Numerical Simulation of Polymeric Liquid Crystalline Flows Under Magnetic Field

Shufang FU

A dissertation submitted to
Kochi University of Technology
in partial fulfillment of the requirements
for the degree of

Doctor of Philosophy

Special Course for International Students
Department of Engineering
Graduate School of Engineering
Kochi University of Technology
Kochi, Japan

March 2006

Abstract

After development of ultrahigh strength polymeric liquid crystalline fibers, which are made of liquid crystalline polyamides, intensive research efforts have been made to enhance the performance of polymeric liquid crystalline materials. The performance, such as tensile strength and modulus, strongly depends on the orientation configuration of constitutive molecules. For example, radial and onion structures are found in the liquid crystal polymer (LCP) fibers. These orientation structures are mainly formed in the processing, where the melted materials flow into dies, and remain in the final products. To optimize the processing of the LCP products, it is useful to know the relation between the flow and the molecular orientation of LCPs.

The relation between the processing and properties of LCPs has long been recognized. A variety of computer simulations predict mold filling flow and fiber orientation in injection-molded parts. However, there is little research on the extensive controlling of the orientation configuration of LCP molecules during the processing. At present, the processing conditions are empirically decided. Therefore, the performance of LCP products only reaches about 10% of theoretical value because of defects or disorders. In order to make an improvement on the performance of the LCP materials it is necessary to investigate the results how the director is controlled by applying appropriate external field in the processing.

In this dissertation the effect of magnetic fields (along the flow and velocity gradient direction) on molecular configuration of LCPs under shear flows are numerically analyzed using the Doi theory. The evolution equation for the probability distribution function of the LCP molecules is directly solved without any closure approximations. The main study discussed in this dissertation is divided into two parts: (1) the effect of the magnetic fields on the director confined into the shear plane, and (2) the effect of the magnetic fields on the director including out-of-plane case.

For the in-plane case the magnetic fields strongly affect the transition among flow-orientation modes, such as tumbling, wagging, and aligning modes. When the magnetic fields are imposed on the LCP shear flow, a new aligning flow-orientation mode emerges at low shear rates, which is macroscopically same with the ordinary aligning mode, but is microscopically quite different from the ordinary one. For the magnetic fields parallel to the flow direction, the fields affect the scalar order parameter rather than the major orientation direction. On the other hand, for the magnetic field parallel to the velocity gradient direction, the effect of the magnetic field is more

remarkable on the major orientation direction in comparison with the effect on the scalar order parameter.

The initial director is oriented at three angles with respect to the shear plane for the out-of-plane case, where the shear plane is parallel to both the velocity and its gradient: (1) along the velocity gradient direction, (2) parallel to the vorticity direction, and (3) set into the plane which is parallel to the vorticity direction and the velocity gradient direction. We find that when the initial director is along the velocity gradient direction in the shear plane, it doesn't rotate out again. Three modes, tumbling, wagging and aligning, are observed, respectively. However, depending on the initial conditions of the probability distribution function of molecular configuration chose in this dissertation in the second and third case a log-rolling orientation state is detected at low shear rates, where the average orientation is perpendicular to the shear plane. The simulation results show that the log-rolling orientation state can be controlled well to align the direction of magnetic fields through the exchange of the longest and second longest axes of molecules. Finally in order to check the effect of the molecular length the simulation results for β=0.9 are also represented.

List of Contents

Chapter 1

General Introduction

1.1 Research Background

The study of liquid crystals (LCs) began in 1888 when an Austrian botanist named Friedrich Reinitzer observed that a material known as cholesteryl benzoate had two distinct melting points – the solid changed first into an opaque liquid, then on raising the temperature further the material became a clear liquid (1). The intermediate, opaque liquid was termed the liquid crystal phase. In addition to the other three distinct states: solid, liquid and gas, LCs are a new state of matter which exhibits a degree of order between that of a liquid and a solid. Therefore LCs are also called mesophases. For this reason LCs possess anisotropic optical properties and fluidity which intrigue the interesting of many scientists even for 100 years they had no practical uses. Since the 1960s, the knowledge they extracted has become profitable: LCs are now used in many applications, such as, liquid crystal displays (LCDs), liquid crystal thermometers and so on. Figure 1.1 shows the chemical formulas of the following typical rodlike liquid crystals: 4-penty1-4' cyanobiphenyl (5CB) and 4-methoxybenzylidene-4'-butylaniline (MBBA) (1).

After the development of ultrahigh strength Kevlar® fibers, which are made of liquid crystalline polyamides by DuPont© in 1971, high strength fibers and high strength engineering plastics have been exploited and widely applied in life, such as Vectran90® and Xydar®. The performance, such as tensile strength and modulus, strongly depends on the orientation configuration of constitutive molecules. But in the process it is difficult to maintain a monodamain orientation state at macroscopic level, or at least control the microstructural orientation state in any flow processing other than fiber spinning (2). For example, when the nematic liquid crystal polymers (LCPs) flow

into a mold, the singular structures (points or lines) will be formed or proliferated in orientation field, which is called defects. The ‘skin-core’ also is a severe problem happened in the LCPs process, which molecules near surface almost align along one direction, however, molecules in the core are distributed at random. These disorders will reduce the performance of LCPs since the strength is stronger along the direction that most molecules align than one perpendicular to this direction. On the other hand, the tumbling (the director rotates endless), wagging (the director oscillates around a steady state) and aligning (the director finally arrives a steady state) modes, which are caused by the LCPs flow, already have been represented by Marrucci and Maffettone (3), and Larson (4). In addition to these three modes, log-rolling and kayaking modes are also found by Larson and Öttinger (8) for the case of out-of-plane orientation configuration. The connection among process, structure, and properties has long been recognized. A variety of computer simulations predict mold filling flow and fiber orientation in injection-molded parts (5-10). However, the simulation results how to control the director in the flow process have not been done, especially for LCP materials. Therefore, in order to further improve the performance of the LCP products it is necessary to simulate the results that how the director is controlled in the process.

For low molar mass liquid crystals (LMMLCs) Leslie-Ericksen (L-E) theory is used to solve flows (11-13). In this theory the local average of the molecular orientation is described by a vector quantity, called the director (**n**). The other classical theory of Doi (14) for LCPs employs the probability orientation function of molecular orientation, which is able to capture the local molecular orientation distribution. The Doi theory gives a detailed view of molecular processes that affect the macroscopic rheological behavior. Based on Doi theory the extended theories (15) were founded, for instance, Tsuji-Ray theory considered short range order elasticity, long range order elasticity and viscous flows. In this dissertation Doi theory included the effect of magnetic fields will be used to discuss how to control the director in the nematic LCPs process.

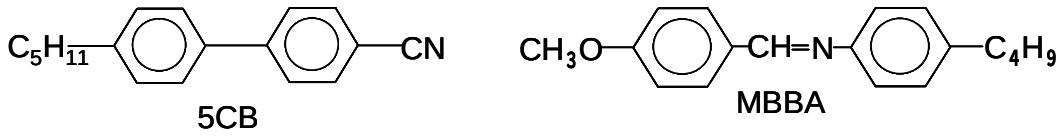

Figure 1.1 Examples of typical rodlike like crystals: 4-penty1-4’ cyanobiphenyl (5CB) and 4-methoxybenzylidene-4’-butylaniline (MBBA).

1.2 Classification of Liquid Crystals (LCs)

LC phase is investigated in the course of phase transfer from a solid state to a liquid state. When the temperature is increased, the crystalline solid formed by spherical symmetrical molecules loses the positional order and directly changes into the liquid. But for the materials composed of oblate or prolate molecules the orientational order is kept with no, or partial, positional order at beginning. Then with further rising the temperature, the liquid state is arrived resulting from losing both the orientational and positional order. The intermediate phase that the molecules have a tendency to point a common direction called the director (**n**) is termed LCs. This distinguishing characteristic of LCs is contrast to the liquid state that molecules are randomly arranged and the solid state that molecules are highly ordered. Therefore, LCs possess both anisotropic optical properties and fluidity.

When molecules show liquid crystalline behavior in their molten state, their anisotropic properties are often directly related to the strongly anisometric molecular shape, i.e. one of their molecular axes strongly deviates from the other two. This leads to two major subclasses: rodlike (calamitic) and disklike (discotic) LCs.

Depending on the degree of orientational and positional order, rodlike LCs can be divided into nematic phase, cholesteric phase and smectic phase. In Figures 1.2 three kinds of LC phases are showed out. The rods describe molecules. a) isotropic phase , b) nematic phase, c) smectic-A phase, d) smectic-C phase, and e) cholesteric phase. In Figure 1.3 the columnar phase constructed by disklike molecules is represented. The disk describes the core of disklike molecules. In the following sections we will explain the main characteristics and applications of LC phases formed by rodlike and disklike molecules.

1.2.1Nematic Phase

The nematic LC phase which is the simplest LCs is characterized by molecules that have no positional order but tend to point in the same direction (along the director **n**). In the following diagram, notice that in Figure 1.2a the molecules are randomly arranged; in Figure 1.2b the molecules point vertically but are arranged with no particular positional order.

Nematics are commonly used in LCDs, such as lap-top computers.

1.2.2 Smectic Phase

The ‘smectic’ word is derived from Greek word for soap. As shown in Figure 1.2d, smectics, which are found at lower temperatures than nematics, possess both orientational and one-dimensional, or layer-like, positional order which is not presented in nematics. Smectic A (S_A) (Fig.1.2c) and smectic C (S_C) (Fig.1.2d) possess highest order in smectic LCs. In the S_A phase, the director is perpendicular to the smectic plane, and there is no particular positional order in the layer. Similarly, in the S_C molecules are oriented as in the S_A, but the director is at a constant tilt angle measured normally to smectic plane. Because of the complicate molecular structures the theoretic research for smectic is very rare. According to L-E theory, however, the continuum theory for smectic C has been put forward. Dr. Terada showed out the detail numerical simulation of smectic C liquid crystalline flow with this continuum theory in his Ph.D. Dissertation (16).

Smectics have been explored as possible lubricants, because they can, in principle, slide readily along surfaces. Recently the study of LCDs used smectics has been noticed by many researchers (17, 18).

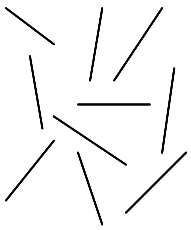

(a) Isotropic

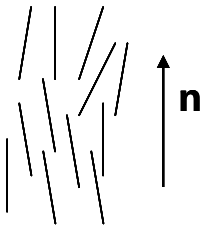

(b) Nematic

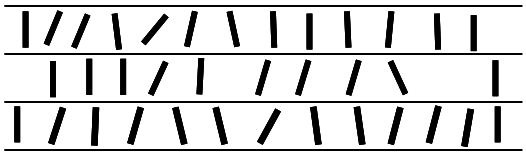

(c) Smectic A

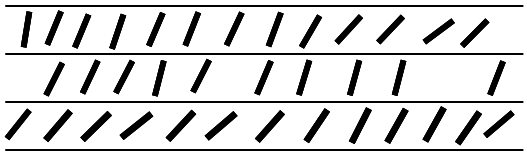

(d) Smectic C

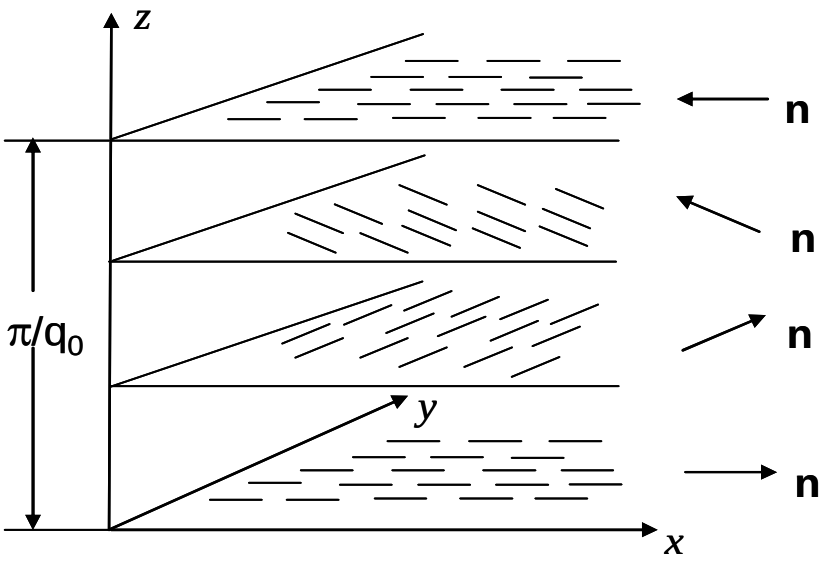

(e) Cholesteric

Figures 1.2 Schematic representations of the (a) isotropic, (b) nematic, (c) smectic-A, (d) smectic-C, and (e) Cholesteric liquid crystalline phases. **n** is the director and π/q_0 is the period.

1.2.3 Cholesteric Phase (1)

Cholesterics are the earliest LCs discovered by Reintzer in 1898. Cholesteric LCs are also called by twisted nematics. The order of cholesterics is same with that of nematics on a local level; i.e., the molecules tend to align with the director. But as shown by Figure 1.2e the directors also make a twist about an axis with a constant angle. On a larger scale, the director follows a helical path with pitch equal to twice the spatial period, since –**n** and **n** are equivalent. Twist structure of cholesteric LCs gives rise to optical rotation and selective reflection.

Cholesterics are used as temperature indictor, since their pitch is often in the range of visible wavelength and strongly dependent on the temperature.

1.2.4 Nematic Discotic Phase

The observation of the first disk-shaped LCs was reported in 1977(19). This new class of LCs has gained increasing interesting, both from scientific and applicative points of view. For discotic LCs, multiple phases have been reported.

The nematic phase for discotic LCs is quite similar to the one for calamitic mesogens. Also, there is only the orientational order. The nematic phase is less common than in calamitic LCs, as the discotic molecules have a great tendency of assembling to columns, forming columnar phases.

1.2.5 Columnar Discotic Phases (20)

The columnar discotic phases are the equivalents of the smectic phases for calamitic LCs. The cores are aligned in columns, surrounded by the side chains. Commonly columnar discotic phases show the two-dimensional positional order. The several columnar phases are distinguished by the order within the columns and the order between the columns. These columns can then be arranged in various ways, for example in a hexagonal or a rectangular lattice. The hexagonal columnar phase is shown in Figure1.3. It proves to be difficult to determine the type of columnar phase exactly, because the optical textures are often ambiguous and X-ray diffraction frequently offers insufficient structure details. Therefore, unlike the smectics, the classification of columnar LCs is still in progress.

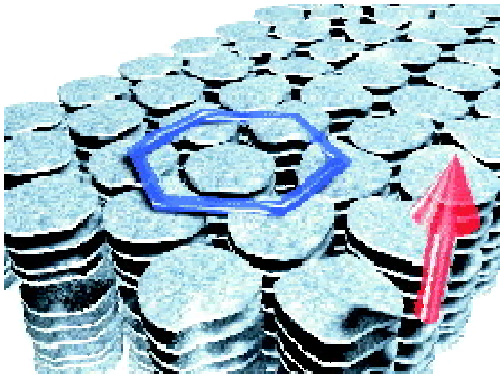

Figure 1.3 Structure of the discotic Col_h phase

Discotic LCs have some unique properties, which are starting to get the commercial applications. The most important aspect is the huge anisotropy in conductivity between the dimension parallel to the column axis and those perpendicular

to that. Based on these, Fuji uses discotic LCs to produce optical compensation films which help to improve the viewing angle properties of LCDs. And discotic LCs are also used by Sanyo to focus electron beams in electron beam lithography. The recent progress in elucidating the properties of the columnar phases as one-dimensional electrical conductors (or molecular wires), fast photoconductors, light emitting diodes and ferroelectrics, all of which have potentially important practical application have been reviewed in the paper written by Chandrasekhar and Prasad (22).

Except this kind of classification, there are also some other ways to classify the LCs. For example, LC phases can be reached by means of increasing temperature of solutions, which is called thermotropic LCs, and some materials can become more order resulting from increasing the concentration of solutions, which are known as lyotropic LCs. In addition, depending on the weight of molecules LCs also can be differentiated into low molecular weight LCs (LMWLCs) and liquid crystalline polymers (LCPs).

1.3. Molecular Characteristics and Applications of LCPs

In this dissertation we will focus on nematic LCPs. LCPs are a class of materials that combine the properties of polymers with those of LCs. LCPs displayed order in the melt (liquid) phase analogous to that exhibited by non-polymeric LCs. The development of the application of LCPs has been carried out after ultrahigh strength Kevlar® fibers which are made of liquid crystalline polyamides by Dupont in 1971. The commercially interesting of LCPs is due to their unusual bulk properties and their processability, resulting from chain stiffness and high molecular orientation. In addition, LCP materials are unusually resistant to solvent attack, moisture uptake, and thermal expansion, softening, or decomposition. Up to now LCPs have been widely used as engineering plastic for electronic materials such as connectors, super fibers for bulletproof vests, and packaging for electrical and optical components. The main molecular characteristics and applications of LCPs are showed in the following sections.

1.3.1Main-chain and Side-chain LCPs

In order to display LC characteristics, rodlike or disklike elements (called mesogens) must be incorporated into their chains. According to the displacements of mesogens along the polymer backbone, the type of LCPs can be determined as main -chain and side-chain LCPs. As illustrated in Figures 1.4, main-chain LCPs (Figure 1.4 (a)) are formed when the mesogens are themselves part of the main chain of a polymer.

The mesogens along the chain allow the polymer to orient in a manner similar to LCs, and thus display LC characteristics. Conversely side-chain LCPs (Figure 1.4 (b)) are formed when mesogens are connected as side chains to the polymer by a flexible "bridge" called spacers. Therefore, there are three parts in a side-chain LCPs: backbone, mesogens and spacers. The presence of long flexible spacers, a low molecular weight and the regular alternation of rigid and flexible units can also influence the mesomorphic of polymers. Main-chain LCPs are attractive materials for applications where their mechanical (e.g. high modulus) and rheological (e.g. low melt viscosity) properties can be exploited. In this dissertation only nematic main-chain LCPs are investigated. Side-chain LCPs are under consideration for electronic and optical applications.

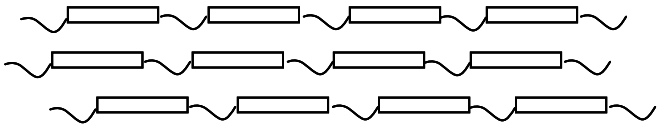

(a) Rigid units and flexible connectors on main chain

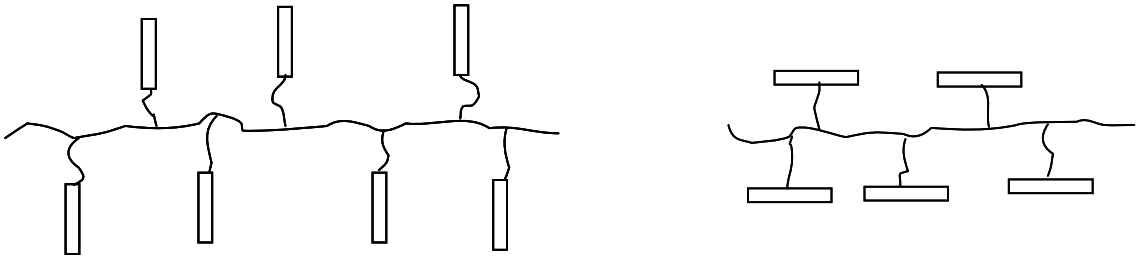

(b) Rigid units and flexible connectors on side chains

Figures 1.4 Schematic illustration of different kinds of LCPs, with rigid units (rectangles) and flexible ones (lines) along the backbone or in side branches: (a) Rigid units and flexible connectors on main chain, (b) Rigid units and flexible connectors on side chains

A well-know main-chain LCP is poly (p-phenylene terephthalamide), which does not melt before decomposing at about 500°-600°C:

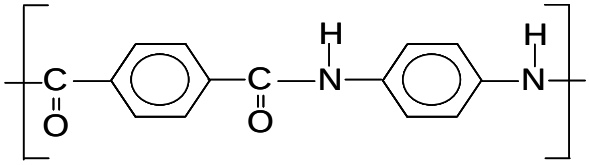

Figure 1.5 Chemical structure of main-chain LCP: poly (*p*-phenylene terephthalamide)

1.3.2 Lyotropic and Thermotropic LCPs

Another classification is lyotropic and thermotropic LCPs. A fiber with a high modulus and strength is obtained by spinning fibers from a lyotropic solution in an elongational flow field (Twaron from AKZO and Kelvlar from Dupont). Thermotropic LCPs are particularly attractive for injection molding, because shrinkage is low, injection and clamping pressure are low (because the melt viscosity is low), and cycle times are fast (because thermal conductivity is high and heat of fusion is low). PPTA (poly (*p*-phenylene terephthalamide)) represented in Figure 1.5 is also used as lyotropic LCPs. Figures 1.6 shows out some other chemical structures of well-studied LCPs (1).

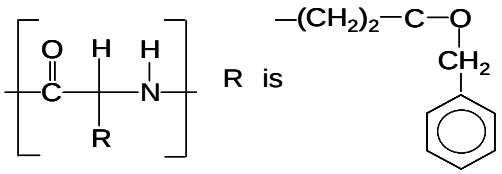

(a) PBLG:
poly(γ-benzyl-L-glutamate)

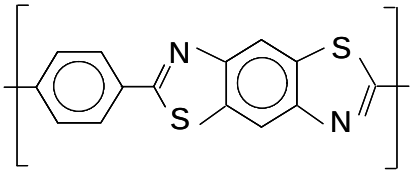

(b) PBZT:
poly(*p*-phenylene benzobisthiazole)

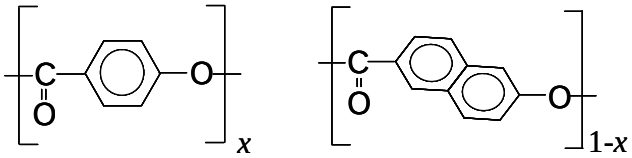

(c) Vectra A

Figures 1.6 Chemical structures of some well-studied LCPs: the top two are used as lyotropic polymers and the bottom is thermotropes.

It is difficult to create LCPs because many times the temperature of the liquid crystalline behavior is above the point where the polymer begins to decompose. Usually there are three ways (22-24) to decrease the melting point of rigid main-chain LCPs by dealing with the arrangement of the monomers in the chain shown in Figures 1.7. In

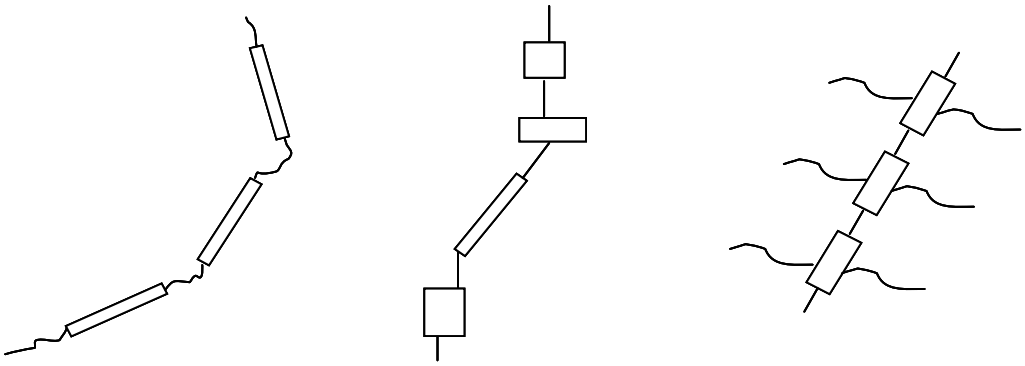

(a) (b) (c)

Figures 1.7 Methods used to decrease the melting point of rigid main-chain LCPs: (a) Insertion of flexible spacers, (b) Random copolymerization and the introduction of crankshaft monomers, (c) Attaching flexible side chains on the backbone

Figure1.7 (a), the melting point is lowered by increasing the flexibility of the main chain when the flexible spacers are inserted. However, too many spacers will cause the LC behavior to disappear. Another way to accomplish this task of lowering the temperature involves copolymerization or/and the introduction crankshaft (or kink like) monomers showed in Figure 1.7(b). The approach using copolymerization as well as the crankshaft monomers has been used commercially by Hoechst-Celance for the Vectra polymers. Finally, shown in Figure 1.7(c), the flexible side chains are attached on the rigid backbone.

1.4 Liquid Crystal Physics

1.4.1 Orientational Order

As mentioned above, molecules in LCs always tend to align a common direction called director **n**. Usually a scalar parameter *S* is defined to show the degree of

molecular alignment along **n**, which is expressed:

$$S = \frac{1}{2} < 3 < \cos^2(\theta) > -1 > \tag{1.1}$$

with -1/2≤*S*≤1. θ is the degree between the molecules and the director as shown in Figure 1.8. <…..> means an average value over all the molecules since the degree is not same for all the molecules oriented about the director.

If all the molecules are aligned along the director, *S* is equal to 1 which defines a perfectly aligned nematic phase. However, this is an ideal state for LCs since the thermal motion at finite temperature always exists. If *S*=0, an isotropic liquid phase is defined, and a value of *S*=-1/2 defines a nematic phase where the molecules are lying in a plane normal to the director. For 5CB illustrated in Figure 1.1, at 25^0C *S*=0.65, which is typical for nematics (25).

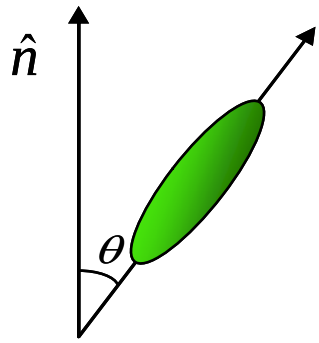

Figure 1.8 Degree between the director and the molecule

1.4.2 Doi Theory (1)

A molecular theory for the effect of flow on the orientation of ideal monodisperse rigid rodlike polymers has been developed by Doi (26) and Hess (27). This theory has successfully modeled the monodomain shear flow problem for rigid, rodlike nematic polymers. Numerical simulations of the Smoluchowski equation for the orientational probability distribution function (pdf) have predicted: monodomain attractors in regions

of the 2-parameter space of nematic concentration and shear rate; and bifurcation curves of monodomain transitions. Theoretical work has focused on approximate constructions of pdf solutions in various linear flow regimes. The Smoluchowski equation is derived for the pdf $f(\mathbf{u})$ that a rodlike molecule is oriented parallel to a unit vector $\mathbf{u}$:

$$\frac{\partial f}{\partial t} = \bar{D}_r \frac{\partial}{\partial \mathbf{u}} \cdot \left(\frac{\partial}{\partial \mathbf{u}} f + f \frac{\partial}{\partial \mathbf{u}} \frac{V_{nem}(\mathbf{u})}{kT} \right) - \frac{\partial}{\partial \mathbf{u}} \cdot \left((\mathbf{u} \cdot \nabla \mathrm{v} - \mathbf{uuu} : \nabla \mathrm{v}) f \right), \tag{1.2}$$

In equation (1.2), $\nabla\mathbf{v}$ is the velocity gradient, $\partial/\partial\mathbf{u}$ is the gradient operator on the unit sphere, and V_{nem} is a nematic potential, such as that of Onsager, or of Maier and Saupe. In this dissertation the part of the potential, V_{nem}, chooses the Maier-Saupe potential. $\bar{D}_r$ is a preaveraged molecular rotary diffusivity in the nematic phase:

$$\frac{1}{\bar{D}_r} = D_r^{-1} \left(\frac{4}{\pi} \right)^2 \left[\int f(\mathbf{u}) f(\mathbf{u}') \sin(\mathbf{u}, \mathbf{u}') d^2u d^2u' \right]^2, \tag{1.3}$$

$\mathbf{S}$ is the order parameter tensor:

$$\mathbf{S} = \int_{|\mathbf{u}|=1} \left(\mathbf{uu} - \frac{\mathbf{I}}{3} \right) f dA = < \mathbf{uu} - \frac{\mathbf{I}}{3} >, \tag{1.4}$$

Here $\mathbf{I}$ is the unit tensor, and <…..> denotes the average over the pdf $f(\mathbf{u})$. The scalar order parameter S is related to the tensor $\mathbf{S}$ by

$$S = \sqrt{\frac{3}{2} \mathbf{S} : \mathbf{S}}, \tag{1.5}$$

S=0 is for a completely isotropic distribution of orientations and S=1 is for rods that are all aligned in the same direction.

If we consider the molecular length, another parameter β called molecular formation coefficient has to be introduced into the equation (1.2):

$$\frac{\partial f}{\partial t} = \bar{D}_r \frac{\partial}{\partial \mathbf{u}} \cdot \left(\frac{\partial}{\partial \mathbf{u}} f + f \frac{\partial}{\partial \mathbf{u}} \frac{V_{nem}(\mathbf{u})}{kT} \right) - \frac{\partial}{\partial \mathbf{u}} \cdot \left((\mathbf{u} \cdot (\mathbf{W} + \beta \mathbf{A}) - \mathbf{u} \cdot \beta \mathbf{A} \cdot \mathbf{uu}) f \right), \tag{1.6}$$

Here $\mathbf{W}$ is the vorticity tensor, and $\mathbf{A}$ is the rate of strain tensor. The molecular

formation coefficient β is described:

$$\beta = \frac{p^2 - 1}{p^2 + 1}, \tag{1.7}$$

with p is the aspect ratio of a molecular:

$$p = \frac{l}{d}, \tag{1.8}$$

l and d is the length and diameter of a rodlike molecule, respectively (Figure 1.9).

When β=1.0, the molecule is infinite long according to equation (1.7). Actually the real molecules have limited length. For typical small-molecule nematics, estimate of p range from 4 to 8, or so, depending on the molecule and how one estimates the molecular diameter.

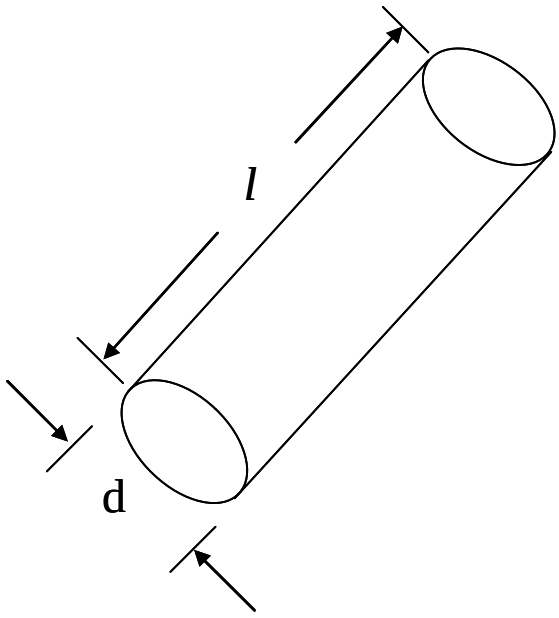

Figure 1.9 A rodlike molecule

1.4.3 External Influences on LCs

In a process a flow field will strongly influent the aligned direction of molecules. At low shear rates the director periodically rotates in the shear plane which is called a tumbling mode. As increasing the shear rate the director oscillates at about fixed angle called a wagging mode. A steady state that the director becomes stationary arrives when the shear rate is further increased, known as a flowing-aligning. If the average direction of molecules lies in the vorticity direction, a mode called 'log-rolling' can be found (28). In addition, defects (lines or points) which break the continuum of orientational order field are also usually produced. Since these phenomena can not be avoided in the process, the performance of the LCPs products, such as the tensile strength, modulus and thermal expansion which is strongly dependent on the aligned level of directors, will be reduced. So how to further improve the properties of LCPs products already has been noticed by many researchers.

As we known, an external field can cause significant changes in the macroscopic properties of the LC system. When an electric or magnetic field is added on the LC system, the director is parallel or perpendicular to the electric or magnetic field. This major characteristic is utilized in industrial applications. As shown in Figure 1.10, the ellipse describes a molecule with electric dipoles, and the arrows represent the electric field vector and the electric force on the molecule, respectively. When an electric field is applied to the LCs, the dipole molecules tend to reorient along the direction of the field. For magnetic fields, the effects on LC molecules are analogous to electric fields since the magnetic dipoles can be caused by moving the electric fields.

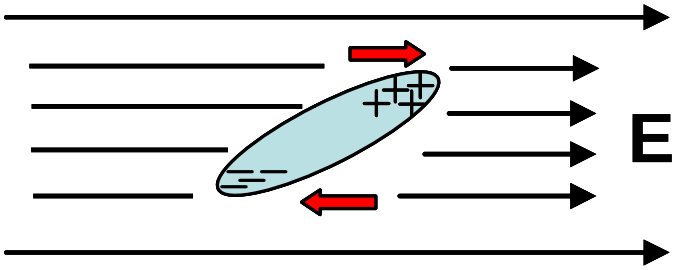

Figure1.10 Dipole molecule applied by an electric or magnetic field

Therefore, if we can control the alignment of directors by means of changing the strength of the electric or magnetic field on LC system, we can tailor the properties of the products. Up to now, most researches have been done to investigate the changing of directors when an electric or magnetic field is applied on a steady state LC system (29-32). Abundant results have been showed out. However, rare simulation results are got for applying the electric or magnetic field on a flowing LC system, especially for a flowing LCP system.

1.5 Dissertation Purpose

A number of LCPs were produced in the 1970s which displayed order in the melt (liquid) phase analogous to that exhibited by non-polymeric LCs. However, the commercial introduction of LCP resins did not occur until 1984, at that time LCPs could not be injection molded. Today, LCPs can be melted processed on conventional equipment at fast speeds with excellent replication of mold details and efficient use of regrind. But as mentioned above, in fact the properties of LCP products only reach 10% of theoretical value since the director is easily affected by an external field. How to further improve the performance of LCP products in the process is also noticed. In the steady state of LCs, many researchers have investigated the changes of the director by adding an electric or magnetic field, or using a special surface treatment in LC devices to force special direction of the director. However, the simulation results about controlling the director of LCPs have not been found, especially in the process of LCP products. So in this dissertation the simulation results with applying magnetic field on a flowing LCP system are presented. As shown in the results, the director can be controlled well by the changes of the magnetic field strength.

1.6 Dissertation Organization

This dissertation contains four chapters. The main study discussed in this dissertation is divided into two parts: 1) the effect of the magnetic field on the director confined into the shear plane; 2) the effect of the magnetic field on the director including out-of-plane case. Chapter 2 and 3 give out the main simulation results. A brief description of each chapter is given blow:

Chapter 1 presents the general introduction required by this dissertation. It includes the basic knowledge about low molecular liquid crystals (LCs) and LCPs, as well as the

theory required to study the LCPs flows under magnetic fields of simulation.

Chapter 2 presents the effect of the magnetic field on molecular orientation of nematic LCPs under simple shear flow when the director is confined into the shear plane. The Doi theory is used including the potential caused by the magnetic field, which is solved directly without any closure approximations. Numerical simulation results that the magnetic field is along the *x*-axis and the *y*-axis are presented and discussed. In addition, the effect of length of molecules is also considered in this part when the magnetic field is applied along the *x*-axis and the *y*-axis.

Chapter 3 presents the simulation results and discussions for out-of-plane case under the magnetic field and the simple shear flow. The Doi theory also is used in this case, where the asymmetry of the probability distribution function with respect to the shear plane is allowed. A log-rolling orientation state is detected at low shear rates depending on the initial condition of the probability density function of the molecular configuration. The comparison between the scalar parameter S and S_{xx} is also discussed in this chapter. Finally in order to check the effect of the molecular length the simulation results for β=0.9 are also represented.

Chapter 4 presents conclusions throughout this study. In this chapter, we mention about the native of the magnetic field on the LCP flows. Also, the efficient way to control the LCP molecular configuration under the flow is proposed.

References

1. Larson, R.G., *The structure and rheology of complex fluids,* 443 (1999) Oxford University press.
2. Sgalari, G., Leal, G.L. and Feng, J.J, *J. Non-Newt. Fluid Mech.* **102**, 361(2002)
3. Marrucci, G. and Maffettone, P. L., *Macromolecules* **22**, 4076 (1989)
4. Larson, R.G., *Macromolecules* **23**, 3983 (1990)
5. Friedl, C. and Brouwer, R., *SPE Tech. Papers* **37**, 326 (1991)
6. Bay, R.S. and Tucker III, C.L., *Polym. Composites* **13**, 317(1992a)
7. Bay, R.S. and Tucker III, C.L., *Polym. Composites* **13**, 322(1992b)
8. de Frahan, H.H., Verleye, V., Dupret, F. and Crochet, M.J., *Polym. Eng. Sci.* **32**, 254(1992)

9. Gupta, M. and Wang, K.K., *Polym. Coposites* **14**, 367(1993)
10. Henry, E., Kjeldsen, S. and Kennedy, P., *SPE Tech. Papers **40***,374(1994)
11. Ericksen, J.L., *Kolloid-Z* **173**, 117-122(1960)
12. Leslie, F.M., *Mech. Appl. Math. **XIX***, 357-370(1966)
13. Leslie, F.M., *Adv. Liq. Cryst.* **4**, 1-84(1979)
14. Doi, M., J. *Polym. Sci. Polym. Phys. Ed.* **19**, 229 (1981)
15. Tsuji, T. and Rey, A.D., *Phys. Rev. E* **57**, 5609-5625(1998)
16. Atsushi Terada, *Ph.D. Thesis*, Department of Intelligent Mechanical Systems Engineering, Kochi University of Technology, (2005)
17. Leslie, F.M., Stewart, I.W. and Nakagawa, M., *Mol. Cryst., Liq. Cryst.*, **198**, 443(1991)
18. Leslie, F.M., *Liq. Crystals*, **14**, 121(1993)
19. Chandrasekhar, S., Sadashiva, B.K. and Surseh, K.A., *Pramana* **9**, 471(1977)
20. home.arcor.de/stefan._lange/uni/in_rep_html/node2.html
21. Chandrasekhar, S. and Prasad, S.K., *Contemp. Phys.* **40**, 237(1999)
22. Chapoy, L.L., *Ed. Recent Advances in Liquid-Cystalline Polymers*, Elsevier Applied Science Publishers, London, 1983
23. Cifcrri, A., Krigbaum, W.R., Mcyer, R.B., Eds., *Polymer Liquid Crystals*, Academis Press, New-York, 1982
24. Ballauff, M., *Angew. Chem*. **101(3)**, 261(1989)
25. Blinov, L.M. and Chigrinov, V.G., *Electroopotic Effects in Liquid Crystalline Materials*, Springer-Verlag, New York (1994)
26. Doi, M., *Ferroelectrics* **30**, 247(1980)
27. Hess, S. *ZNaturforsch* **31A**, 1034(1976)
28. Larson, R.G. and Öttinger, H.C., *Macromolecules* **24**, 6270 (1991)
29. Andrews, N.C., Edwards, B.J. and McHcgh, A., *J. Rheol.* **39**, 1161-1181(1995)
30. Belyaev, V.V, *Phys. Usp.*, **44 (3),** 255-284(2001)
31. Lukaschek, M. and Kothe, G., *J. Phys. Chem.* **117(9)**, 4550-4556(2002)
32. Luckhurst, G.R., Timimi, B.A., Nakatsuji, M., Okumoto, K., Sugimura, A., and Zimmermann, H., *Mol. Cryst. Liq. Cryst.*, **398**, 235-248(2003)

Chapter 2

Effect of Magnetic Field on Molecular Orientation of Nematic Liquid Crystalline Polymers Under Simple Shear Flow:I In-Plane Case

The effect of magnetic fields on molecular configuration of liquid crystalline polymers under shear flows are numerically analyzed using the Doi theory. The evolution equation for the probability density function of the LCP molecules is directly solved without any closure approximations. Two cases of the magnetic fields are considered:(1) the magnetic field parallel to the flow direction, and (2) the magnetic field parallel to the velocity gradient direction. For both cases, the magnetic fields strongly affect on the transition among flow-orientation modes, such as tumbling, wagging, and aligning modes. When the magnetic field is imposed on the LCP shear flow, a new aligning flow-orientation mode emerges at low shear rate, which is macroscopically same as the ordinary aligning mode, but is microscopically quite different from the ordinary one. For the magnetic field parallel to the flow direction, the field affects on the scalar order parameter rather than the major orientation direction. On the other hand, for the magnetic field parallel to the velocity gradient direction, the effect of the magnetic field is more remarkable on the major orientation direction in comparison with the effect on the scalar order parameter.

2.1 Introduction

After development of ultrahigh strength Kevlar® fibers, which are made of liquid crystalline polyamides by DuPont© in 1971, intensive research efforts have been achieved to enhance the performance of polymeric liquid crystalline materials. The performance, such as tensile strength and modulus, strongly depend on the orientation configuration of constitutive molecules. For example, radial and onion structures are found in the LCP fibers. These orientation structures are mainly formed in the processing, where the melted materials flow into dies, and remain in the final products. To optimize the processing of the LCP products, it is useful to know the relation between the flow and the molecular orientation of LCPs.

For the last few decades, many researches have been performed on the molecular orientation in the LCP flows, especially by means of theoretical and computational analysis (1~5). One of the major advances in the theoretical LCP rheology was made by Doi in 1981, who extended the theory for semi-dilute polymeric fluids to that for concentrated rod-like polymeric fluids. The theory is well applicable to the flow of LCPs in the absence of the long range order of the molecular orientation configuration. Using the Doi theory, Marrucci and Maffettone (6) and Larson (7) found that for simple shear flows LCPs show three flow-orientation modes depending on the shear rate; they are tumbling, wagging, and aligning modes. These three modes correspond to the rotational, oscillatory, and stationary behaviors of the macroscopic molecular orientation direction, respectively. In addition to these three modes, log-rolling and kayaking modes are found by Larson and Öttinger (8) for the case of out-of-plane orientation configuration. On the other hand, the behaviors of macroscopic orientation are not necessarily same as those of microscopic molecules (i.e., behaviors of individual molecules). Using the Langevin simulation technique, it has been shown that the individual molecules continue rotating even in the wagging or aligning modes (9~10). Although the flow-orientation modes are of apparent, they are successfully connected with the complex phenomena in the rheological quantities of LCPs, such as shear viscosity thinning (11~13), negative first normal stress difference (14~17), and the kink in viscosity (14, 16, 18~19).

To obtain the desired performance and to optimize the process of the LCP products, one must carefully find the best coupling of the condition parameters which emerge in the process, such as a temperature, a flow rate, and the shape of die. Of course, the previous investigations on LCP flows mentioned above are greatfully useful for determining those parameters, but it is still hard to determine all of them.

If one can freely control the molecular orientation configuration during the processing, the processing optimization may become much simpler. It is known that the LC molecules are sensitive to a magnetic field. The LC molecules tend to align parallel or perpendicular to the field, depending on the sign of the magnetic susceptibility coefficient. Thus, it may be useful to use the magnetic field for controlling the orientation of LC molecules. Some studies on the effect of a magnetic field on the flowing LC molecular orientation field have been reported for low molecular weight liquid crystals (LMWLCs) (20~23). In the studies (21,22), the Leslie-Ericksen theory (24~26) was used to solve the flows. The L-E theory employs a vector notation to represent the local averaged molecular orientation direction, and thus the orientation order of LC molecules is not taken into account. On the other hand, the probability density function of the molecular orientation is employed in the Doi theory (1). The major difference between the low molecular and the polymeric liquid crystals is in the strength of the short range order elasticity (i.e., magnitude of a rotational diffusivity of rod-like molecules). The rotational diffusivities of LMWLCs are much higher than those of LCPs, and the time and/or spatial change in the molecular orientation order is negligible for LMWLCs. Thus the vector notation is enough for LMWLCs. However, for LCPs the molecular orientation order is easily affected by the flow or other external fields, and the previous results for LMWLCs are hard to be used to infer the LCP flow behaviors under the magnetic field.

In this paper, we focus our attention on the effect of magnetic fields on the flow-orientation behaviors. The behaviors are computed using the Doi theory and the results are organized in terms of the flow-orientation modes. The organization of this paper is as follows. In section 2.2 we briefly review the Doi theory, and section 2.3 presents the main simulation results that the director is affected by the magnetic field within the shear plane. In this section we also discuss the effect of the molecular formation coefficient β which can be defined in terms of the aspect ratio of the ideal rodlike molecules on the flow-orientation modes, for instants, β =1.0 and 0.9 are chose in this paper.

2.2 Theory Model

The LCP dynamical system used in this study is subjected to a magnetic field in addition to Hydrodynamic, Brownian and the intermolecular forces. In the Doi theory the polymer molecules were modeled as rigid axisymmetric rods with infinite aspect ratio, and the governing equation for the orientation distribution function *f*, which gives

the probability of finding a rod at an orientation within the solid angle $d\mathbf{u}$ of the unit vector **u,** is written as:

$$\frac{\partial f}{\partial t} = \overline{D}_r \frac{\partial}{\partial \mathbf{u}} \cdot \left(\frac{\partial}{\partial \mathbf{u}} f + f \frac{\partial}{\partial \mathbf{u}} \frac{V(\mathbf{u})}{kT} \right) - \frac{\partial}{\partial \mathbf{u}} \cdot (\dot{\mathbf{u}} f), \tag{2.1}$$

Here $\overline{D}_r$ denotes the average rotational diffusivity:

$$\overline{D}_r = D_s \left(1 - \frac{3}{2} \mathbf{S} : \mathbf{S} \right)^{-2}, \tag{2.2}$$

Where D_s is the rotational diffusivity of an isotropic state, and the order parameter tensor **S**, which is the second moment of the orientation distribution *f*, is defined by the following equation:

$$\mathbf{S} = \int_{|\mathbf{u}|=1} \left(\mathbf{uu} - \frac{\mathbf{I}}{3} \right) f dA, \tag{2.3}$$

Here **I** is a unit tensor. When the effect of the magnetic field on the LCP molecules is taken into account, the mean field potential $V(\mathbf{u})$ in eq.(2.1) can be described as a sum of the Maier-Saupe potential and the potential due to the magnetic field, as follows

$$V(\mathbf{u}) = -\frac{3kTU}{2} (\mathbf{S} : \mathbf{uu}) - \frac{\mu_0 \Delta\chi}{2} (\mathbf{u} \cdot \mathbf{H})^2, \tag{2.4}$$

Where k is the Boltzmann constant, T the absolute temperature, and U the dimensionless nematic potential intensity. μ_0 is the permeability of vacuum, **H** the vector of the magnetic field, and $\Delta\chi (=\chi_{\parallel}-\chi_{\perp})$ the magnetic anisotropy. $\dot{\mathbf{u}}$ in eq.(1) represents the rate of change of **u** by the macroscopic flow, given by

$$\dot{\mathbf{u}} = \boldsymbol{\kappa} \cdot \mathbf{u} - \boldsymbol{\kappa} : \mathbf{uuu}, \tag{2.5}$$

Here $\boldsymbol{\kappa}$ is the velocity gradient tensor.

2.3 Numerical Calculation

We consider simple shear flow, as shown in Figure 2.1, where *x*-axis is the flow direction, *y*-axis is the direction of the velocity gradient, and *z*-axis is co-axial with the vorticity axis. The material is sheared with the shear rate of $\dot{\gamma}$ in the *x*-*y* plane, and the velocity gradient tensor is given by,

$$\boldsymbol{\kappa}=\begin{bmatrix} 0 & \frac{1}{2}\dot{\gamma}(\beta+1) & 0 \\ \frac{1}{2}\dot{\gamma}(\beta-1) & 0 & 0 \\ 0 & 0 & 0 \end{bmatrix}, \tag{2.6}$$

The orientation of a single molecule represented by a unit vector **u** is characterized with an azimuthal angle ϕ and a polar angle θ. The orientation distribution function *f* keeps symmetry with respect to the *x*-*y* plane, when the director which represents the local average of the molecular orientation always remains in the shear plane. That is,

$$f(\theta,\phi,t)=f(\pi-\theta,\phi,t)\,, \tag{2.7}$$

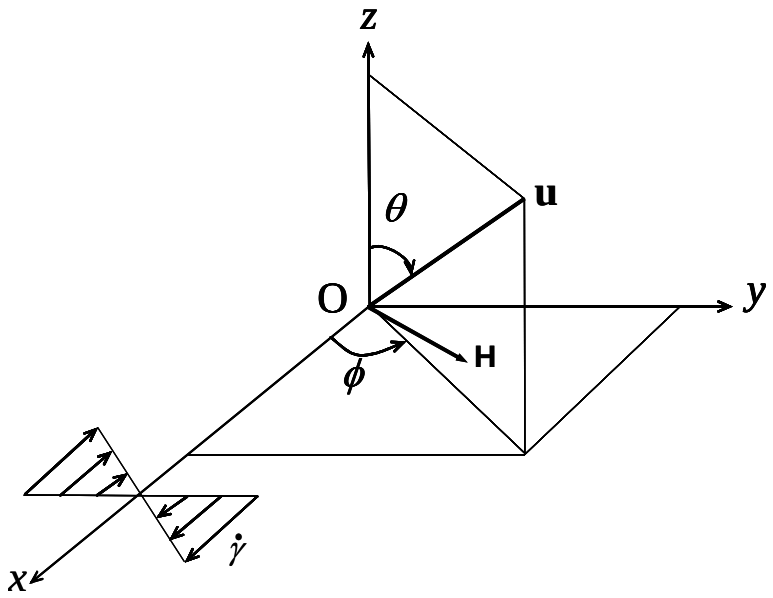

Figure 2.1 Geometry and coordinate systems

Also, it should be mentioned here that since there is no distinction between head and tale of the model rods, the function *f* must has the point symmetry:

$$f(\theta,\phi,t) = f(\pi-\theta,\pi+\phi,t)\,, \tag{2.8}$$

From above conditions for the distribution function *f*, the non-zero components of the order parameter tensor **S** are:

$$\mathbf{S} = \begin{bmatrix} S_{xx} & S_{xy} & 0 \\ S_{xy} & S_{yy} & 0 \\ 0 & 0 & S_{zz} \end{bmatrix}. \tag{2.9}$$

After non-dimensionalization using the time scale 1/Ds and the magnetic force $\sqrt{2kT/\mu_0\Delta\chi}$, eq.(2.1) for two dimensional magnetic field (**H**=(H_x,H_y,0)) becomes

$$\begin{aligned}
\frac{\partial f}{\partial t^*} &= \left(1-\frac{3}{2}\mathbf{S}:\mathbf{S}\right)^{-2}\left(\frac{\partial^2 f}{\partial\theta^2}+\cot\theta\frac{\partial f}{\partial\theta}+\frac{1}{\sin^2\theta}\frac{\partial^2 f}{\partial\phi^2}\right) \\
&+3U\left(1-\frac{3}{2}\mathbf{S}:\mathbf{S}\right)^{-2}\left\{3f\left(S_{xx}\sin^2\theta\cos^2\phi+S_{yy}\sin^2\theta\sin^2\phi+S_{zz}\cos^2\theta+S_{xy}\sin^2\theta\sin 2\phi\right)\right. \\
&\left.-\frac{1}{2}\frac{\partial f}{\partial\theta}\sin 2\theta\left(S_{xx}\cos^2\phi+S_{yy}\sin^2\phi-S_{zz}+S_{xy}\sin 2\phi\right)+\frac{1}{2}\frac{\partial f}{\partial\phi}\left(S_{xx}\sin 2\phi-S_{yy}\sin 2\phi-2S_{xy}\cos 2\phi\right)\right\}, \\
&+\left(1-\frac{3}{2}\mathbf{S}:\mathbf{S}\right)^{-2}\left\{2f\left[H_x^{*2}\left(3\sin^2\theta\cos^2\phi-1\right)+H_y^{*2}\left(3\sin^2\theta\sin^2\phi-1\right)+3H_x^*H_y^*\sin 2\phi\sin^2\theta\right]\right. \\
&\left.-\frac{\partial f}{\partial\theta}\left[\sin 2\theta\left(H_x^{*2}\cos^2\phi+H_y^{*2}\sin^2\phi+H_x^*H_y^*\sin 2\phi\right)\right]+\frac{\partial f}{\partial\phi}\left[\sin 2\phi\left(H_x^{*2}-H_y^{*2}\right)-2H_x^*H_y^*\cos 2\phi\right]\right\} \\
&+\dot\gamma^*\left\{\beta\left(\frac{3}{2}f\sin^2\theta\sin 2\phi-\frac{1}{4}\frac{\partial f}{\partial\theta}\sin 2\theta\sin 2\phi\right)+\frac{\partial f}{\partial\phi}(1-\beta\cos 2\phi)/2\right\}
\end{aligned} \tag{2.10}$$

where

$$H_x^* = \frac{H_x}{\sqrt{2kT/(\mu_0\Delta\chi)}}\,, \tag{2.11}$$

$$H_y^* = \frac{H_y}{\sqrt{2kT/(\mu_0\Delta\chi)}}\,, \tag{2.12}$$

$$\dot\gamma^* = \frac{\dot\gamma}{D_s}\,, \tag{2.13}$$

$$t^* = tD_s, \tag{2.14}$$

The superscripts * denote non-dimensionalized variables and parameters. Above equation is computed using the finite difference method for spatial discretization and the Crank-Nicolson method for time integration. Because of the conditions eq.(2.7) and eq.(2.8), the computation area for f can be restricted in the region $0 \le \theta \le \pi/2$ and $-\pi/2 \le \phi \le \pi/2$. Boundary conditions for the function are:

$$\partial f(0,\phi,t^*)/\partial\theta = 0, \tag{2.15}$$

$$\partial f(\pi/2,\phi,t^*)/\partial\theta = 0, \tag{2.16}$$

$$f(\theta,-\pi/2,t^*) = f(\theta,\pi/2,t^*), \tag{2.17}$$

$$\partial f(\theta,-\pi/2,t^*)/\partial\phi = \partial f(\theta,\pi/2,t^*)/\partial\phi. \tag{2.18}$$

The normalization condition,

$$4\int_0^{\pi/2} d\theta \int_0^{\pi} d\phi\, f \sin\theta = 1, \tag{2.19}$$

is also required. An initial profile of the function, $f(\theta,\phi,t^*=0)$, is derived from the Boltzmann profile with the major orientation direction along the x-axis (flow direction). The time step and the spatial mesh width are set to be $\Delta t^* = 0.005/\dot{\gamma}^*$ and $\Delta\theta = \Delta\phi = 3$deg.

2.3.1 Results and Discussions for β=1.0

Computational parameters in eq.(2.10) are the dimensionless nematic potential intensity U, the dimensionless magnetic field strength H^*, and dimensionless shear rate $\dot{\gamma}^*$. Throughout this paper, the nematic potential intensity U is set to be 5 which corresponds to the lowest order of the nematic state, to make easy to see the effect of the magnetic field on the orientation order. In the following discussions, the computation results for the orientation distribution function will be mainly organized in terms of the major orientation angle ϕ_m and the scalar order parameter S, defined by

$$\tan 2\phi_m = \frac{2S_{xy}}{S_{xx} - S_{yy}}, \tag{2.20}$$

and

$$S = \sqrt{\frac{3}{2}\mathbf{S}:\mathbf{S}}\ . \tag{2.21}$$

In this paper, we choose two simple cases of the magnetic fields; (1) the magnetic field along the flow direction (**H**=(H_x,0,0)) and (2) the magnetic field along velocity gradient direction (**H**=(0,H_y,0)).

2.3.1.1 The Magnetic Field along the *x*-axis

In this section, we deal with the case that the magnetic field is parallel to the flow direction (i.e., **H**=(H_x,0,0)). Both of the shear flow and the magnetic field are simultaneously imposed at t^*=0.

Figures 2.2 show the time evolutions of the major orientation angle ϕ_m and scalar order parameter S for $\dot{\gamma}^*$=2 and H_x^*=0, 1×10^{-6}, and 1.8×10^{-6}. The horizontal axis γ(=$t^*\dot{\gamma}^*$) represents the strain by the shear flow which is equivalent to the dimensionless time. ϕ_m shows the typical tumbling behavior for H_x^*=0 where ϕ_m periodically decreases with γ. When the magnetic field is imposed, the decrease period becomes longer ($H_x^*=1\times10^{-6}$). Above a certain critical magnetic field strength, ϕ_m no longer changes with time and the system shows an aligning like behavior. This new aligning behavior at low shear rates is quite different from the aligning behavior at high shear rates. As mentioned in the introduction, although the major orientation angle remains stationary, the individual molecules continue rotating, in the aligning behavior at high shear rates. However, the rotation of the individual molecules is suppressed in the aligning behavior at low shear rates, since the torque on the molecules by the magnetic field overcomes the torque by the flow. The behaviors of S reflect the behaviors of ϕ_m, and the steady value of S for $H_x^*=1.8\times10^{-6}$ is slightly higher than that at the equilibrium state. Figures 2.3 show the time evolutions of the major orientation angle ϕ_m and scalar order parameter S for $\dot{\gamma}^*$=4 and H_x^*=0, 1×10^{-6}, and 1.8×10^{-6}. For H_x^*=0, the system exhibits the wagging behavior. As the magnetic field is imposed, for $H_x^*=1\times10^{-6}$, the period and the amplitude of the oscillatory behavior of ϕ_m increase. Similar to the case for $\dot{\gamma}^*$=2, the system shows the new aligning behavior above a

certain critical H_x*. Figures 2.4 are the time evolutions of the major orientation angle ϕ_m and scalar order parameter S for $\dot{\gamma}^*$=10, at which the system shows the aligning behavior at no magnetic field. The damping behaviors of ϕ_m and S can be seen for all values of H_x* and only the ordinary aligning behaviors are found. The steady values of ϕ_m decrease and the steady values of S increase with increasing H_x*.

To analyze the influence of H_x^* on the scalar order parameter, the time-averaged scalar order parameter $\bar{S}$ as a function of H_x^* is shown in Figure 2.5. For $\dot{\gamma}^*$=10 and 50, S increases slightly in this magnetic field strength range. However, for $\dot{\gamma}^*$=2 and 4, S increases drastically with increasing H_x^*, since the effect of the magnetic field can easily over the shear flow effect. Figure 2.6 shows the effect of the shear rate $\dot{\gamma}^*$ on the time-averaged scalar order parameter $\bar{S}$ for H_x^*=0, 1×10^{-6}, 1.6×10^{-6}, and 1.8×10^{-6}. For H_x^*=0, $\bar{S}$ decreases continuously toward the minimum value at $\dot{\gamma}^*\approx$4.7, and then increases monotonically as the shear rate increases. This tendency in $\bar{S}$ does not change for $H_x^*=1\times10^{-6}$ and 1.6×10^{-6}. However, for $H_x^*=1.8\times10^{-6}$, a discontinuous decrease in $\bar{S}$ is found at $\dot{\gamma}^*\approx$5.2, where the flow-orientation mode transition from the new aligning mode to the ordinary aligning mode arises.

Next, we discuss about the effect of the magnetic field on the flow-orientation mode transition. Figure 2.7 represents a flow-orientation mode diagram spanned by the shear rate $\dot{\gamma}^*$ and the magnetic field strength H_x^*. For the case that only the shear flow is applied to the system (i.e., H_x^*=0), the tumbling, wagging, and aligning modes appear depending on the shear rate. At $H_x^*=1\times10^{-6}$, the new aligning mode regime emerges at low shear rate. This new aligning mode regime spreads toward the higher shear rate with the increase of H_x^*, and takes over whole the tumbling regime at $H_x^*=1.4\times10^{-6}$. The wagging mode regime also disappears, when H_x^* is increased up to 1.8×10^{-6}. A dashed line at $H_x^*=1.8\times10^{-6}$ represents the mode transition shear rate between the new aligning mode and the ordinary aligning mode, and corresponds to the discontinuous decrease in $\bar{S}$ in Figure 2.6. It is expected that his transition shear rate becomes higher if H_x^* is increased further more.

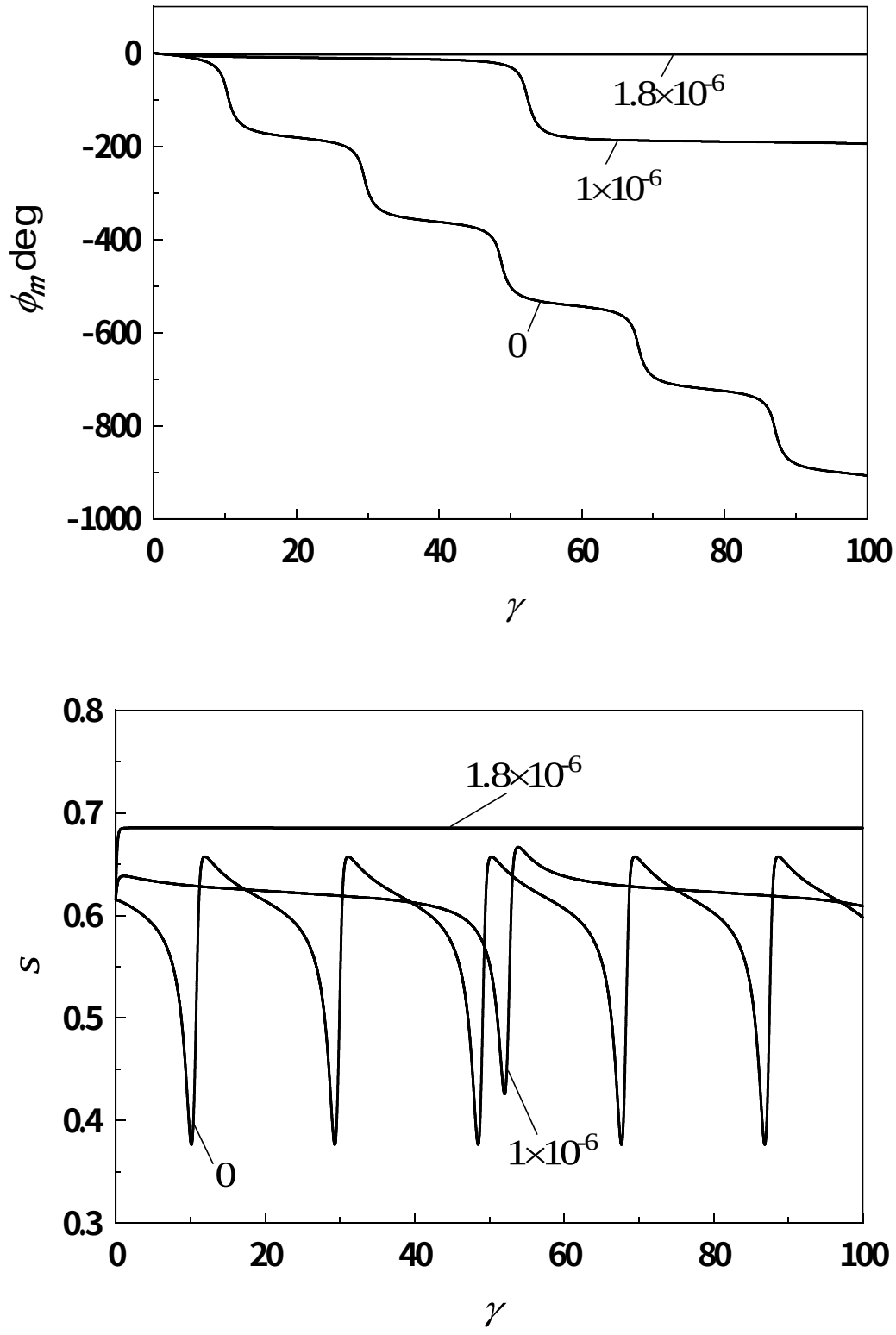

Figures 2.2 Transient behaviors of preferred angle ϕ_m and scalar order parameter S versus strain same with the dimensionless time at a given dimensionless shear rate: $\dot{\gamma}^*=2$ for various values of dimensionless magnetic field: $H_x^*=0$, 1×10^{-6}, and 1.8×10^{-6}at $\beta=1.0$.

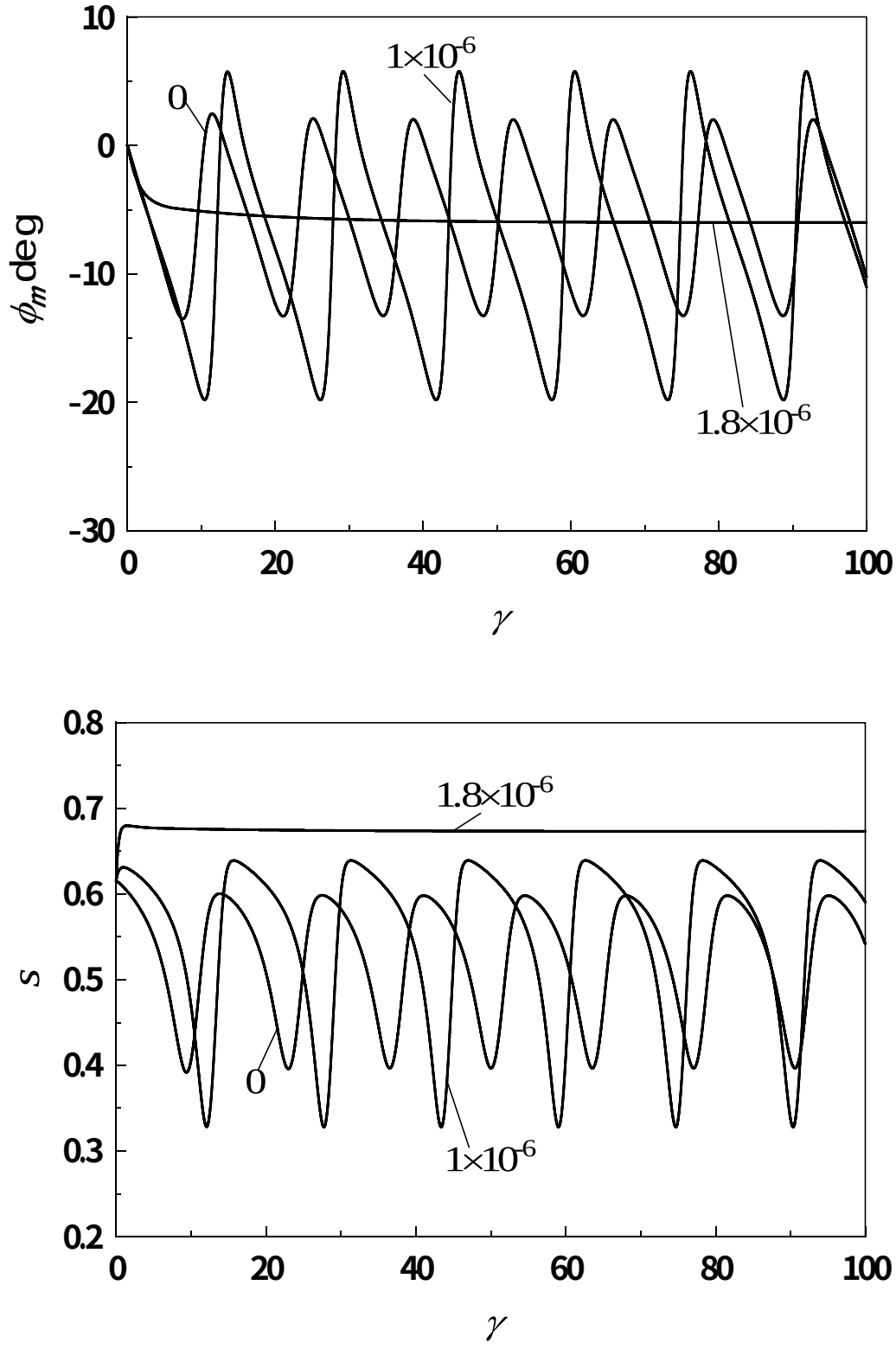

Figures 2.3 Transient behaviors of ϕ_m and S versus strain at $\dot{\gamma}^*$=4 for various values of H_x^*: H_x^*=0, 1×10^{-6}, and 1.8×10^{-6} at β=1.0.

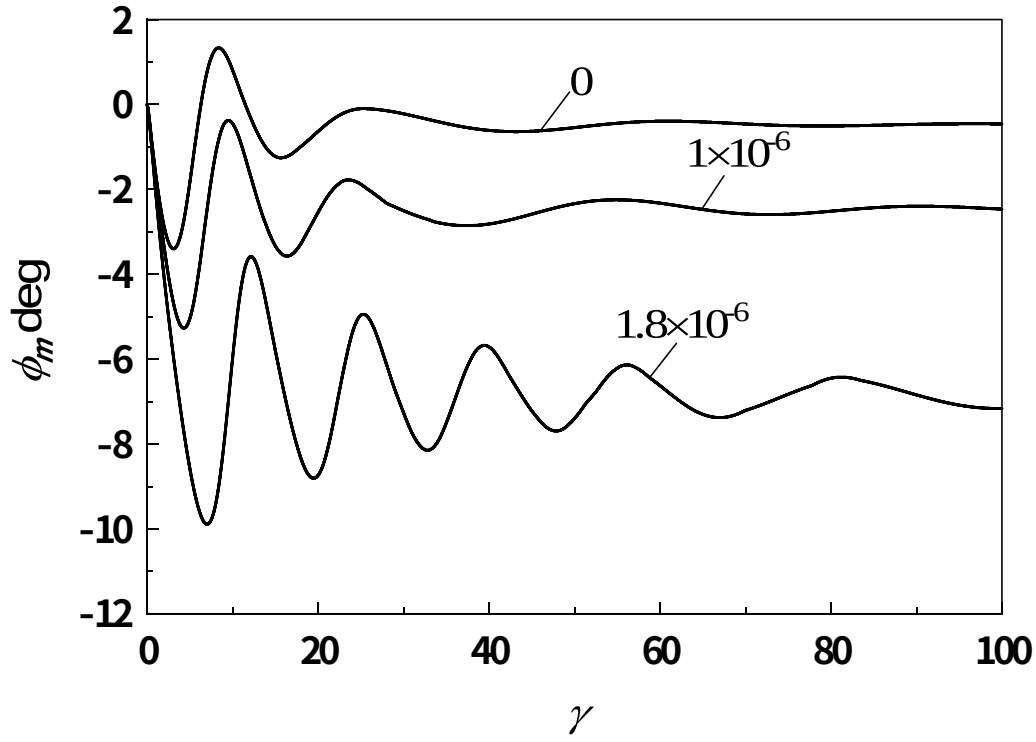

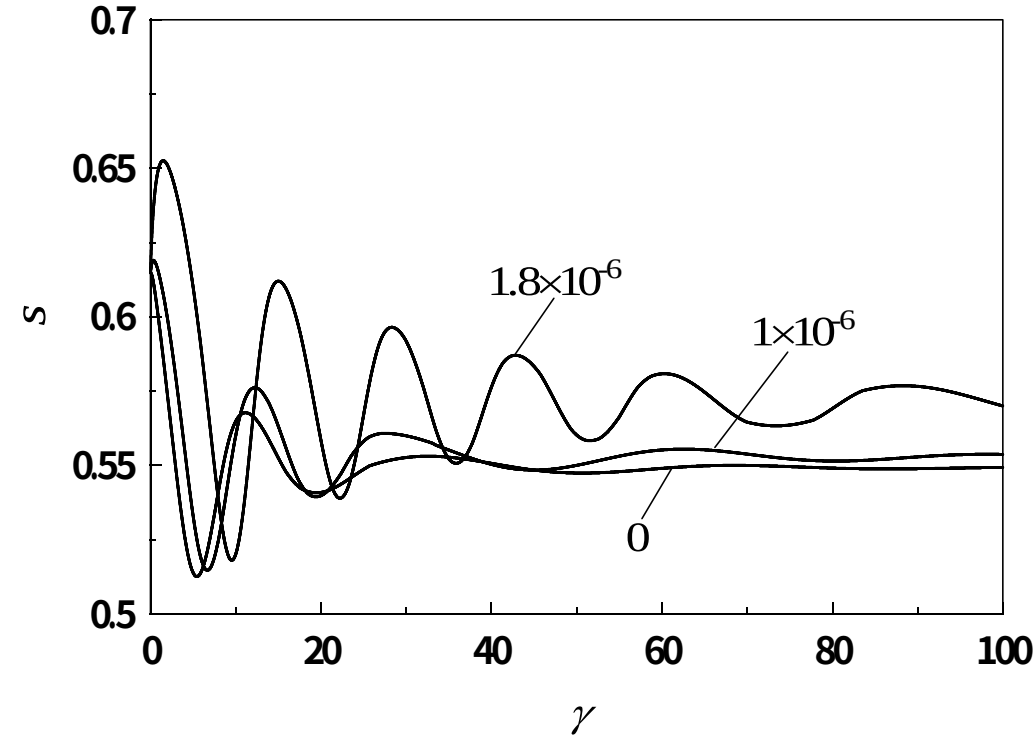

Figures 2.4 Transient behaviors of ϕ_m and S versus strain at $\dot{\gamma}^*$=10 for various values of H_x^*: H_x^*=0, 1×10^{-6}, and 1.8×10^{-6} at β=1.0.

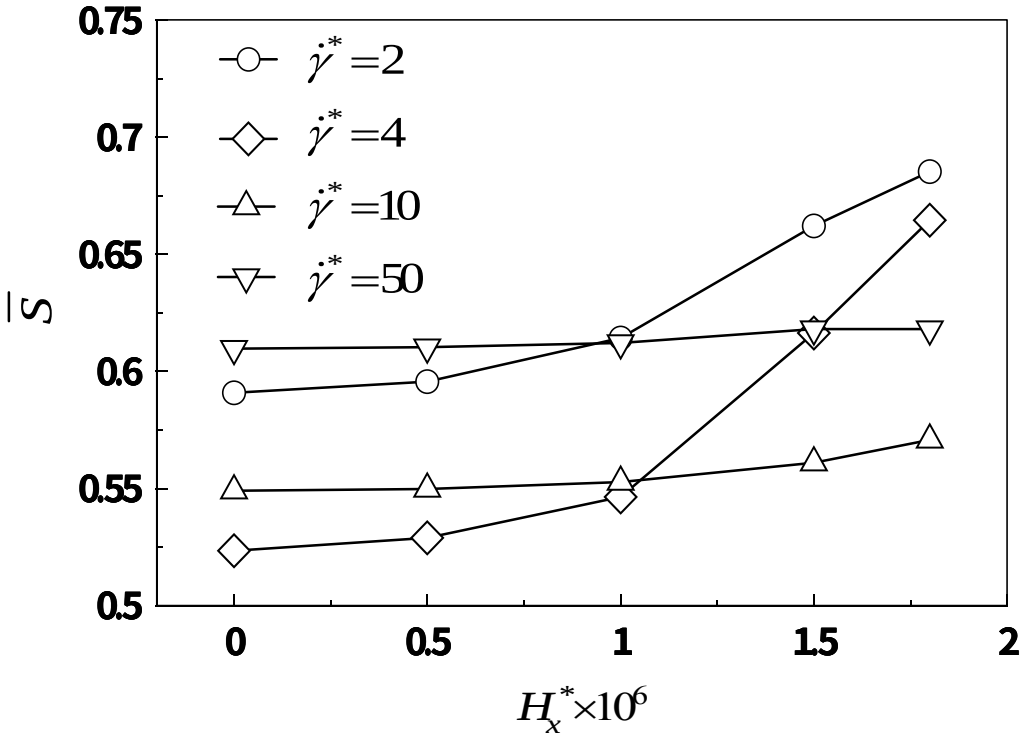

Figure 2.5 Effect of magnetic field parallel to the *x*-axis on average scalar order parameter $\bar{S}$ for various values of shear rates: $\dot{\gamma}^*$=2, 4, 10, and 50 at β=1.0.

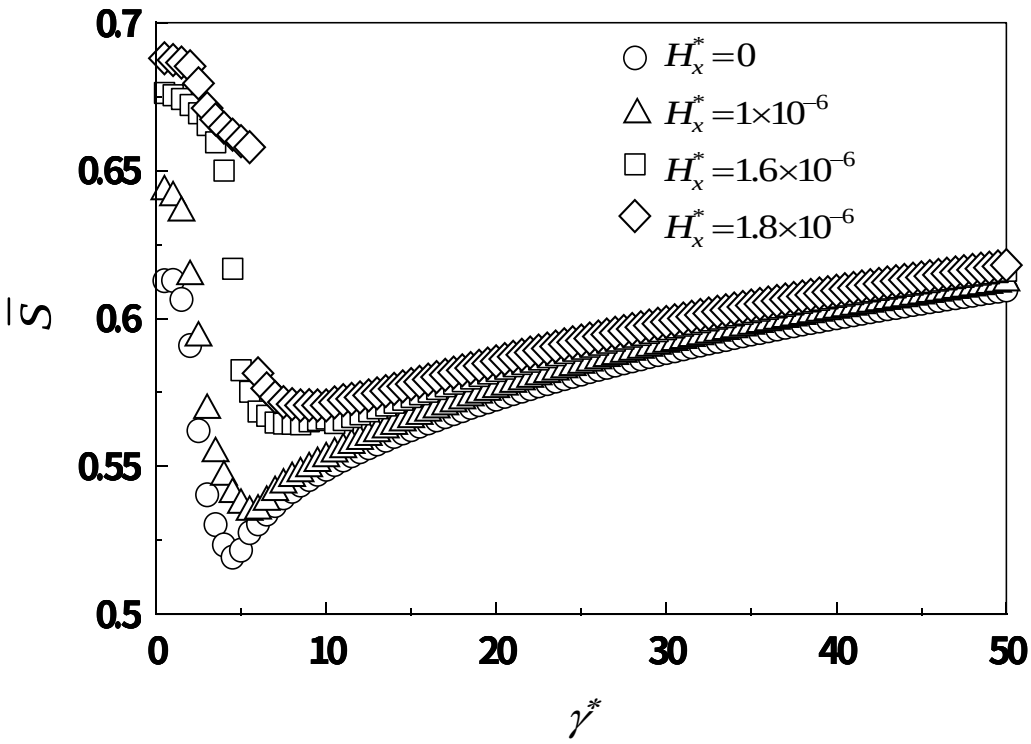

Figure 2.6 Average order parameter $\bar{S}$ as a function of shear rate $\dot{\gamma}^*$ at H_x^*=0, 1×10^{-6}, 1.6×10^{-6}, and 1.8×10^{-6} at β=1.0.

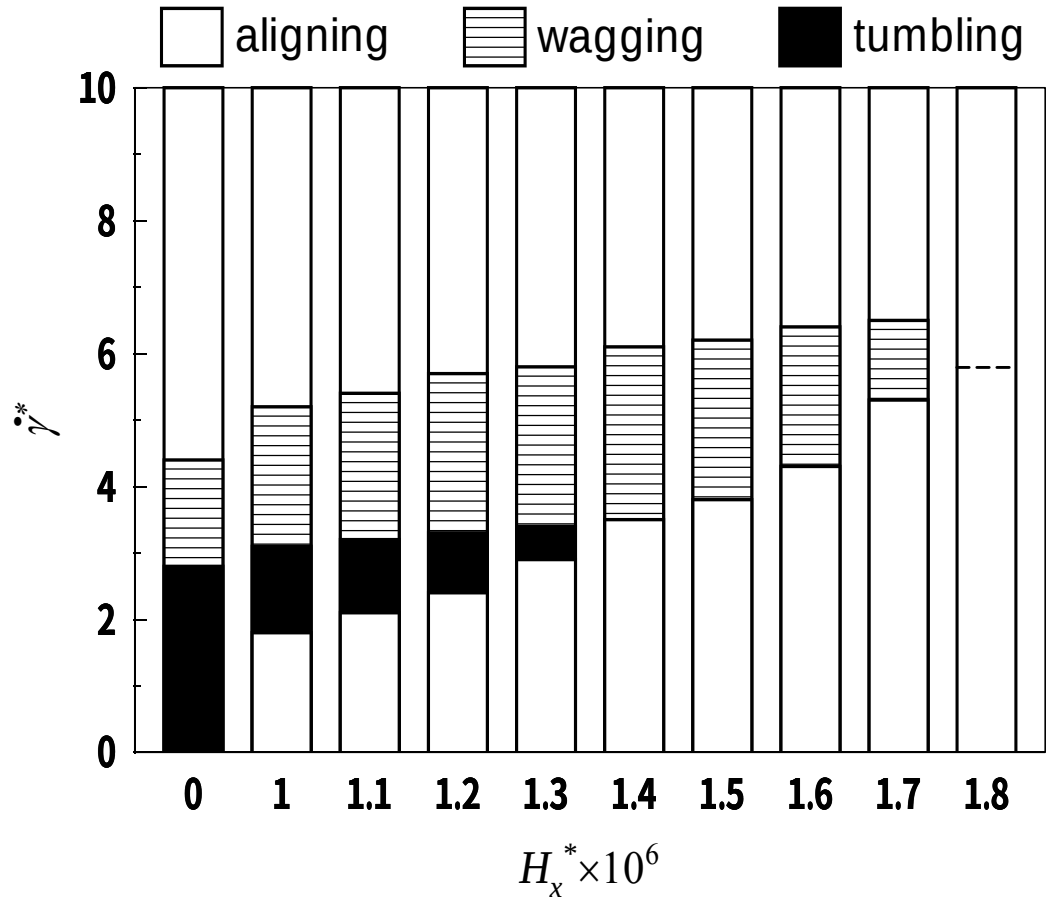

Figure 2.7 Critical shear rates as a function of magnetic field along the *x* direction at β=1.0.

2.3.1.2 The Magnetic Field along the *y*-axis

In this section, the case that the magnetic field is imposed parallel to the velocity gradient direction is considered. Figures 2.8 show the time evolutions of the major orientation angle ϕ_m and the scalar order parameter S for $\dot{\gamma}^*$=2 and H_y^*=0, 1×10^{-6}, and 1.8×10^{-6}. Behaviors of ϕ_m and S for H_y^*=0 and 1×10^{-6} are similar to those shown in Figure 2.2 in the case of the magnetic field along *x*-axis, but the results for $H_y^*=1.8\times10^{-6}$ are somewhat different from the results in Figure 2.2 for $H_x^*=1.8\times10^{-6}$. The major orientation angle ϕ_m decreases at first and then increases to a steady value. It should be noticed that the steady direction of the major molecular orientation is not parallel to *y*-axis. Figure 2.9 shows the torques exerted on a LCP molecule. The torque on a LCP molecule by the shear flow becomes the minimum when the molecules are along the flow direction, while the magnetic field tends to align the molecules along the velocity gradient direction. The major orientation angles at steady states are determined as a result of the competition between the torques by the shear flow and the magnetic field.

Figures 2.10 are the time evolutions of ϕ_m and S for $\dot{\gamma}^*$=4 and H_y^*=0, 1.4×10^{-6}, and 1.8×10^{-6}. The behaviors of S and ϕ_m exhibit same tendency as those shown in Figures 3, except for $H_y^*=1.8\times10^{-6}$. The steady state value of $\phi_m\approx$30deg obtained for $H_y^*=1.8\times10^{-6}$ is also the result of the competition discussed above. Figures 2.11 represent the time evolutions of ϕ_m and S for $\dot{\gamma}^*$=10 and H_y^*=0, 1×10^{-6}, and 1.8×10^{-6}. Within the magnetic field strength region used here, all the results look like the ordinary aligning state. However, as shown in Figure 2.12, a discontinuous decrease in the time-averaged scalar order parameter $\bar{S}$ exists for $H_y^*=1.6\times10^{-6}$, and corresponds to the transition shear rate between the ordinary and the new aligning modes as mentioned above. The effect of the magnetic field strength H_y^* on the steady major orientation angle ϕ_m^{steady} is shown in Figure 2.13 for $\dot{\gamma}^*$=2, 4, and 10. The angles ϕ_m^{steady} increase with increasing the magnetic field strength H_y^*. Finally, a flow-orientation mode diagram spanned by the shear rate $\dot{\gamma}^*$ and the magnetic field strength H_y^* is shown in Figure 2.14. As the magnetic field strength increases, the new aligning mode emerges at low shear rate, and then it covers whole the tumbling mode regime, similar to the diagram for the case of the magnetic field along the *x*-axis (Figure 2.7). On the other hand, the wagging-ordinary aligning mode transition shear rate in Figure 2.14 decreases with increase of the magnetic field strength, while that shear rate in Figure 2.7 increases.

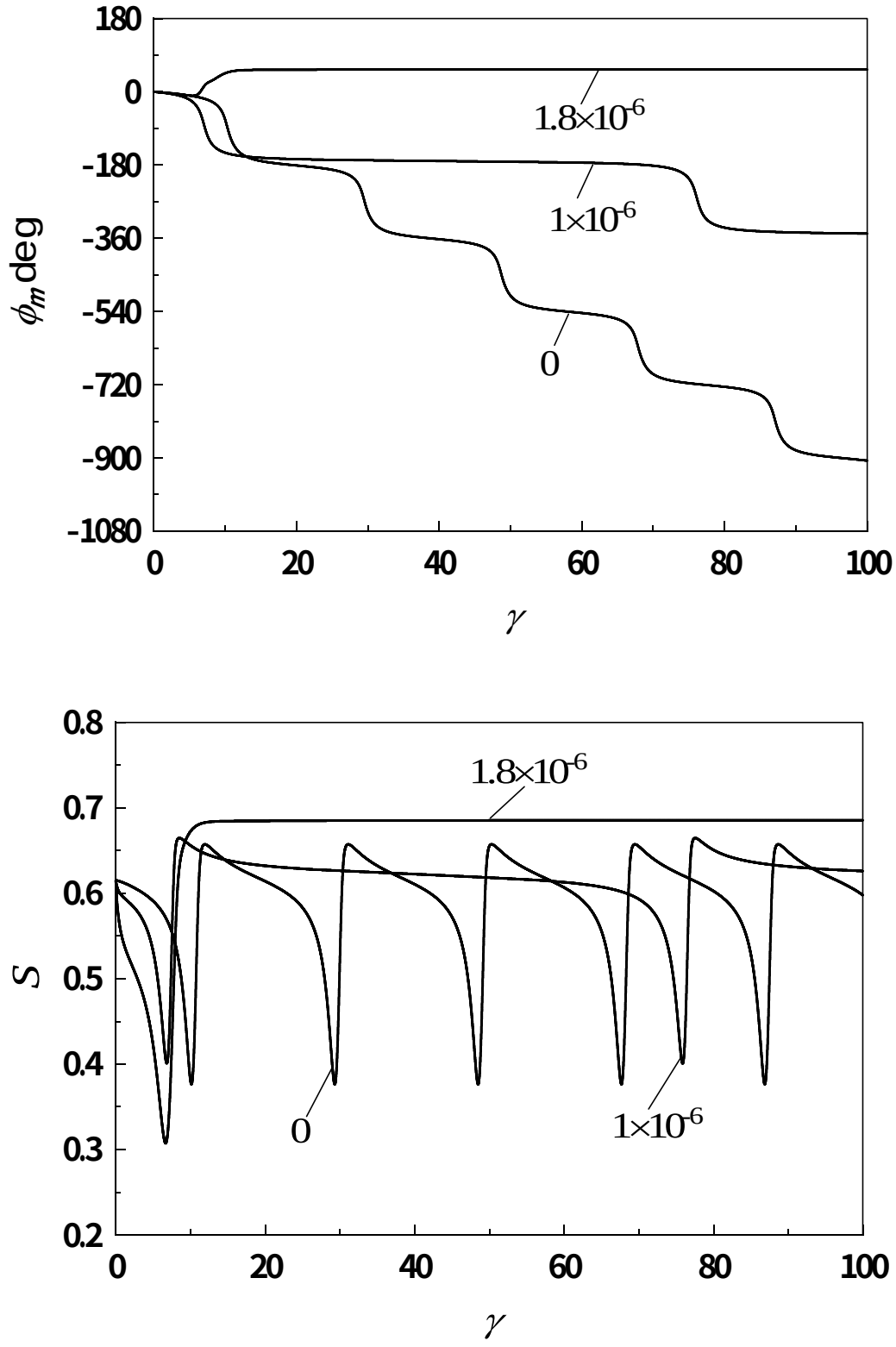

Figures 2.8 Transient behaviors of ϕ_m and S versus strain at $\dot{\gamma}^*$=2 for various values of H_y^*: H_y^*=0, 1×10^{-6}, and 1.8×10^{-6} at β=1.0.

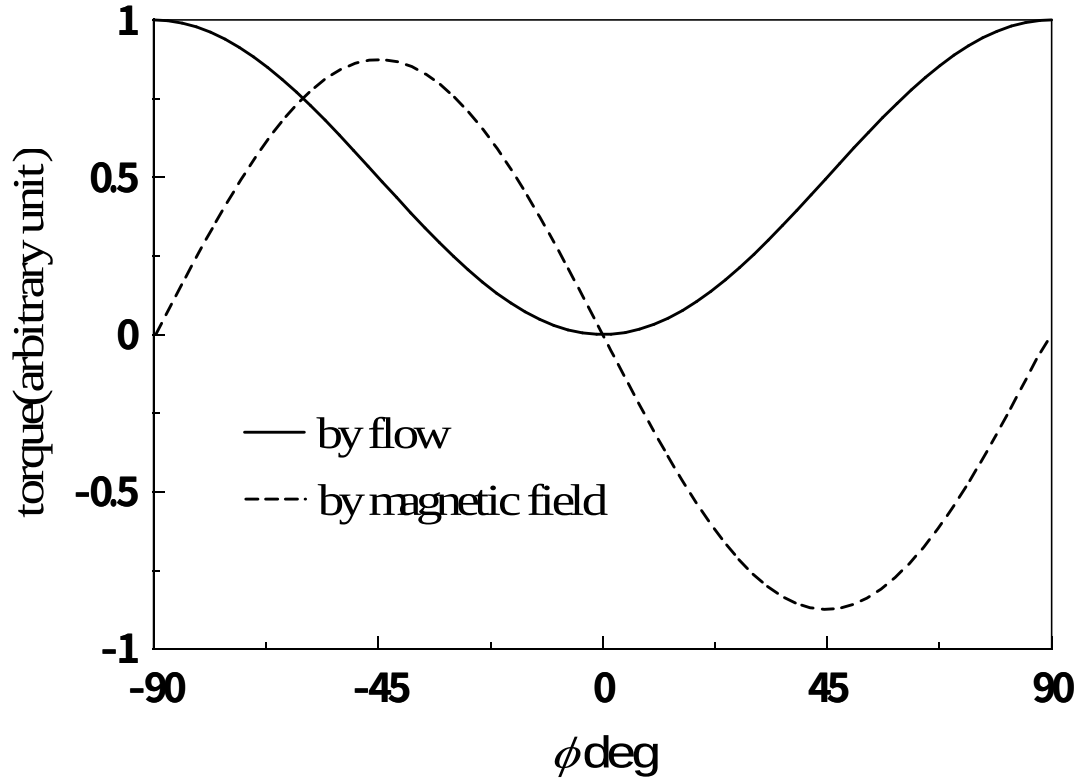

Figure 2.9 Torques (arbitrary unit) on a LCP molecule as a function of the azimuthal angle at β=1.0.

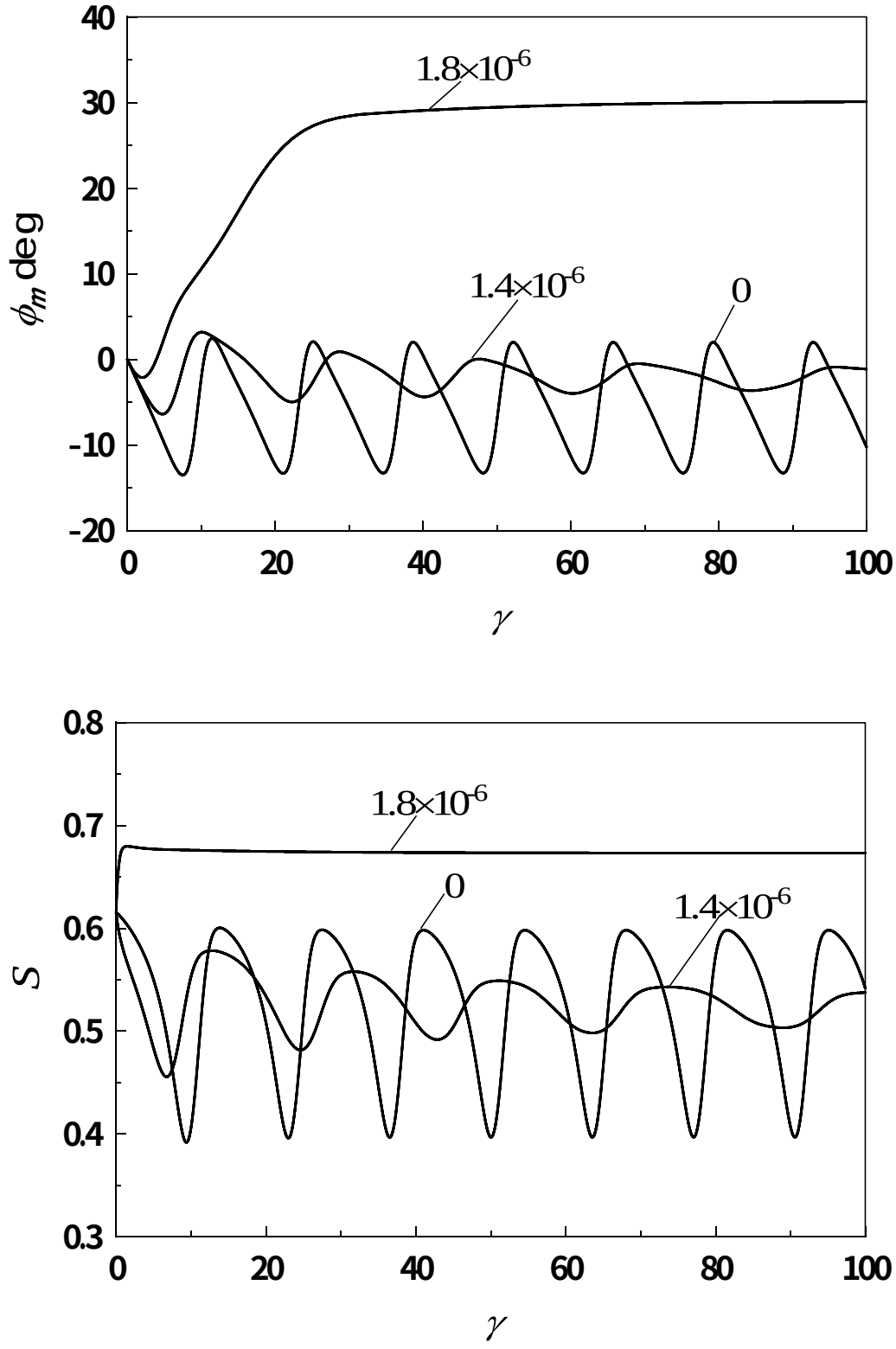

Figures 2.10 Transient behaviors of ϕ_m and S versus strain at $\dot{\gamma}^*$=4 for various values of H_y^*: H_y^*=0, 1.4×10^{-6}, and 1.8×10^{-6} at β=1.0.

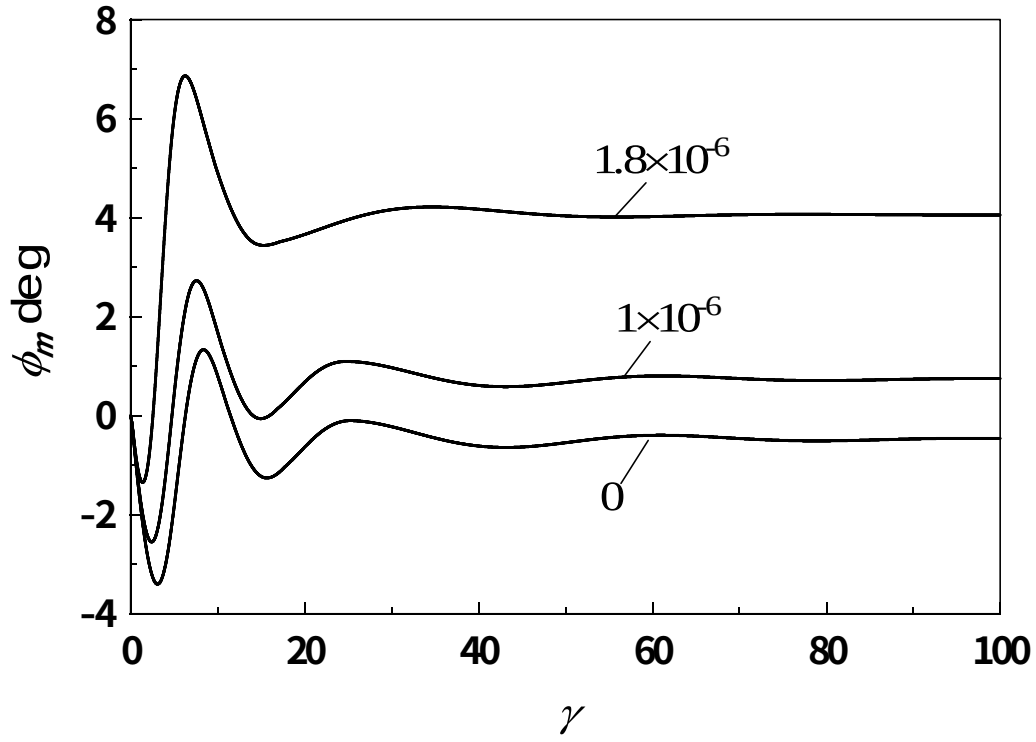

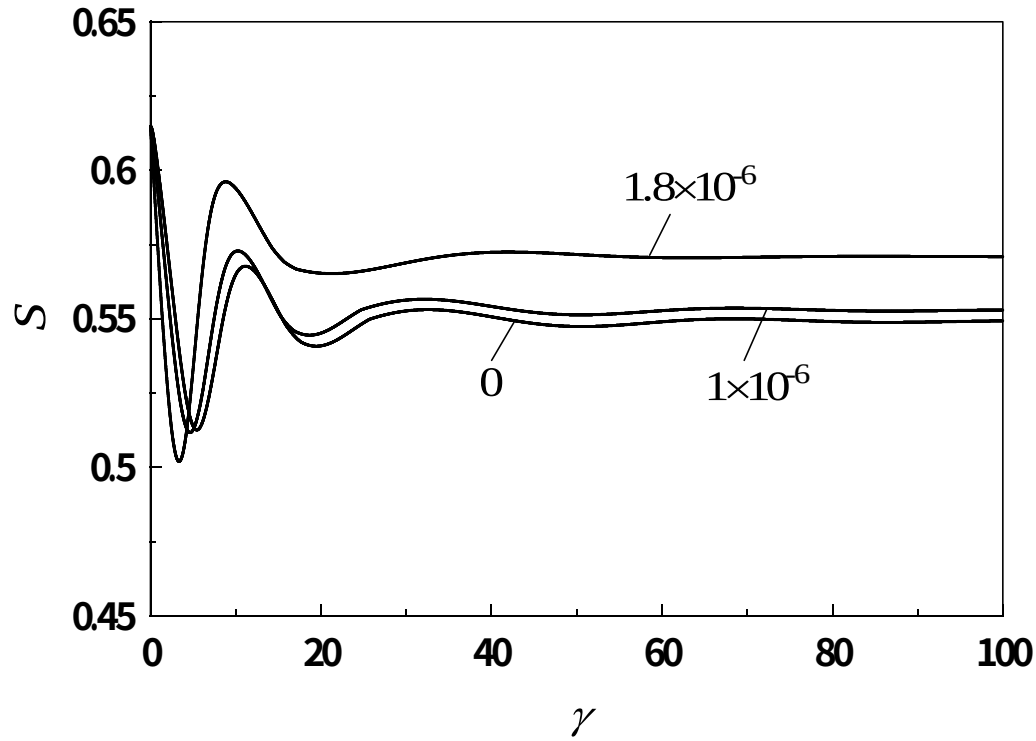

Figures 2.11 Transient behaviors of ϕ_m and S versus strain at $\dot{\gamma}^*$=10 for various values of H_y^*: H_y^*=0, 1×10^{-6}, and 1.8×10^{-6} at β=1.0.

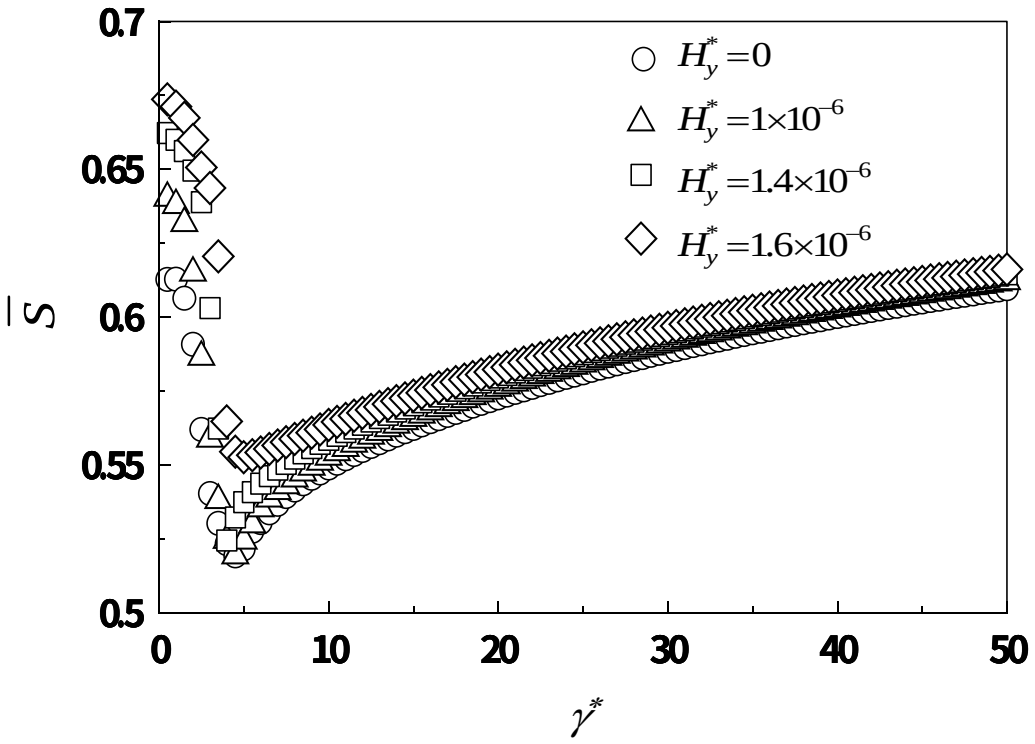

Figure 2.12 Average order parameter $\bar{S}$ as a function of shear rate $\dot{\gamma}^*$ at H_y^*=0, 1×10^{-6}, 1.4×10^{-6}, and 1.6×10^{-6} at β=1.0.

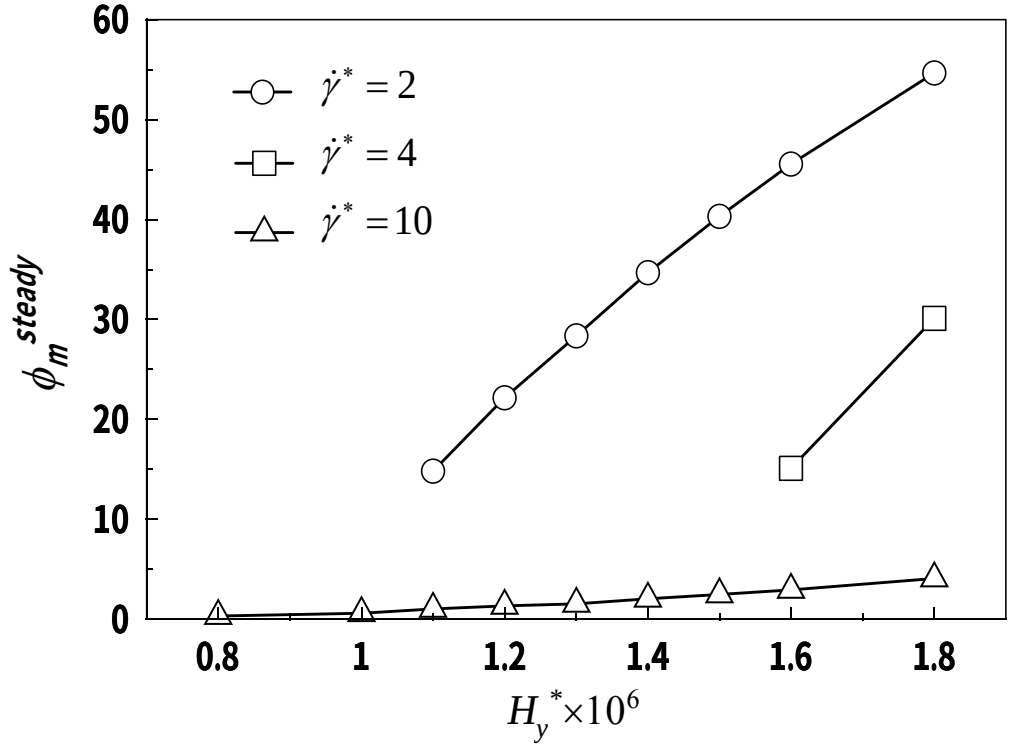

Figure 2.13 Effect of the magnetic field strength H_y^* on the steady major orientation angle ϕ_m^{steady} at β=1.0.

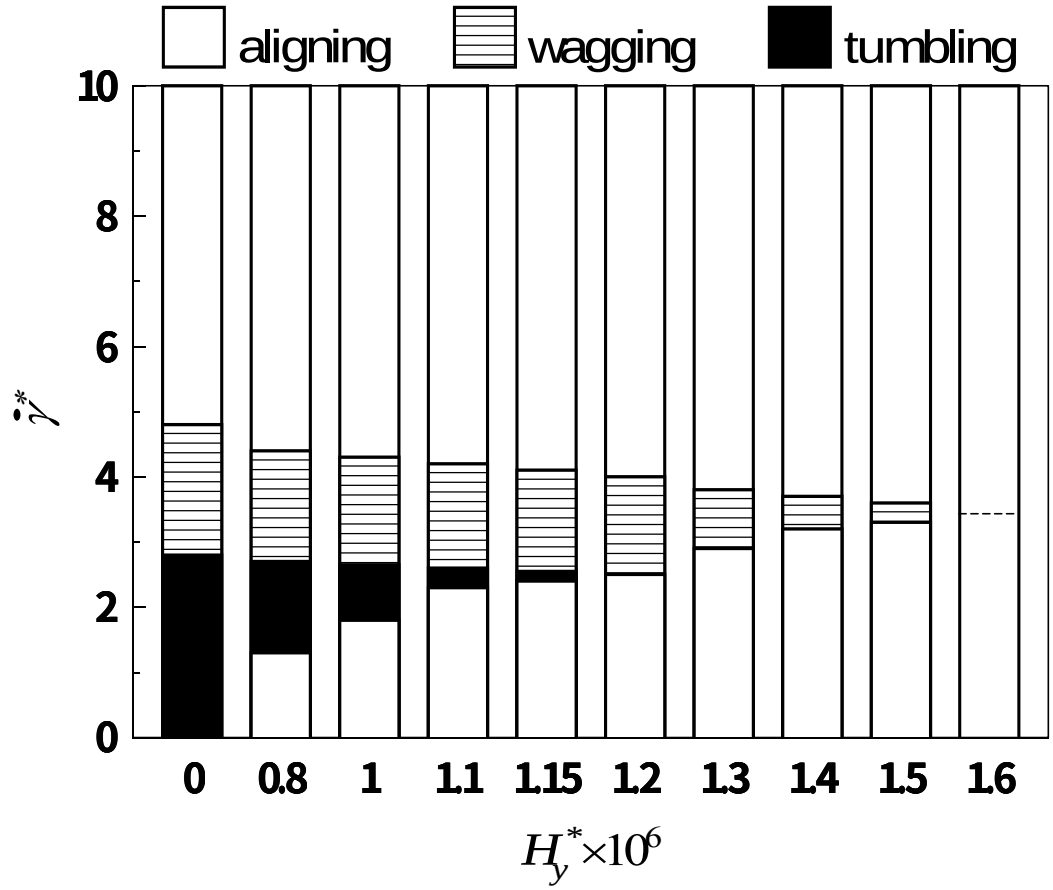

Figure 2.14 Critical shear rates as a function of magnetic field along the *y* direction at β=1.0.

2.3.2 Results and Discussions for β=0.9

In this part, the molecular length will be considered since the real molecules are not infinite. We choose β=0.9 in equation (2.1). With the relation (1.7), we can know the length is about 4.5 times to the diameter. In addition to the value of β, other parameters are same with the case when β=1.0. Also two cases are discussed: 1) the magnetic field along the *x*-axis, 2) the magnetic field parallel to the *y*-axis.

2.3.2.1 The Magnetic Field along the *x*-axis

Figures 2.15 show that the transient behaviors of preferred angle ϕ_m and scalar order parameter *S* versus strain at $\dot{\gamma}^*$=3 for various values of dimensionless magnetic field: H_x^*=0, 1.5×10^{-6}, and 2×10^{-6}. When H_x^*=0, the preferred angle monotonously decreases from 0^o, namely, tumbling modes are presented. As shown in Figures 2.15, the rotational periodic of the director increases with the increasing strength of the magnetic field. A new aligning mode also appears at $H_x^*=2\times10^{-6}$. The scalar order parameter *S* increases with the magnetic field. Increased the shear rate at 5, the director oscillates at a fixed angle when only the flow is added on the LCP system. With increasing the strength of the magnetic field the oscillation of the director becomes slow and finally at $H_x^*=2\times10^{-6}$ a steady state arrives, namely, the new aligning defined in the last part is detected. The higher orientational state can be arrived with increasing the strength of the magnetic field as shown in Figures 2.16. The ordinary aligning at H_x^*=0 is given out at $\dot{\gamma}^*$=20 in Figures 2.17. Even increasing the strength of the magnetic field in the range chose by this part the new aligning modes can not be found in the range of ordinary aligning. However, the scalar order parameter *S* also increases under the increasing magnetic field. From Figure 2.18, we also can get two groups that one is the new aligning at the low shear rates $\dot{\gamma}^*$=3, 5; another is the ordinary aligning represented at the high shear rates $\dot{\gamma}^*$=20, 50. Figure 2.19 describes the orientation distribution function versus the degree ϕ at $\dot{\gamma}^*$=3, 50. The orientatioal distribution function at $\dot{\gamma}^*$= 50 becomes wider than the one at $\dot{\gamma}^*$=3 and the peak of it shifts to the bigger degree. To analyze the influence of H_x^* on the scalar order parameter, the time-averaged scalar order parameter $\bar{S}$ as a function of H_x^* is shown in Figure 2.20. It is similar to Figure 2.7, at the low shear rates $\dot{\gamma}^*$=3, 5 the time-averaged scalar order parameter can be increased very quickly after a critical value of the magnetic filed; however, at the high shear rates $\dot{\gamma}^*$=20, 50, the $\bar{S}$ is increased slightly with the magnetic field. Figure 2.21 shows the effect of the shear rate $\dot{\gamma}^*$ on the time-averaged scalar order parameter $\bar{S}$ for

H_x^*=0, 1.5×10^{-6}, and 2×10^{-6}. The discontinuous happens at about $\dot{\gamma}^* \approx 5.4$ when $H_x^*=2\times10^{-6}$. As can be seen in Figure 2.22 where a flow-orientation mode diagram spanned by the shear rate $\dot{\gamma}^*$ and the magnetic field strength H_x^*, this discontinuous describes the boundary of the new aligning modes and the wagging modes. The range of tumbling is repressed and the new aligning modes appear at low shear rates.

Compared the simulation results obtained at β=1.0 the main difference resulting from the molecular length is that the wagging mode doesn't disappear, on the contrary, the range of it is enlarged with the increasing magnetic field strength represented in Figure 2.22.

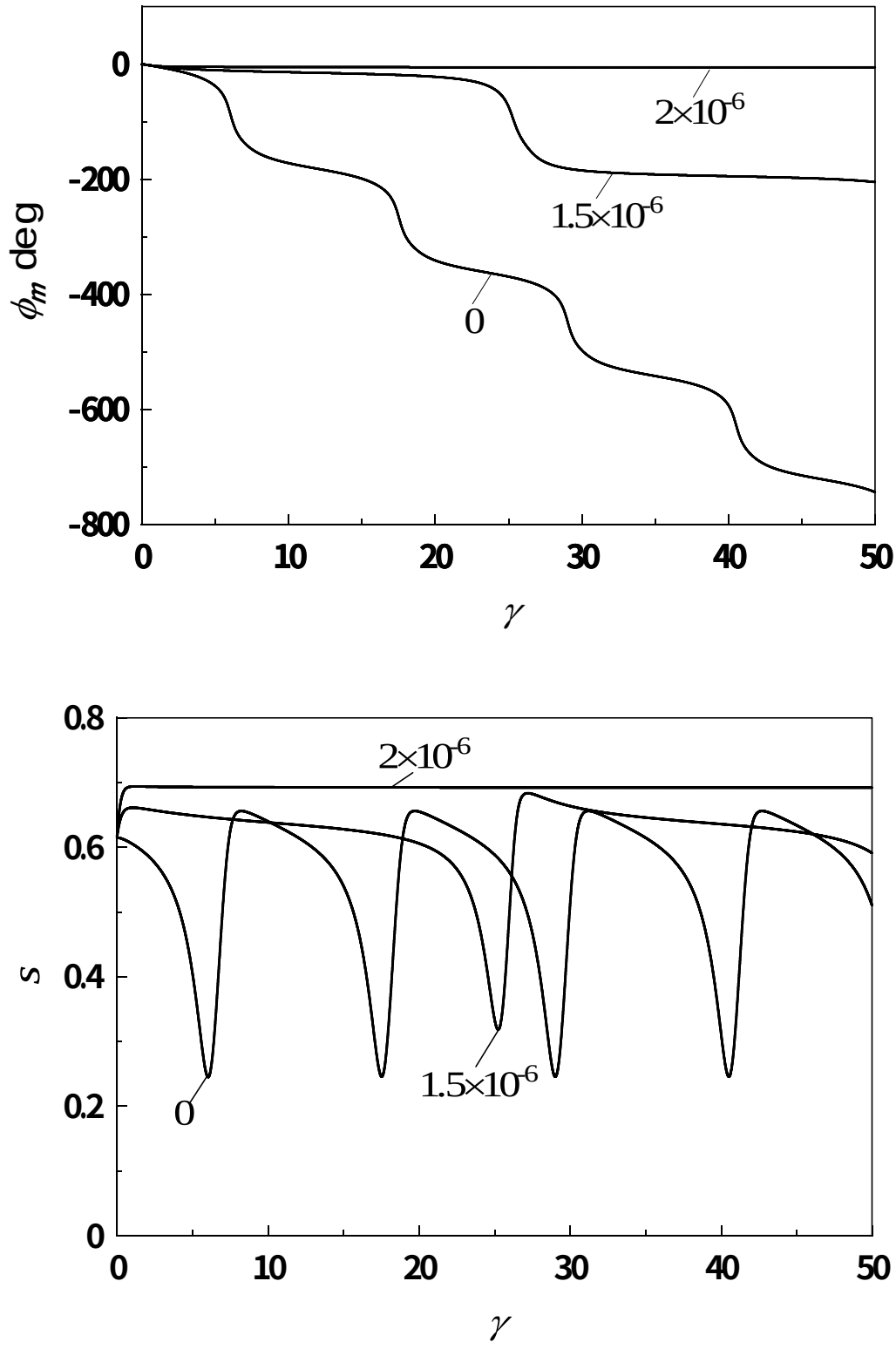

Figures 2.15 Transient behaviors of ϕ_m and S versus strain at $\dot{\gamma}^*$=3 for various values of H_x^*: H_x^*=0, 1.5×10^{-6}, and 2×10^{-6} at β=0.9.

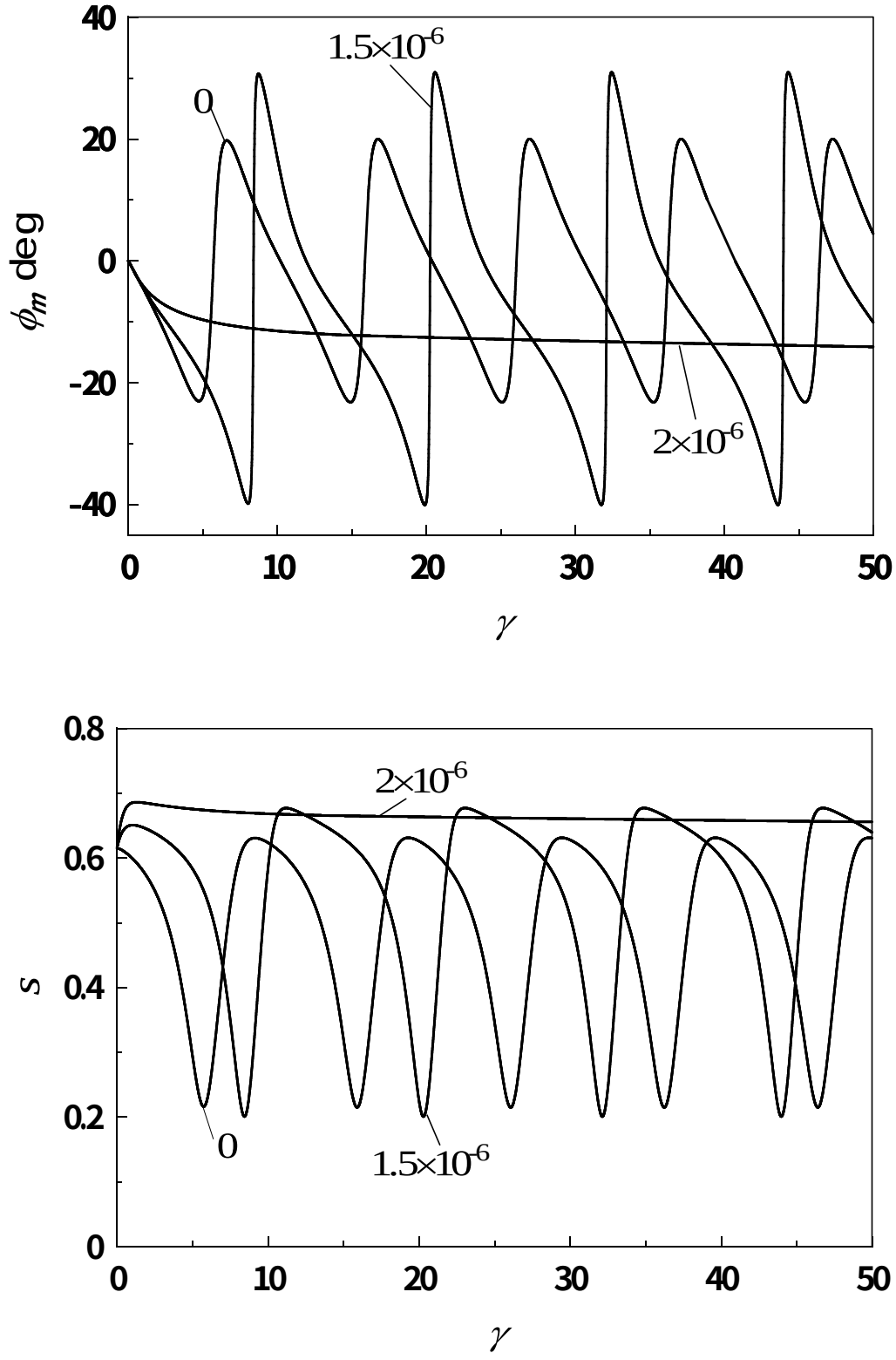

Figures 2.16 Transient behaviors of ϕ_m and S versus strain at $\dot{\gamma}^*$=5 for various values of H_x^*: H_x^*=0, 1.5×10^{-6}, and 2×10^{-6} at β=0.9.

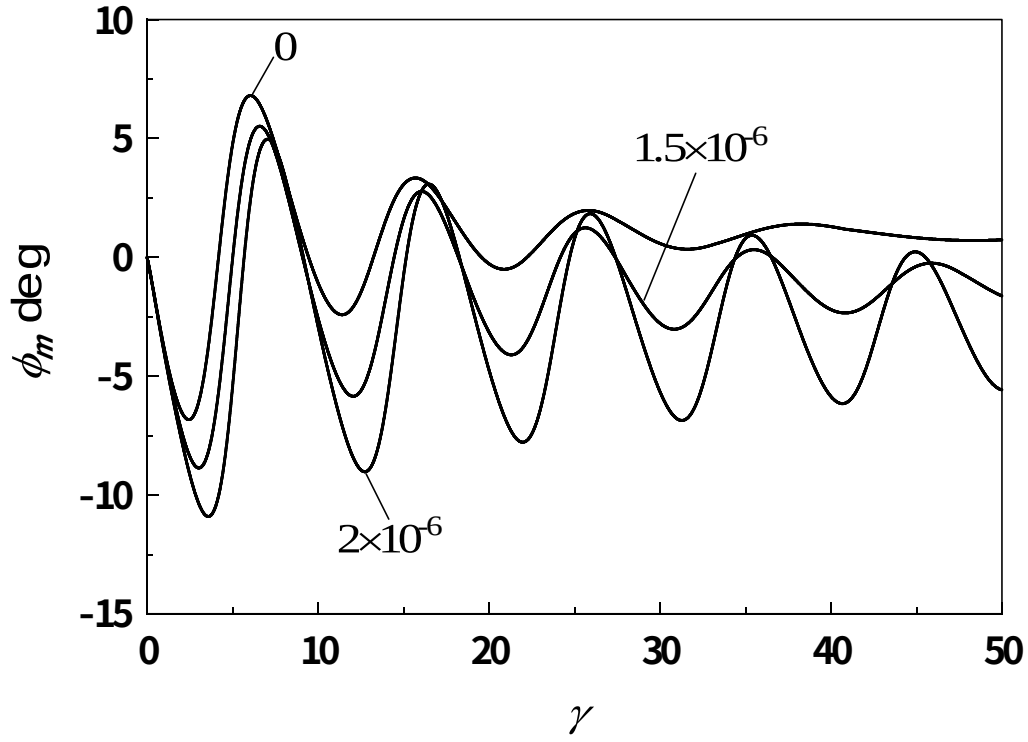

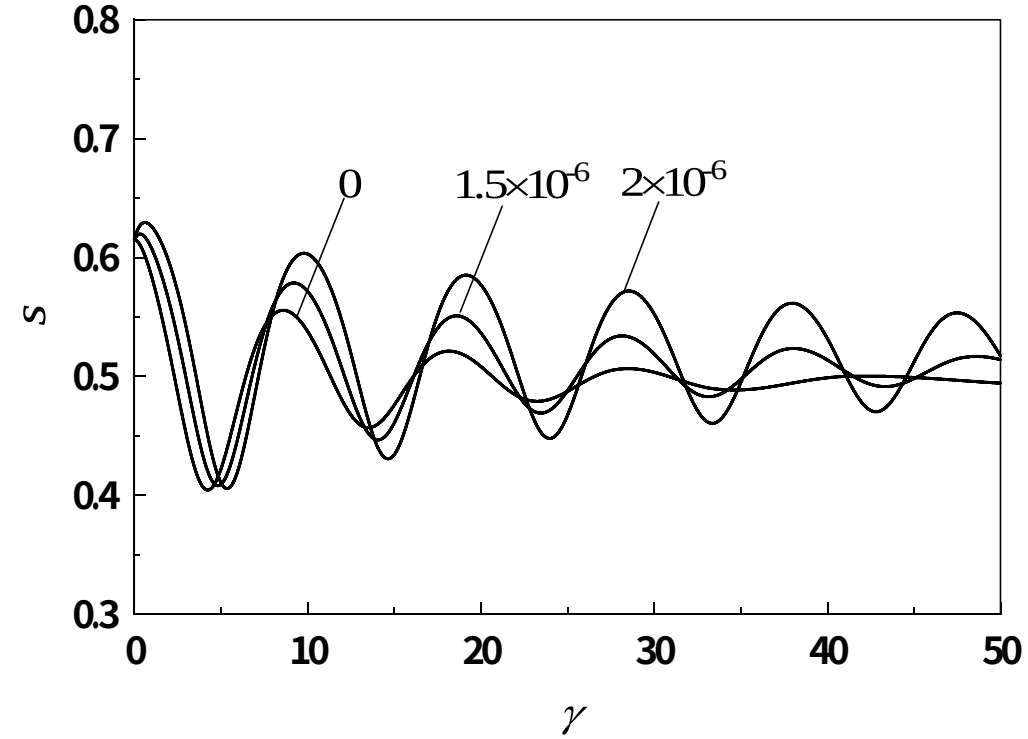

Figures 2.17 Transient behaviors of ϕ_m and S versus strain at $\dot{\gamma}^*$=20 for various values of H_x^*: H_x^*=0, 1.5×10^{-6}, and 2×10^{-6} at β=0.9.

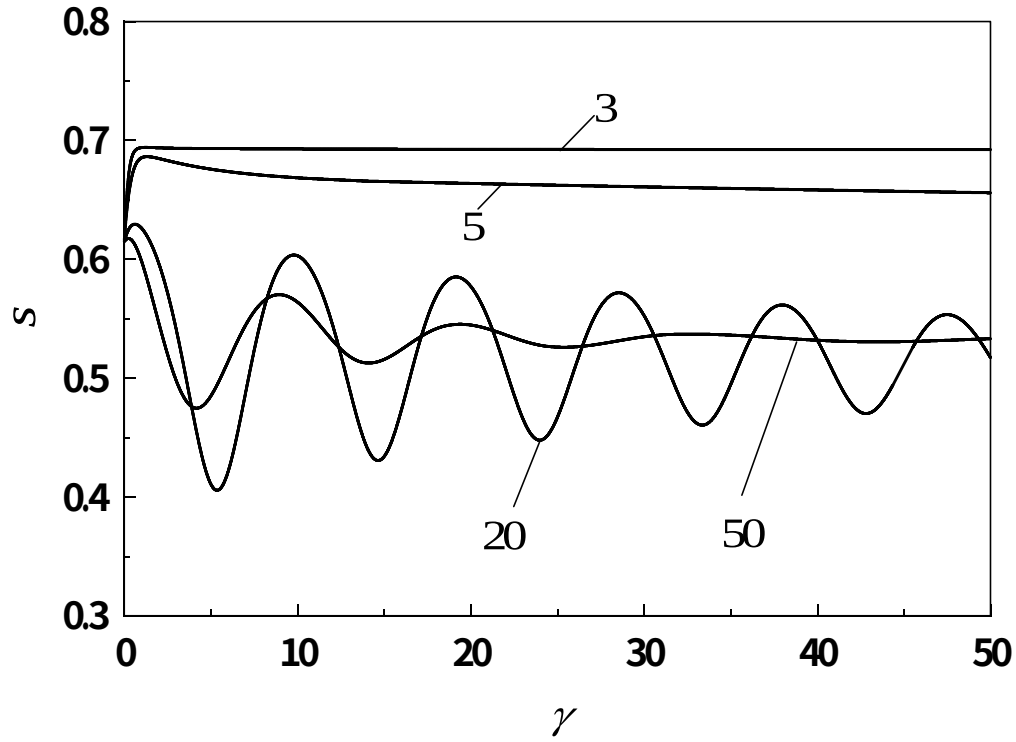

Figure 2.18 Transient behavior of order parameter S at $\dot{\gamma}^*$=3, 5, 20, 50 for H_x^*=2×10^{-6} at β=0.9.

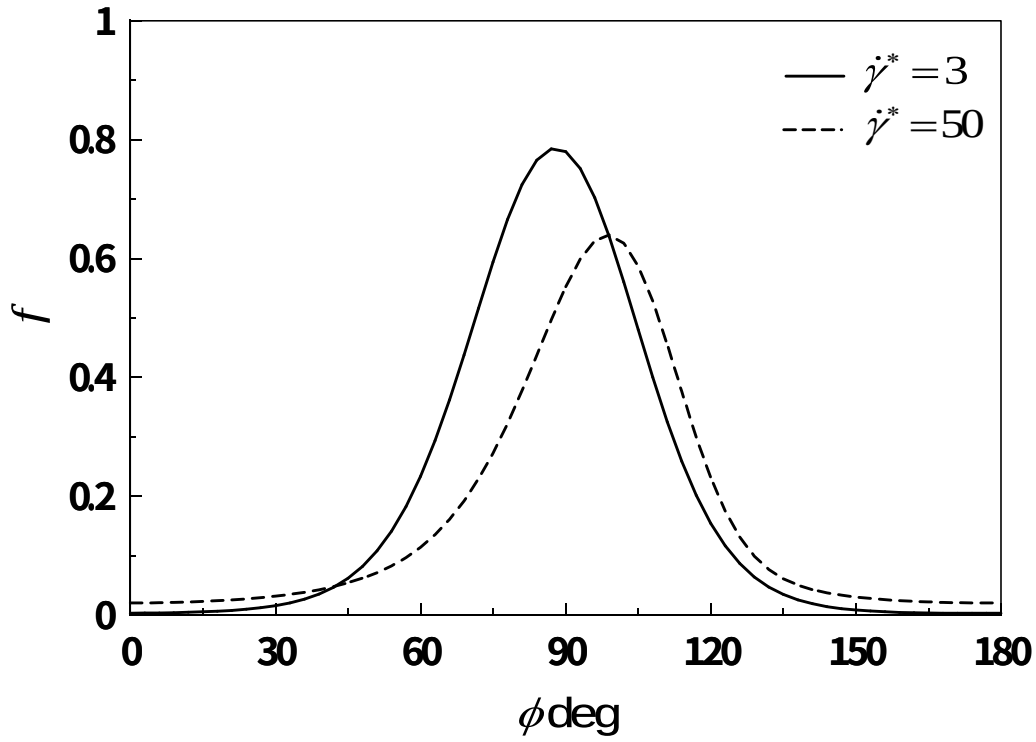

Figure 2.19 Orientation distribution function versus the degree ϕ at $\dot{\gamma}^*$=3, 50 at β=0.9.

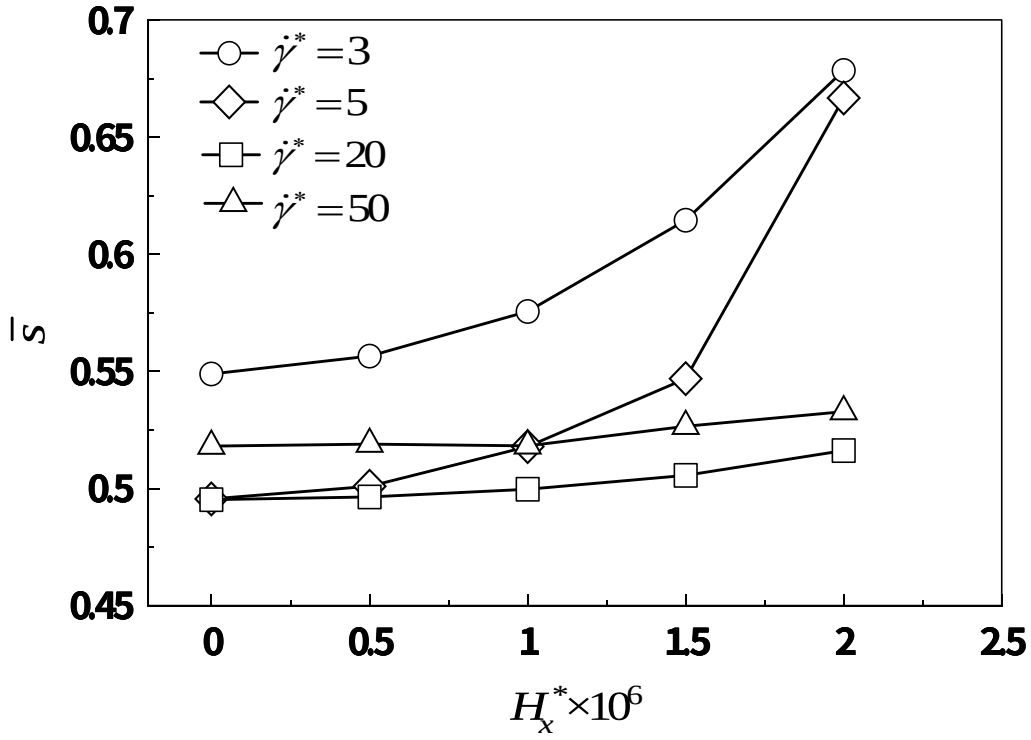

Figure 2.20 Effect of magnetic field parallel to the *x* direction on average scalar order parameter $\bar{S}$ for various values of shear rates: $\dot{\gamma}^*$=3, 5, 20, and 50 at β=0.9.

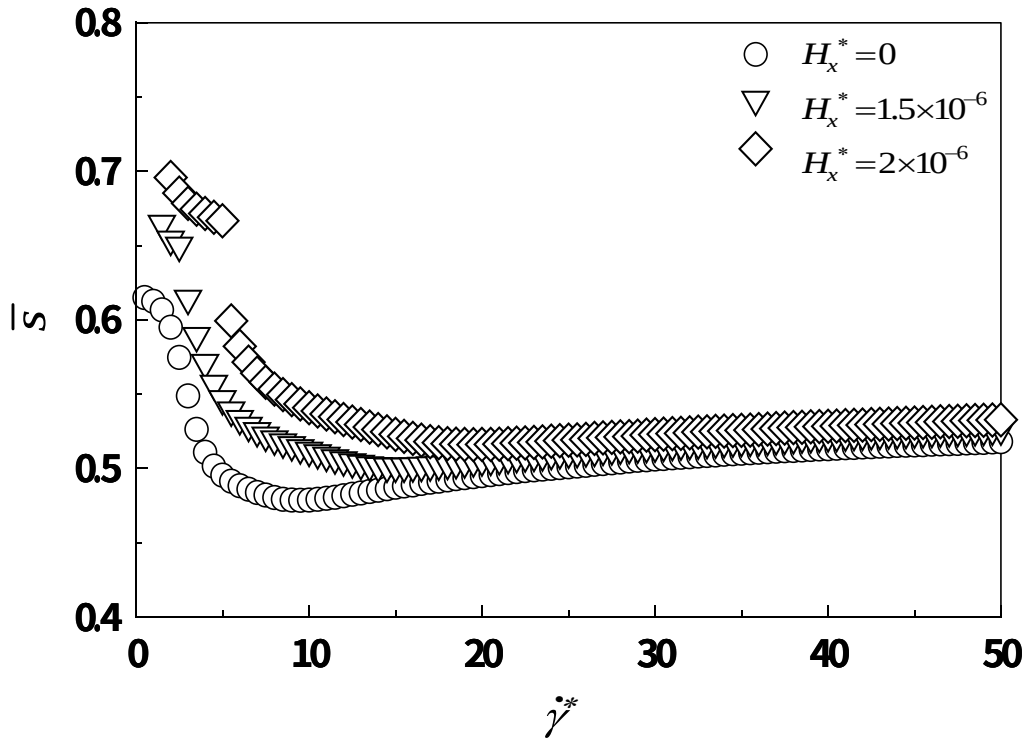

Figure 2.21 Average order parameter $\bar{S}$ as a function of shear rate $\dot{\gamma}^*$ at H_x^*=0, 1.5×10^{-6}, and 2×10^{-6} at β=0.9.

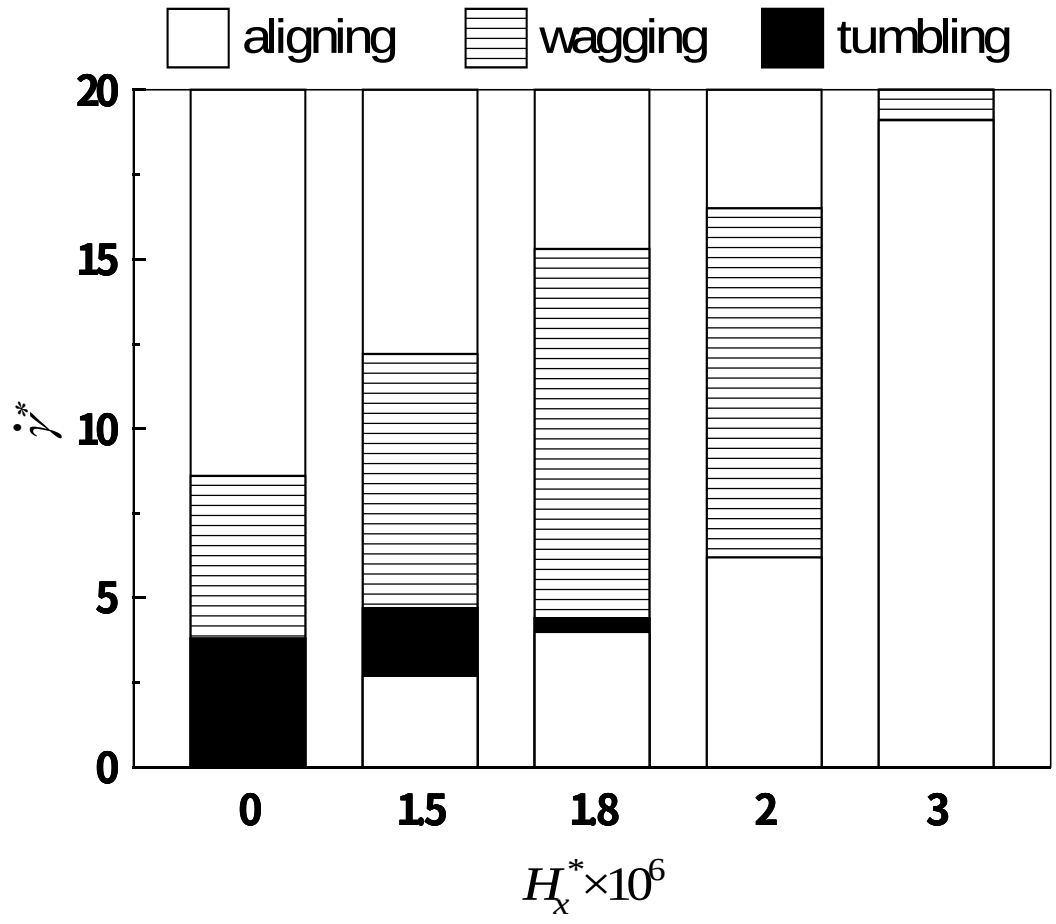

Figure 2.22 Critical shear rates as a function of magnetic field along the *x* direction at β=0.9.

2.3.2.2 The Magnetic Field along the *y*-axis

As we can see from Figures 2.23 to 2.26 the results for the magnetic field along the *y*-axis are almost same with the simulation results shown in the part 2.3.1.1when β=1.0. Also two groups can be defined from Figure 2.26, which are the new aligning with higher orientation states at low shear rates defined in the last section and the ordinary aligning at high shear rates. Figure 2.27 shows that the orientation distribution function changes with the degree ϕ. When the shear rate decreases the peak of the orientation distribution function obviously shifts to the right and becomes much sharper than the one at high shear rate $\dot{\gamma}^*$=50. In Figure 2.28 the effect of the shear rate on the time-averaged scalar order parameter $\bar{S}$ is represented at H_y^*=0, 1.5×10^{-6}, and 2.0×10^{-6}. It can be seen that the higher orientational state can be got at low shear rates resulting from the comparison between the torques caused by the shear flow and the magnetic field. A discontinuous decrease, corresponding to the boundary between the ordinary and new aligning, also appears at $\dot{\gamma}^* \approx 5.0$ in Figure 2.29 which shows the effect of the magnetic field on the time-averaged scalar parameter $\bar{S}$. A flow-orientation mode diagram spanned by the shear rate $\dot{\gamma}^*$ and the magnetic field strength H_y^* also is plot in Figure 2.30. The new aligning range also can be observed at low shear rates, however, the range of the wagging mode will be reduced with the magnetic field, and finally disappears at $H_y^*=2.0\times10^{-6}$. The dot line means the boundary between the ordinary and new aligning modes.

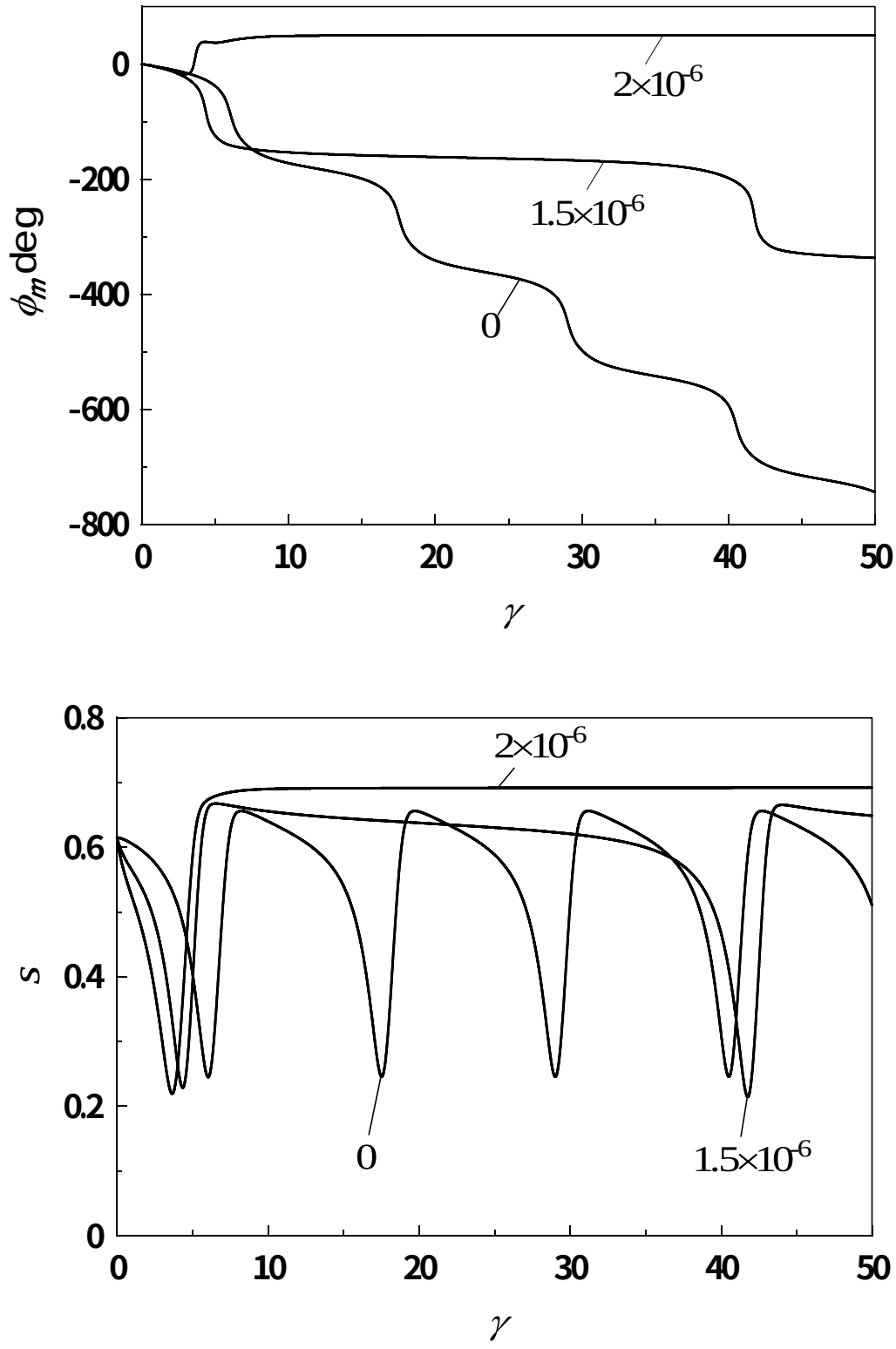

Figures 2.23 Transient behaviors of ϕ_m and S versus strain at $\dot{\gamma}^*$=3 for various values of H_y^*: H_y^*=0, 1.5×10^{-6}, and 2×10^{-6} at β=0.9.

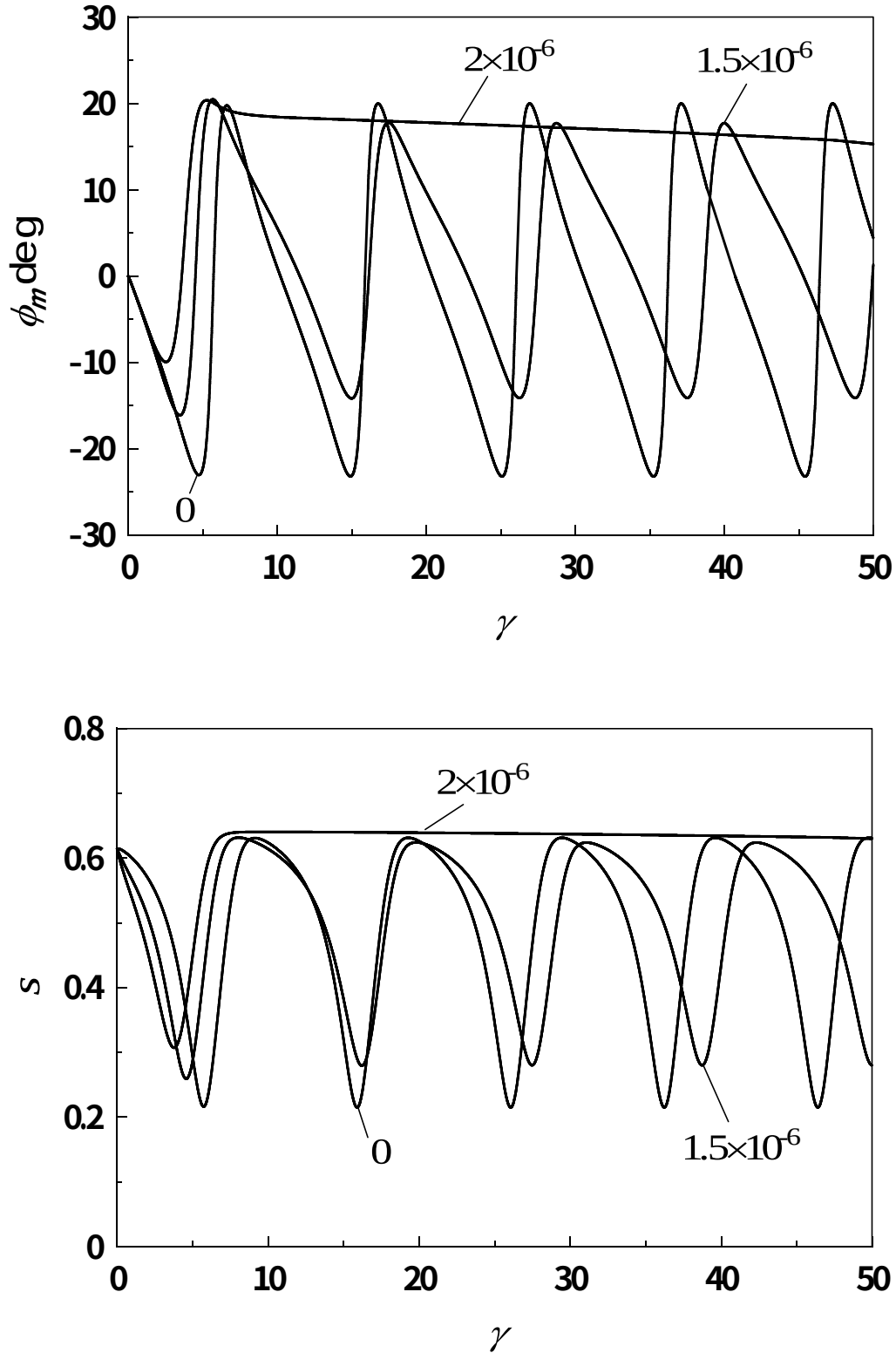

Figures 2.24 Transient behaviors of ϕ_m and S versus strain at $\dot{\gamma}^*$=5 for various values of H_y^*: H_y^*=0, 1.5×10^{-6}, and 2×10^{-6} at β=0.9.

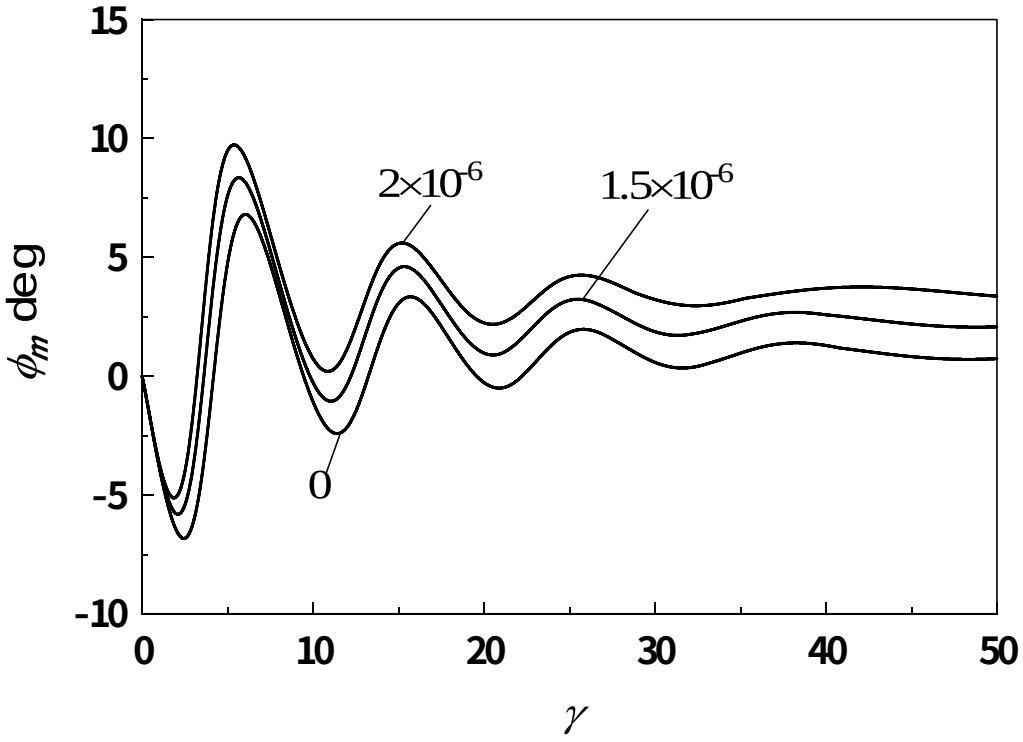

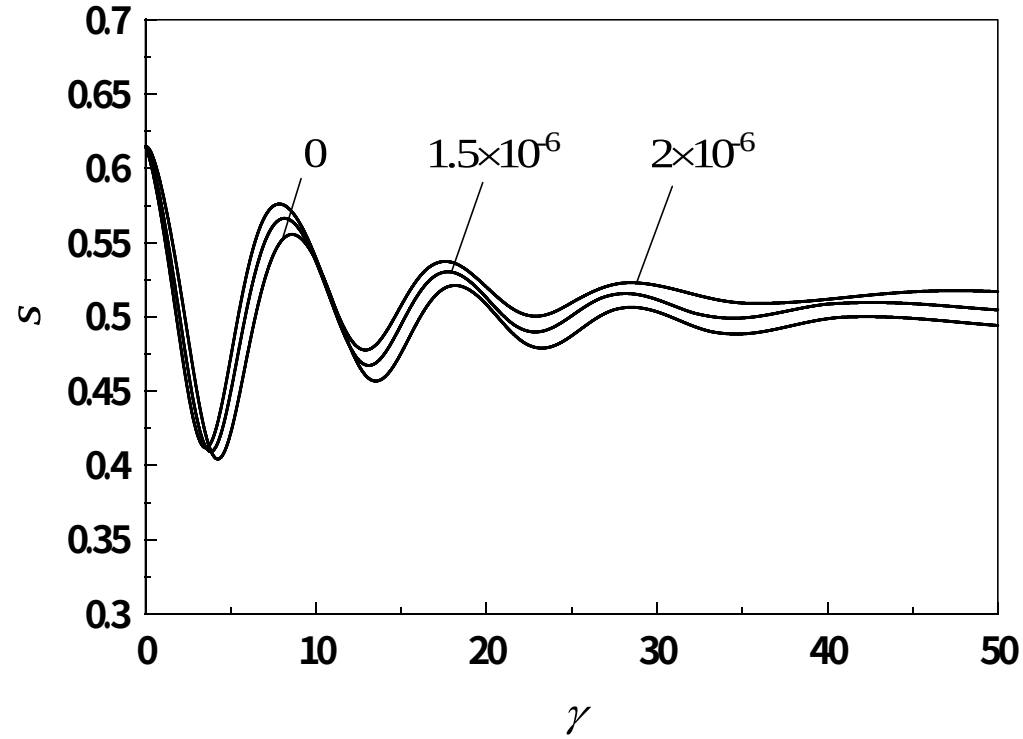

Figures 2.25 Transient behaviors of ϕ_m and S versus strain at $\dot{\gamma}^*$=20 for various values of H_y^*: H_y^*=0, 1.5×10^{-6}, and 2×10^{-6} at β=0.9.

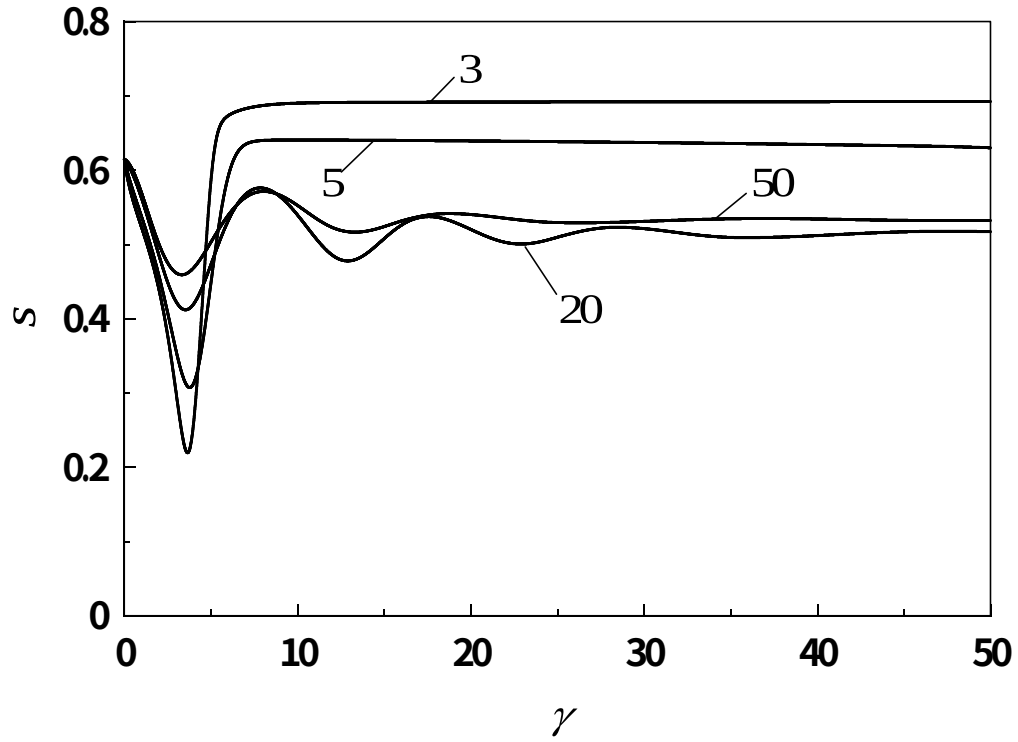

Figure 2.26 Transient behavior of order parameter S at $\dot{\gamma}^*$=3, 5, 20, 50 for $H_y^*=2\times10^{-6}$ at β=0.9.

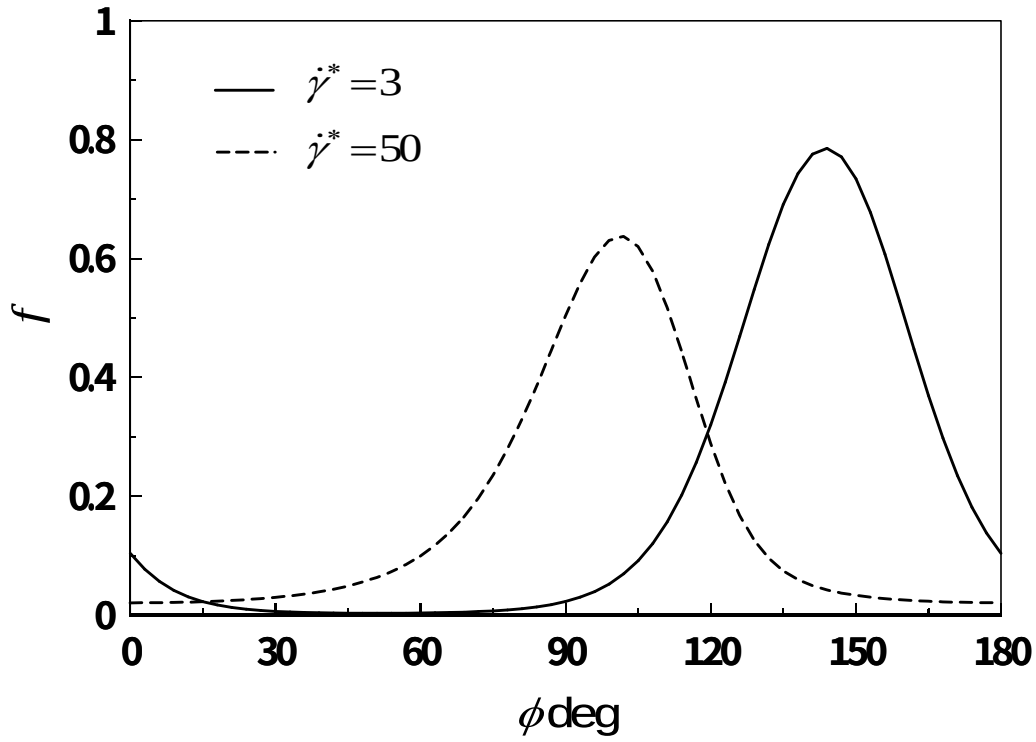

Figure 2.27 Orientation distribution function f versus the degree ϕ at $\dot{\gamma}^*$=3, 50 for $H_y^*=2\times10^{-6}$ at β=0.9.

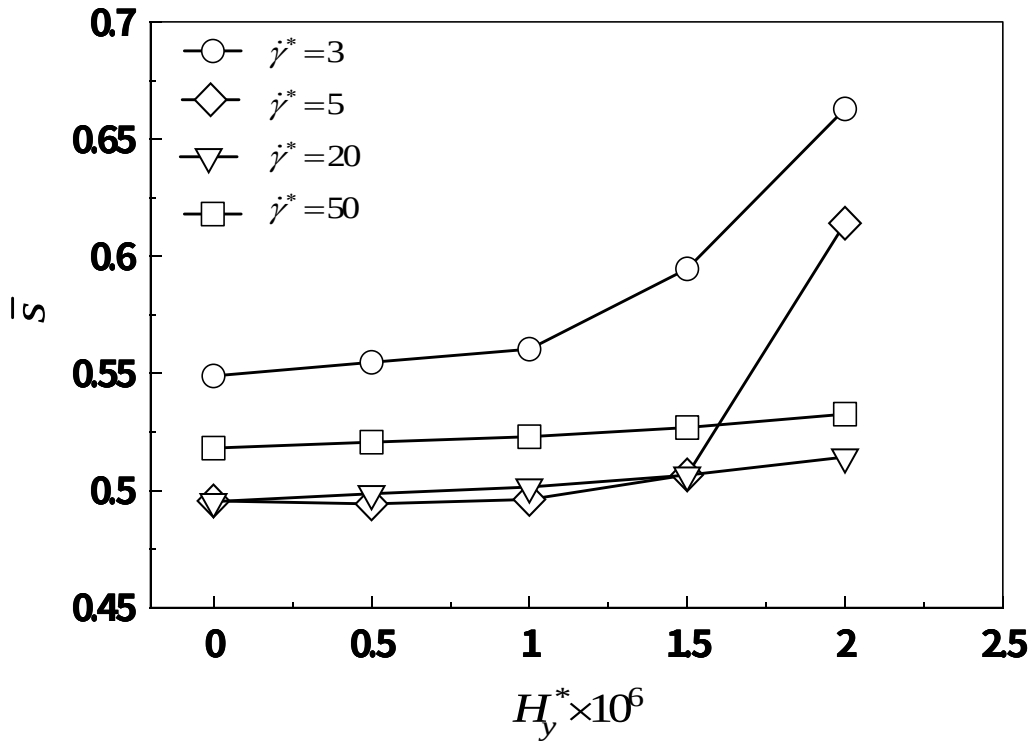

Figure 2.28 Effect of magnetic field parallel to the *y* direction on average scalar order parameter $\bar{S}$ for various values of shear rates: $\dot{\gamma}^*$=3, 5, 20, and 50 at β=0.9.

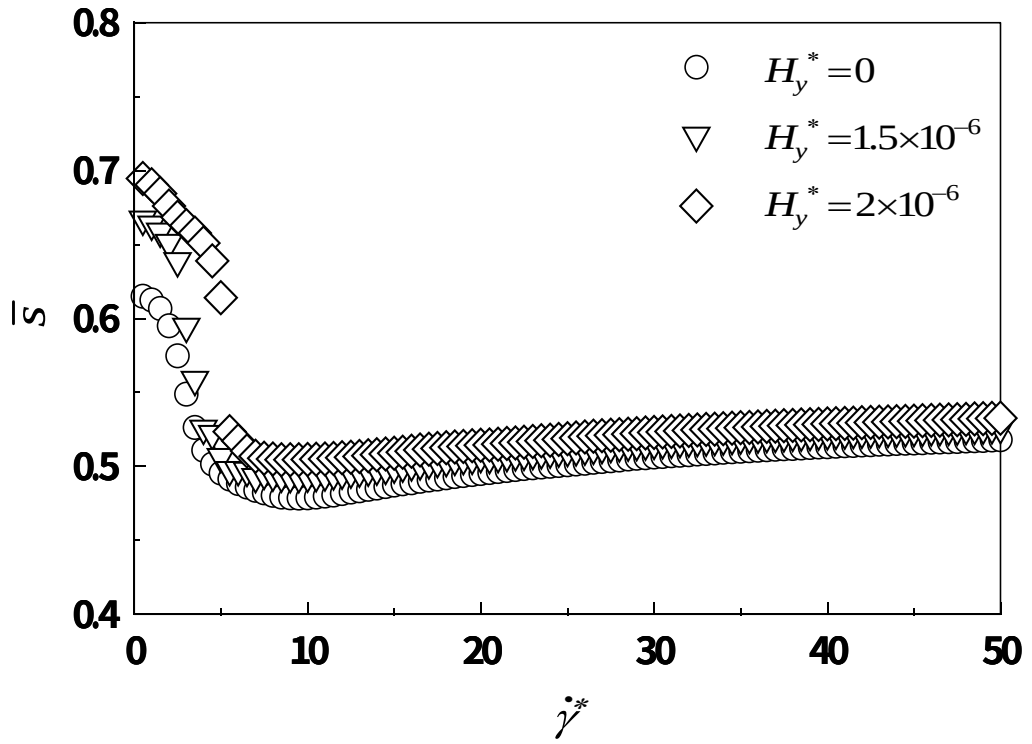

Figure 2.29 Average order parameter $\bar{S}$ as a function of shear rate $\dot{\gamma}^*$ at H_y^*=0, 1×10^{-6}, 1.4×10^{-6}, and 1.6×10^{-6}at β=0.9.

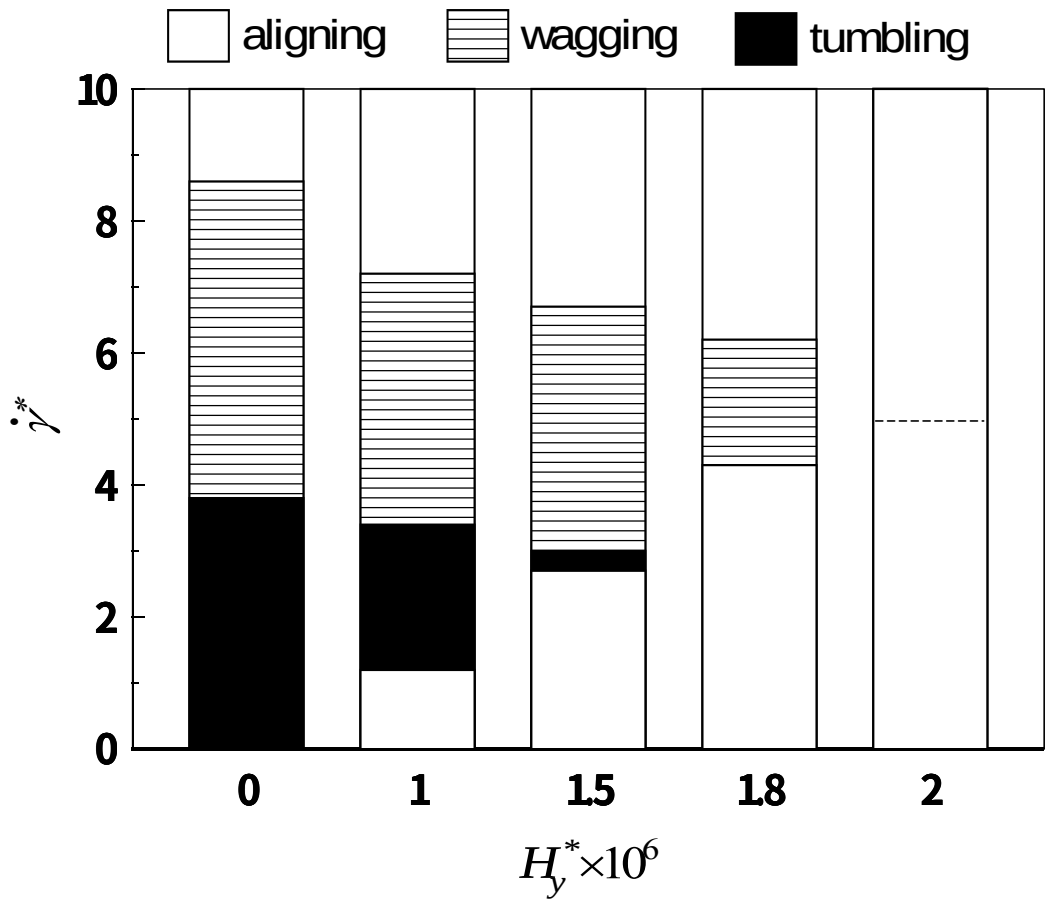

Figure 2.30 Critical shear rates as a function of magnetic field along the *y* direction at β=0.9

2.4 Conclusions

In this paper, we have simulated the evolution of LCP molecular configuration under the shear flow. In the Doi theory used for the computation, the molecular configuration is represented by the probability density function of LCP molecules. The computation results are analyzed and discussed in terms of the major orientation direction, the scalar order parameter, and the flow-orientation mode transitions. When the magnetic field is imposed in the flow direction (*x*-direction), the scalar parameter becomes higher for entire shear rate regime because of the magnetic field. Also, the existence of the new aligning state is found at low shear rate regime in which the effect of the shear flow prevails the effect of the magnetic force, and the rotation of individual molecules is suppressed. On the other hand, for the case of the magnetic field along the velocity gradient direction (*y*-direction), the magnetic fields drastically affect on the steady angle of the major orientation direction, in addition to the effects mentioned above. The major difference between the two cases of the magnetic field is the relations between the orientation direction preferred by the shear flow and the magnetic field; the flow-orientation direction is same as the magnetic field-orientation direction for $\boldsymbol{H}^*=(H_x^*,0,0)$, but the flow-orientation direction is perpendicular to the magnetic field-orientation direction for $\boldsymbol{H}^*=(0,H_y^*,0)$. Thus, for the former case the magnetic fields affect on the scalar parameter rather than the major orientation direction, and for the latter case the effect of the magnetic field is more remarkable on the major orientation direction in comparison with the effect on the scalar order parameter.

The effect of the molecular length by setting $\beta=0.9$ also is discussed in the two cases that the magnetic field is along the *x*-axis and the *y*-axis, respectively. The major difference from $\beta=1.0$ is the effect of the magnetic field along the *x*-axis on the flow-orientation mode, which the wagging state doesn't disappear with the increasing magnetic filed.

In this calculation all of the quantities are non-dimensionalized with equations (2.11) to (2.14). In particularly, the real value of the magnetic field what we need in the process is noticed. For instance, if we choose 1kg PAA (t=399K and$\Delta\chi=1.21\times10^{-7}$cgs), the real strength of the magnetic field at $H_x^*=1\times10^{-6}$ is about 2.4×10^{-8} A/m.

Through this simulation, we obtained the conclusion that the magnetic fields affect not only on the scalar order parameter and the major orientation direction, but also on the flow-orientation modes. In other word, using the proper magnetic field, one can obtain the arbitrary desired molecular orientation configurations which enhance the functionality of the LCP materials.

References

1. Doi, M., J. *Polym. Sci. Polym. Phys. Ed.* **19**, 229-243(1981)
2. Marrucci, G. and Greco, F., *Mol. Cryst. Liq. Cryst.* **206**, 17-30(1991)
3. Tsuji, T. and Rey, A.D., *J. Non-Newtonian Fluid Mech.* **73**, 127-152 (1997)
4. Tsuji, T. and Rey, A.D., *Phys. Rev. E* **57**, 5609-5625(1998)
5. Feng, J.J., Sgalari, G. and Leal, L.G., *J. Rheol.* **44**, 1085-1101(2000)
6. Marrucci, G. and Maffettone, P. L., *Macromolecules* **22**, 4076-4082(1989)
7. Larson, R.G., *Macromolecules* **23**, 3983-3992(1990)
8. Larson, R.G. and Öttinger, H.C., *Macromolecules* **24**, 6270-6282(1991)
9. Marrucci, G., *Rheol Acta* **29**,523-528(1990)
10. Chono, S., Tsuji, T., *Trans. Jpn. Soc. Mech. Eng.*, Part B **65**, 3539-3545(1999)(in Japanese)
11. Asada, T., Tanaka, T. and Onogi, S., *J. Appl. Polym. Symp.* **41**, 229-239(1985)
12. Larson, R.G. and Mead, D.W., *Liq. Cryst.* **15**, 151-169(1993)
13. Walker, L.M., Wagner, N.J. and Larson, R.G., Mirau, P.A. and Moldenaers, P, *J. Rheol.* **39**, 925-952(1995)
14. Kiss, G. and Porter, R.S., *J. Polym. Sci., Polym, Symp.* **65**, 193-211(1978)
15. Moldenaers, P. and Mewis, J., *J. Rheol.* **30**, 567-584(1986)
16. Grizzuti, N., Cavella, N.S. and Cicarelli, P., *J. Rheol.* **34**, 1293-1310(1990)
17. Baek, S.-G., Magda, J.J. and Cementwala, S.," *J. Rheol.* **37**, 935-945(1993a)
18. Kiss, G. and Porter, R.S., *J. Polym. Sci.,Part A-2, Polym.Phys.* **18**, 361-388(1980b)
19. Berry, G.C., *Mol. Cryst. Liq. Cryst.* **165**, 333-360(1988)
20. Andrews, N.C., Edwards, B.J. and McHcgh, A., *J. Rheol.* **39**, 1161-1181(1995)
21. Belyaev, V.V, *Phys. Usp.*, **44 (3),** 255-284(2001)
22. Lukaschek, M. and Kothe, G., *J. Phys. Chem.* **117(9)**, 4550-4556(2002)
23. Luckhurst, G.R., Timimi, B.A., Nakatsuji, M., Okumoto, K., Sugimura, A., and Zimmermann, H., *Mol. Cryst. Liq. Cryst.*, **398**, 235-248(2003)
24. Ericksen, J.L., *Kolloid-Z* **173**, 117-122(1960)
25. Leslie, F.M., *Mech. Appl. Math.* **XIX**, 357-370(1966)
26. Leslie, F.M., Adv. *Liq. Cryst.* **4**, 1-84(1979)

Chapter 3

Effect of Magnetic Field on Molecular Orientation of Nematic Liquid Crystalline Polymers Under Simple Shear Flow:II Out-of-Plane Case

The effect of magnetic fields on molecular configuration of liquid crystalline polymers (LCPs) under simple shear flows is numerically analyzed using the Doi theory when the out-of-plane case is considered. The evolution equation for the probability distribution function of the LCP molecules is directly solved without any approximation closure. The initial director is oriented at three angles with respect to the shear plane, where the shear plane is parallel to both the velocity and its gradient:(1) along the direction of the flow, (2) parallel to the vorticity direction, and (3) set into the plane which parallel to the vorticity direction and the flow. Two cases of the magnetic fields which are parallel to the flow and velocity gradient direction are considered. We find that when the initial position of the director is along the flow, it doesn't rotate out from the shear plane. Three modes, tumbling, wagging and aligning, are observed, respectively. However, depending on the initial conditions of the probability distribution function of molecular configuration chose in this chapter in the second and third case a log-rolling orientation state is detected at low shear rates, where the average orientation is perpendicular to the shear plane. The simulation results show that the director can be controlled well to align the direction of magnetic fields. It is an efficient way to improve the performance of LCP materials. Finally in order to check the effect of the molecular length the simulation results for β=0.9 are also represented.

3.1 Introduction

In the Chapter 2 the effect of magnetic fields on molecular configuration of LCPs under simple shear flows for the in-plane case are numerically analyzed using the Doi theory (1). The simulation results are discussed through investigating the effect of magnetic fields on the major orientation direction, the scalar order parameter, and the flow-orientation mode transitions. A conclusion was made that the strength of LCPs can be tailored by applying the appropriate magnetic fields. However, the director doesn't always be confined into the shear plane in the LCP processing. Also the calculations, which had been done by Zuniga and Leslie (2), show that director gradients can create flow instabilities that drive the director out of the shear plane in tumbling range. The detail discussions for the out-of-plane case were done by Larson and Ö̈ttinger (3) with Doi equation which was solved by two numerical solution technique: one was an expansion in spherical harmonic functions, and another was a stochastic method that integrates the equations of motion for a large ensemble of molecules. A steady log-rolling orientation state where the average orientation is always perpendicular to the shear plane, and a time-periodic kayaking state with an orbit oblique to the shear plane were observed depending on the initial conditions of the molecular configuration of LCPs. Recently a constitutive model for dispersions of acicular magnetic particles has been developed by modeling the particles as rigid dumbbells dispersed in a solvent by Bhandar and Wiest (4, 5). Based on the Doi theory an average alignment parameter J (J=<**u**>) is introduced into the probability orientation function of the molecular orientation because of the difference between the two "beads" of the dumbbell. However, as we known, the alignment parameter J will be equal to zero because the probability distribution function f(**u**,t) has for-aft symmetry for molecules of LCPs. In this case the constitutive equation for the modeling of magnetic dispersions will be returned into Doi equation solved through second tensor equation. As a result, the mesoscal constitutive modeling of magnetic dispersions can not show out the tumbling and wagging modes of LCPs.

In the process basically the strength of LCP products along the flow direction is noticed. If the director rotates out of the shear plane, the strength along the flow direction will be reduced since it depends on the degree of the molecular alignment. How the magnetic fields affect the molecular configuration of flowing LCPs is further investigated with Doi theory when the out-of-plane case is considered. The degree of molecular alignment along the director direction and the flow direction is also calculated, respectively.

The organization of this chapter is as follows. In section 3.2 we give out the basic equations used in the calculations. And the main simulation results are presented into section 3.3 for β=1.0 and section 3.4 for β=0.9. Finally a brief conclusion is made in section 3.5.

3.2 Basic Equations

The Doi theory is used to solve the out-of-plane case which has been described in the section 2.2. We also consider a simple shear flow, and define *x* to be the flow direction, *y* to be the velocity gradient direction, and *z* to be the vorticity direction as shown in Figure 3.1. The orientation of a single molecule represented by a unit vector **u** is characterized with an azimuthal angle ϕ and a polar angle θ. The magnetic field is applied in the shear plane, and two cases will be considered: 1) the magnetic field along the *x*-axis, 2) the magnetic field along the *y*-axis. The Doi equation represented in the part 2.2 is showed:

$$\frac{\partial f}{\partial t} = \overline{D}_r \frac{\partial}{\partial \mathbf{u}} \cdot \left(\frac{\partial}{\partial \mathbf{u}} f + f \frac{\partial}{\partial \mathbf{u}} \frac{V(\mathbf{u})}{kT} \right) - \frac{\partial}{\partial \mathbf{u}} \cdot (\dot{\mathbf{u}} f), \tag{3.1}$$

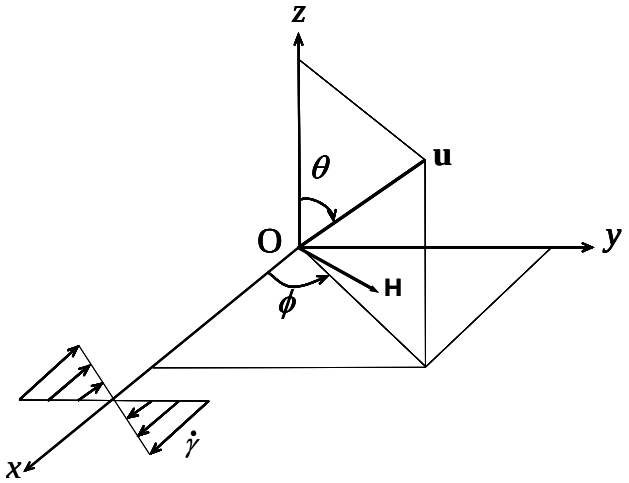

Figure 3.1 Geometry and coordinate systems

When the probability distribution function $f(\mathbf{u},t)$ is confined into the shear plane, it is symmetry with respect to the *x*-*y* plane. However, this symmetry will be broken if

the restriction on the director is removed.

The material is sheared with the shear rate of $\dot{\gamma}$ in the *x*-*y* plane, and the velocity gradient tensor is given by,

$$\boldsymbol{\kappa}=\begin{bmatrix} 0 & \frac{1}{2}\dot{\gamma}(\beta+1) & 0 \\ \frac{1}{2}\dot{\gamma}(\beta-1) & 0 & 0 \\ 0 & 0 & 0 \end{bmatrix}, \tag{3.2}$$

β is the molecular formation coefficient. Because the director doesn't always remain in the shear plane, all the components of the order parameter tensor will be considered:

$$\mathbf{S}=\begin{bmatrix} S_{xx} & S_{xy} & S_{xz} \\ S_{xy} & S_{yy} & S_{yz} \\ S_{zx} & S_{zy} & S_{zz} \end{bmatrix}, \tag{3.3}$$

Using the same way with the part 2.3 to non-dimensionlize the equation (3.1) for two dimensional magnetic field (**H**=(H_x,H_y,0)) then

$$\begin{aligned}
\frac{\partial f}{\partial t^*} &= \left(1-\frac{3}{2}\mathbf{S}:\mathbf{S}\right)^{-2}\left(\frac{\partial^2 f}{\partial\theta^2}+\cot\theta\frac{\partial f}{\partial\theta}+\frac{1}{\sin^2\theta}\frac{\partial^2 f}{\partial\phi^2}\right) \\
&+3U\left(1-\frac{3}{2}\mathbf{S}:\mathbf{S}\right)^{-2}\left\{3f\left(S_{xx}\sin^2\theta\cos^2\phi+S_{yy}\sin^2\theta\sin^2\phi+S_{zz}\cos^2\theta+S_{xy}\sin^2\theta\sin2\phi+\sin2\theta\left(S_{xz}\cos\phi+S_{yz}\sin\phi\right)\right)\right. \\
&-\frac{1}{2}\frac{\partial f}{\partial\theta}\sin2\theta\left(S_{xx}\cos^2\phi+S_{yy}\sin^2\phi-S_{zz}+S_{xy}\sin2\phi+2\cos2\theta(S_{xz}\cos\phi+S_{yz}\sin\phi)\right) \\
&\left.+\frac{1}{2}\frac{\partial f}{\partial\phi}\left(S_{xx}\sin2\phi-S_{yy}\sin2\phi-2S_{xy}\cos2\phi+2\cot\theta(S_{xz}\sin\phi-S_{yz}\cos\phi)\right)\right\} \\
&+\left(1-\frac{3}{2}\mathbf{S}:\mathbf{S}\right)^{-2}\left\{2f\left[H_x^{*2}\left(3\sin^2\theta\cos^2\phi-1\right)+H_y^{*2}\left(3\sin^2\theta\sin^2\phi-1\right)+3H_x^*H_y^*\sin2\phi\sin^2\theta\right]\right. \\
&\left.-\frac{\partial f}{\partial\theta}\left[\sin2\theta\left(H_x^{*2}\cos^2\phi+H_y^{*2}\sin^2\phi+H_x^*H_y^*\sin2\phi\right)\right]+\frac{\partial f}{\partial\phi}\left[\sin2\phi\left(H_x^{*2}-H_y^{*2}\right)-2H_x^*H_y^*\cos2\phi\right]\right\} \\
&+\dot{\gamma}^*\left\{\beta\left(\frac{3}{2}f\sin^2\theta\sin2\phi-\frac{1}{4}\frac{\partial f}{\partial\theta}\sin2\theta\sin2\phi\right)+\frac{\partial f}{\partial\phi}(1-\beta\cos2\phi)/2\right\}
\end{aligned} \tag{3.4}$$

The superscripts * denote non-dimensionalized variables and parameters. Above equation is computed using the finite difference method for spatial discretization and the Crank-Nicolson method for time integration. The computation area for f can be

restricted in the region $0 \le \theta \le \pi$ and $-\pi/2 \le \phi \le \pi/2$ due to the broken symmetry with respect to the *x*-*y* plane. Boundary conditions for the function are:

$$\partial f(0,\phi,t^*)/\partial\theta = 0, \tag{3.5}$$

$$\partial f(\pi,\phi,t^*)/\partial\theta = 0, \tag{3.6}$$

$$f(\theta,-\pi,t^*) = f(\theta,\pi,t^*), \tag{3.7}$$

$$\partial f(\theta,-\pi,t^*)/\partial\phi = \partial f(\theta,\pi,t^*)/\partial\phi. \tag{3.8}$$

The normalization condition,

$$2\int_0^{\pi} d\theta \int_0^{\pi} d\phi\, f \sin\theta = 1, \tag{3.9}$$

is also required.

An initial profile of the function, $f(\theta,\phi,t^*=0)$, is derived from the Boltzman profile with the major orientation direction along the *x*-axis (flow direction). The time step and the spatial mesh width are set to be $\Delta t^* = 0.005/\dot{\gamma}^*$ and $\Delta\theta = \Delta\phi = 3$deg. The nematic potential intensity *U* also is set to be 5 in order to compare with the results getting from the section 2.3. Here we allow the director to exist an angle φ between the *y* and *z* axes similar to the method done by Larson and Öttinger(3). Thus when $\varphi = 0^o$ the director is parallel to the *x*-axis, and when $\varphi = -90^o$, it is parallel to the *z*-axis, namely the vorticity direction. In general the initial director is defined as $\mathbf{n}=(n_x,n_y,n_z)=(\cos\varphi,0,\sin\varphi)$. In this thesis $\varphi = 0^o$, -90^o and -50^o are chosen. According to the equation (2.3), the order parameter tensor can be solved by the integration of the probability distribution function $f(\mathbf{u},t)$.

A quantity $S_2 = S_{yy} - S_{zz}$ defined same with the paper by Larson and Öttinger(1991) is also discussed in the following results, especially, the effect of the magnetic fields on it will be investigated. When $S_2 = 0$, it can be seen that $S_{eq} \times (n_y^2 - n_z^2) = 0$. It is impossible that n_y is equal to n_z. As a result, the director is aligned along *x* axis. Here n_x, n_y, n_z are the three components of the director **n** obtaining by solving the eigenvalues and eigenvectors of the order parameter tensor **S**. And S_{eq} is obtained at the equilibrium state. Using the same method the conclusions as follows can be made that if S_2 is

roughly S_{eq}, the director is along the y-axis; if S_2 is roughly -S_{eq}, the director is oriented to be parallel to the *z* axis. Therefore, we can easily distinguish any drift of the director and how the magnetic fields control it.

The azimuthal angle ϕ and the polar angle θ of the director can be defined as:

$$\theta = \arccos(n_z), \tag{3.10}$$

$$\phi = \arctan(\frac{n_y}{n_x}), \tag{3.11}$$

As we known the scalar parameter *S* can show out the molecular alignment of LCPs along the director. Actually, the tensile strength of LCPs along the flow direction always is noticed in the process. Therefore, in this part we will focus on the strength of LCPs along the flow direction through showing out the component S_{xx} of the order parameter tensor **S**, and the effect of the magnetic field parallel to the *x*-axis on it also will be investigated.

3.3 Results and Discussions for β=1.0

3.3.1 Initial Position of the Director along the *x*-axis

In this section, the director starts rotating from the *x*-axis, namely **n** = (±1, 0, 0). Figure 3.2 shows S_2 oscillates with time in the range of 0~S_{eq} at $\dot{\gamma}^*$=1. Obviously the director is confined into the shear plane: when S_2=0, the director is parallel to the flow direction, and when $S_2 \approx S_{eq}$, the director is almost along the *y*-axis. With the equation (3.10) the major orientation angle ϕ_m with time in the shear plane is represented in Figures 3.3. A typical tumbling mode is showed where ϕ_m periodically decreases with strain γ. The scalar parameter *S* and S_{xx} as the function of time also is showed in Figures 3.3. Since the director periodically rotates in the shear plane, S_{xx} also shows periodically oscillation. Compared with Figure 3.2, $S_{xx\,max}$ is related to S_2=0, namely, the director is along the *x*-axis; on the contrary, $S_{xx\,min}$ indicates the director almost is parallel to the *y*-axis. When $\dot{\gamma}^*$=2.85 in Figure 3.4, the amplitude of S_2 is reduced compared with the one at $\dot{\gamma}^*$=1, which shows that the *x*-axis tends to become an attractor for the director. A wagging mode is exhibited in Figures 3.5 where the director periodically oscillates in the shear plane after several damping oscillations. The changing of the scalar parameter *S* and S_{xx} with time are also represented in Figures 3.5. With the increasing shear rate ($\dot{\gamma}^*$=10 Figure 3.6), the oscillatory peak of S_2 decreases very quickly, and within a short

time it becomes zero. From Figures 3.7, the director in the shear plane describes an aligning mode which oscillates several times then reaches a steady state at $\phi_m \approx 0^o$. The director is aligned almost along the *x*-axis because the torque caused by the shear rate is strong enough. The scalar parameter *S* and S_{xx} also is described in Figures 3.7, where reflect the behaviors of ϕ_m. Obviously, the molecular alignment along the direction of the flow is smaller than the one along the director.

The time-averaged $\overline{S}$ and $\overline{S}_{xx}$ affected by the shear rate $\dot{\gamma}^*$ are investigated in Figure 3.8. The changes of $\overline{S}$ with the shear rate is almost same with the simulation results when the director is confined into the shear plane for $H_x^*=0$ described in Figure 2.6. $\overline{S}_{xx}$ decreases continuously, and then increases monotonically as the shear rate increases. It can be seen that both the time-averaged $\overline{S}$ and $\overline{S}_{xx}$ increase with the shear rate and $\overline{S}$ is much higher than $\overline{S}_{xx}$.

As we can see from the simulation results from Figures 3.2 to 3.8 that once we set the director along the *x*-axis at $t^*=0$, then the director doesn't rotate out from the shear plane. Three modes, tumbling, wagging and aligning, also can be detected. The molecular alignment along the flow also can be increased by increasing the shear rate. In this part we will not discuss the effect of the magnetic field on the director since it will be similar to the discussions in the part of 2.3.

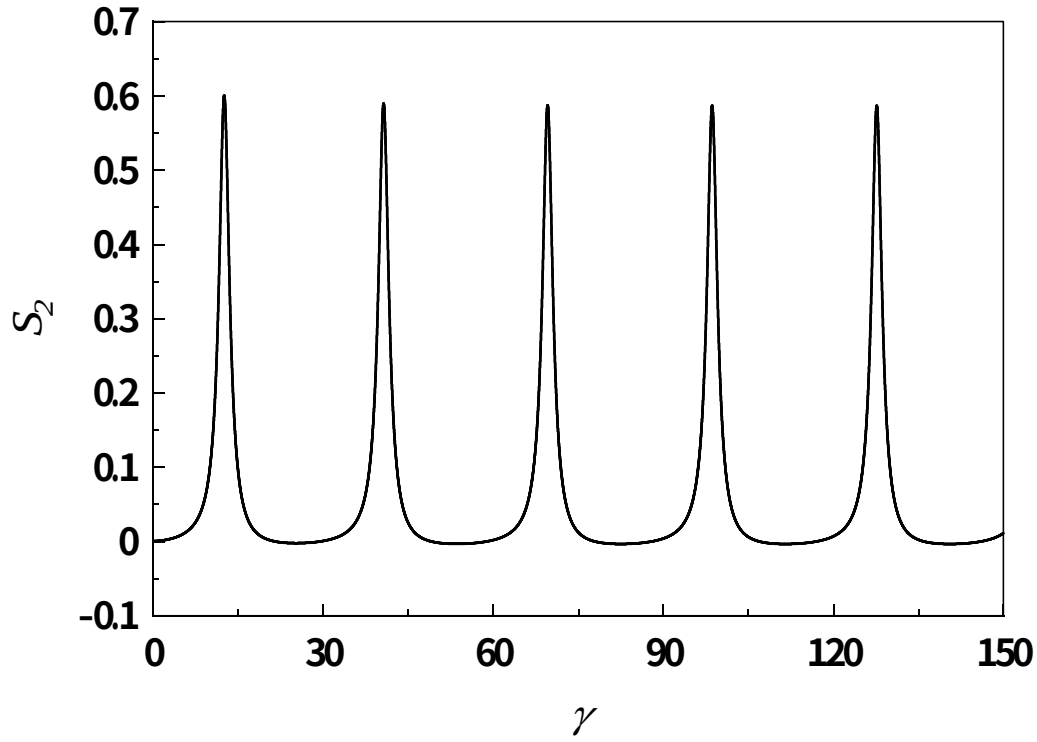

Figure 3.2 S_2 versus strain at $\dot{\gamma}^*$ =1 for β=1.0.

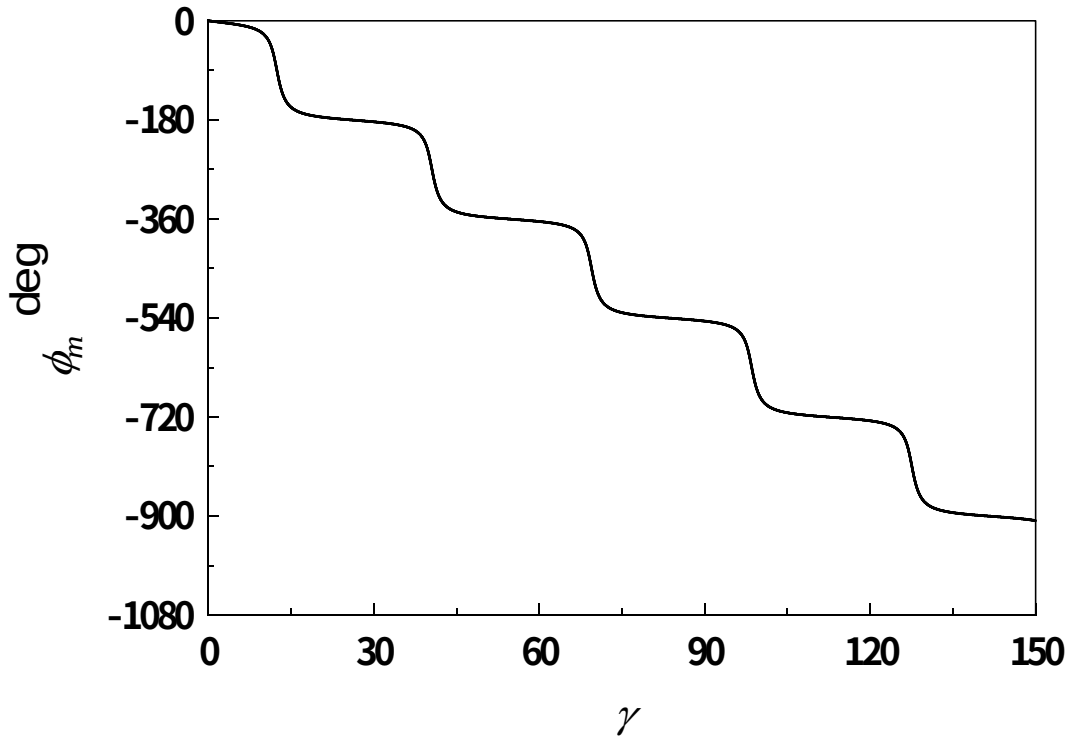

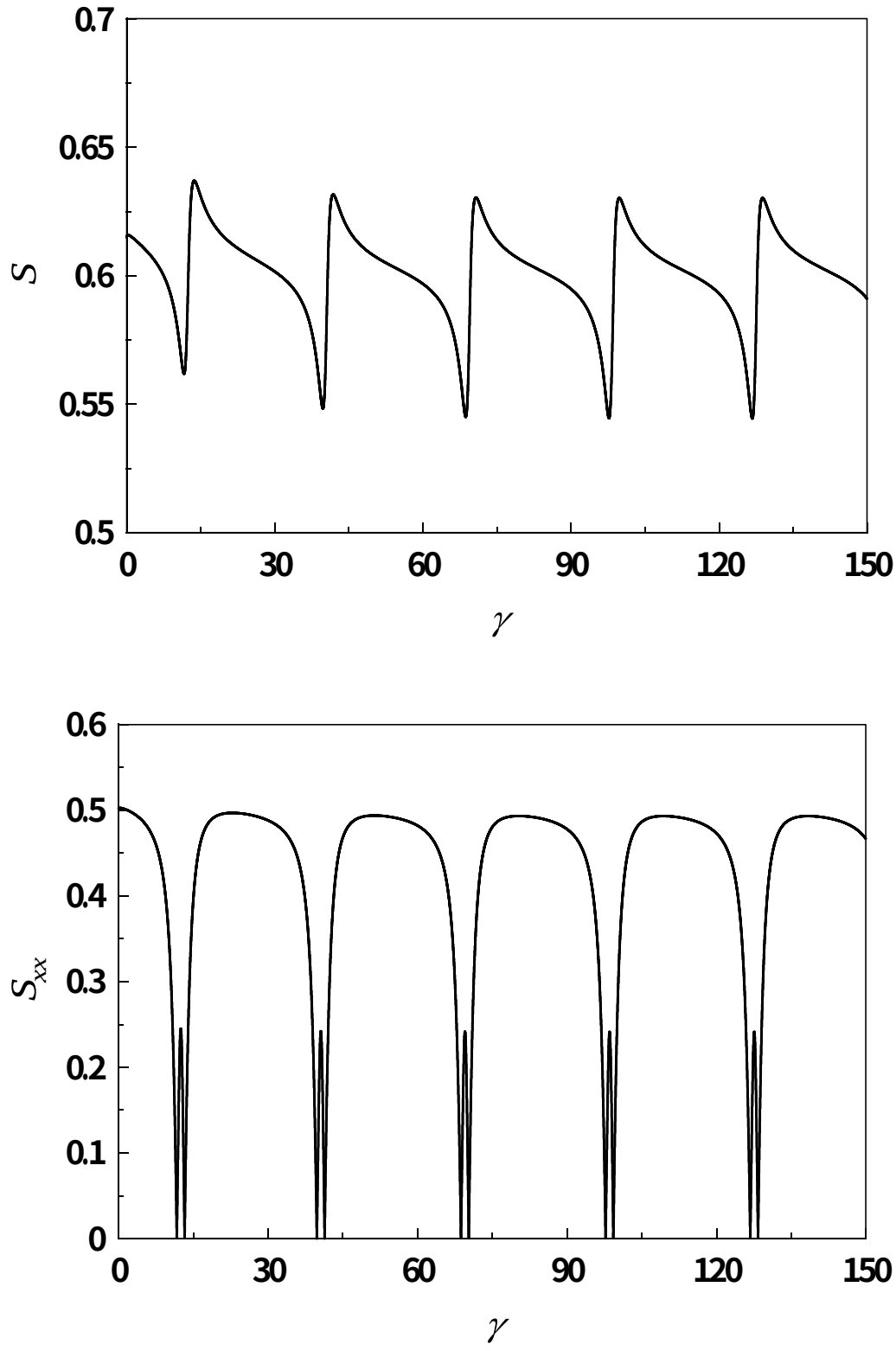

Figures 3.3 Transient behaviors of preferred angle ϕ_m and scalar order parameter S and S_{xx} versus strain at a given shear rate $\dot{\gamma}^*$=1 for β=1.0.

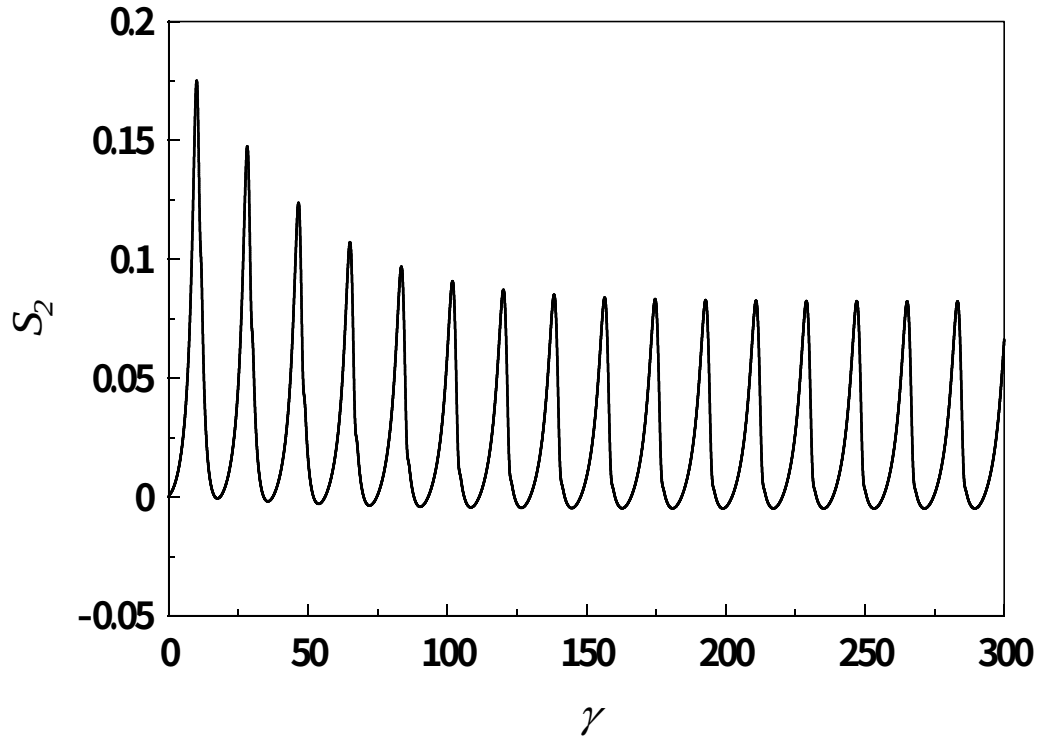

Figure 3.4 S_2 versus strain at $\dot{\gamma}^*$ =2.85 for β=1.0.

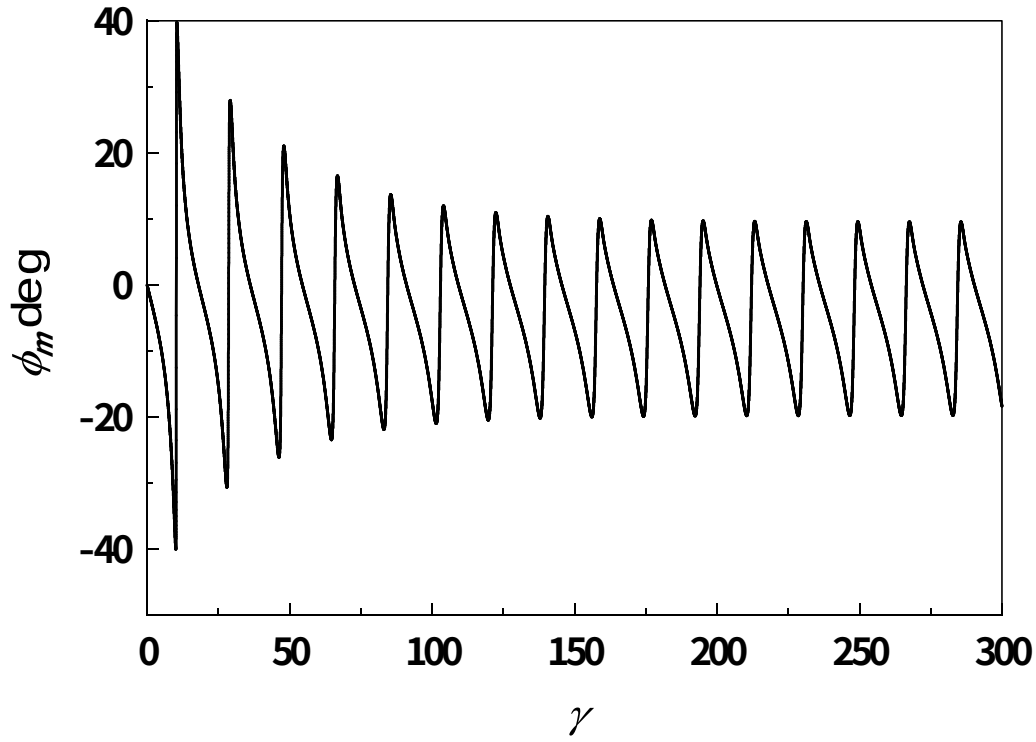

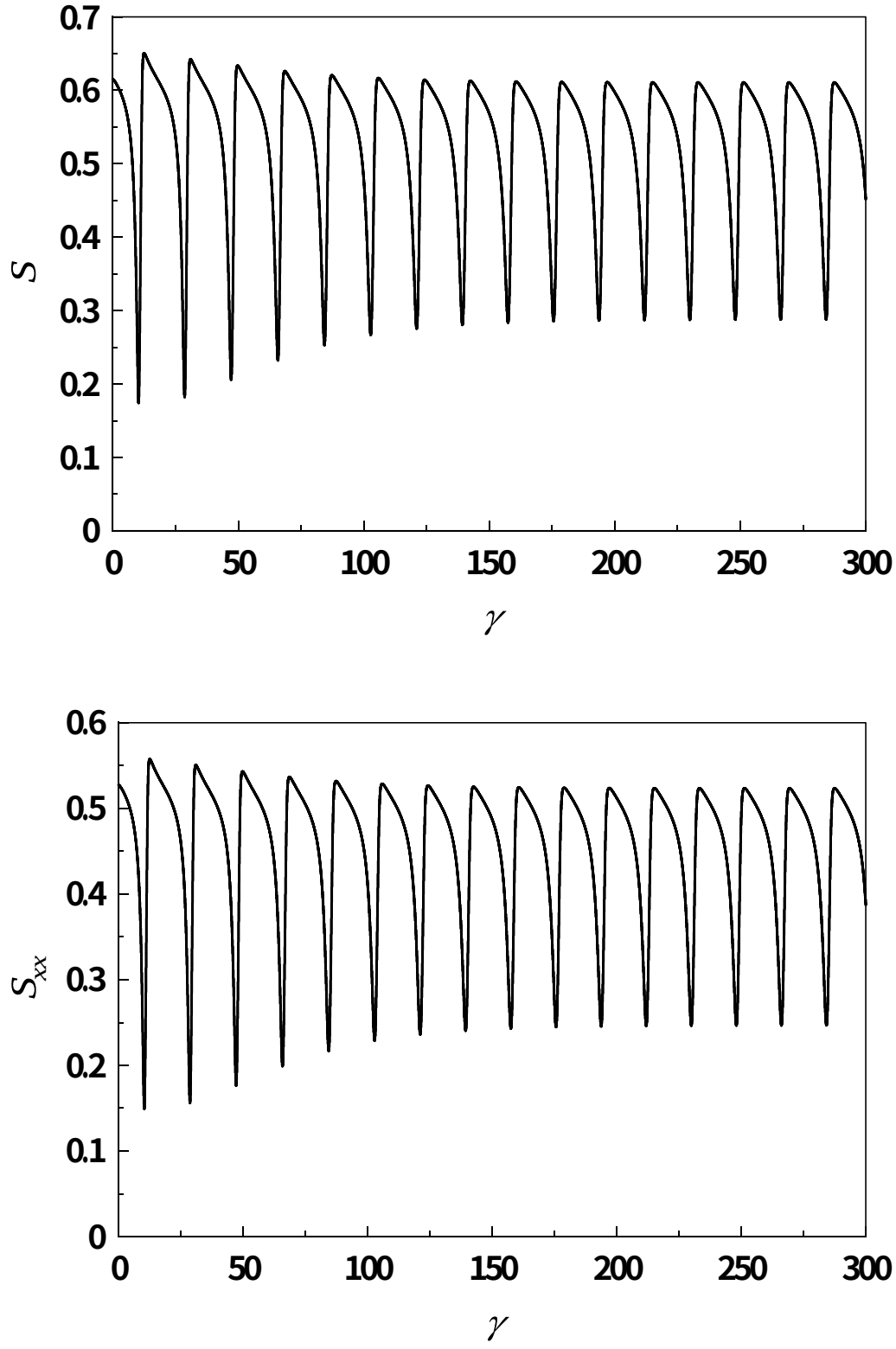

Figures 3.5 Transient behaviors of preferred angle ϕ_m and scalar order parameter S and S_{xx} versus strain at a given shear rate $\dot{\gamma}^*$=2.85 for β=1.0.

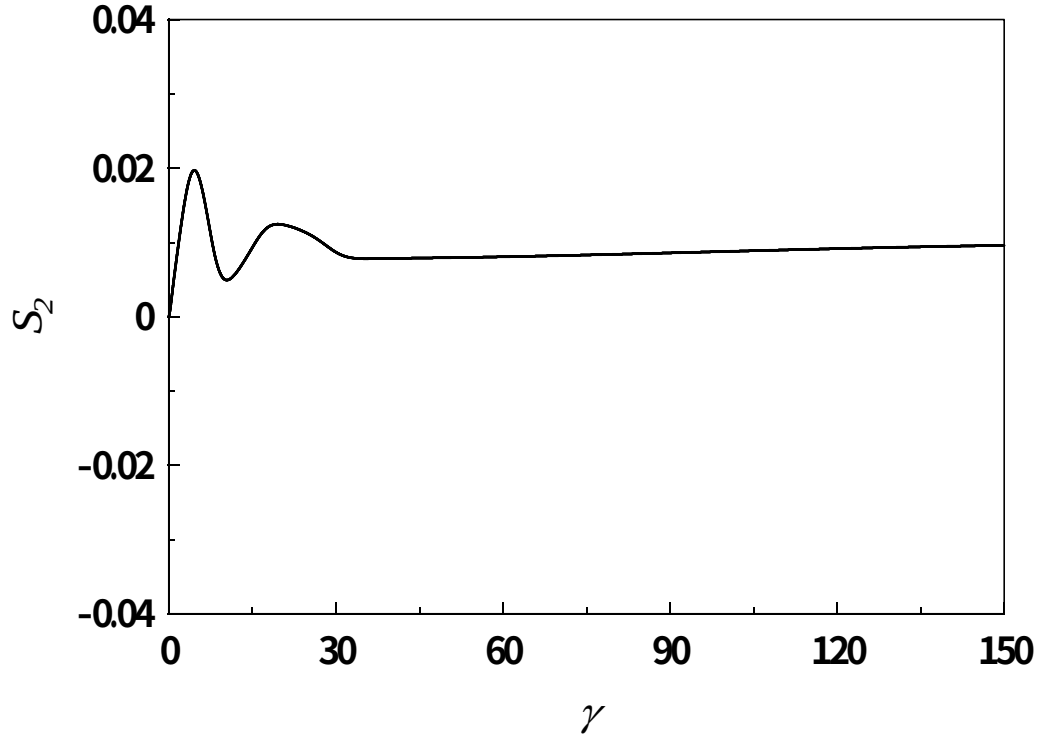

Figure 3.6 S_2 versus strain at $\dot{\gamma}^*$ =10 for β=1.0.

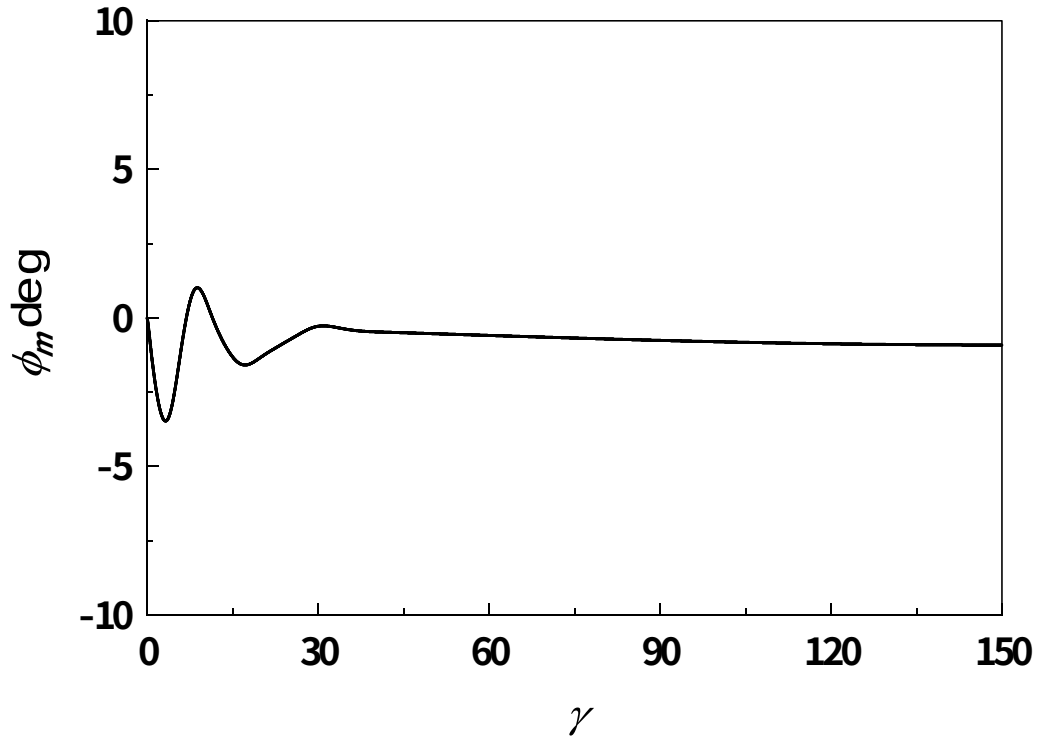

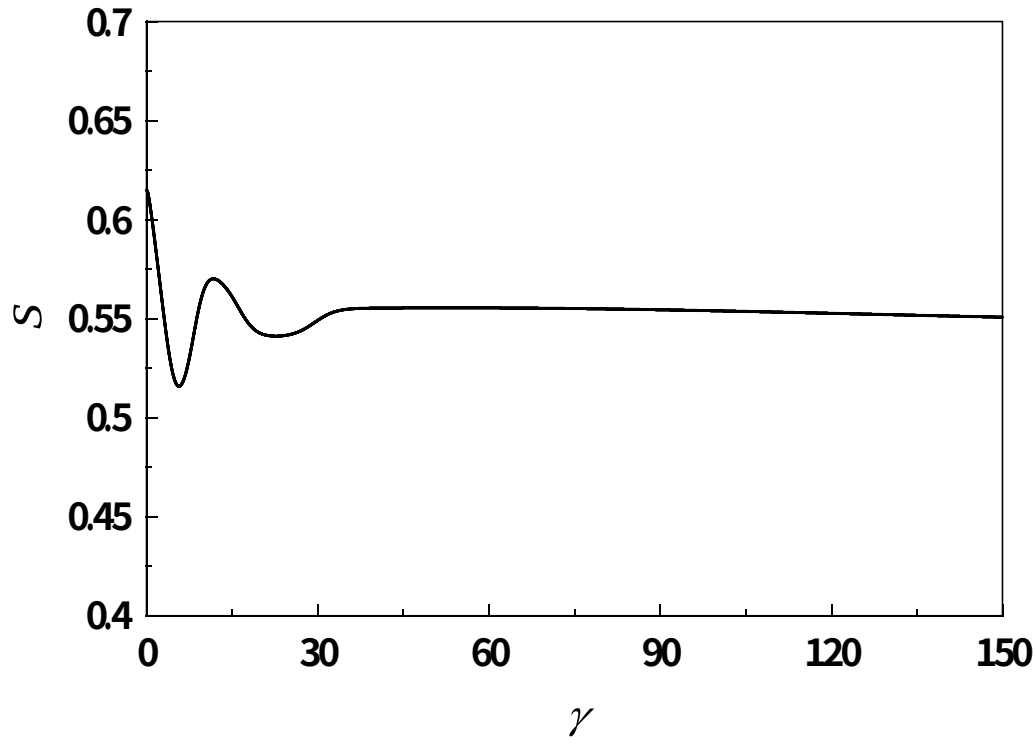

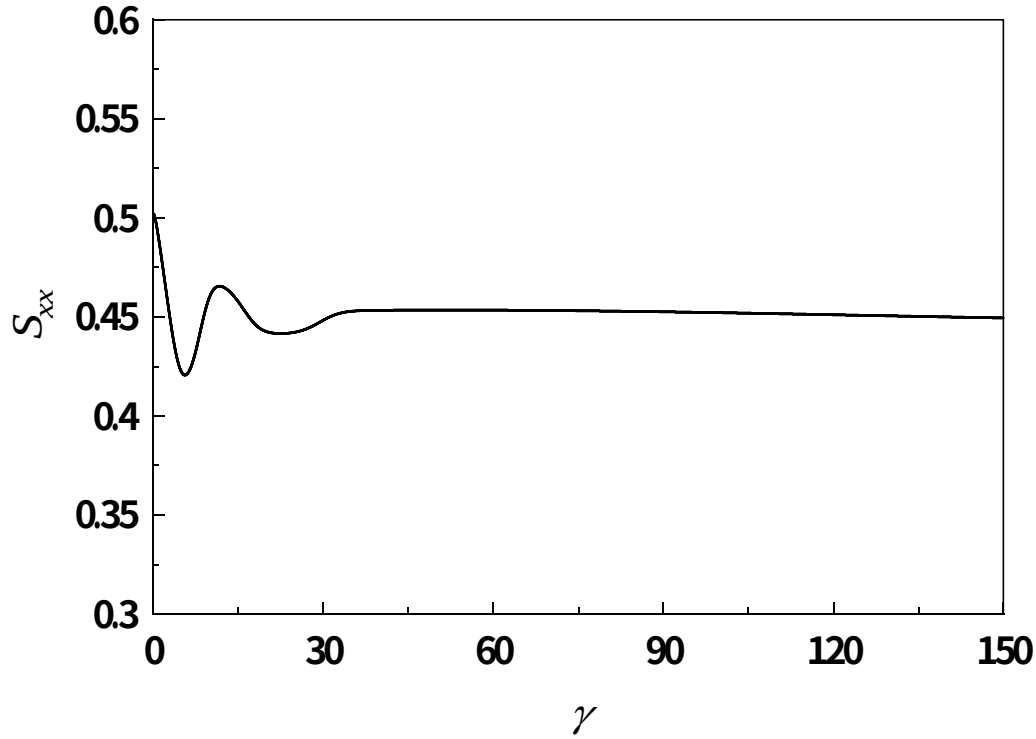

Figures 3.7 Transient behaviors of preferred angle ϕ_m and scalar order parameter S and S_{xx} versus strain at a given shear rate $\dot{\gamma}^*$=10 for β=1.0.

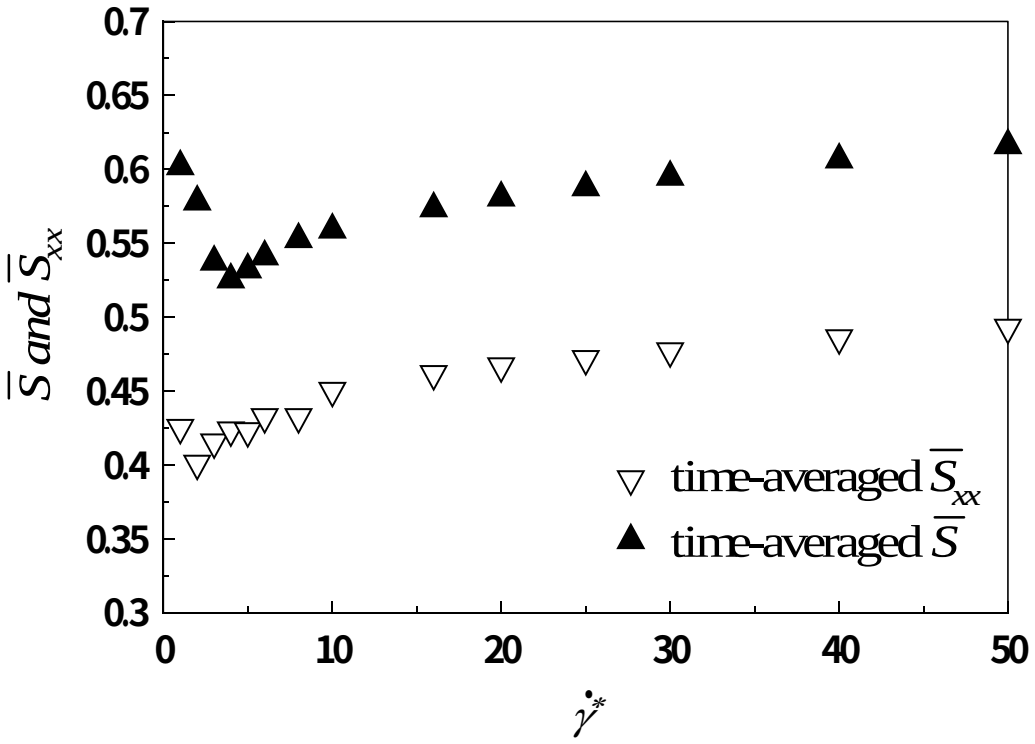

Figure 3.8 Average order parameter $\bar{S}$ and $\bar{S}_{xx}$ as a function of shear rate.

3.3.2 Initial Position of the Director along the *z*-axis

We will set the director to be orthogonal to the shear plane in this section. When the director **n** is parallel to the vorticity axis, **n** = (0, 0, ±1), the bi-steady state depending on the tumbling parameter, which is discussed when molecular elasticity is absent(6), has to be considered: if $|\lambda|<1$, the nematic is called tumbling nematic. The solution, **n** = (0, 0, ±1), is neutrally stable to homogeneous disturbances, that is, such disturbances neither grow nor decay away, but produce neutrally stable orbits. This orientation is called log-rolling orientation (5) since the director merely orbits about the vorticity axis; if $|\lambda|>1$, the nematic is flow-aligning. The log-rolling orientation is unstable to small disturbances and the director always finds its way to the flow alignment angle in the shear plane. Based on these known results, the case considering the effect of molecular elasticity has been discussed by Larson and Öttinger in 1991 with Doi theory solved by two numerical solution techniques: an expansion in spherical harmonic functions and a stochastic method. The initial director decides the final state that is either a time-periodic tumbling orbit in shear plane or log-rolling (or kayaking) state at a low and modest shear rates. In order to control the orbit of the director in the

LCP process we will further investigate the effect of the magnetic field along the *x* and *y* direction on the log-rolling orientation. The simulation results described the degree of molecular alignment along the flow direction under the magnetic field parallel to the *x*-axis, which S_{xx} changes with non-dimensional time, are also represented. The simulation results show out an efficient method to obtain a high orientation state along the flow direction.

3.3.2.1 The Magnetic Field along the *x*-axis

In this section, we deal with the case that the magnetic field is parallel to the flow direction (i.e., **H**=(H_x,0,0)). Figure 3.9 shows the time evolutions of S_2 for $\dot{\gamma}^*$=1 and H_x*=0, 1.5×10^{-6}, and 2.0×10^{-6}. When H_x*=0, S_2 almost is equal to $-S_{eq}$ with time. As explained above the director is parallel to the vorticity direction, namely, the log-rolling orientation is detected. With applying the magnetic field along the *x*-axis for H_x*=1.5×10^{-6}, S_2 shifts up slightly and remains a constant. The vorticity direction also is an attractor for the director. The magnetic field, however, is increased at H_x*=2.0×10^{-6}, S_2 at first is increased slowly, then suddenly becomes zero and keeps it with time. The director from the vorticity direction goes into the shear plane and is controlled along the direction of the magnetic field. The Figure 3.10 describes the polar angle θ of the director changes with the increasing strength of the magnetic field at $\dot{\gamma}^*$=1. When H_x*=0, the polar angle θ of the director remains zero since the director is parallel to the vorticity direction at $\dot{\gamma}^*$=1. Increasing the magnetic field at H_x*=2.0×10^{-6}, the polar angle θ of the director at beginning keeps 0^o, and then suddenly becomes 90^o. It shows that the director doesn't continuously rotate into the shear plane from the vortictity direction. As we known a biaxial nematic must be described by two directors that are mutually perpendicular; the longest axis of the molecule tends to be parallel to one of the directors, the second longest axis is parallel to the other director. Figures 3.11 show the schematics of the molecular deformation under the magnetic field and the shear flow along the *x*-axis. The ellipse in the origin represents a rodlike molecule of LCPs. At *t**=0 the longest axis of the molecule is along the *z*-axis and suppose that the second axis of it is parallel to the *x*-axis. The molecules are deformed with time, which caused mainly by the effect of the magnetic field since the shear rate is so small that it can not deform the molecule which can be proved when H_x*=0 in Figure 3.10. As can be seen from Figures 3.11, the longest axis along the *z*-axis becomes shorter and shorter; on the contrary, the second longest axis along the *x*-axis becomes longer and longer, then finally is changed into the longest one. As a result, the

director suddenly becomes to be parallel to the direction of the magnetic field, namely, the *x*-axis. This course also can be reflected by the changing of the scalar parameter *S* with time because when the molecule becomes a sphere, the scalar parameter *S* is near zero resulting from reaching an isotropic phase. Figure 3.12 shows out the result just like what we speculated on the course of molecular deformation in Figures 3.11. When H_x*=0 and 1.5×10^{-6}, *S* is a constant because of the log-rolling orientation represented in the two cases. However, when the magnetic field is increased at 2×10^{-6}, *S* decreases slowly and a very small value is arrived, which shows the isotropic phase due to the deformation of molecules under the magnetic field, and then quickly becomes a high value, which shows that the deformed molecules are parallel to the direction of the magnetic field. And also we can see that *S* increases with the magnetic field. In order to investigate the strength of LCPs along the flow, Figures 3.12 represent S_{xx} changes with time at $\dot{\gamma}^*$=1 for H_x*=0 and 2×10^{-6}. When H_x*=0, the value of S_{xx} is very small resulting from molecules almost along the voiticity direction. When we increase the magnetic field at 2×10^{-6}, S_{xx} increases slightly at first time, and then suddenly becomes a very high value.

We directly increase the shear rate into a higher range since a small shear rate can not affect the log-rolling orientation. Figure 3.13 shows S_2 as a function of time changes with the magnetic field at $\dot{\gamma}^*$=10. When H_x*=0, the shear plane is an attractor for the director because the stronger shear rate results in the deformation of molecules as explained by Figures 3.11. The magnetic filed is applied and increased from 1.5×10^{-6} to 2×10^{-6}. The director is accelerated to be close by the shear plane as can be seen from the changes of S_2 after adding the magnetic field along the *x*-axis. If the strength of the magnetic field is increased again, it can shorten the time that the director is aligned to be parallel to the shear plane; in addition, a higher orientational state can be arrived where most molecules will be controlled to be aligned along the direction of the magnetic field as well as the direction of the flow. Figures 3.14 give out the scalar parameter *S* and S_{xx} changes with time at $\dot{\gamma}^*$=10 for H_x*=0, $1.5\times10^{-6}$and 2×10^{-6}. We can see *S* decreases at first and increases again for all the cases, which also reflect the molecular deformation caused by the high shear rate and the magnetic field. With the increasing strength of the magnetic field *S* also increases. On the other hand, although S_{xx} is low at the beginning due to the log-rolling orientation state at the initial state, it increases very quickly with time because molecules are aligned along the flow direction under the effect of the torques caused by the shear flow and the magnetic field. With increasing the magnetic field S_{xx} also is increased.

During the LCP process it hopes that the molecular alignment can be improved

after applying the magnetic field. In order to investigate the effect of the magnetic field on it, the time-averaged $\bar{S}$ and $\bar{S}_{xx}$ changing with the magnetic field at $\dot{\gamma}^*$=1,10,100 are plot in Figures 3.15. When $\dot{\gamma}^*$=1, the director keeps the log-rolling orientation state if the magnetic field is smaller than 1.5×10^{-6}. However, when the magnetic field is larger than it, the director is confined into the shear plane in a short time, and then is parallel to the *x*-axis. Therefore, the time-averaged $\bar{S}$ increases quickly with the magnetic field. When $\dot{\gamma}^*$=10 and 100, the shear plane is the attractor even without the magnetic field. The final state of the director shows an aligning where the director is along the *x*-axis. The time-averaged $\bar{S}$ increases apparently when the magnetic field is larger than 2×10^{-6} at $\dot{\gamma}^*$=10. However, when $\dot{\gamma}^*$=100, the effect of the magnetic field on $\bar{S}$ is not evident in the magnetic field strength range chose by this paper. It can be seen that the time-averaged $\bar{S}_{xx}$ is very small near to zero and decreases continuously toward the minimum value at $H_x^*=1.5\times10^{-6}$, and then suddenly changes into a big value at $H_x^*=2\times10^{-6}$ when $\dot{\gamma}^*$=1. After that $\bar{S}_{xx}$ smoothly increases with the magnetic field. As the shear rate increases at $\dot{\gamma}^*$=100 the evident effect of the magnetic field chose by this part can not be observed.

Figures 3.16 describe the time-averaged $\bar{S}$ and $\bar{S}_{xx}$ changes with the shear rate when the magnetic field is considered as a parameter. As the shear rates increases $\bar{S}$ decreases at first time, and then slowly increases for all the cases at H_x^*=0, 1.5×10^{-6}, 2×10^{-6}, 3×10^{-6}. At low shear rates if the strength of the magnetic field is not stronger enough to rotate the director into the shear plane $\bar{S}$ will be smaller than the one at H_x^*=0 due to the molecular deformation as can be shown in Figures 3.16 at $H_x^*=1.5\times10^{-6}$. Also a discontinuous is observed at H_x^*=0, 1.5×10^{-6} corresponding to the boundary between the log-rolling orientation and the aligning state along the *x*-axis. When the magnetic field is increased at 2×10^{-6} and 3×10^{-6}, the discontinuousness disappears since the torque caused by the magnetic field is so strong that the shear plane becomes the attractor even the director along the vorticity direction at the initial state. The time-averaged $\bar{S}_{xx}$ increases with the increasing strength of the magnetic field. At low shear rates $\bar{S}_{xx}$ is very small due to the log-rolling orientation state at H_x^*=0, 1.5×10^{-6}, and then suddenly becomes a high value. This discontinuousness also indicates the boundary between the log-rolling orientation state and the aligning along the *x*-axis.

From these simulation results it can be made a conclusion that when the initial state of the director is along the vorticity direction, a log-rolling orientation can be detected in the tumbling range of the shear rate. The method applying the magnetic field along the flow direction in LCP process can reduce the log-rolling orientation; at

the same time the molecular alignment is controlled to align the direction of the magnetic field.

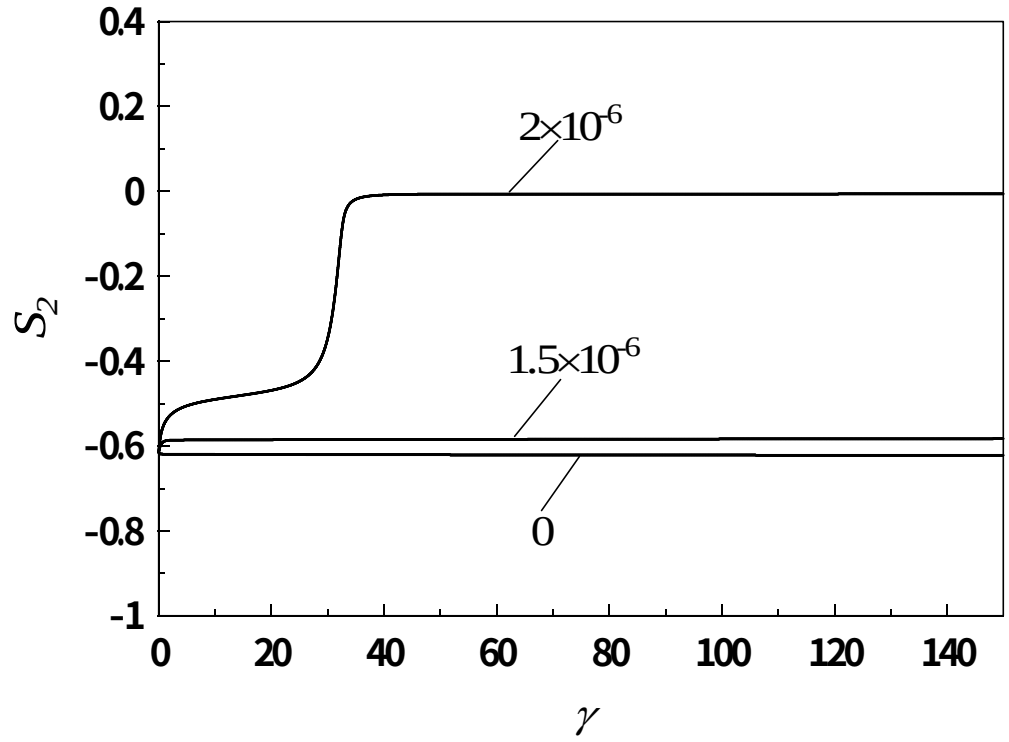

Figure 3.9 S_2 versus strain at $\dot{\gamma}^*$ =1 for β=1.0 when H_x^*=0, 1.5×10^{-6}, and 2×10^{-6}.

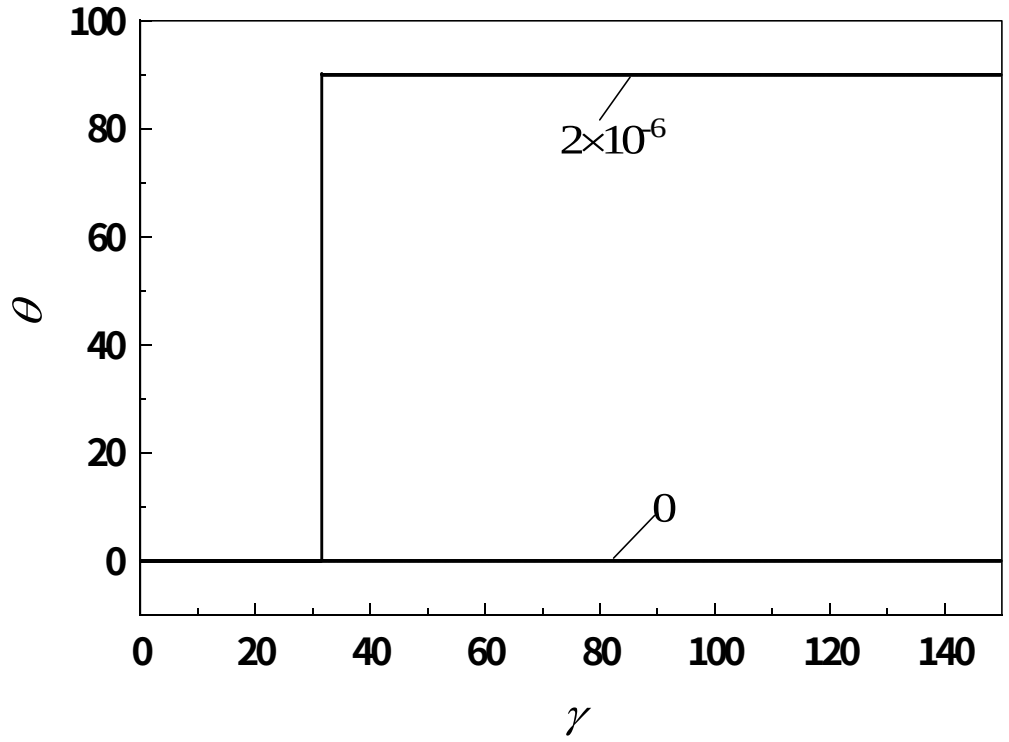

Figure 3.10 Polar angle θ versus strain at $\dot{\gamma}^*$ =1 for β=1.0 when H_x^*=0 and 2×10^{-6}.

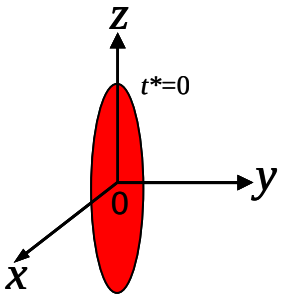

(a)

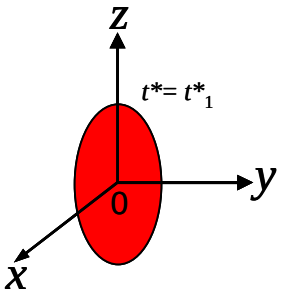

(b)

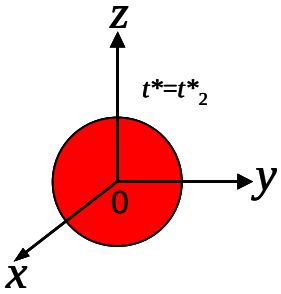

(c)

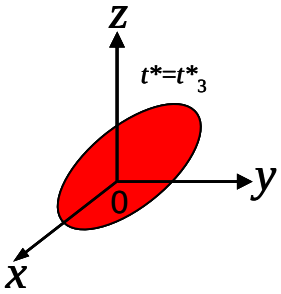

(d)

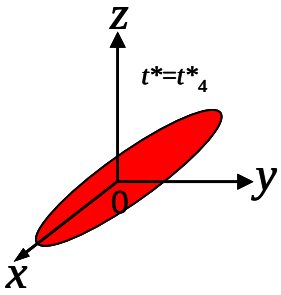

(e)

Figures 3.11 Schematics of the molecular deformation under the magnetic field and the shear flow along the *x*-axis.

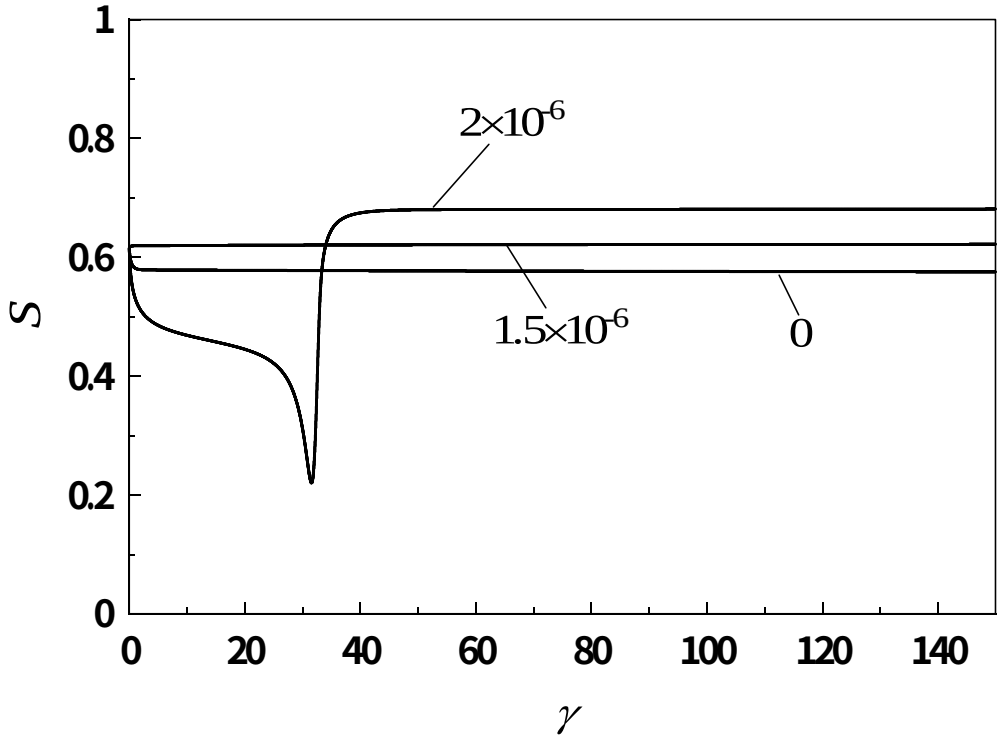

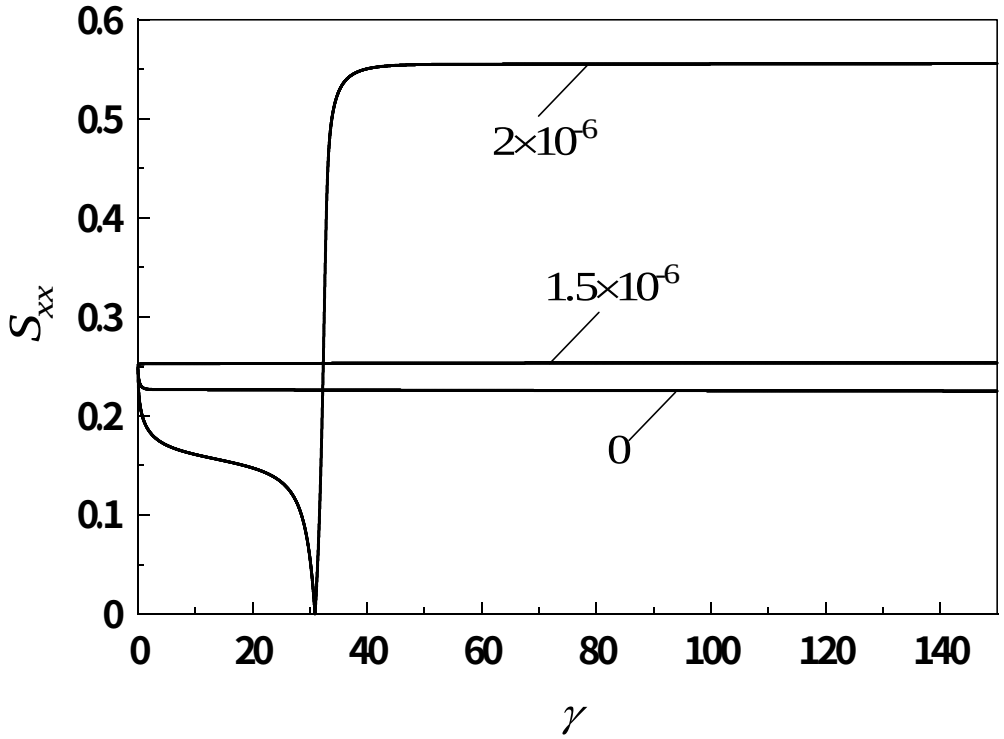

Figures 3.12 Transient behaviors of scalar order parameter S and S_{xx} versus strain at $\dot{\gamma}^*$=1 for β=1.0 when H_x^*=0, 1.5×10^{-6}, and 2×10^{-6}.

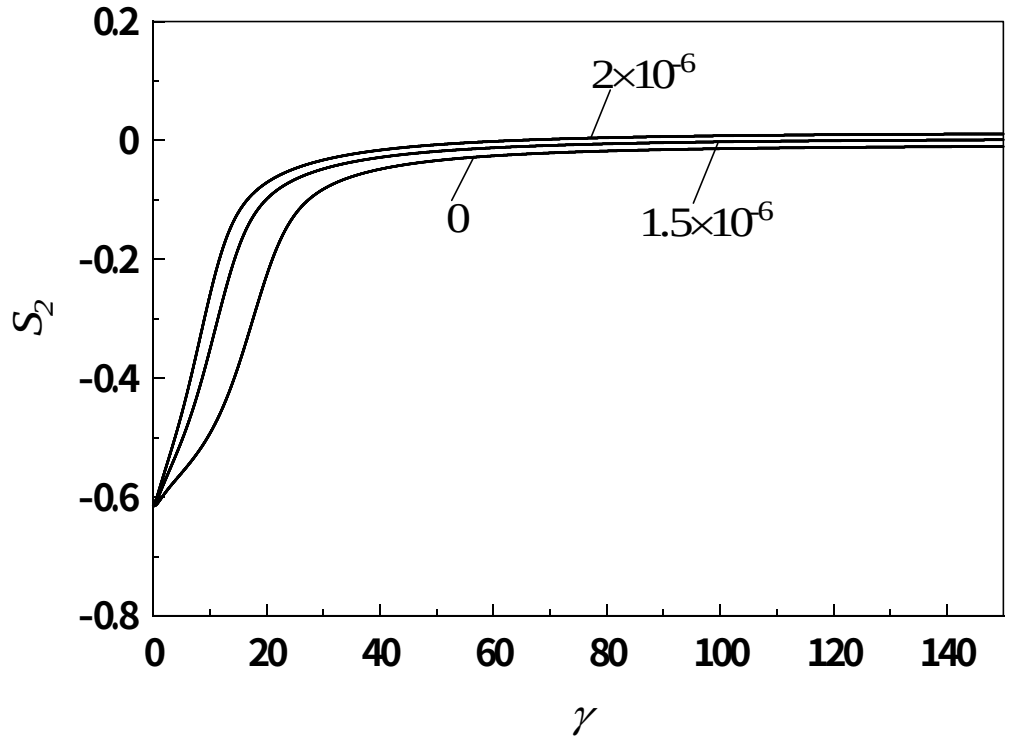

Figure 3.13 S_2 versus strain at $\dot{\gamma}^*$ =10 for β=1.0 when H_x^*=0, 1.5×10^{-6}, and 2×10^{-6}.

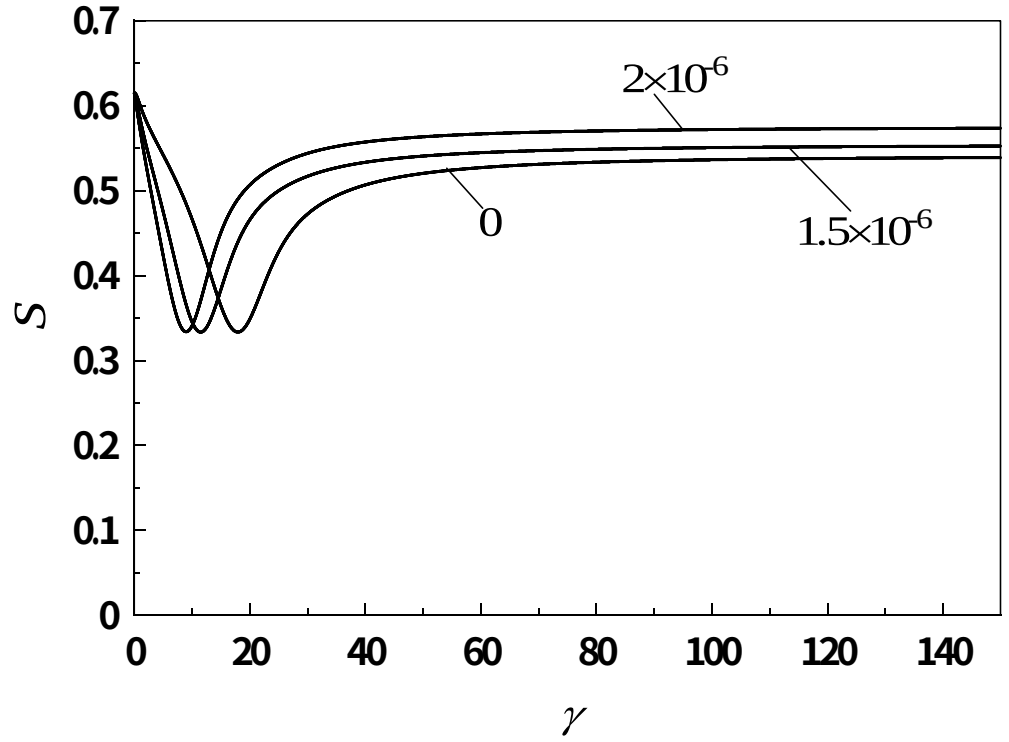

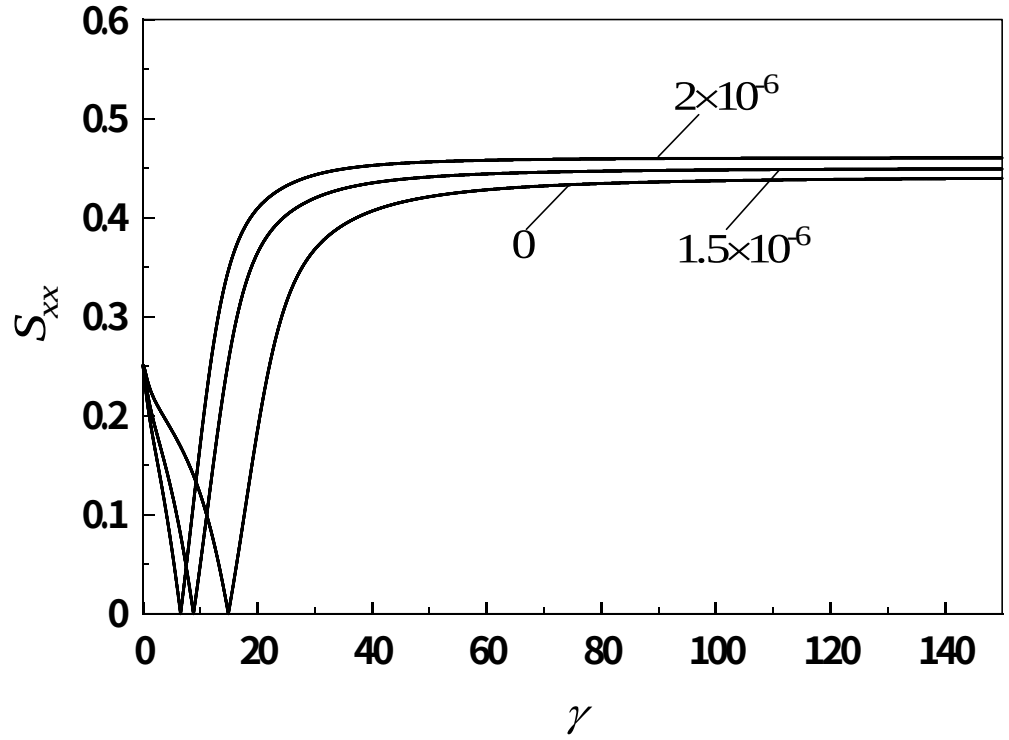

Figures 3.14 Transient behaviors of scalar order parameter S and S_{xx} versus strain at $\dot{\gamma}^*$=10 for β=1.0 when H_x^*=0, 1.5×10^{-6}, and 2×10^{-6}.

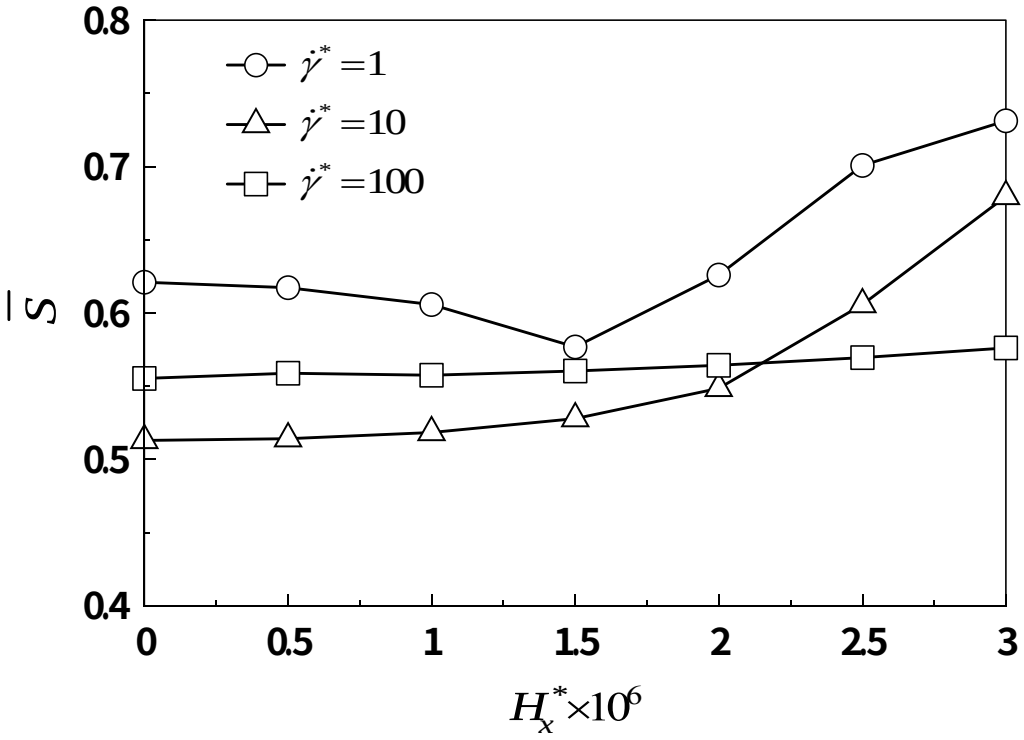

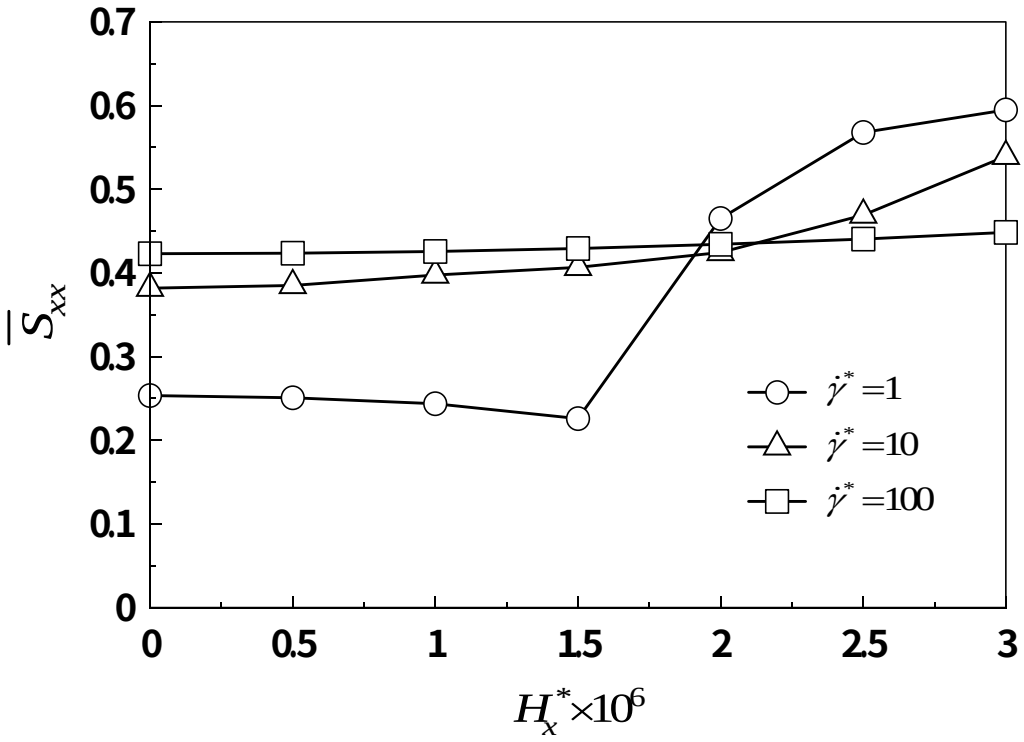

Figures 3.15 Effect of magnetic field parallel to the *x*-axis on average scalar order parameter $\bar{S}$ and $\bar{S}_{xx}$ at $\dot{\gamma}^*$=1, 10, 100 for β=1.0.

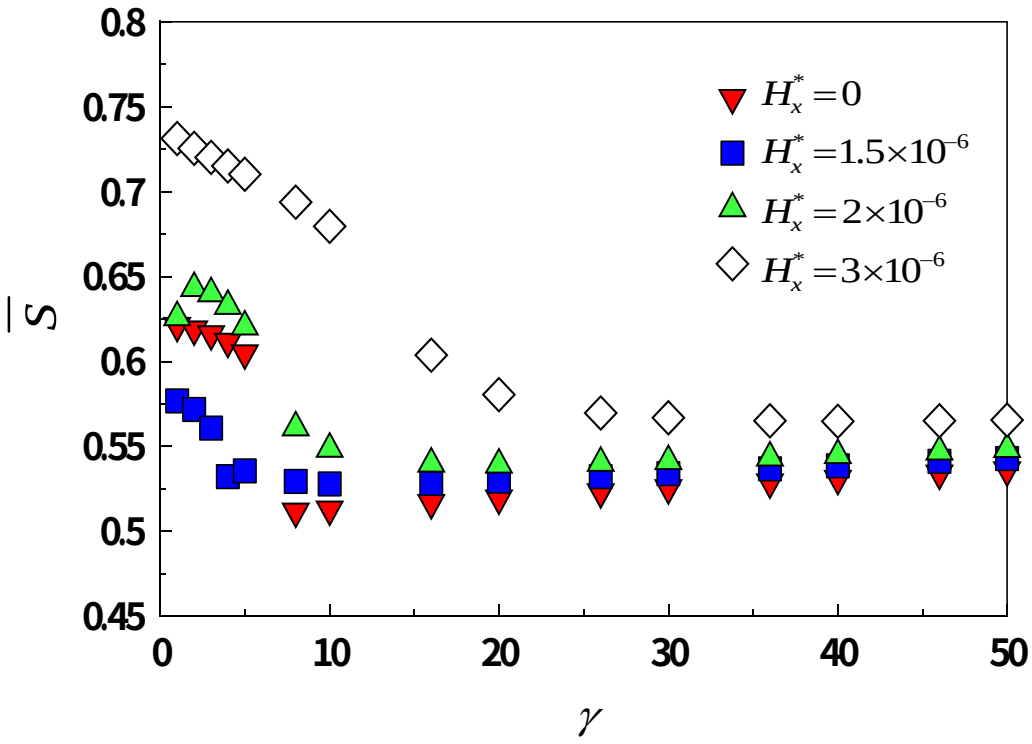

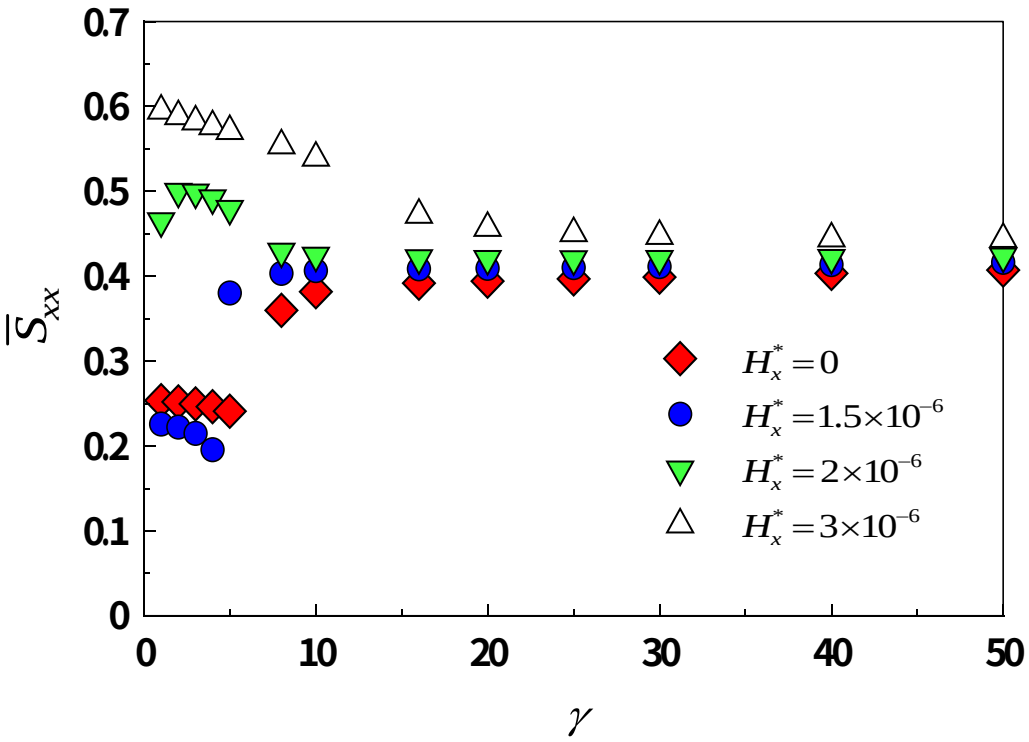

Figures 3.16 Average order parameter $\overline{S}$ and $\overline{S}_{xx}$ as a function of shear rate forβ=1.0 at H_x^*=0, 1.5×10^{-6}, 2×10^{-6}and 3×10^{-6}.

3.3.2.2 The Magnetic Field along the y-axis

In this section, the case that the magnetic field is imposed parallel to the velocity gradient direction is considered. Figure 3.17 shows that S_2 as the function of time changes with the increasing strength of the magnetic field along the *y*-axis at $\dot{\gamma}^*$=1. The log-rolling orientation state also can be found when H_y*=0 and 1.5×10^{-6}. Further increasing the magnetic field at H_y*=2×10^{-6}, the molecules are deformed and aligned along the *x*-axis, which is indicated by the changes of S_2 with time. Because the direction of the flow is different from the one of the magnetic field, the final position of the director is decided by the comparison of the torques resulting from the flow and the magnetic field. If we hope that molecules have a tendency to align along the *y*-axis, the more magnetic field strength is needed. When H_y*=3×10^{-6}, S_2 directly becomes a very high value in a short time, which illustrates that the director is controlled to align along the *y*-axis by the torque caused by the magnetic field. Figure 3.18 shows that the scalar parameter *S* increases with the magnetic field. When H_y*=2×10^{-6} and 3×10^{-6}, *S* continually decreased toward the minimum because the rodlike molecules are deformed

into the spherical molecules by the stronger magnetic field. After that the director is aligned along the direction of the magnetic field as explained in Figure 3.11. Figure 3.19 describes the orbits of the director in a three dimensional space at H_y*=3×10^{-6}. When n_z=1 and n_x=n_y=0, the director is along the vorticity direction. When n_z=0, the tracks of the director in the shear plane show that the director almost is aligned along the *y*-axis. The discontinuous change of the director can be explained by the exchange of the two axes resulting from the molecular deformation as described in Figure 3.11.

We also increase the shear rate at a high value $\dot{\gamma}^*$=10 (Figure 3.20), where the shear plane becomes an attractor for the director when H_y*=0. Because the torque added along the *x*-axis becomes stronger with the increasing shear rate, S_2 doesn't reach a bigger value than the one at $\dot{\gamma}^*$=1 at H_y*=3×10^{-6}. Only further increasing the magnetic field, the torque caused by the magnetic field along the *y*-axis can conquer the torque caused by the flow along the *x*-axis so that the state where the molecules are parallel to the *y*-axis is obtained. Figure 3.21 presents that the scalar parameter *S* increases with the strength of the magnetic field, and the minimum value indicates that the rodlike molecules are deformed. The tracks of the director affected by the flow and the magnetic field (H_y*=3×10^{-6}) are also showed out in Figure 3.22. The orbits of the director in the shear plane lie between the *x*-axis and the *y*-axis, which reflects the competition of the torques caused by the flow and the magnetic field.

The time-averaged $\bar{S}$ as the function of the shear rate at H_y*=0, 1.5×10^{-6}, 2×10^{-6} and 3×10^{-6} is described in Figure 3.23. We can see that $\bar{S}$ decreases at low shear rates, and only when H_y*=0, a discontinuous decrease is found, which is a boundary between the log-rolling orientation and the alignment in the shear plane.

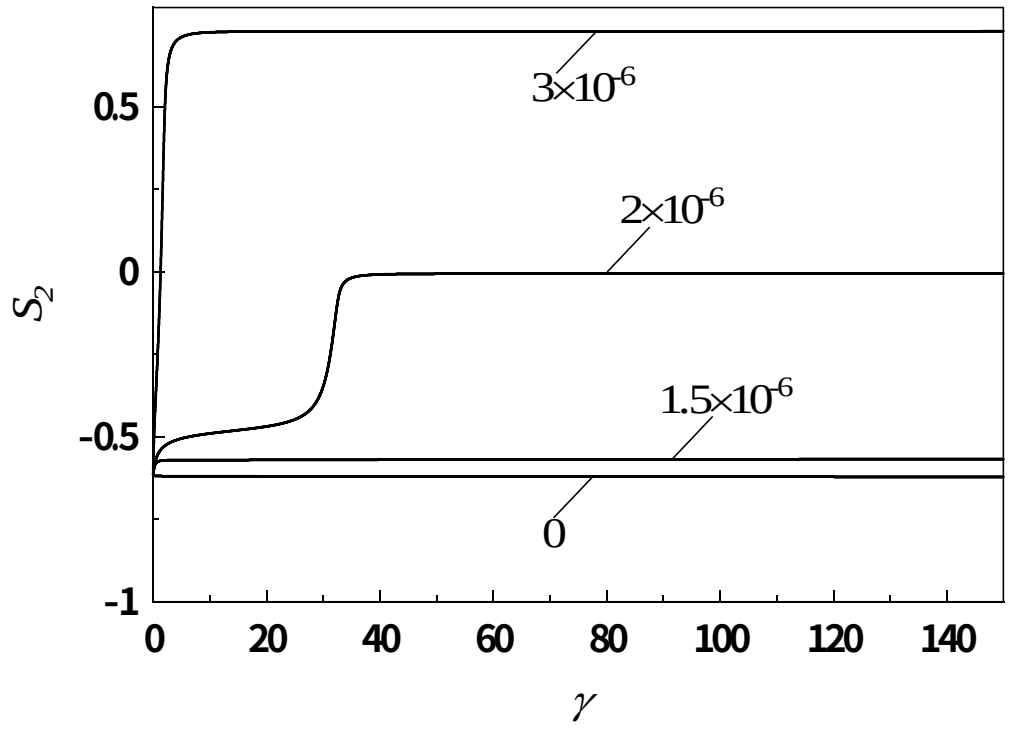

Figure 3.17 S_2 versus strain at $\dot{\gamma}^*$=1 for β=1.0 when H_y^*=0, 1.5×10^{-6}, 2×10^{-6}and 3×10^{-6}.

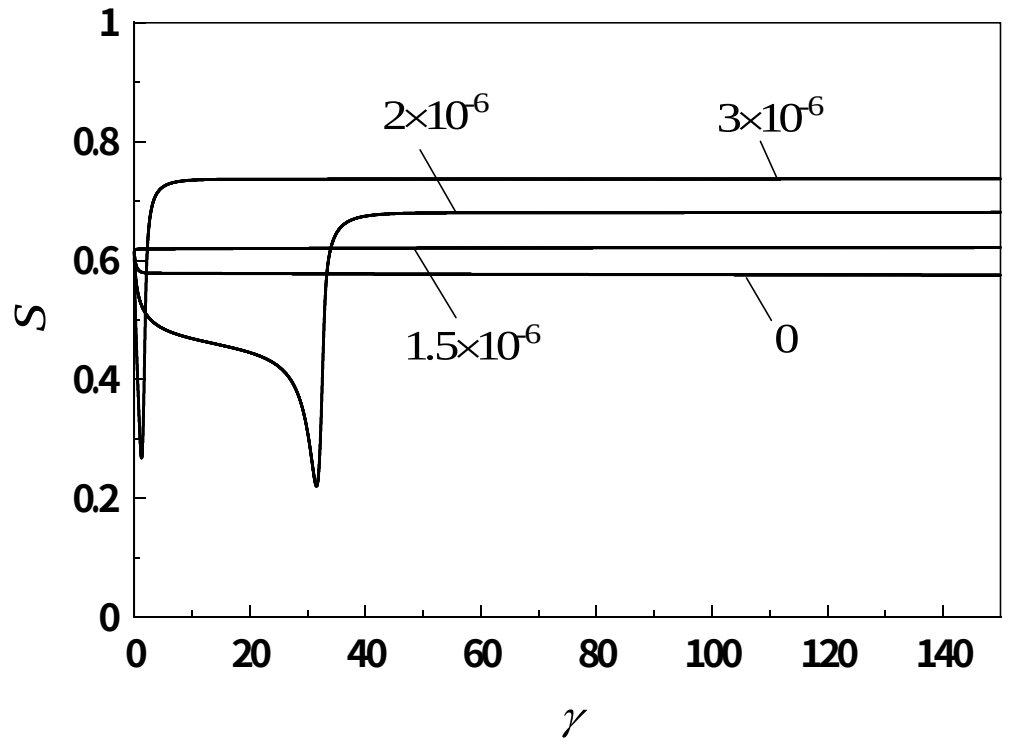

Figure 3.18 Transient behaviors of scalar order parameter S versus strain at $\dot{\gamma}^*$=1 for β=1.0 when H_y^*=0, 1.5×10^{-6}, 2×10^{-6}and 3×10^{-6}.

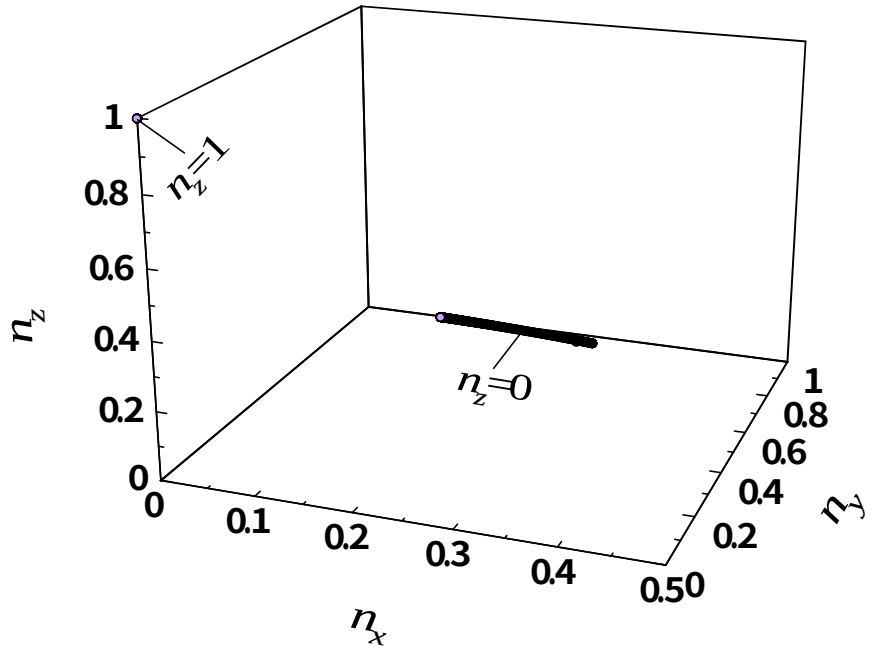

Figure 3.19 Orbits of the director in a three dimensional space at $\dot{\gamma}^*$=1 for β=1.0 when H_y*=3×10^{-6}.

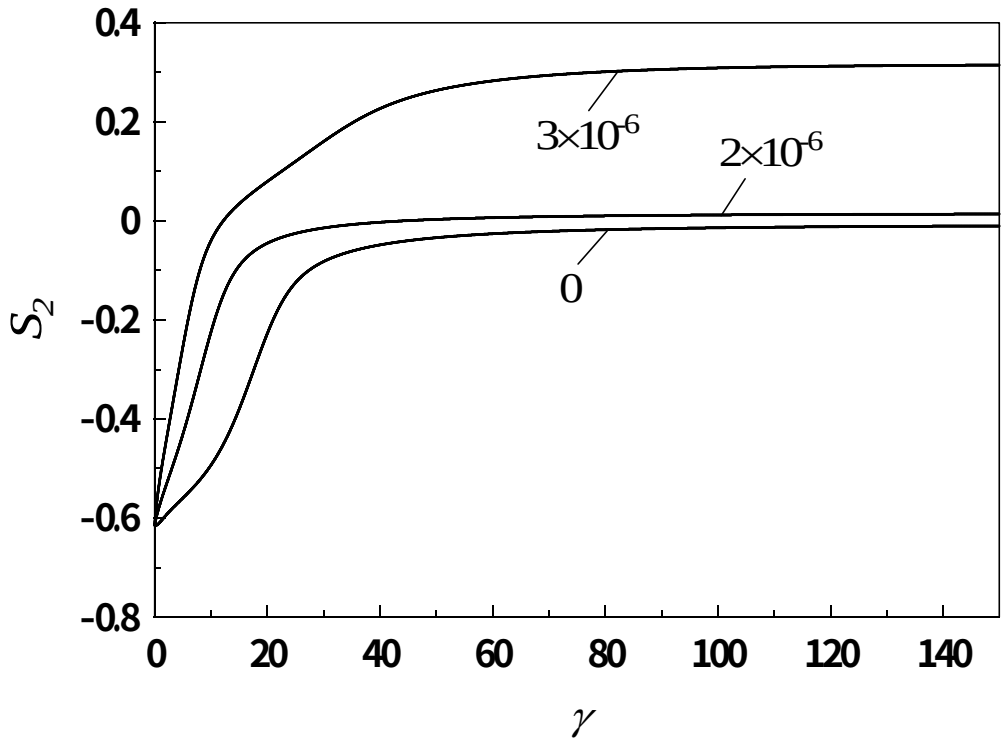

Figure 3.20 S_2 versus strain at $\dot{\gamma}^*$=10 for β=1.0 when H_y^*=0, 2×10^{-6}and 3×10^{-6}.

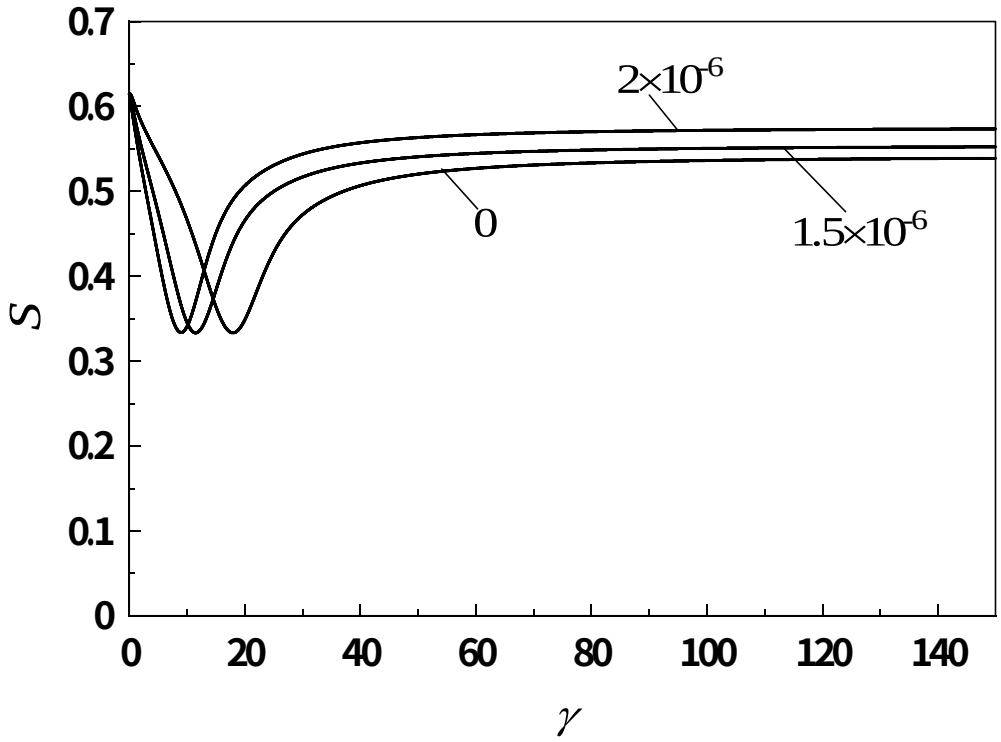

Figure 3.21 Transient behaviors of scalar order parameter S versus strain at $\dot{\gamma}^*$=10 for β=1.0 when H_y^*=0, $2\times10^{-6}$and 3×10^{-6}.

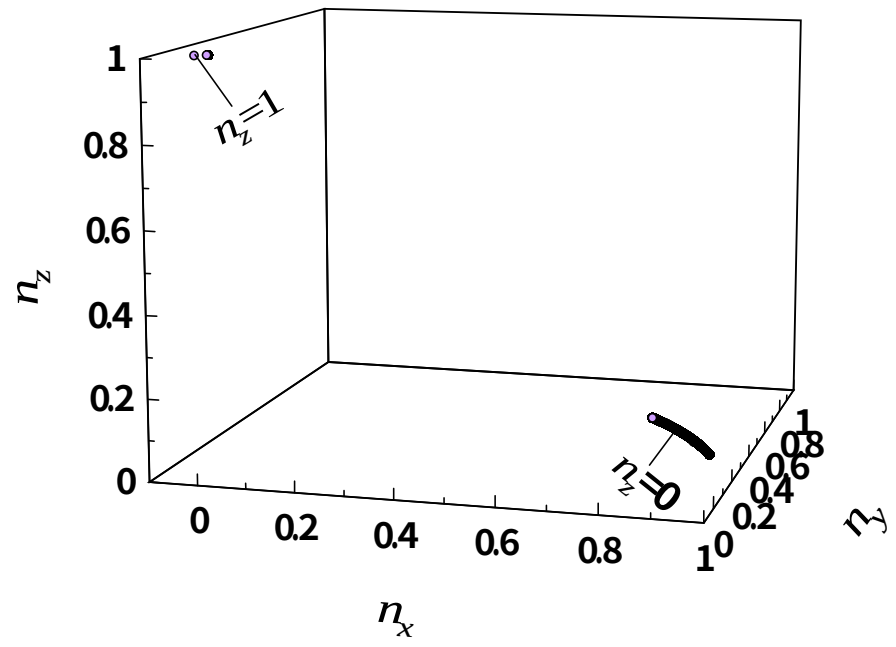

Figure 3.22 Orbits of the director in a three dimensional space at $\dot{\gamma}^*$=10 for β=1.0 when H_y*=3×10^{-6}.

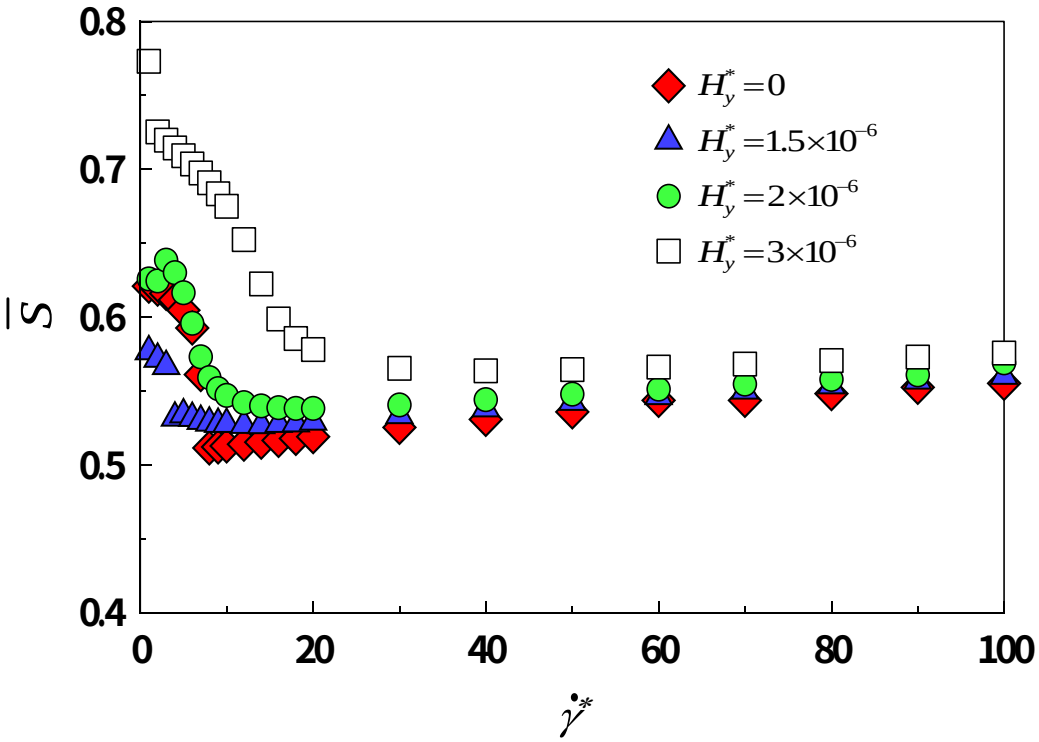

Figure3.23 Average order parameter $\bar{S}$ as a function of shear rate for β=1.0 at H_y^*=0, 1.5×10^{-6}, $2\times10^{-6}$and 3×10^{-6}.

3.3.3 Initial Position of the Director at φ=-50°

In this section, the director is set into the *x*-*z* plane at φ=-50°. Under the shear flow and the magnetic field the tracks of the director will be discussed. Also the degree of molecular alignment along the flow direction is investigated when the magnetic field is applied along the *x*-axis.

3.3.3.1 The Magnetic Field along the *x*-axis

We will consider in this part that the direction of the torque caused by the magnetic field is same with the one caused by the shear flow. Figure 3.24 shows S_2 changes with time at $\dot{\gamma}^*$=1 for H_x*=0 and 1.5×10^{-6}. When H_x*=0, S_2 reduces and reaches a steady state at $-S_{eq}$. The vorticity direction is an attractor for the director because the force coming from the shear flow is weaker so that it can not control the director to align along it. However, after applying the magnetic field, the torque controlling the director to align along the *x*-axis is reinforced. As can be seen from

Figure 3.24 S_2 becomes zero in a short time under the magnetic field at $H_x^*= 1.5\times10^{-6}$. The scalar parameter S and S_{xx} also increases with the magnetic field represented in Figures 3.25. Due to the log-rolling orientation state at $H_x^*=0$ S_{xx} describing the molecular alignment along the x-axis is very small, however, it becomes very high under the force of the magnetic field when $H_x^*= 1.5\times10^{-6}$.

With the increasing shear rate at $\dot{\gamma}^*=2$ the shear plane becomes an attractor for the director as shown as in the Figure 3.26, where S_2 will oscillate between $0\sim S_{eq}$ even $H_x^*=0$. The director can not be controlled to align along the direction of the shear flow since the torque caused by the flow is not stronger enough. In order to tailor the properties of LCPs the alignment of the director must be freely decided in terms of the strength of the magnetic field. The magnetic field, $H_x^*= 1.5\times10^{-6}$, is added on the director along the shear flow, then the director ceases the oscillation in the shear plane and aligns along the direction of the shear flow and the magnetic field, namely, the x-axis. The scalar parameter S and S_{xx} are presented in Figures 3.27, where the aligning state is arrived at $H_x^*=1.5\times10^{-6}$. In addition, the degree of molecular alignment along the x-axis increases with the magnetic field as can be seen from the changes of S_{xx} with time.

When the shear rate is increased at 6, the director is controlled to be parallel to the x-axis by the shear flow described by Figure 3.28 at $H_x^*=0$. After applying the magnetic field (1.5×10^{-6}) along the x-axis, the exchange of two axes is accelerated and much higher orientational state can be arrived. S increases with the increasing magnetic field and the minimum value of it hints the maximum deformation of molecules showed in Figures 3.29.

The time-averaged $\overline{S}$ and $\overline{S}_{xx}$ as the function of the magnetic field are plot in Figures 3.30 at $\dot{\gamma}^*=1$, 10, 100. $\overline{S}$ slightly decreases at $\dot{\gamma}^*=1$ when H_x^* is smaller than 1×10^{-6} since the anisotropy of the rodlike molecules is reduced when the director keeps the log-rolling orientation state. After that $\overline{S}$ will increases with the magnetic field. The apparent changes of $\overline{S}$ with the magnetic field chose by this part can not be found as increasing the shear rate. $\overline{S}_{xx}$ is near to zero at $\dot{\gamma}^*=1$ when H_x^* is smaller than 1×10^{-6} because the log-rolling orientation state is remained. As the increasing magnetic field $\overline{S}_{xx}$ quickly increases and reaches a high value. With the increasing shear rate the excellent effect of the magnetic field on it can not be observed in the scope chose by this part.

The time-averaged $\overline{S}$ and $\overline{S}_{xx}$ as the function of the shear rate also is investigated in Figures 3.31 at $H_x^*=0$, 2×10^{-6}, 3×10^{-6}. For all the cases $\overline{S}$ decreases at first, and then slowly increases with the shear rate. When $H_x^*=0$, a discontinuousness is detected as

the boundary of a log-rolling orientation state and an aligning state along the magnetic field. As the increasing magnetic field $\bar{S}$ also increases with the shear rate. At low shear rates because of the log-rolling orientation state at H_x*=0, the molecular alignment is very low, with increasing the shear rate $\bar{S}_{xx}$ becomes bigger and bigger due to the stronger torque caused by the shear rate. $\bar{S}_{xx}$ also increases with the increasing strength of the magnetic field.

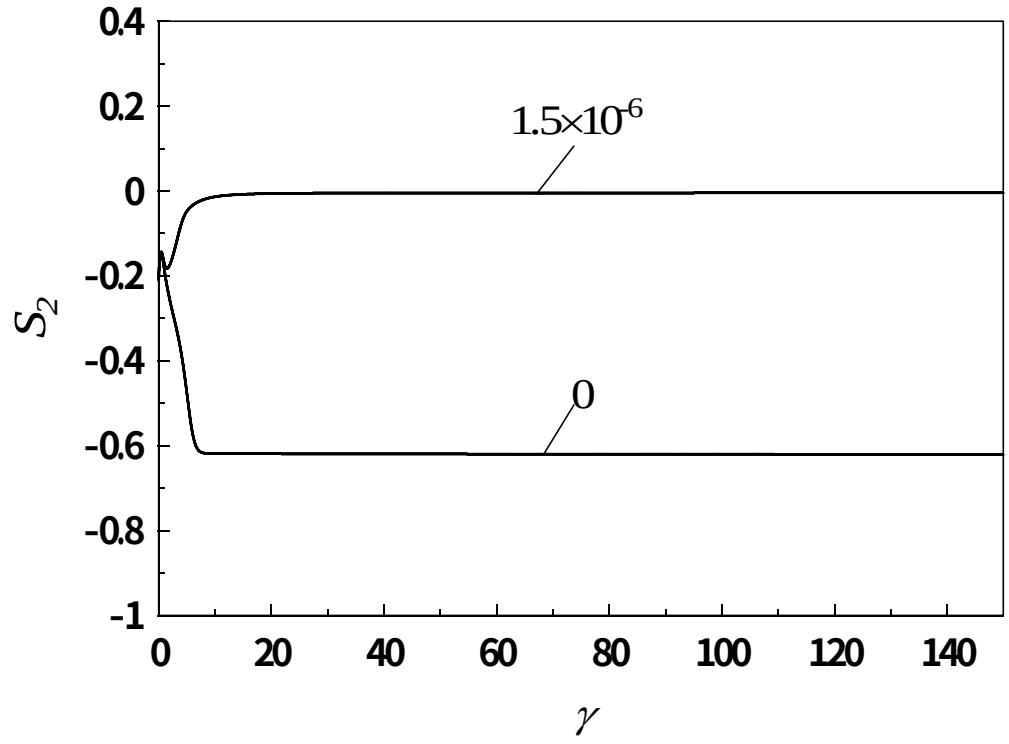

Figure 3.24 S_2 versus strain at $\dot{\gamma}^*$=1 for β=1.0 when H_x^*=0, and 1.5×10^{-6}.

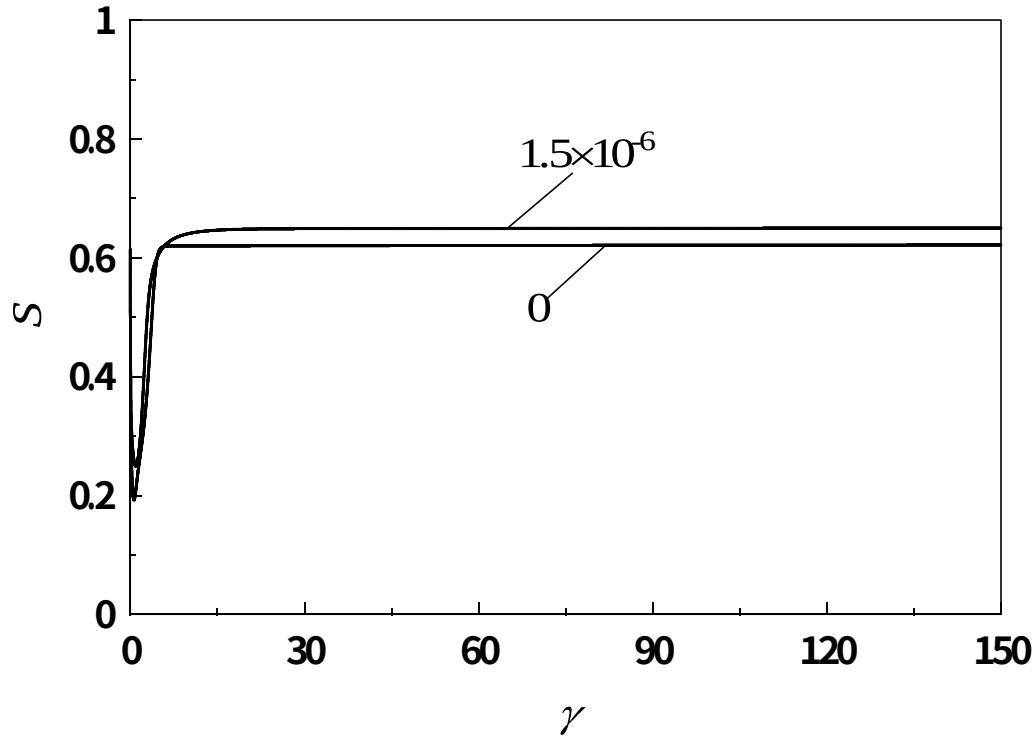

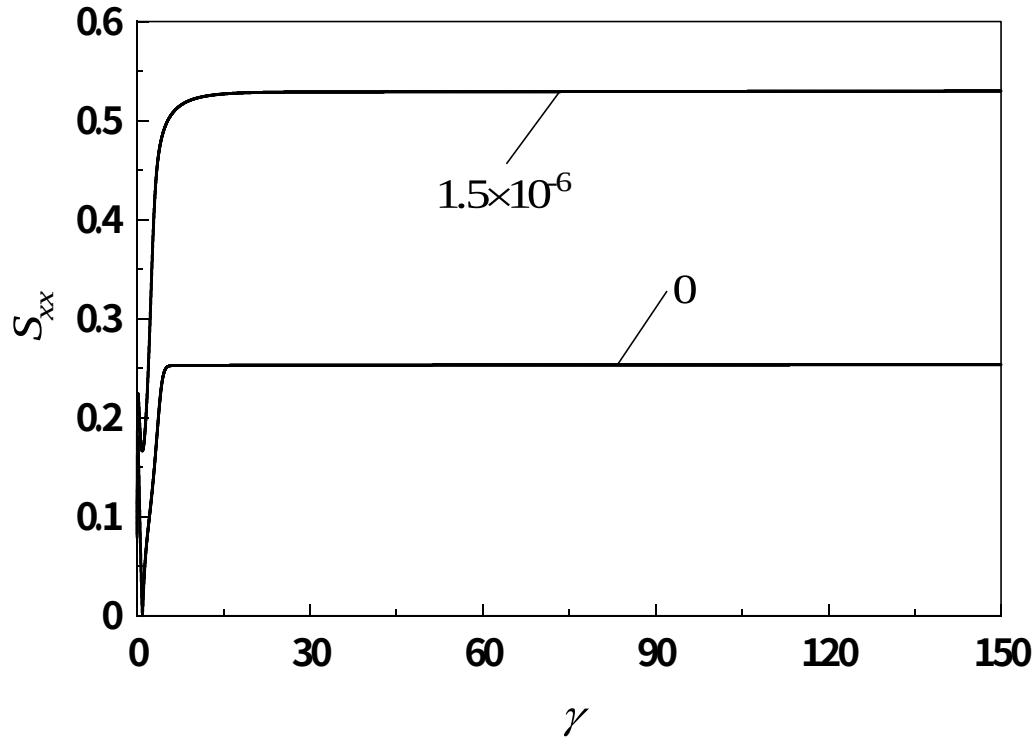

Figures 3.25 Transient behaviors of scalar order parameter S and S_{xx} versus strain at $\dot{\gamma}^*$=1 for β=1.0 when H_x^*=0, and 1.5×10^{-6}.

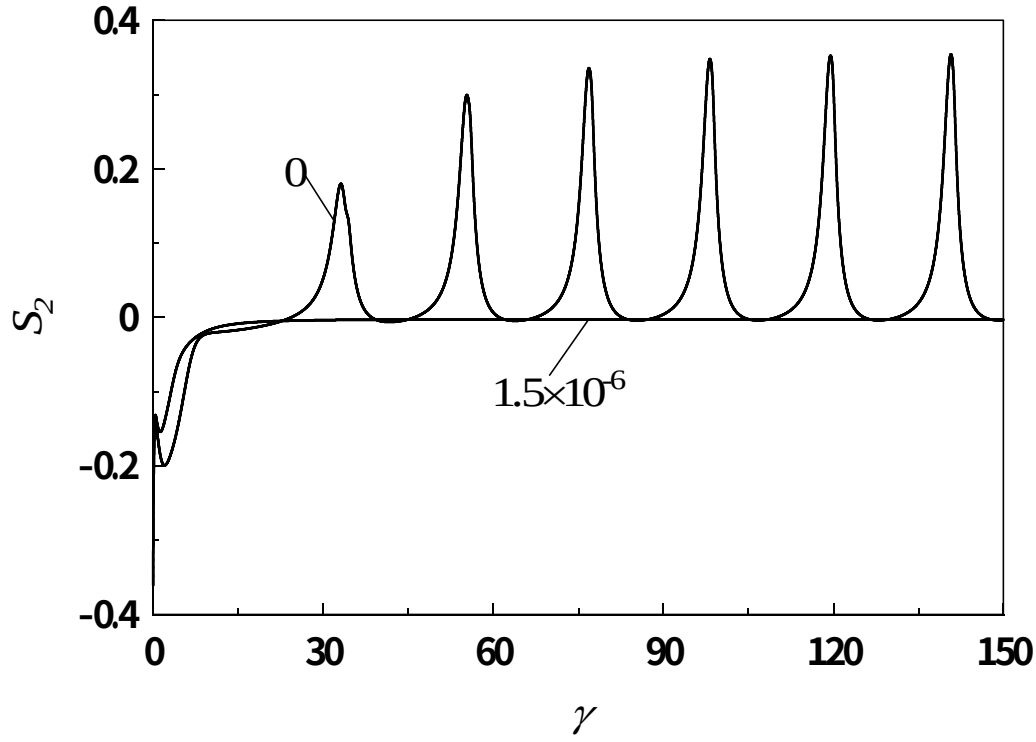

Figure 3.26 S_2 versus strain at $\dot{\gamma}^*$=2 for β=1.0 when H_x^*=0, and 1.5×10^{-6}.

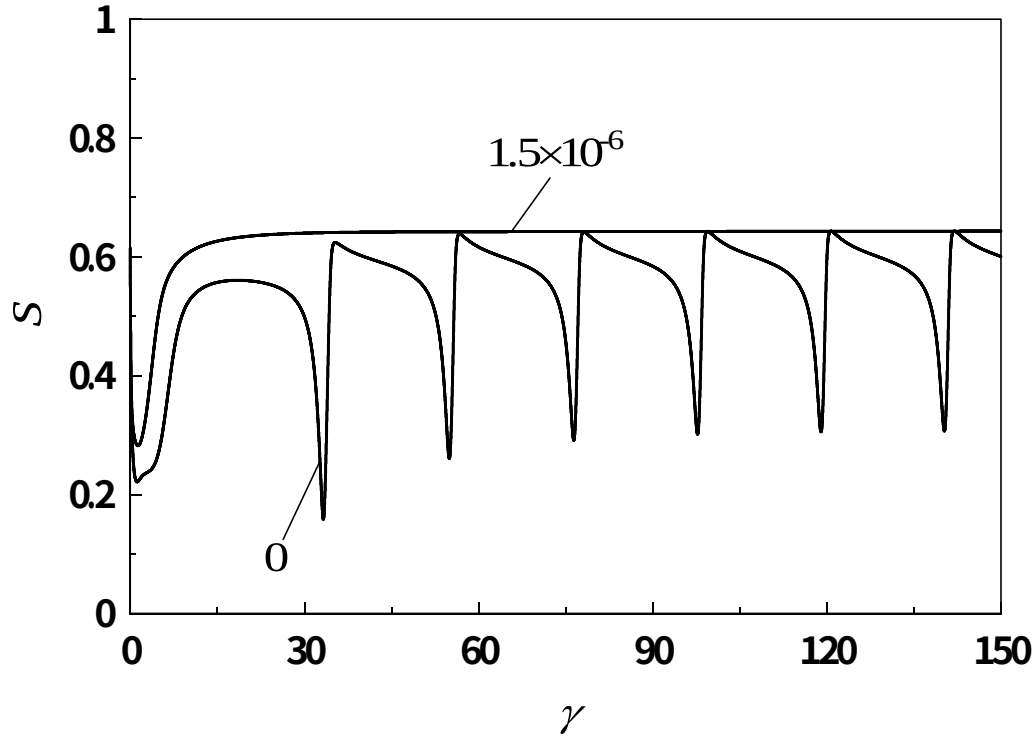

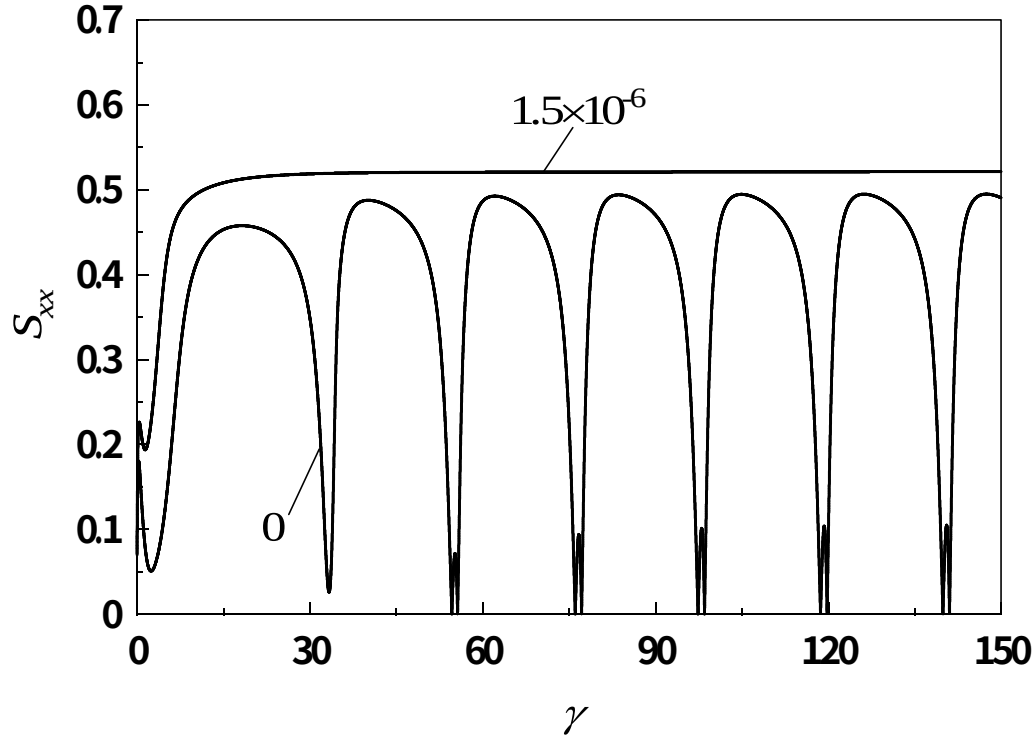

Figures 3.27 Transient behaviors of scalar order parameter S and S_{xx} versus strain at $\dot{\gamma}^*$=2 for β=1.0 when H_x^*=0 and 1.5×10^{-6}.

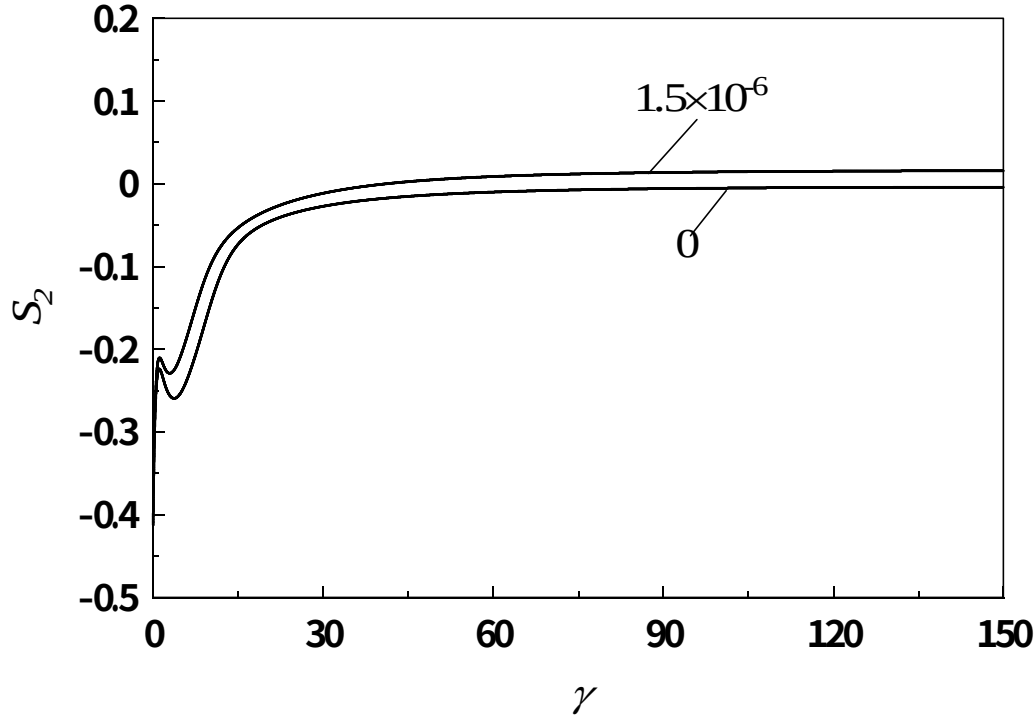

Figure 3.28 S_2 versus strain at $\dot{\gamma}^*$=6 for β=1.0 when H_x^*=0, and 1.5×10^{-6}.

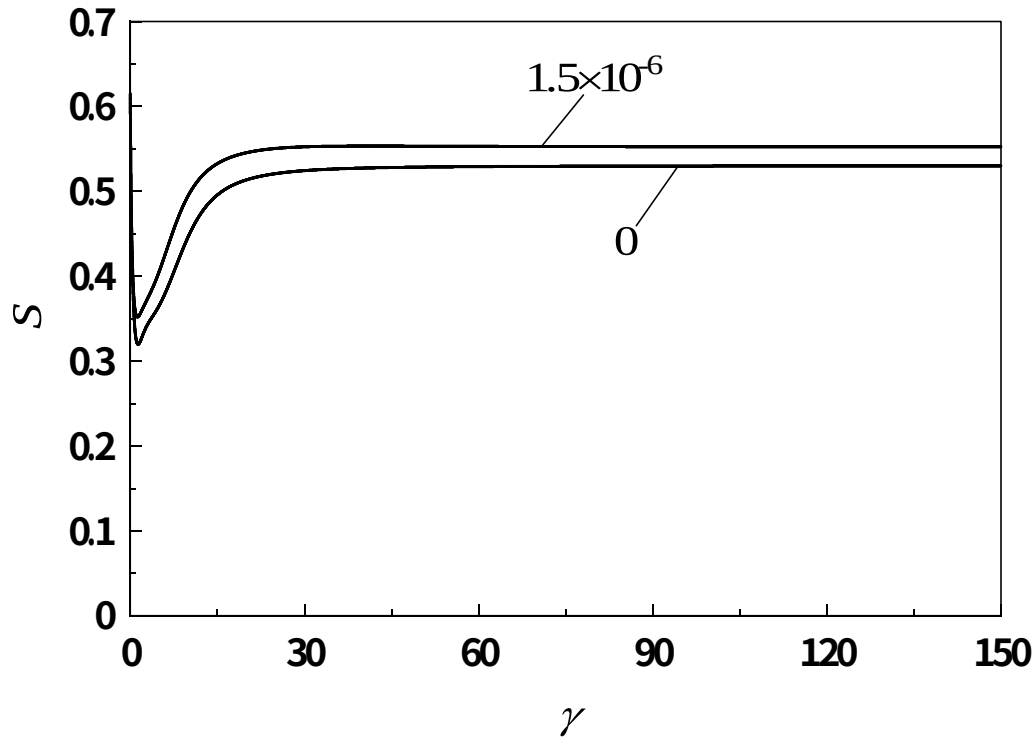

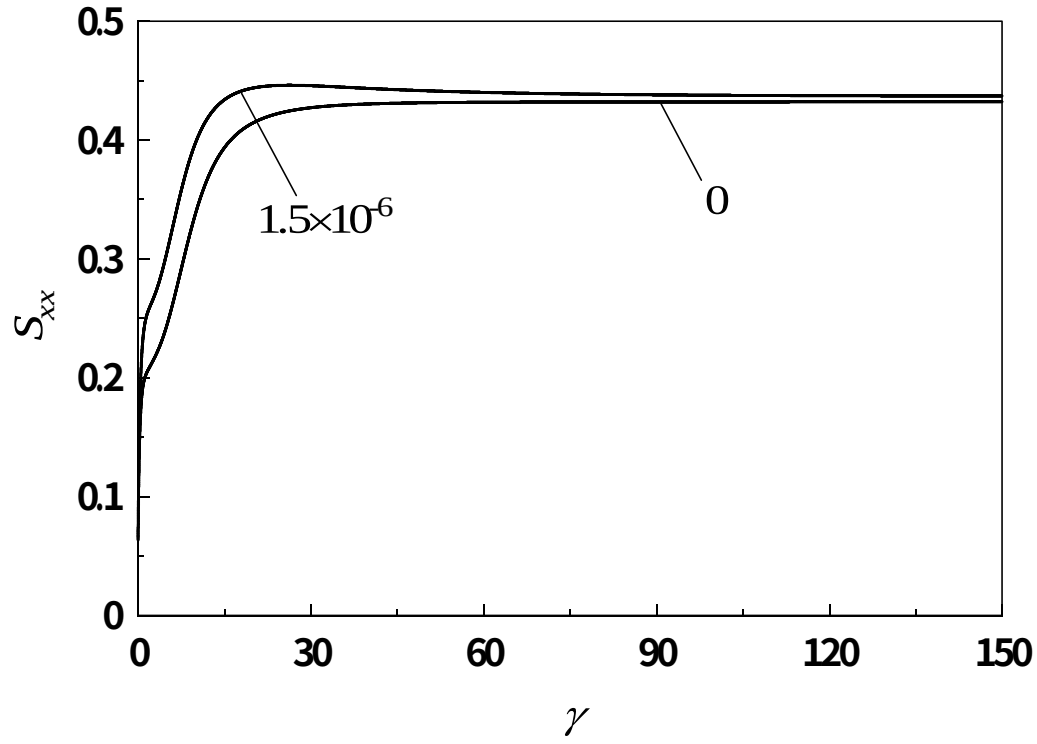

Figures 3.29 Transient behaviors of scalar order parameter S and S_{xx} versus strain at $\dot{\gamma}^*$=6 for β=1.0 when H_x^*=0 and 1.5×10^{-6}.

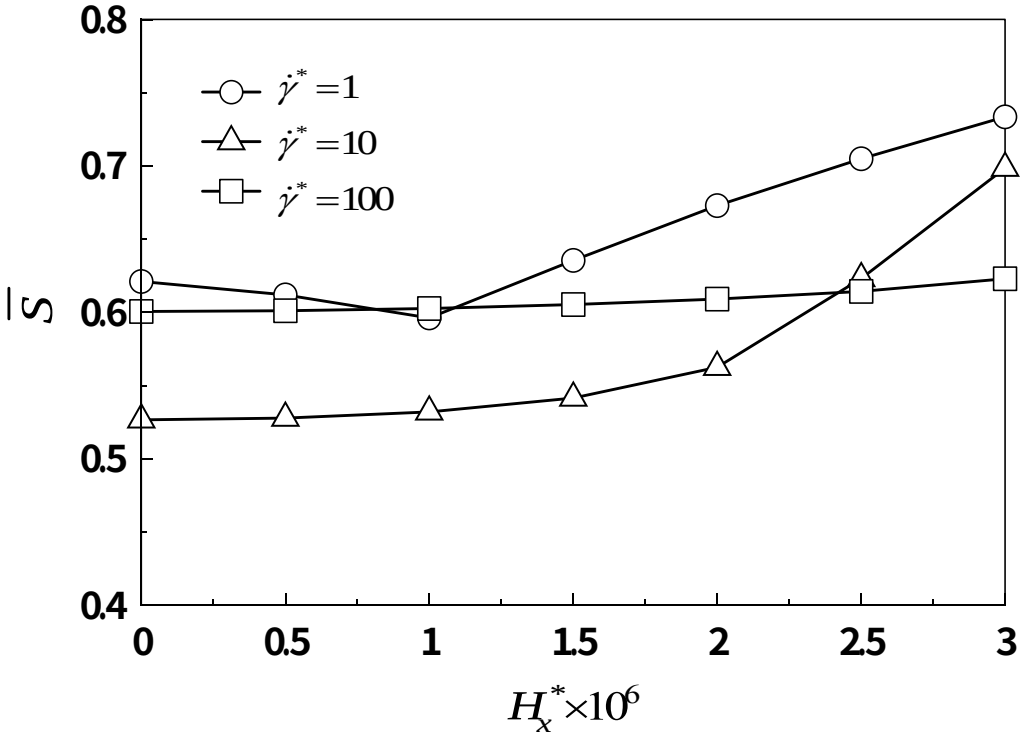

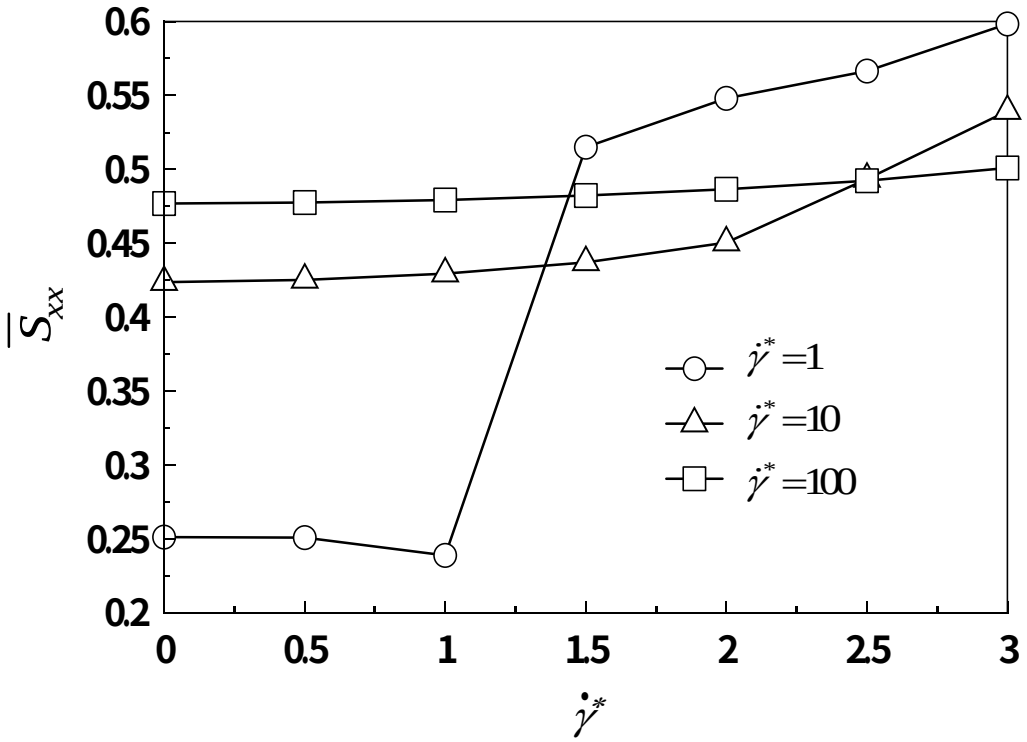

Figures 3.30 Effect of magnetic field parallel to the *x*-axis on average scalar order for β=1.0 parameter $\bar{S}$ and $\bar{S}_{xx}$ at $\dot{\gamma}^*$=1, 10, 100.

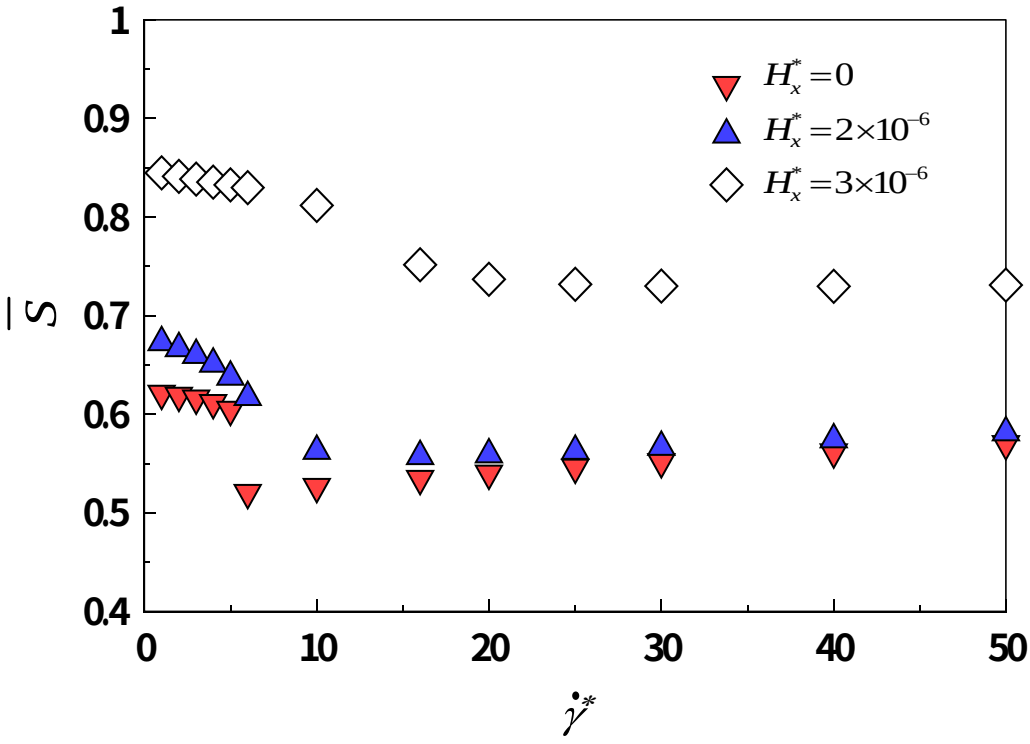

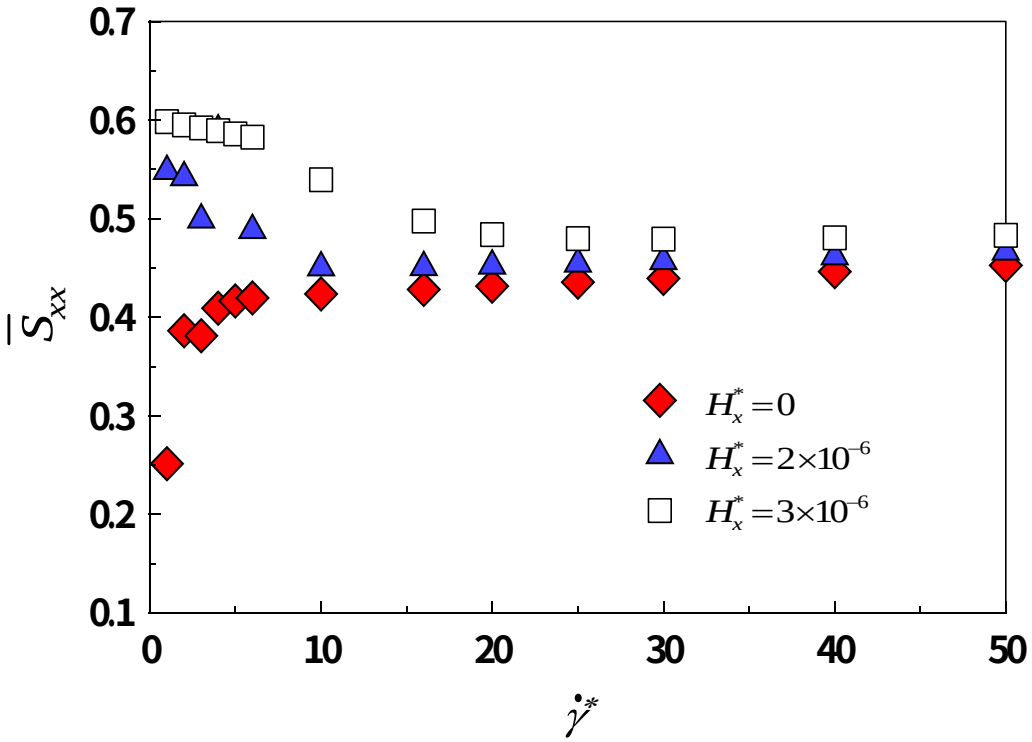

Figures 3.31 Average order parameter $\overline{S}$ and $\overline{S}_{xx}$ as a function of shear rate for β=1.0

3.3.3.2 The Magnetic Field along the *y*-axis

In this part, the effect of the magnetic field along the *y*-axis on the director is discussed. Figure 3.32 shows that S_2 changes with time at $\dot{\gamma}^*$=1 for H_y*=0, 1.5×10^{-6}, 2×10^{-6}. The director rotates into the vorticity direction without adding a magnetic field. When H_y*= 1.5×10^{-6}, S_2 increases and keeps a constant in the range of 0~S_{eq}. Increasing the strength of the magnetic field (H_y*=2×10^{-6}) again, the value of S_2 also is increased to be near S_{eq}. The alignment of the director can be controlled well according to the change of the magnetic field. The scalar parameter *S* versus the time is showed out in Figure 3.33, in which it increases with the magnetic field.

When $\dot{\gamma}^*$=2, we have already known that the director rotates into the shear plane and oscillates between the *x*-axis and the *y*-axis without adding the magnetic field. The effect of the magnetic field along the *y*-axis is plot in Figure 3.34. The oscillation of the director in the shear plane is eliminated by applying the magnetic field at H_y*= 1.5×10^{-6}, 2×10^{-6}. And at the same time the director also deviates from the direction of the shear flow to keep a steady state between the direction of the shear flow and the direction of the magnetic field. With the increasing strength of the magnetic field the director is

nearer to the direction of the magnetic field. Figure 3.35 describes S changes with the magnetic field as the function of the time.

Figure 3.36 shows the simulation results of S_2 at $\dot{\gamma}^*$=6 for H_y*=0, $1.5\times10^{-6}$and 2×10^{-6}. The shear plane becomes an attractor since the torque caused by the shear rate along the x-axis is strong enough. The more strength of the magnetic field is needed to control the director along the y-axis compared with the one of $\dot{\gamma}^*$=2. The changes of S with time at H_y*=0, $1.5\times10^{-6}$and 2×10^{-6} is described in Figure 3.37, in which S increases with the applying magnetic field.

The time-averaged $\bar{S}$ changing with the shear rate at H_y*=0, 1.5×10^{-6}, $2\times10^{-6}$and 3×10^{-6} is plot in Figure 3.38. $\bar{S}$ decreases at first time, and then slowly decreases with the shear rate. We can see with the increasing magnetic field $\bar{S}$ also increases.

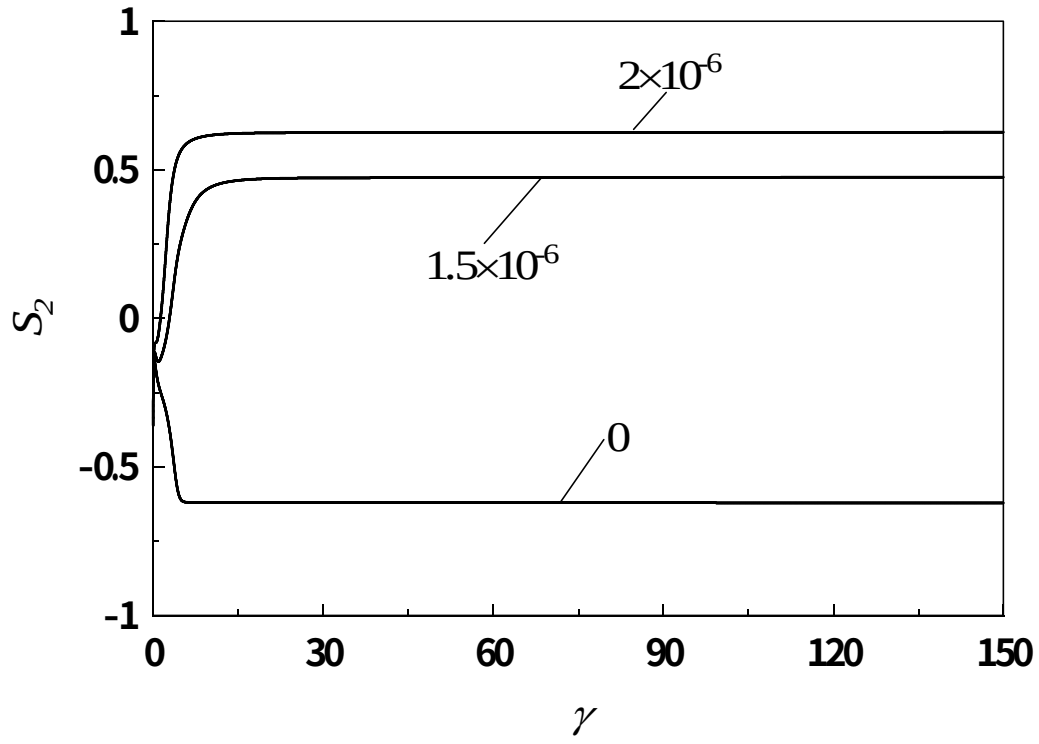

Figure 3.32 S_2 versus strain at $\dot{\gamma}^*$=1 for β=1.0 when H_y^*=0, 1.5×10^{-6} and 2×10^{-6}.

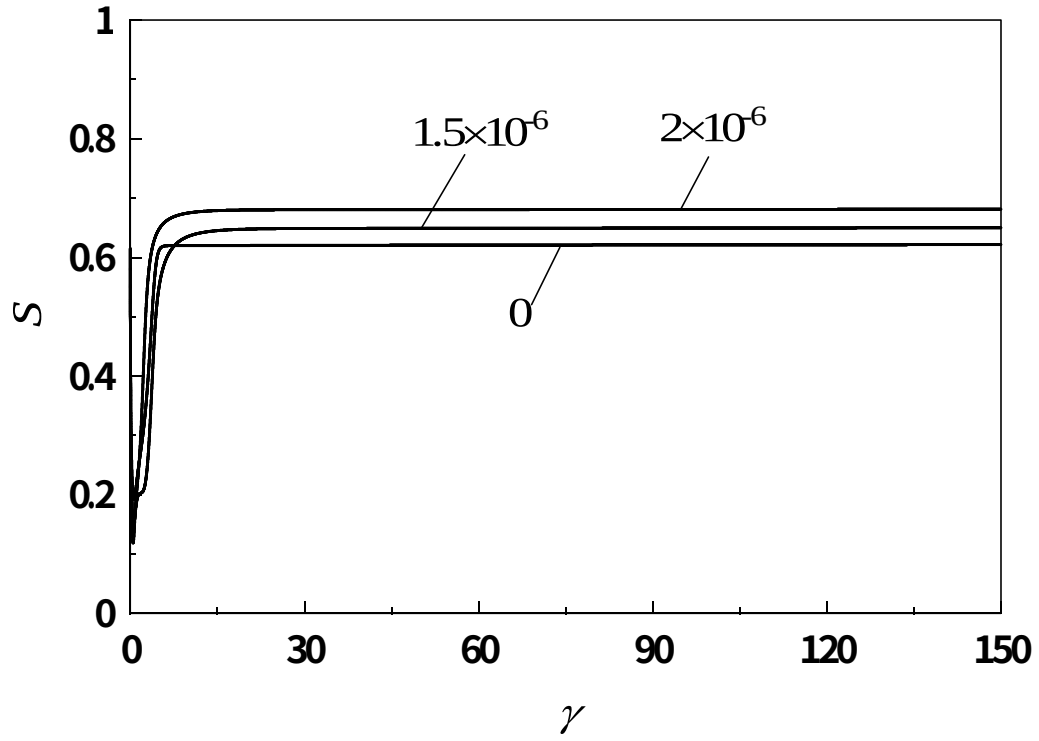

Figure 3.33 Transient behaviors of scalar order parameter S versus strain at $\dot{\gamma}^*$=2 for β=1.0 when H_y^*=0, 1.5×10^{-6} and 2×10^{-6}.

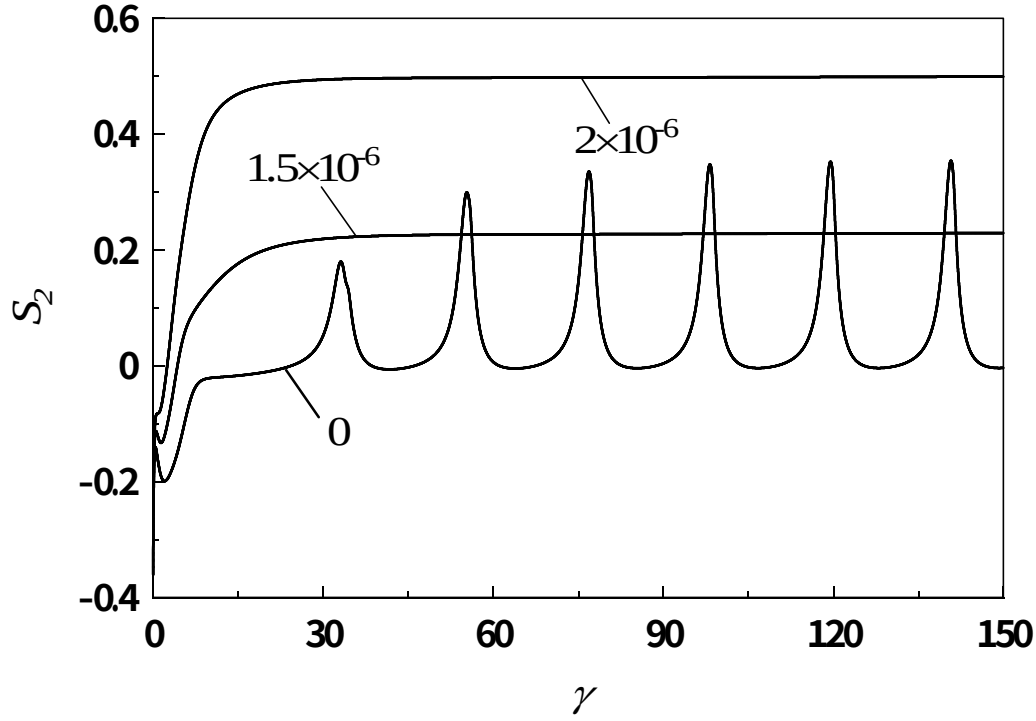

Figure 3.34 S_2 versus strain at $\dot{\gamma}^*$=2 for β=1.0 when H_y^*=0, 1.5×10^{-6} and 2×10^{-6}.

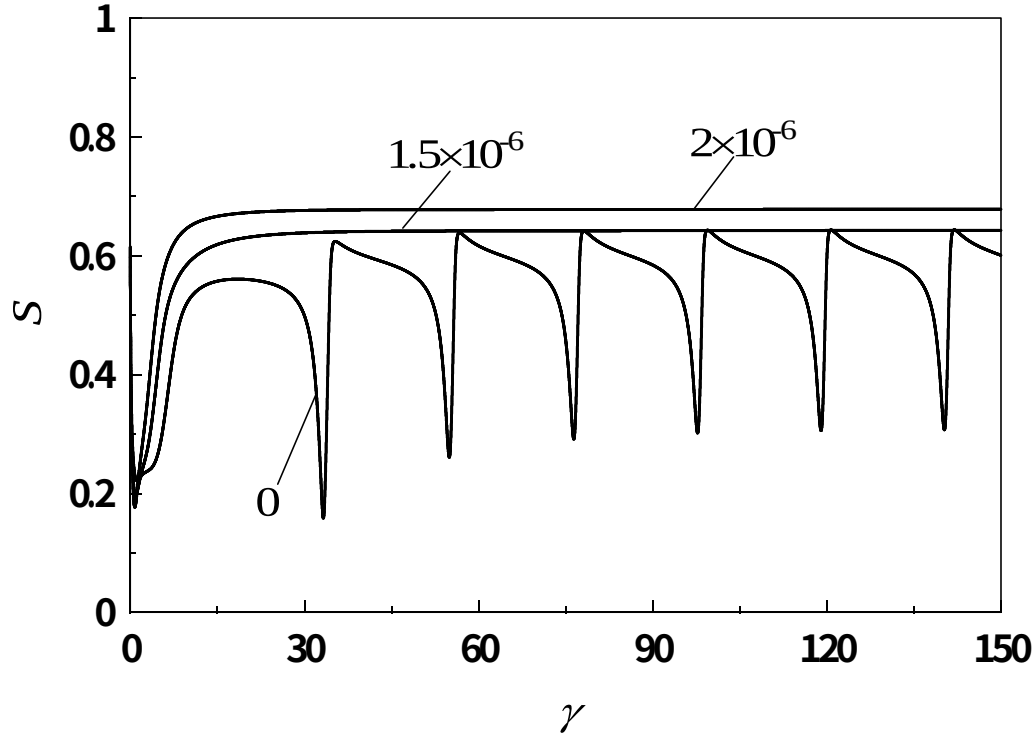

Figure 3.35 Transient behaviors of scalar order parameter S versus strain at $\dot{\gamma}^*$=2 for β=1.0 when H_y^*=0, 1.5×10^{-6} and 2×10^{-6}.

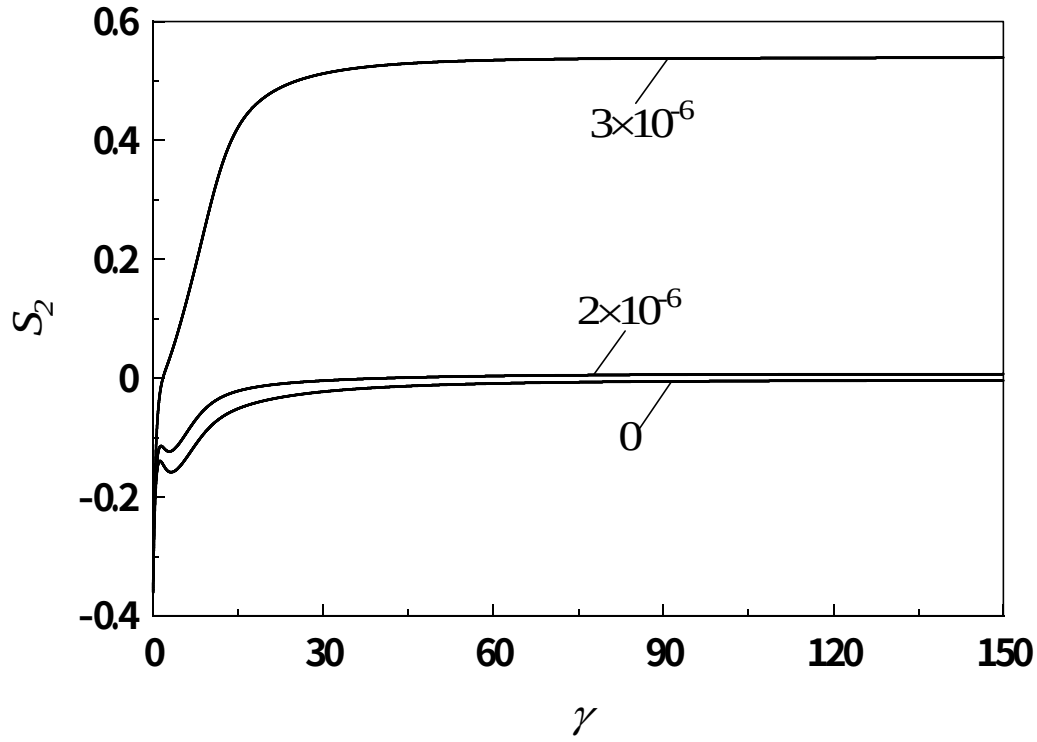

Figure 3.36 S_2 versus strain at $\dot{\gamma}^*$ =6 for β=1.0 when H_y^*=0, 2×10^{-6} and 3×10^{-6}.

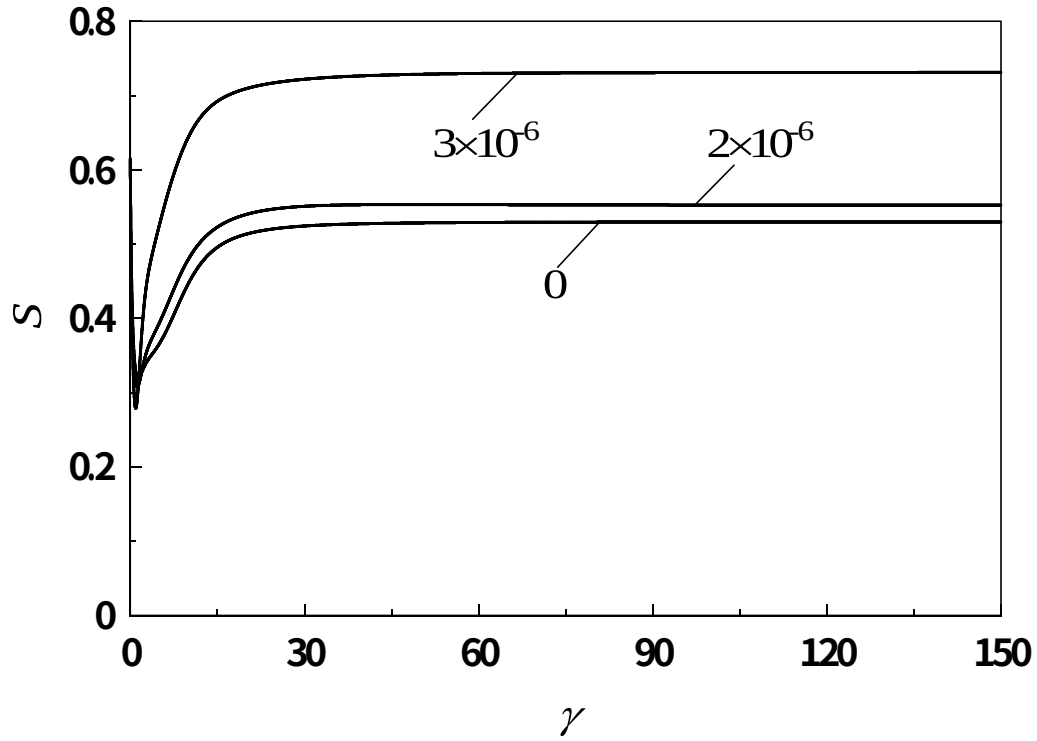

Figure 3.37 Transient behaviors of scalar order parameter S versus strain at $\dot{\gamma}^*$ =6 for β=1.0 when H_y^*=0, 1.5×10^{-6} and 2×10^{-6}.

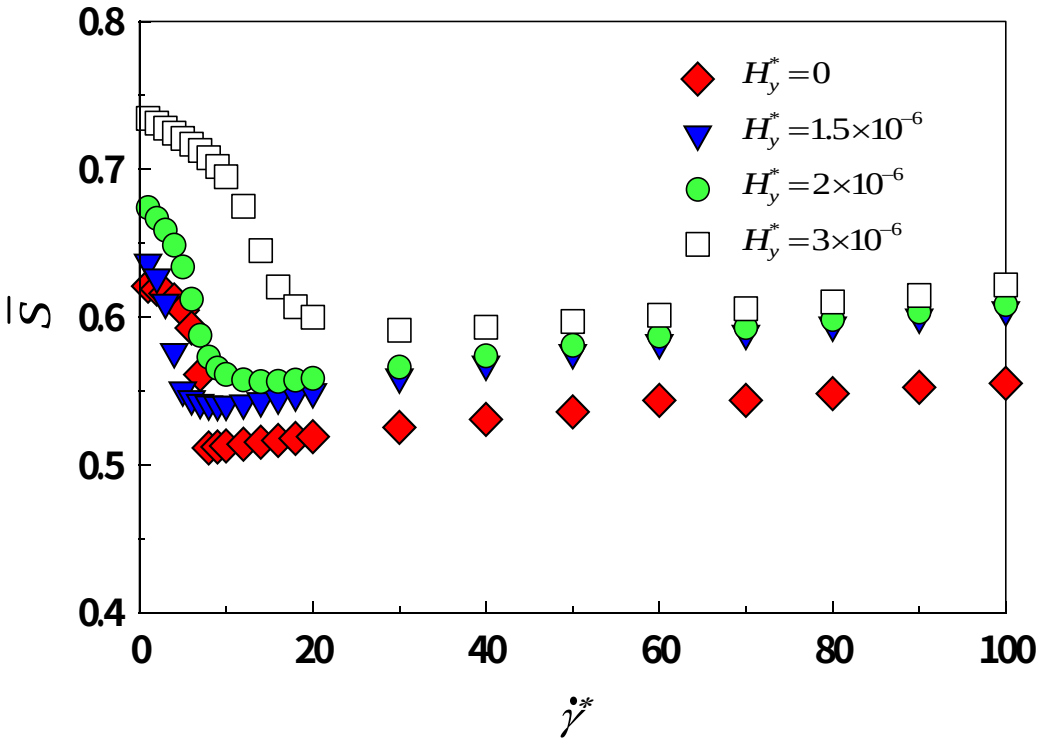

Figure 3.38 Average order parameter $\bar{S}$ as a function of shear rate for β=1.0 at H_y^*=0, 1.5×10^{-6}, 2×10^{-6} and 3×10^{-6}.

3.4 Results and Discussions for β=0.9

In this part, we will discuss the effect of the molecular length on the director by choosing β=0.9 in the equation (3.4) in out-of-plane cases. The three initial directors investigated in the part 3.3 are considered when the magnetic field is applied along the *x*-axis and the *y*-axis.

3.4.1 Initial Position of the Director along the *x*-axis

In this section the initial director is set to be along the *x*-axis. Figure 3.39 shows S_2 as the function of time oscillates between 0~S_{eq} in the shear plane. Compared with Figure 3.2 the oscillation periodic obviously increases. Transient behaviors of preferred angle and order parameters in the shear plane at $\dot{\gamma}^*$=1 is described in Figures 3.40. The endless rotation of the major orientation indicates that a tumbling mode is detected. With increasing the shear rate at $\dot{\gamma}^*$=5 the amplitude of S_2 in Figure 3.41 is apparently reduced, and infers that the director oscillates in the shear plane. A wagging mode is

found as can be seen from Figures 3.42, where the director periodically oscillates in the shear plane. Figure 3.43 describes S_2 changes with time when $\dot{\gamma}^*$=12, which the amplitude of it decreases as the oscillation, finally becomes a constant near to zero. An alignment is found when $\dot{\gamma}^*$=12 where the major orientation direction remains a constant along the shear flow in Figures 3.44.

The time-averaged scalar order parameter $\overline{S}$ and $\overline{S}_{xx}$ as the function of the shear rate are represented in Figures 3.45. Apparently, $\overline{S}_{xx}$ is smaller than the one at β=1.0 shown in Figure 3.8.

Compared with the results in part 3.3 at β=1.0 the oscillation periodicity of the director is obviously increased. And at the same calculation conditions the molecular alignment atβ=0.9 is lower than the one when β=1.0. From the simulation results we can make a conclusion same with before that the director shows out the three modes, tumbling, wagging and aligning, in the shear plane once the initial director is set into it. Therefore, the effect of the magnetic field on the director also will not be investigated since the results are almost same with the ones discussed in Chapter 2 where the director is always confined into the shear plane.

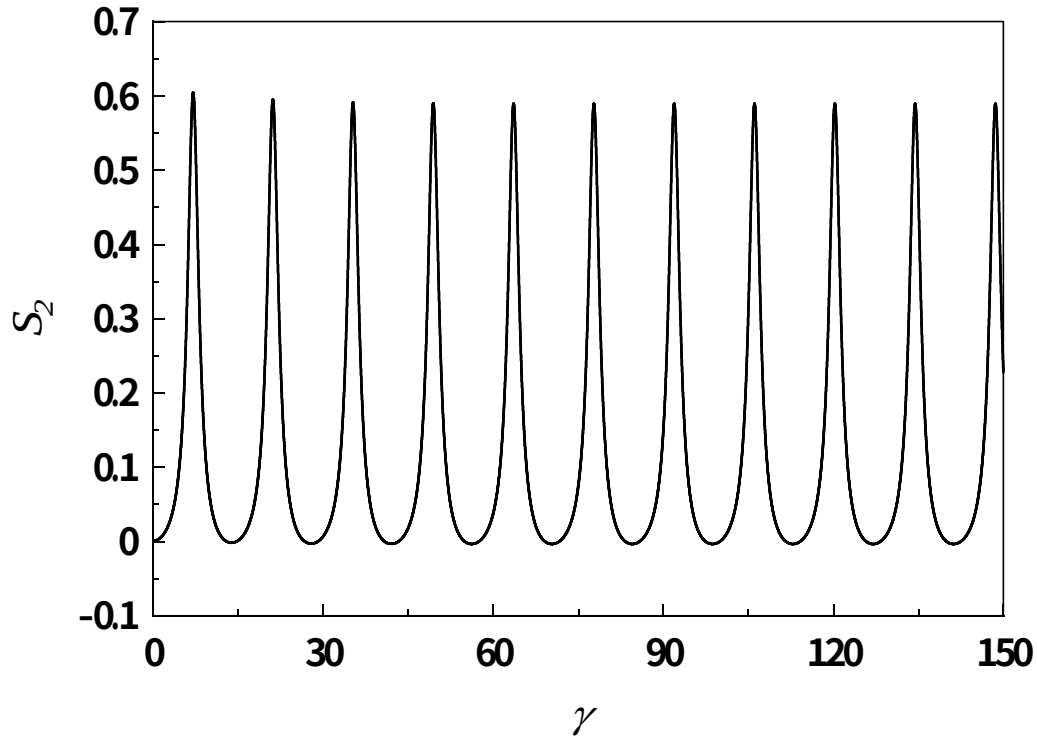

Figure 3.39 S_2 versus strain at $\dot{\gamma}^*$ =1 for β=0.9.

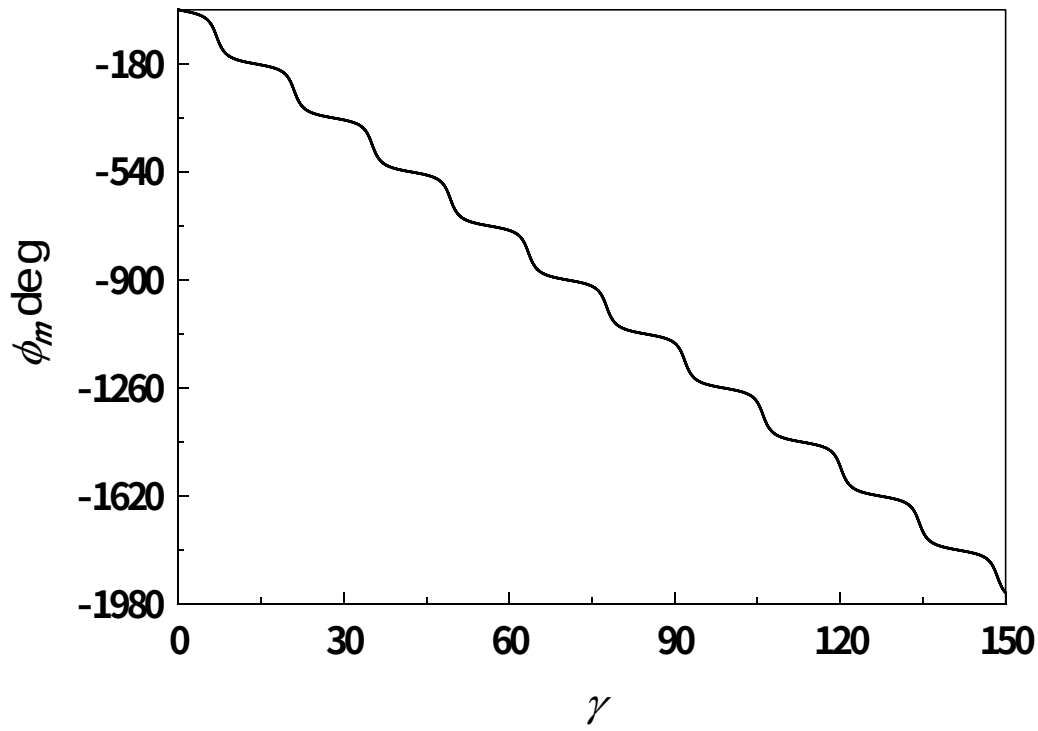

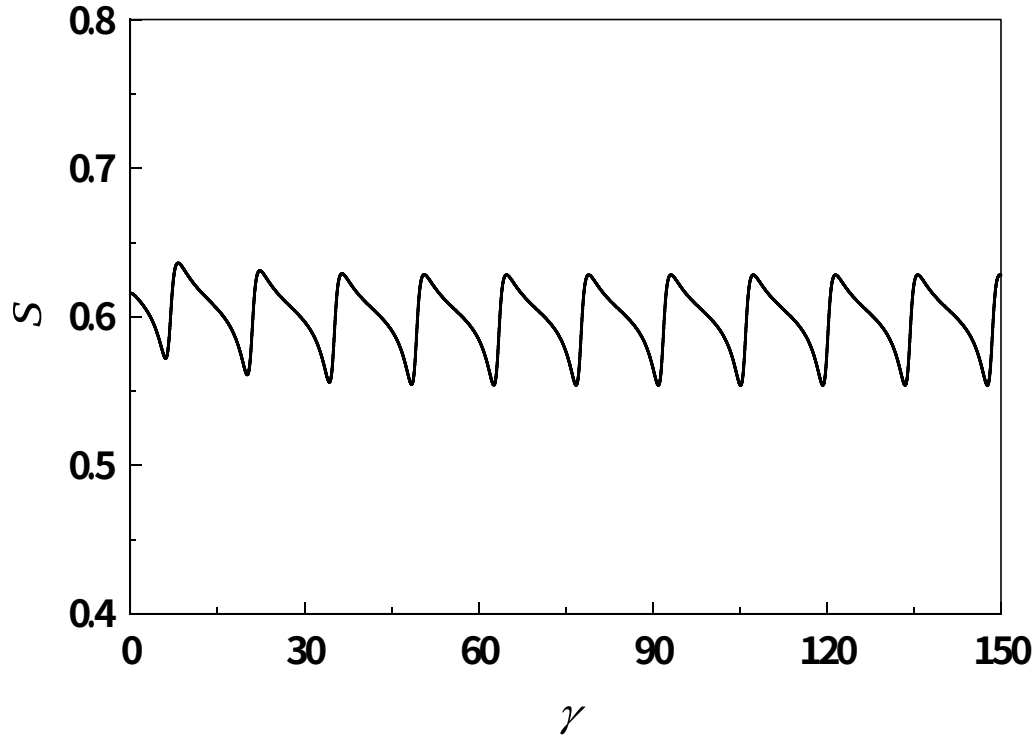

Figures 3.40 Transient behaviors of preferred angle ϕ_m and scalar order parameter S versus strain at $\dot{\gamma}^*$=1 for β=0.9.

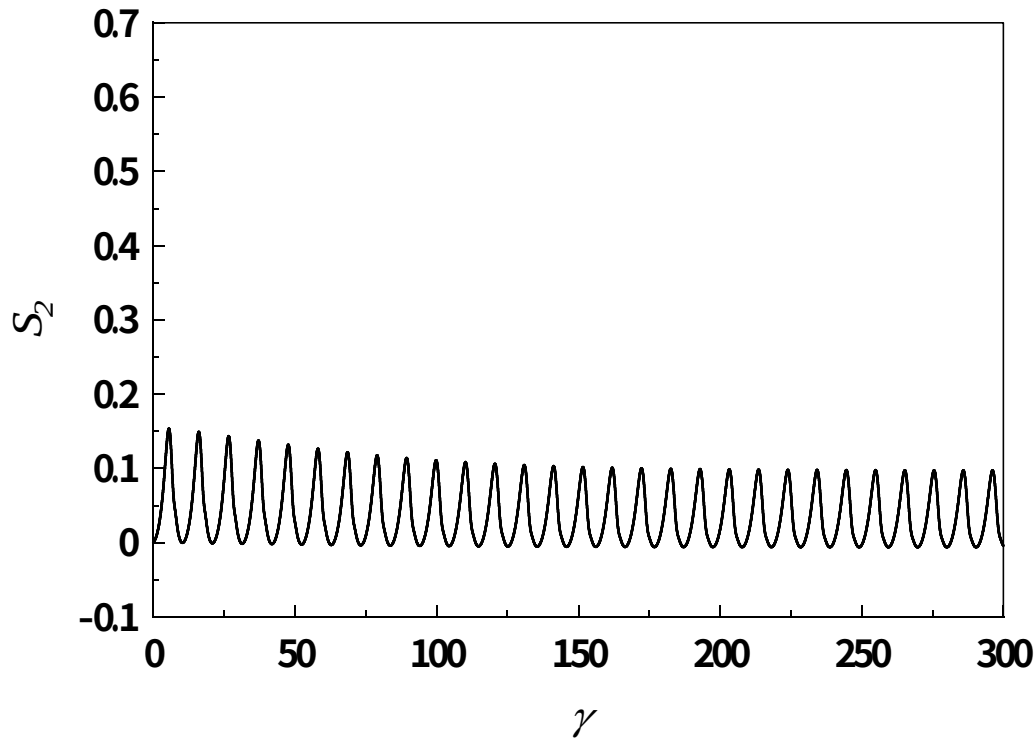

Figure 3.41 S_2 versus strain at $\dot{\gamma}^*$=5 for β=0.9.

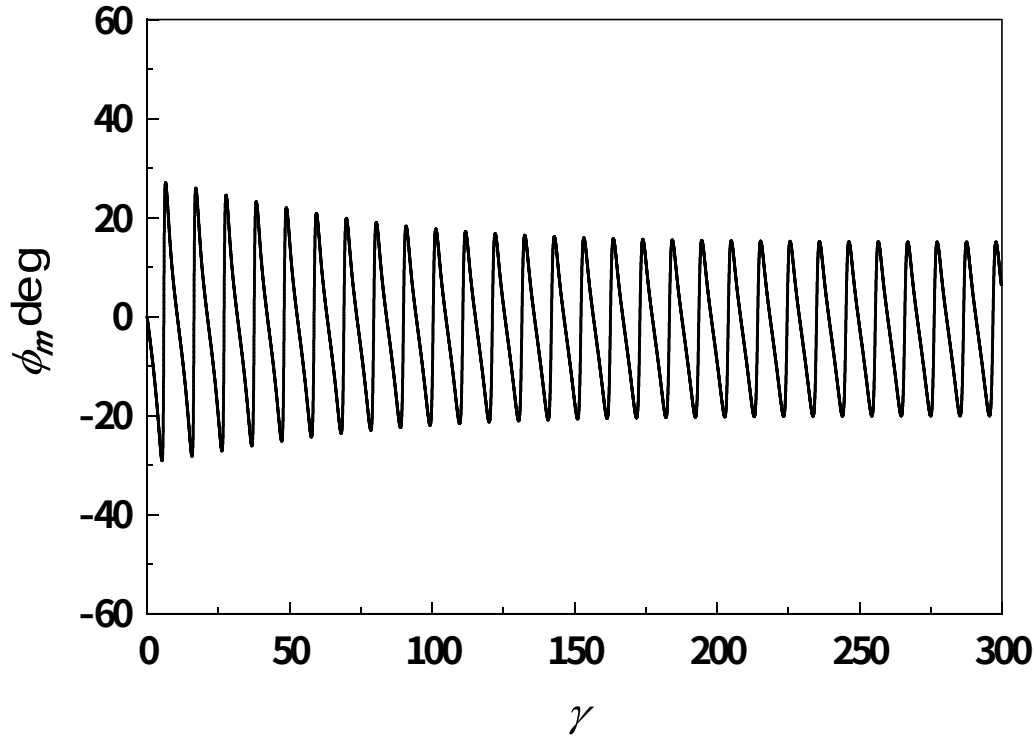

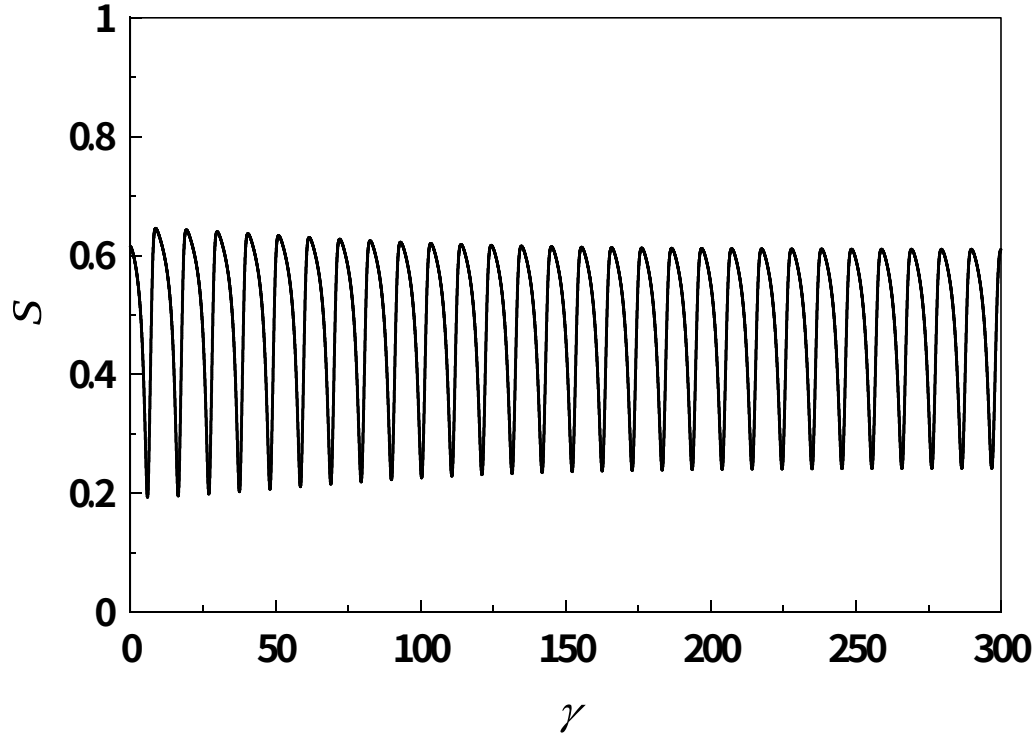

Figures 3.42 Transient behaviors of preferred angle ϕ_m and scalar order parameter S versus strain at $\dot{\gamma}^*$=5 forβ=0.9.

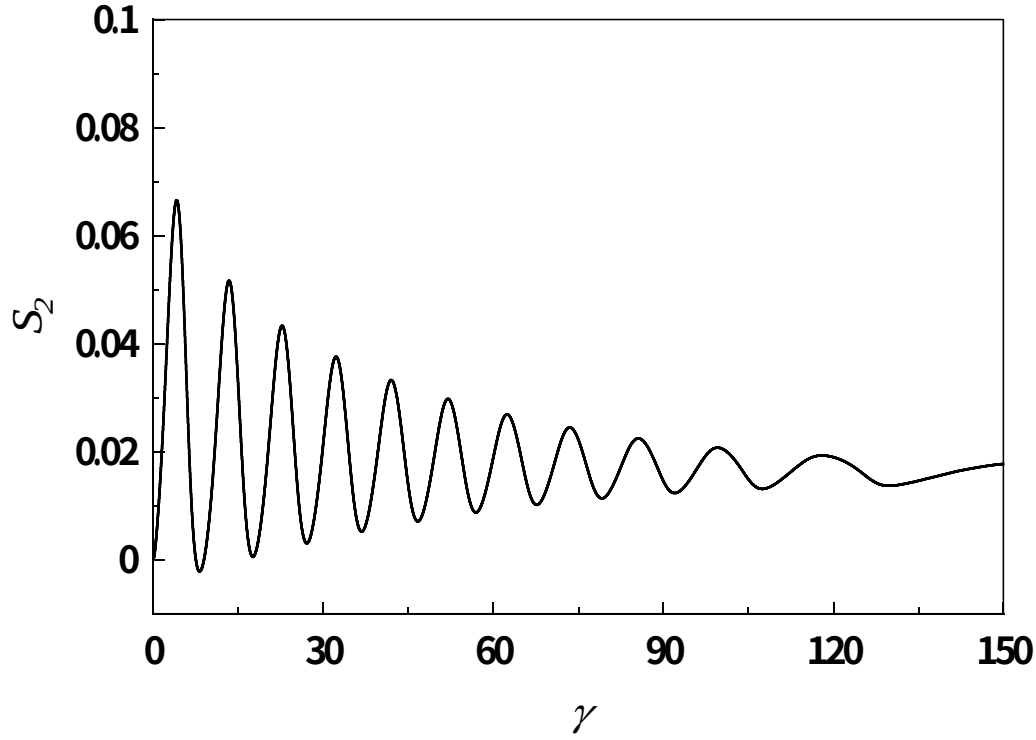

Figure 3.43 S_2 versus strain at $\dot{\gamma}^*$ =12 for β=0.9.

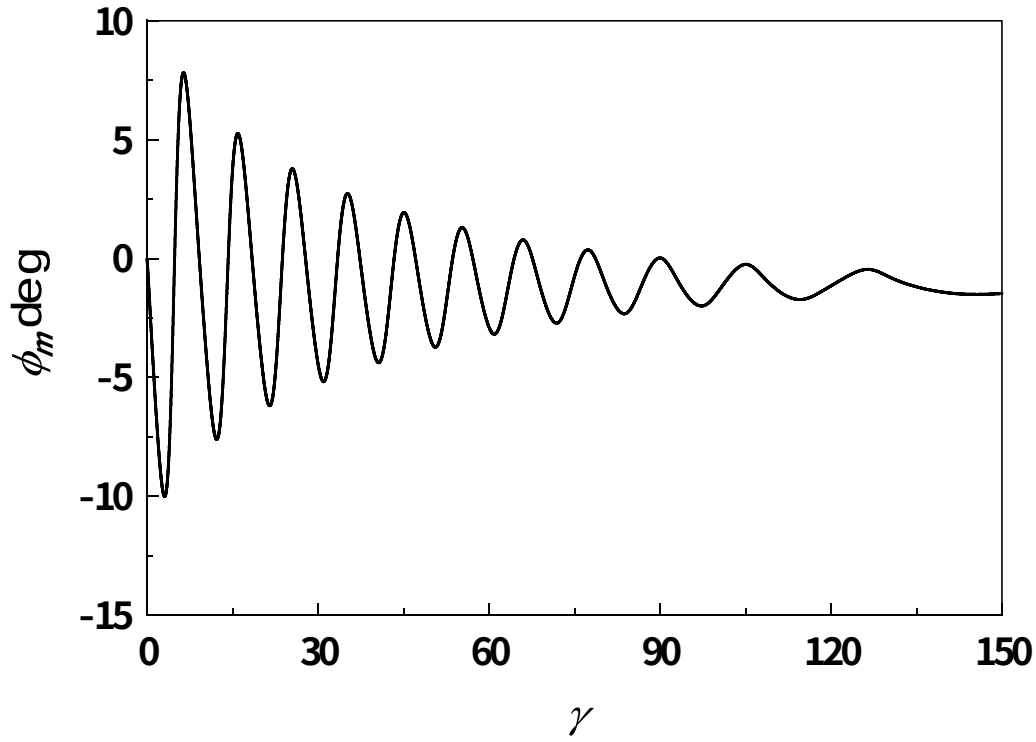

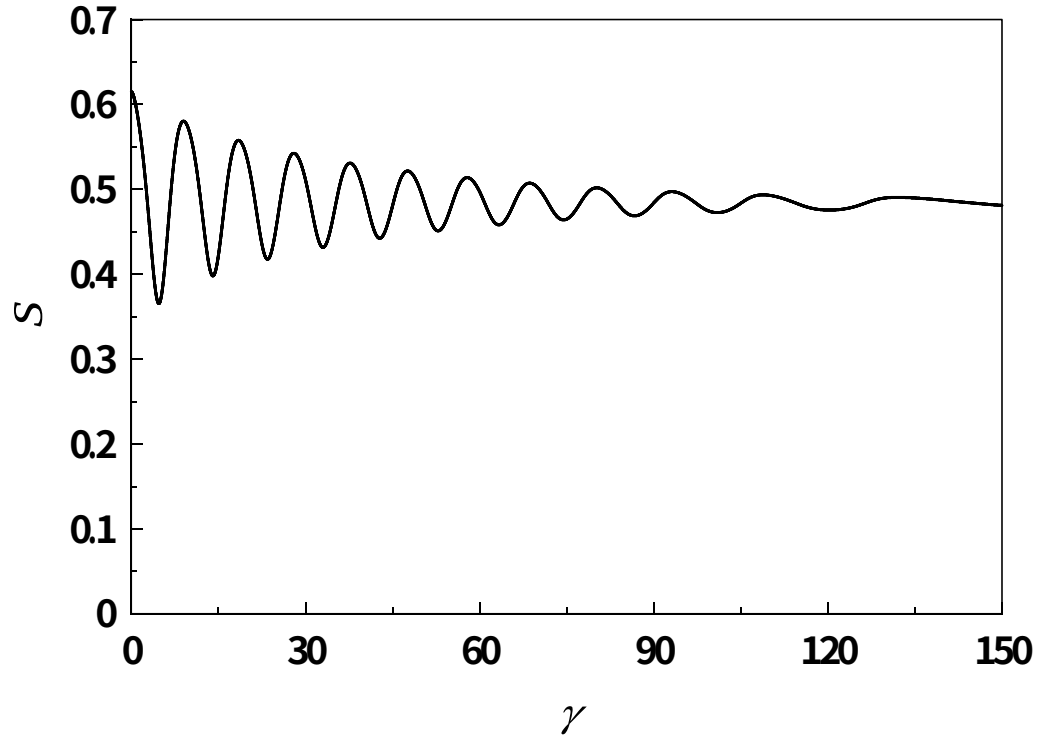

Figures 3.44 Transient behaviors of preferred angle ϕ_m and scalar order parameter S versus strain at $\dot{\gamma}^*$ =12 for β=0.9

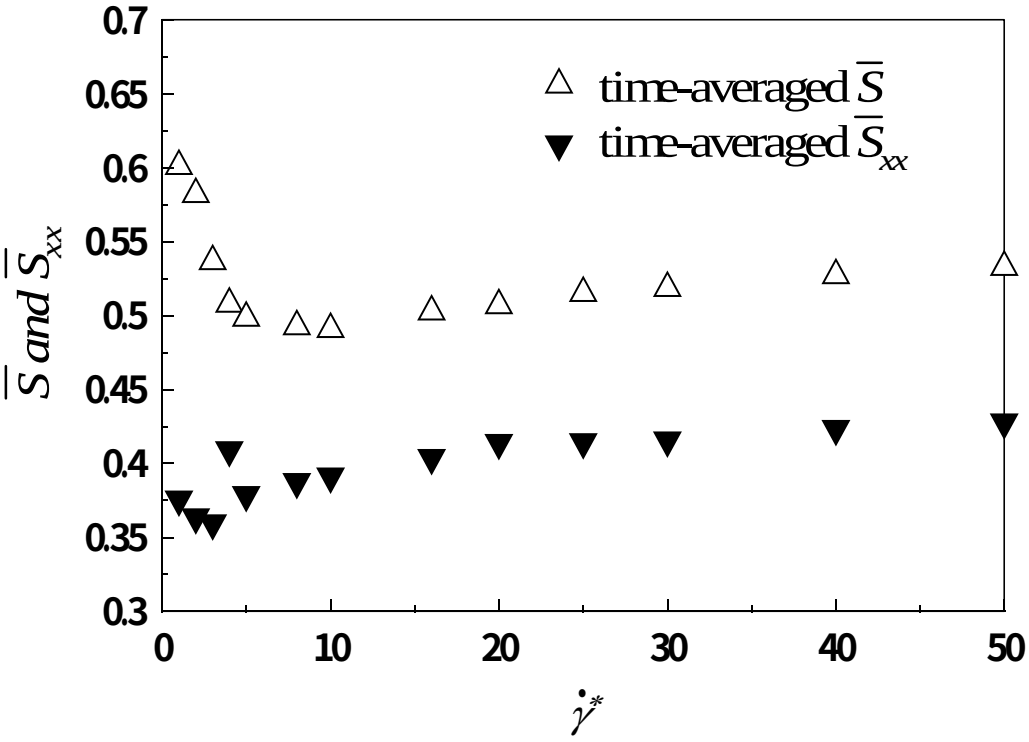

Figure 3.45 Average order parameter $\bar{S}$ and $\bar{S}_{xx}$ as a function of shear rate.

3.4.2 Initial Position of the Director along the *z*-axis

In this section the initial director will be parallel to the voriticity direction, namely, along the *z*-axis. As explained above a log-rolling orientation state will be found in this case. In order to control the director freely the effect of the magnetic field applied along the *x*-axis and the *y*-axis on the director also is discussed, respectively.

3.4.2.1 The Magnetic Field along the *x*-axis

The simulation results that the magnetic field is applied along the *x*-axis ((H_x, 0, 0)) are given out in this section. Figure 3.46 describes S_2 as the function of time changes with the magnetic field at $\dot{\gamma}^*$=1 for H_x*=0, 1.5×10^{-6} and 2×10^{-6}. From the figure we can see that when H_x*=0 and 1.5×10^{-6}, the vorticity also is an attractor for the director. The log-rolling orientation state is kept. However, once further increasing the magnetic field at 2×10^{-6}, the director will be aligned along the *x*-axis after the course of molecular deformation by the magnetic field (Figures 3.11) which also can be testified by the changing of *S* with the time in Figures 3.47. It is obvious that the alignment of the molecules is improved by adding the magnetic field along the flow direction. S_{xx} versus time also is described in Figures 3.48, where it becomes a big value after the director aligns in the shear plane.

We directly increase the shear rate into a high value in order to further investigate the effect of the shear rate on the log-rolling orientation state. Figure 3.49 gives out that the shear plane becomes an attractor when $\dot{\gamma}^*$=10 even without applying the magnetic field. After applying the magnetic field along the flow direction the alignment along the director is reinforced again which is showed out in Figures 3.50. At the same time the molecular alignment along the flow direction described by S_{xx} also is improved by the magnetic field.

The time-averaged scalar order parameter $\overline{S}$ and $\overline{S}_{xx}$ versus the shear rate also is plot at H_x*=0, $2\times10^{-6}$and 3×10^{-6} in Figures 3.51. When H_x*=0, at low shear rates a discontinuous decrease is observed, which is the boundary between the log-rolling orientation state and the aligning state along the flow direction. Also at high shear rates $\overline{S}$ increases with the magnetic field. When H_x*=$2\times10^{-6}$and 3×10^{-6}, the log-rolling orientation state is conquered. The time-averaged $\overline{S}_{xx}$ also is represented with the shear rate. At low shear rates $\overline{S}_{xx}$ is very small because of the log-rolling orientation state when H_x*=0. After that $\overline{S}_{xx}$ becomes bigger suddenly at a critical value then slowly increases with the shear rate.

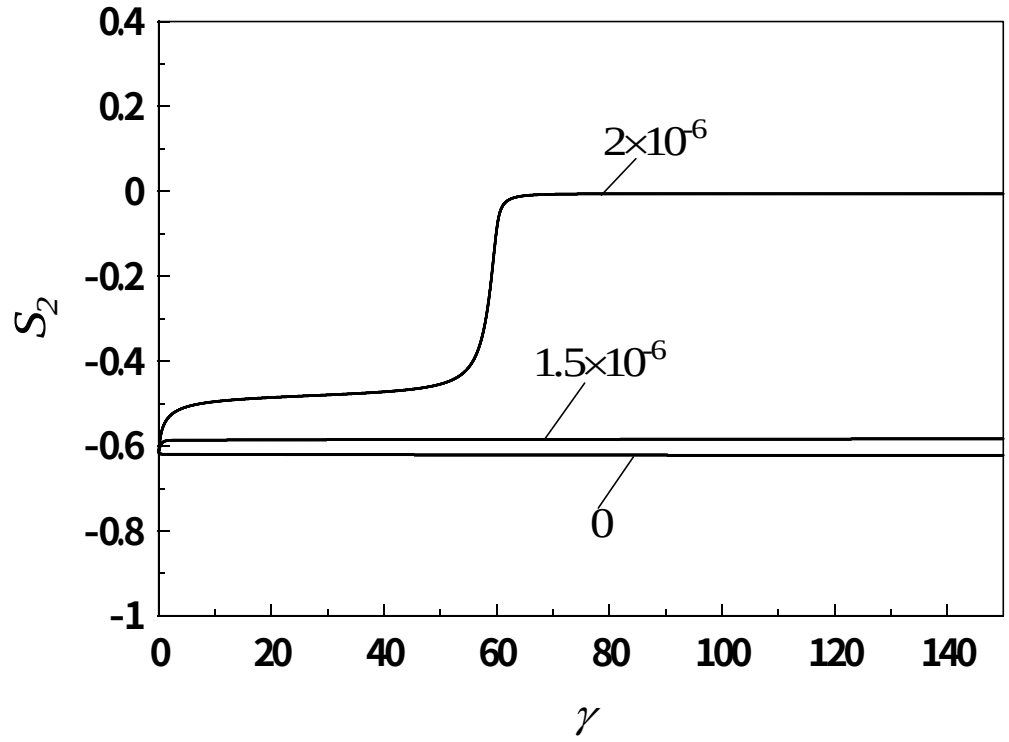

Figure 3.46 S_2 versus strain at $\dot{\gamma}^*$ =1 for β=0.9 when H_x^*=0, 1.5×10^{-6} and 2×10^{-6}.

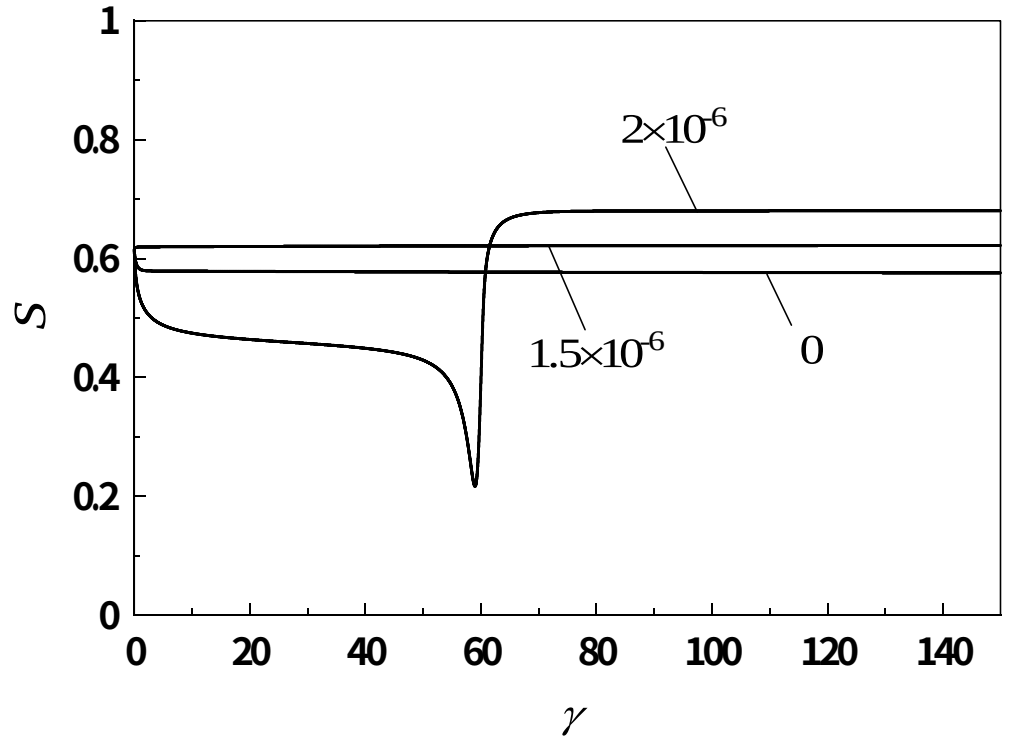

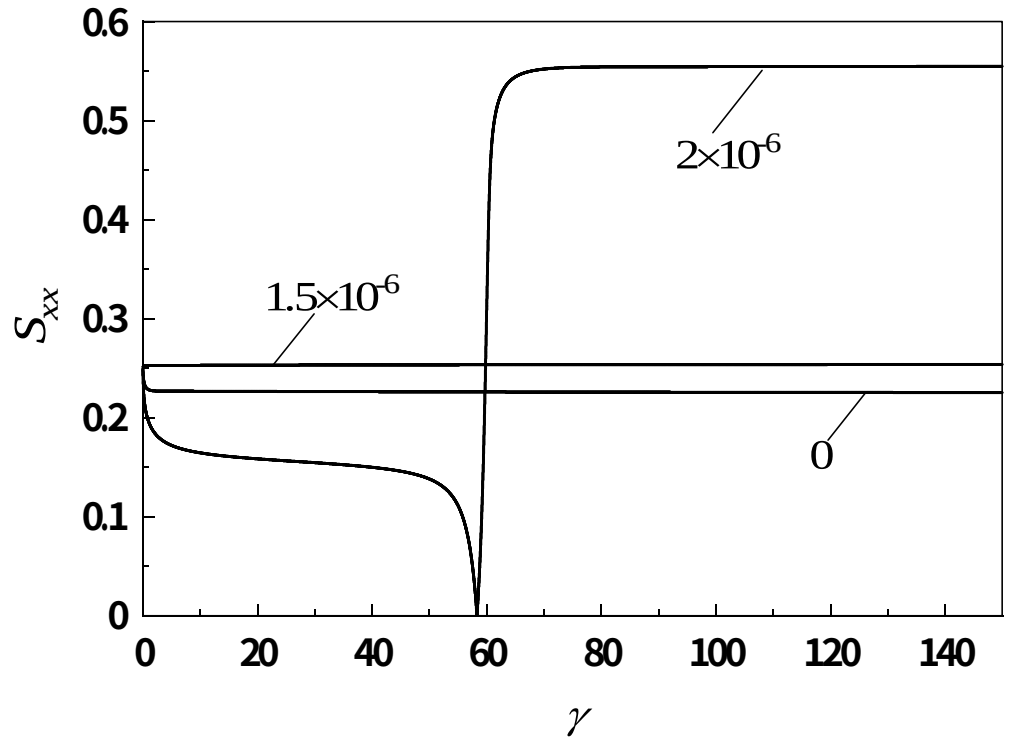

Figures 3.47 Transient behaviors of scalar order parameter S and S_{xx} versus strain at $\dot{\gamma}^*$ =1 for β=0.9 when H_x^*=0, 1.5×10^{-6}and 2×10^{-6}.

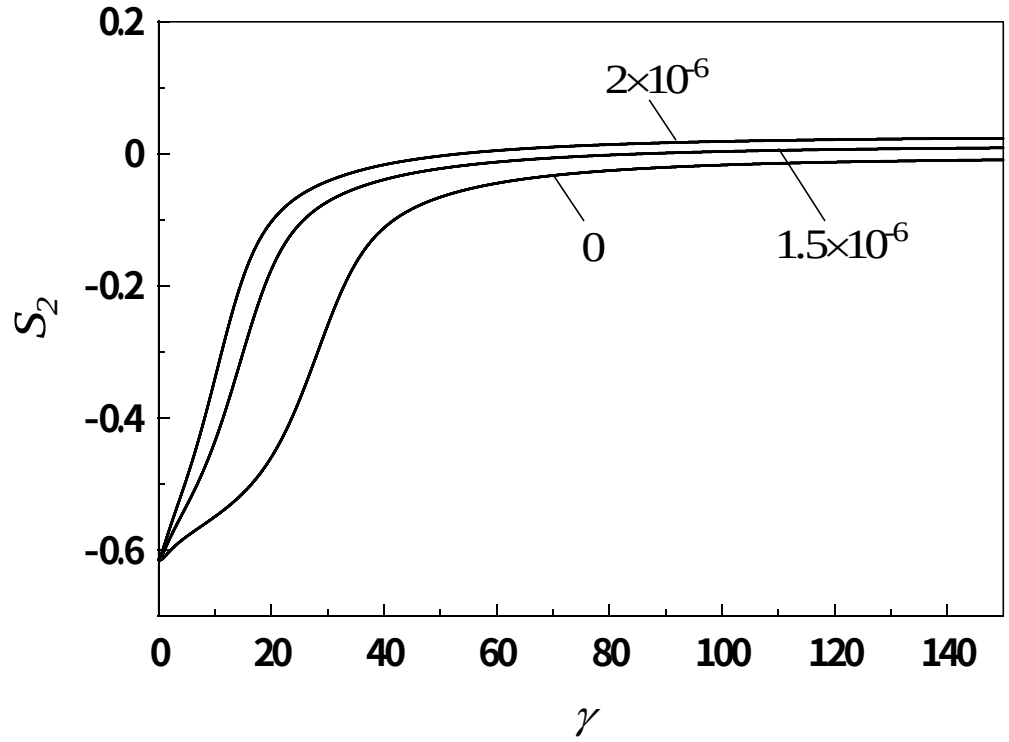

Figure 3.48 S_2 versus strain at $\dot{\gamma}^*$ =10 for β=0.9 when H_x^*=0, 1.5×10^{-6} and 2×10^{-6}.

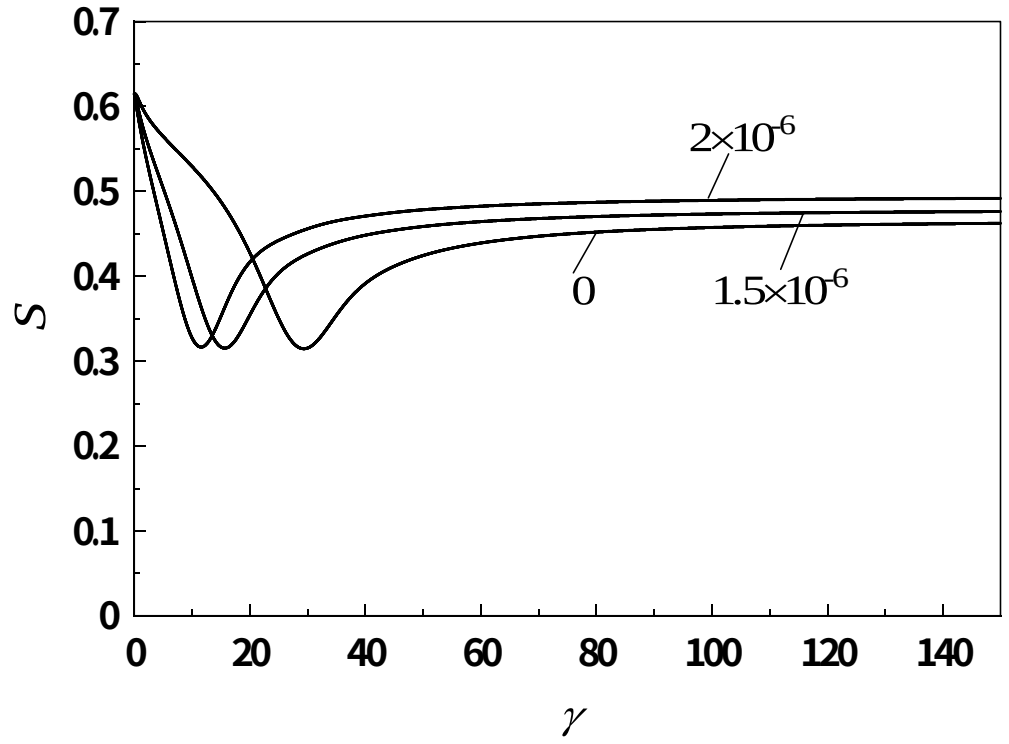

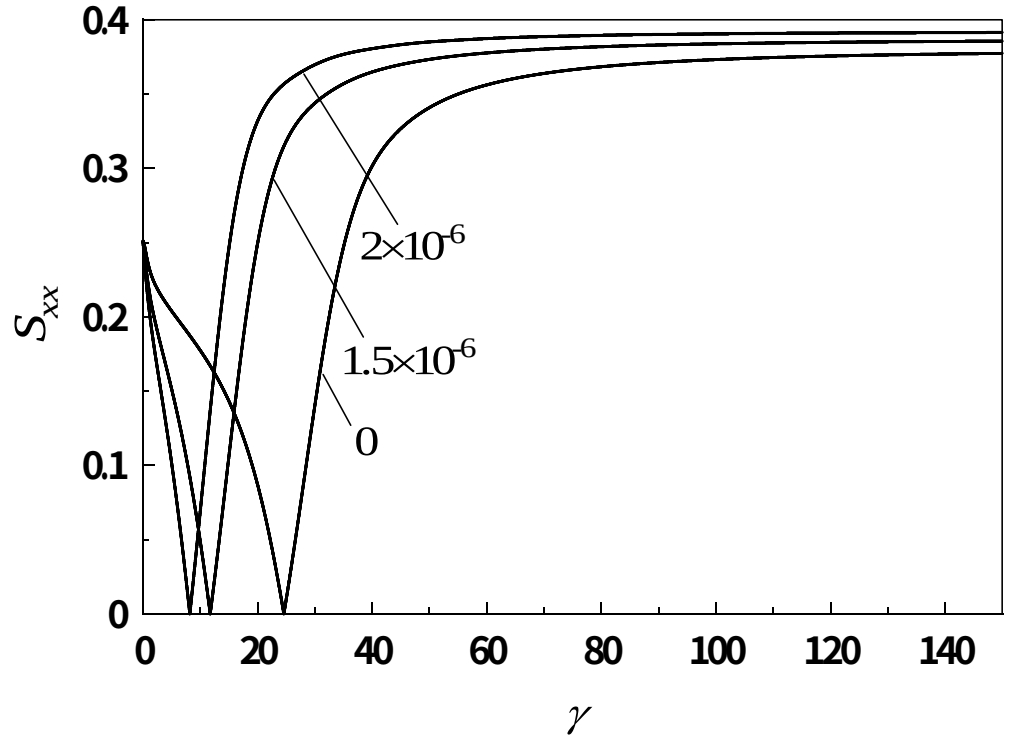

Figures 3.49 Transient behaviors of scalar order parameter S and S_{xx} versus strain at $\dot{\gamma}^*$ =10 for β=0.9 when H_x^*=0, $1.5\times10^{-6}$and 2×10^{-6}.

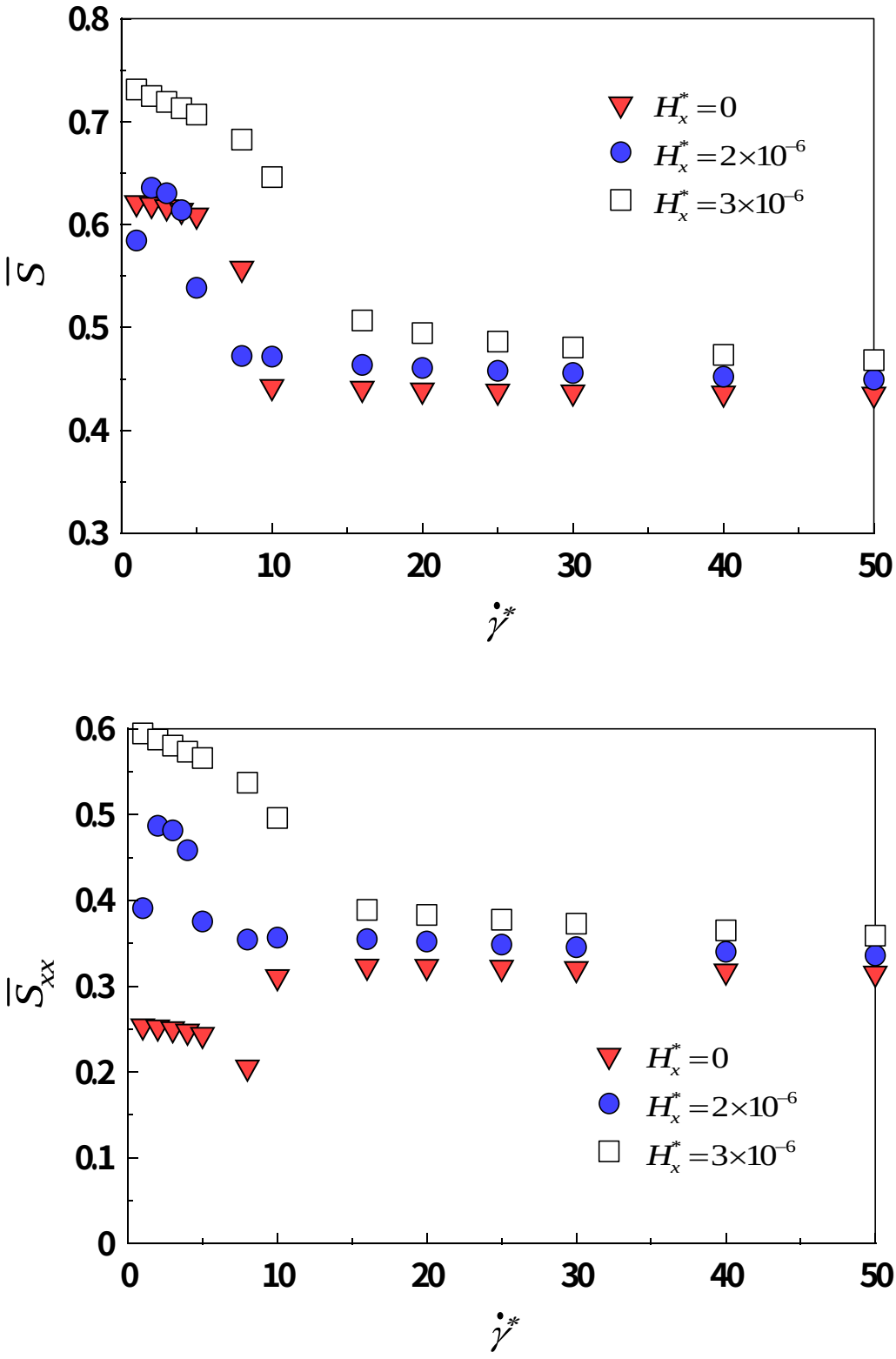

Figures 3.50 Average order parameter $\bar{S}$ and $\bar{S}_{xx}$ as a function of shear rate for β=0.9 at H_x^*=0, 1.5×10^{-6}, 2×10^{-6} and 3×10^{-6}.

3.4.2.2 The Magnetic Field along the *y*-axis

The discussions of the simulation results are represented in the following part when the magnetic field is parallel to the *y*-axis. As we known in this case the toques caused by the flow and the magnetic field is not along the same direction. Therefore the final director will be decided by the competition made by the torques caused by the flow and the magnetic field. Figure 3.51 indirectly shows out the director changes with the time through checking S_2 at $\dot{\gamma}^*$=1. It is almost same with the results when we set β=1.0 except that the time of the molecular deformation becomes longer as can be seen from the results at $H_y^*= 2\times10^{-6}$. The scalar parameter *S* versus time also shows out this point in Figure 3.52. When the shear rate is increased at $\dot{\gamma}^*$=10, the director is aligned along the flow direction shown in Figure 3.53. The director doesn't always align the flow direction once the magnetic field is stronger enough as can be obtained at $H_y^*= 3\times10^{-6}$. The scalar order parameter *S* also is given out in Figure 3.54. In order to investigate the time-averaged $\bar{S}$ changes with the shear rate at the different strength of the magnetic field, Figure 3.55 is plot. Both of them have a discontinuous decrease as explained above.

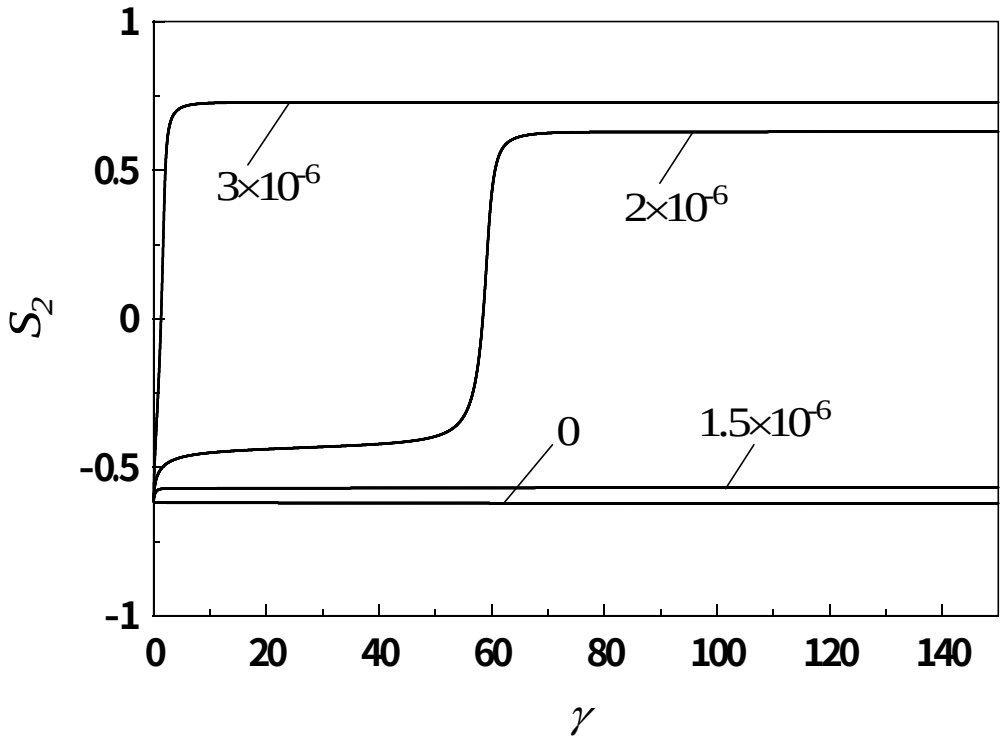

Figure 3.51 S_2 versus strain at $\dot{\gamma}^*$ =1 for β=0.9 when H_y^*=0, 1.5×10^{-6}, 2×10^{-6} and 3×10^{-6}.

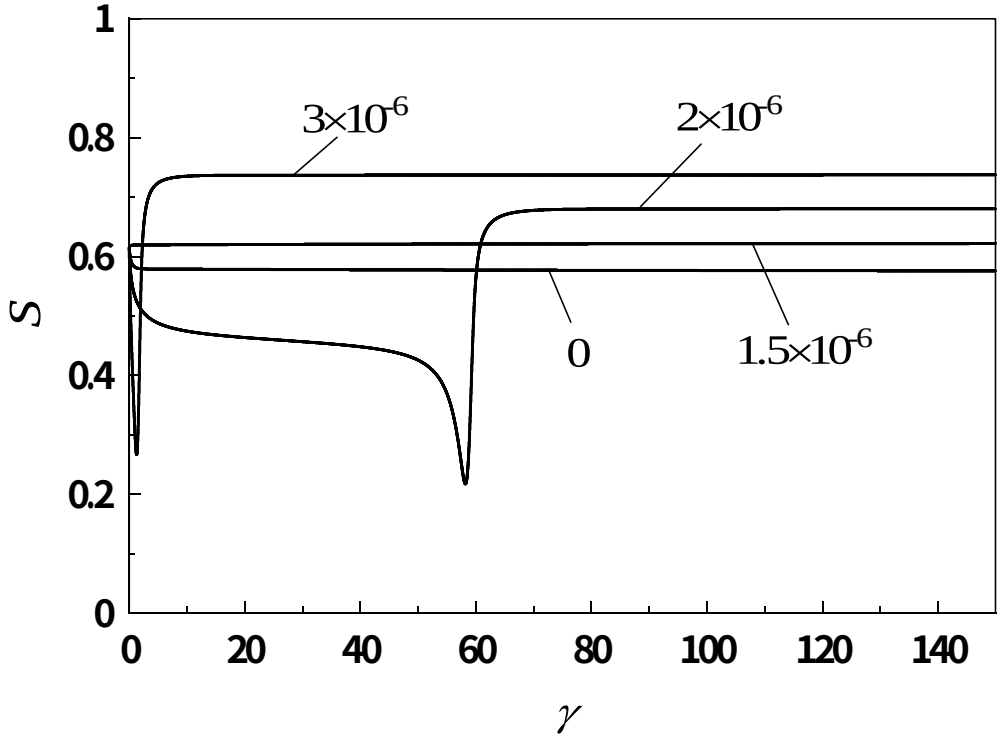

Figure 3.52 Transient behaviors of scalar order parameter S versus strain at $\dot{\gamma}^*$ =1 for β=0.9 when H_y^*=0, 1.5×10^{-6}, 2×10^{-6} and 3×10^{-6}.

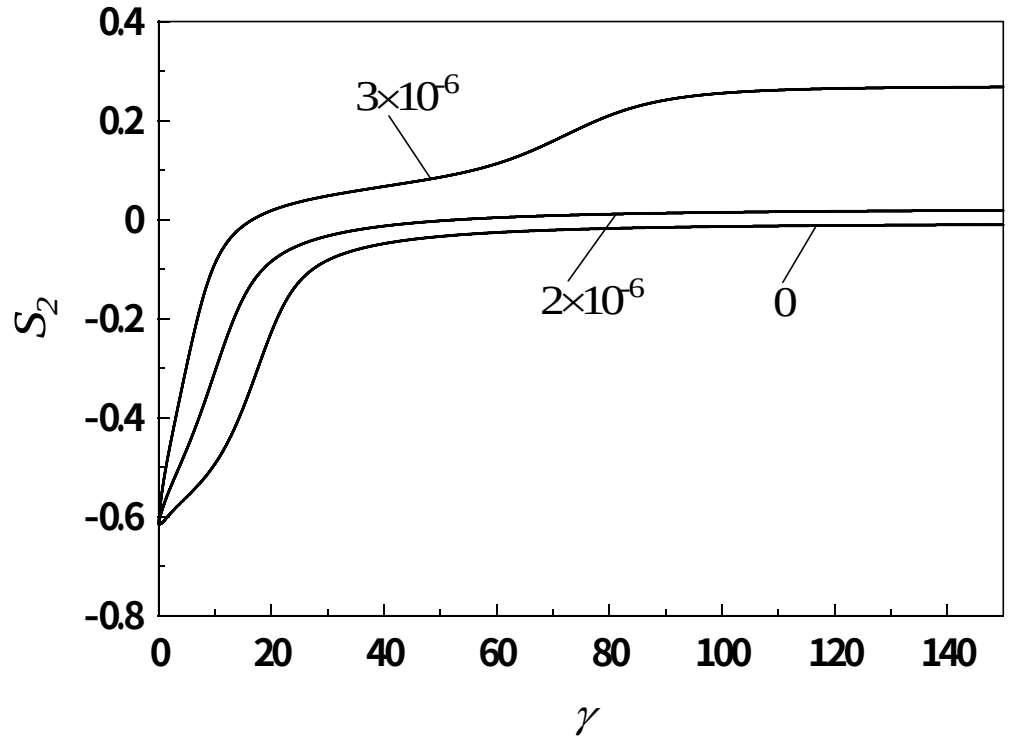

Figure 3.53 S_2 versus strain at $\dot{\gamma}^*$ =10 for β=0.9 when H_y^*=0, 2×10^{-6} and 3×10^{-6}.

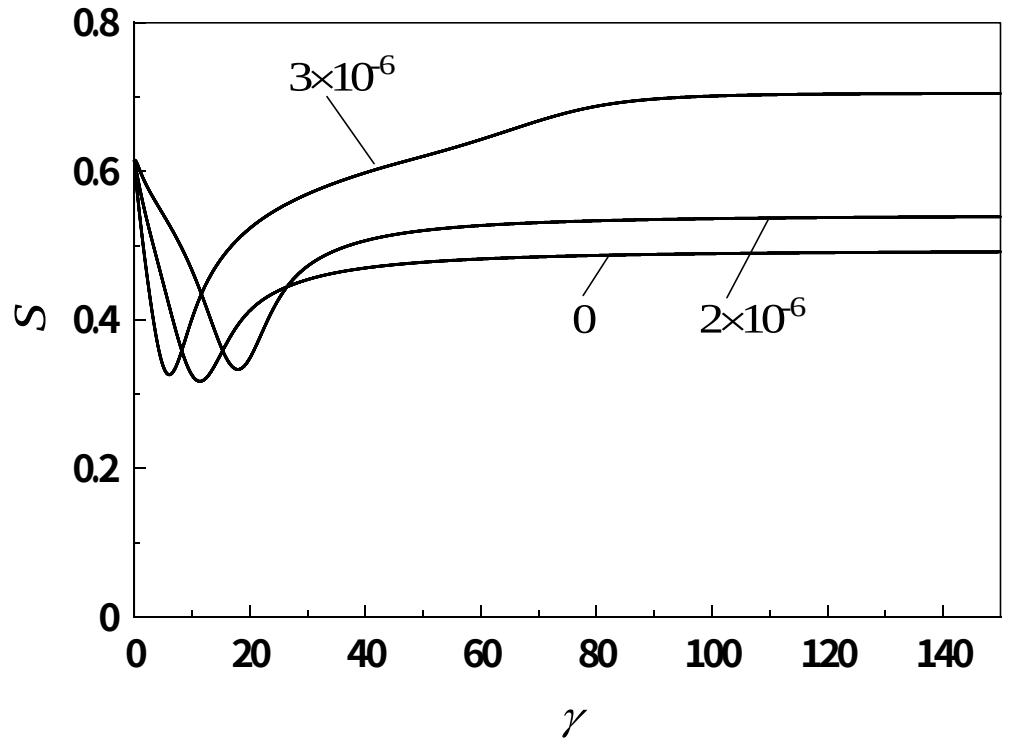

Figure 3.54 Transient behaviors of scalar order parameter S versus strain at $\dot{\gamma}^*$ =10 for β=0.9 when H_y^*=0, 2×10^{-6} and 3×10^{-6}.

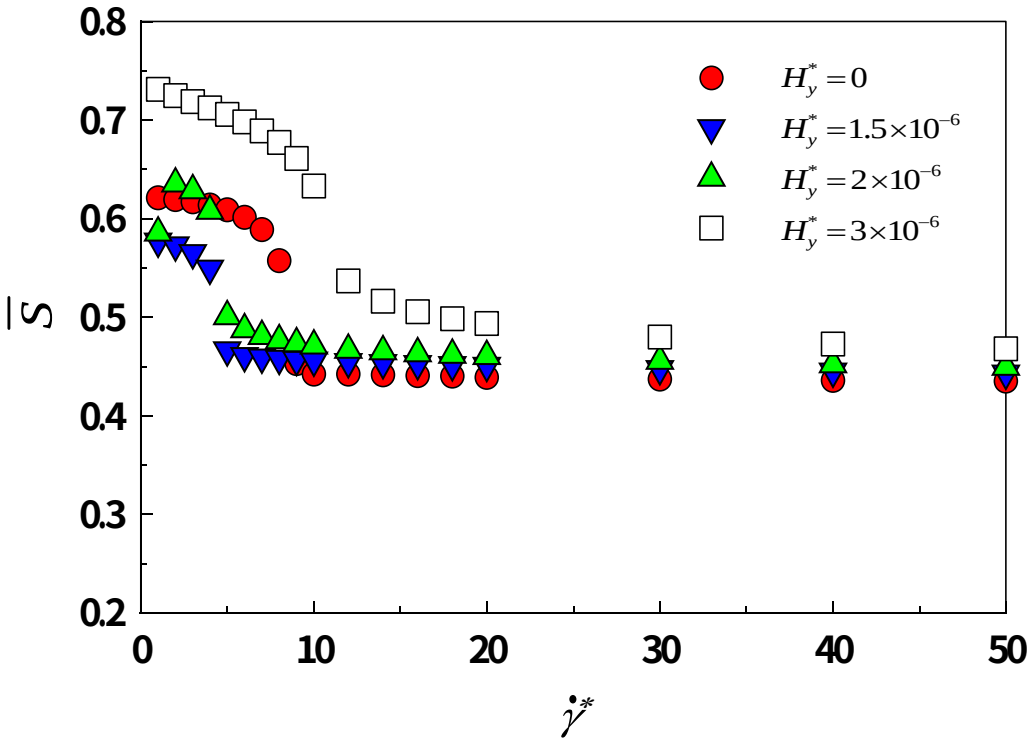

Figure 3.55 Average order parameter $\bar{S}$ as a function of shear rate for β=0.9 at H_y^*=0, 1.5×10^{-6}, 2×10^{-6} and 3×10^{-6}.

3.4.3 Initial Position of the Director at φ=-50°

In this part, we will consider a general situation that the initial director is set to be into the *x*-*z* plane at φ=-50°. The two cases that the magnetic field is along the *x*-axis and the *y*-axis are considered, respectively.

3.4.3.1 The Magnetic Field along the *x*-axis

The simulation results that the magnetic field applies along the *x*-axis are given out in the following discussions. Figure 3.56 describes the orbit of the director at $\dot{\gamma}^*$=1 through S_2 changes with time, where the director rotates to align along the vorticity direction at H_x*=0, however, when H_x*=1.5×10^{-6} the shear plane becomes the attractor for the director. Compared the two figures in Figures 3.57 we can obtain that the molecular alignment along the flow direction is increased after the magnetic field is applied. Increasing the shear rate at $\dot{\gamma}^*$=2 in Figure 3.58 the director will rotates into the shear plane and oscillates in it. The periodicity is obviously increased compared the

one at β=1.0. After applying the magnetic field (H_x*=1.5×10^{-6}) the director ceases oscillations in the shear plane and aligns along the direction of the magnetic field. Figures 3.59 describes the scalar parameter S and S_{xx} changes with time at H_x*=0 and H_x*=1.5×10^{-6}. Further increasing the shear rate at $\dot{\gamma}^*$=6 in Figure 3.60 the shear plane becomes an attractor, and at the same time the director is aligned along the flow direction without applying the magnetic field. The scalar parameter S is very low which is showed out in Figures 3.61.

The time-averaged scalar parameter $\overline{S}$ and $\overline{S}_{xx}$ versus the shear rate at H_x*=0, 2×10^{-6} and 3×10^{-6} is plot in Figures 3.62. Only when H_x*=0 at low shear rates, the log-rolling orientation state is observed, which is indicated when $\overline{S}_{xx}$ is very low.

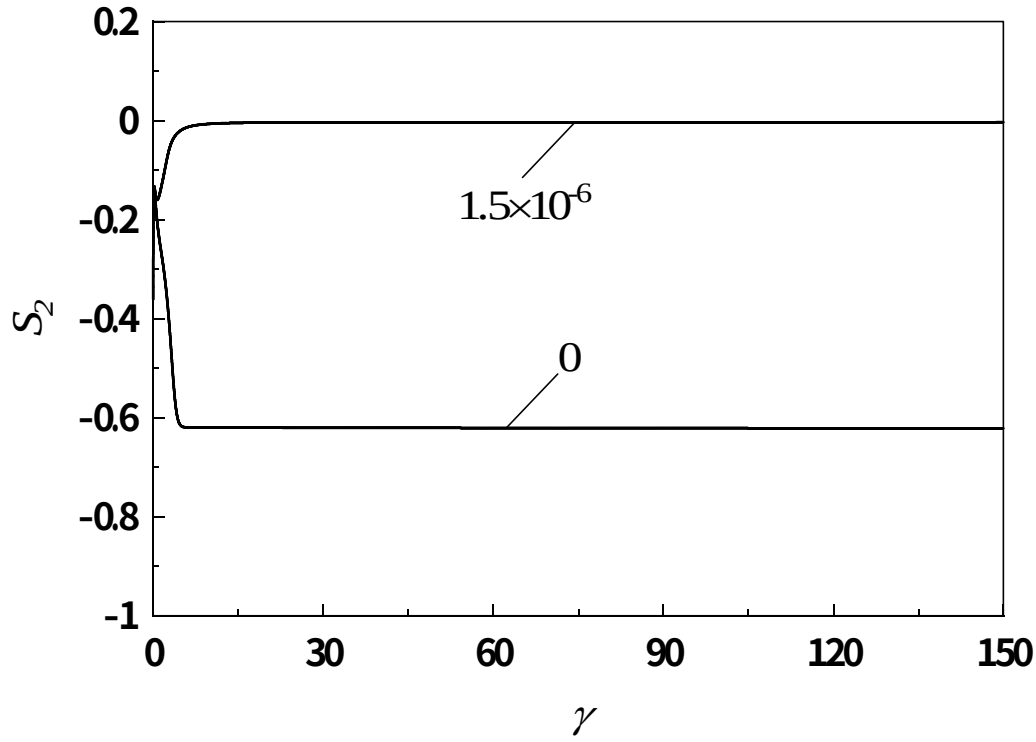

Figure 3.56 S_2 versus strain at $\dot{\gamma}^*$ =1 for β=0.9 when H_x^*=0 and1.5×10^{-6}.

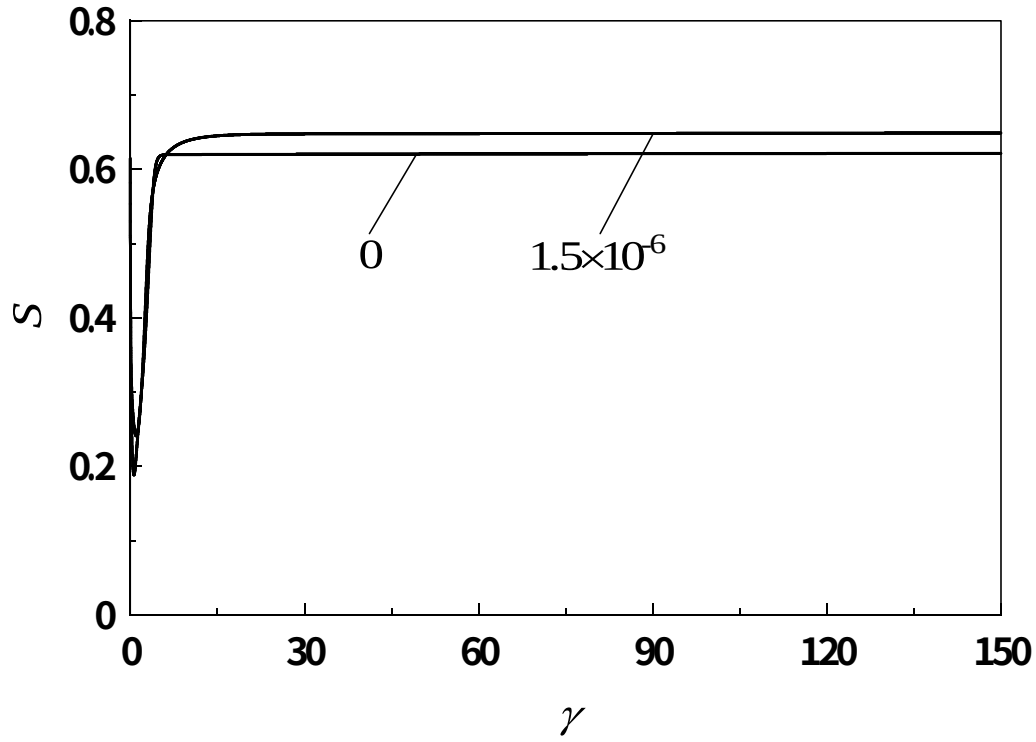

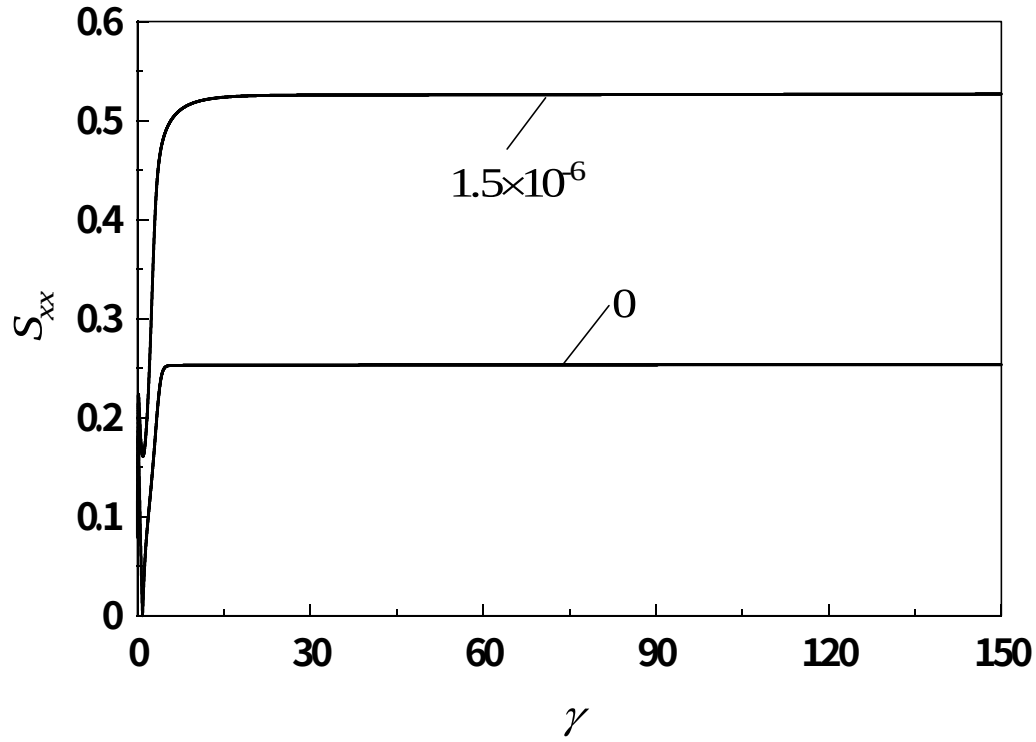

Figures 3.57 Transient behaviors of scalar order parameter S and S_{xx} versus strain at $\dot{\gamma}^*$ =1 for β=0.9 when H_x^*=0 and 1.5×10^{-6}.

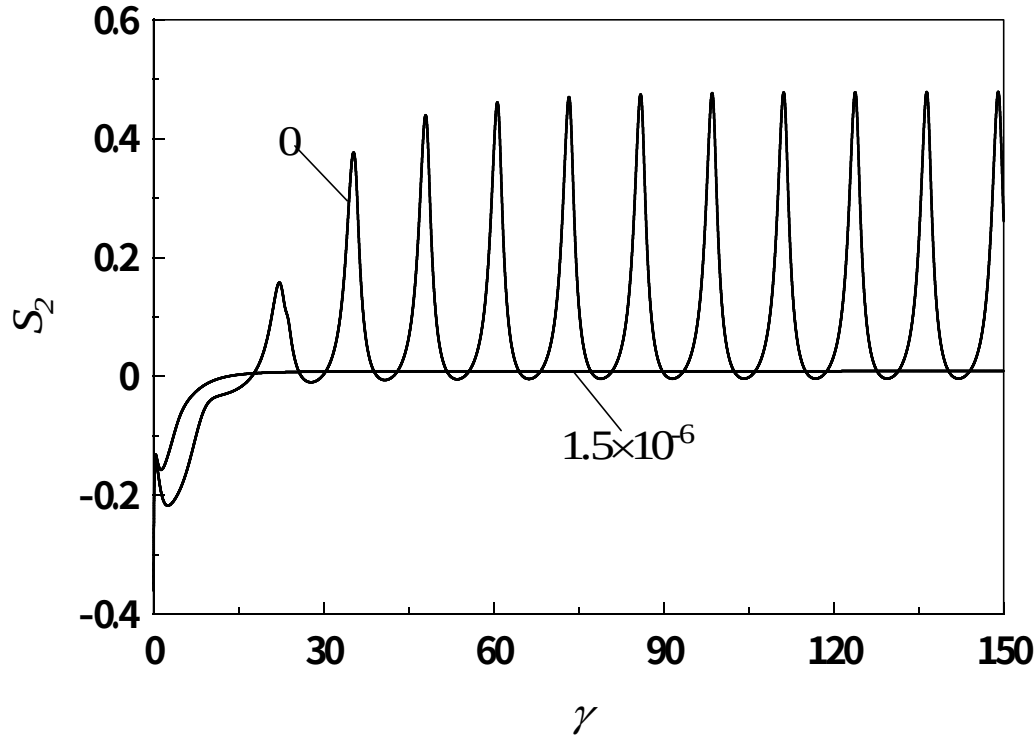

Figure 3.58 S_2 versus strain at $\dot{\gamma}^*$ =2 for β=0.9 when H_x^*=0 and1.5×10^{-6}.

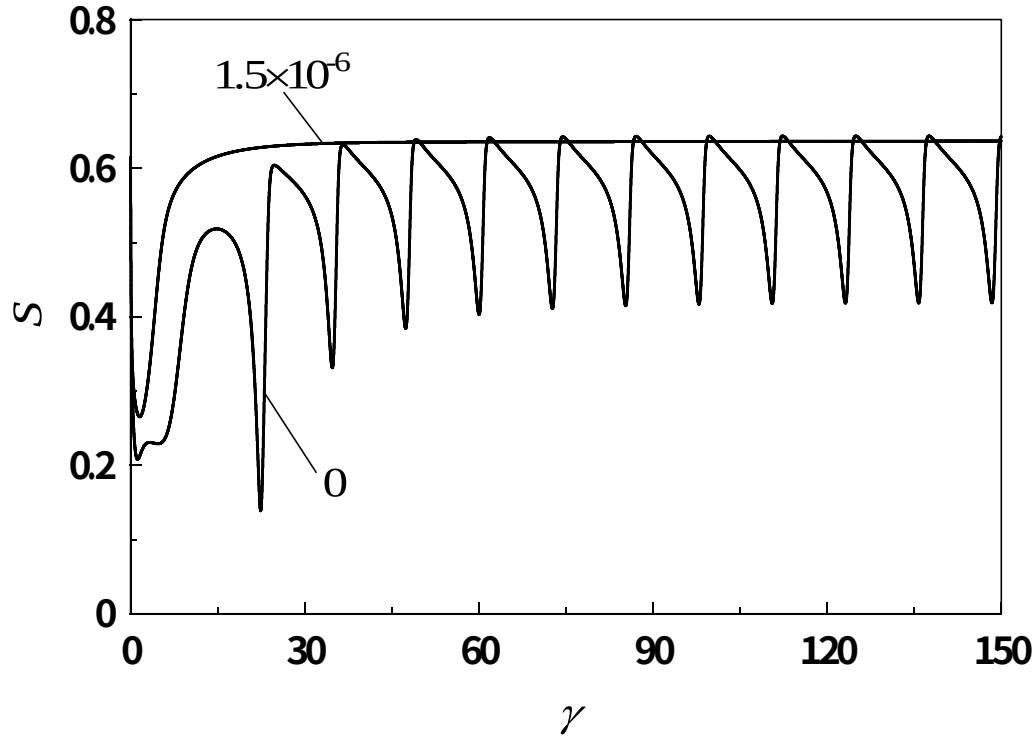

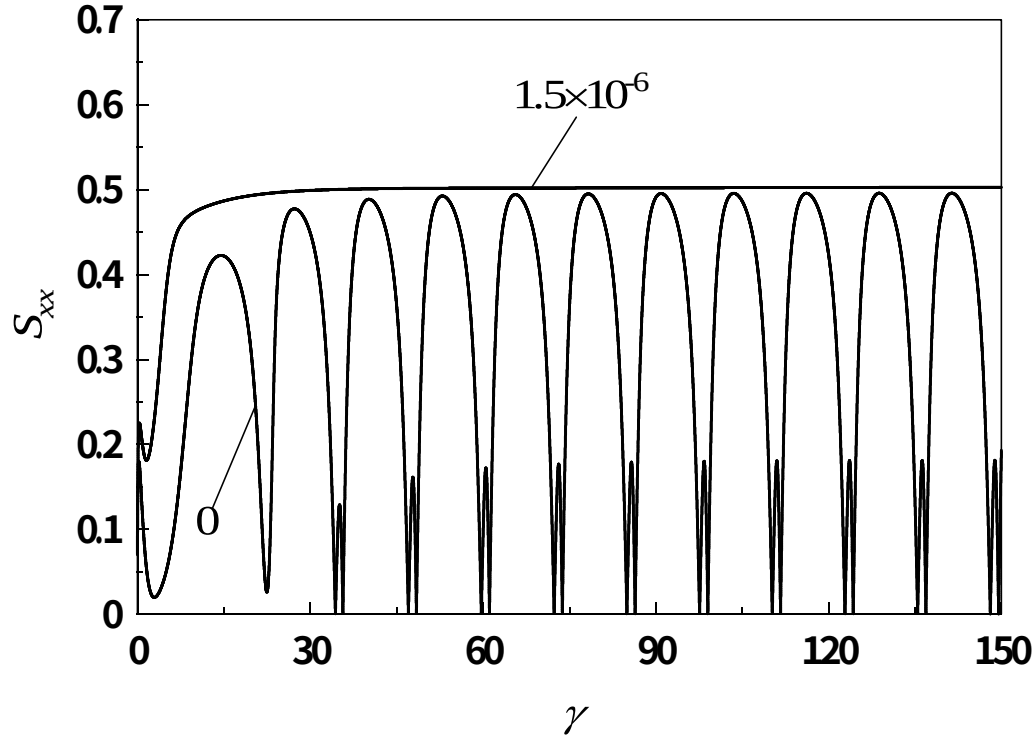

Figures 3.59 Transient behaviors of scalar order parameter S and S_{xx} versus strain at $\dot{\gamma}^*$ =2 for β=0.9 when H_x^*=0 and 1.5×10^{-6}.

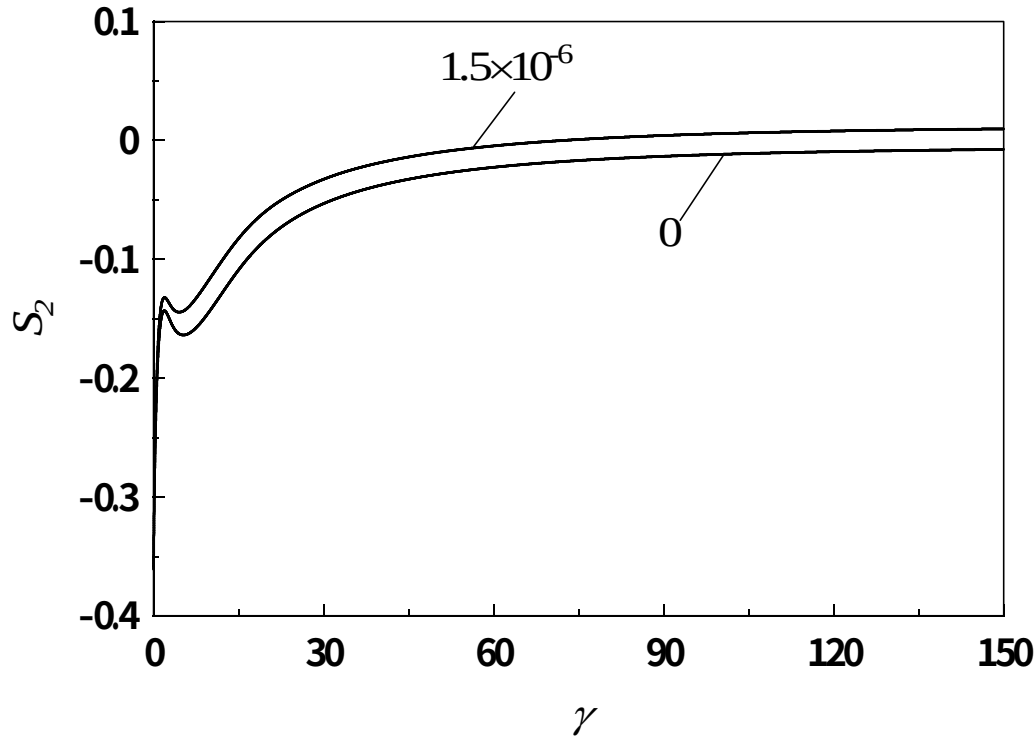

Figure 3.60 S_2 versus strain at $\dot{\gamma}^*$ =10 for β=0.9 when H_x^*=0 and1.5×10^{-6}.

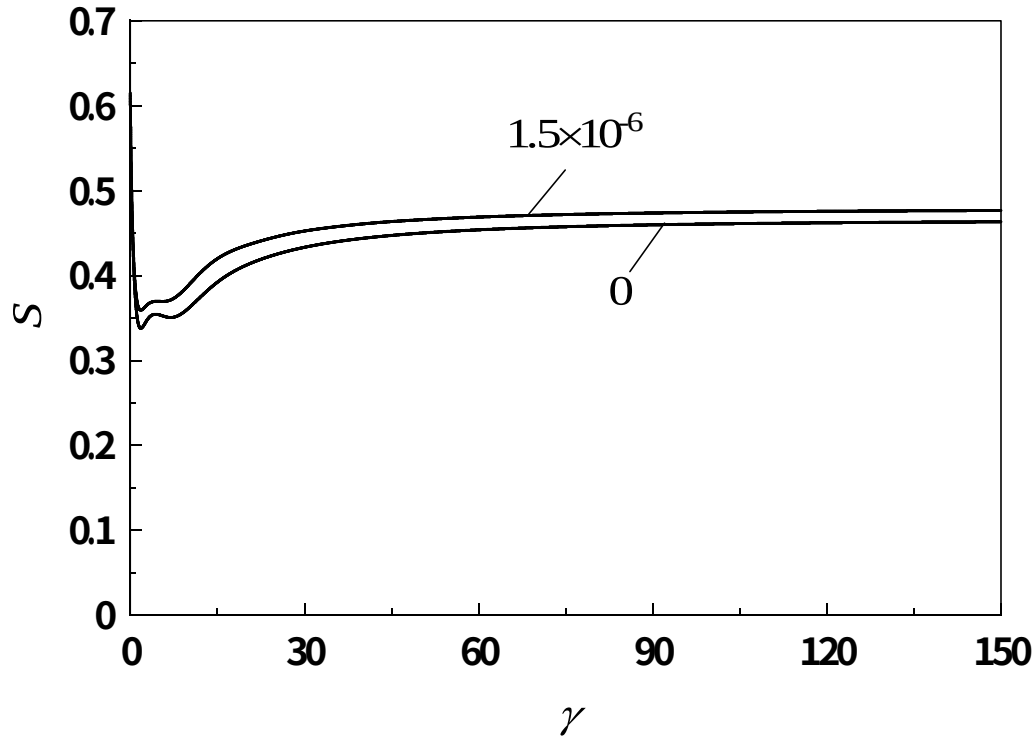

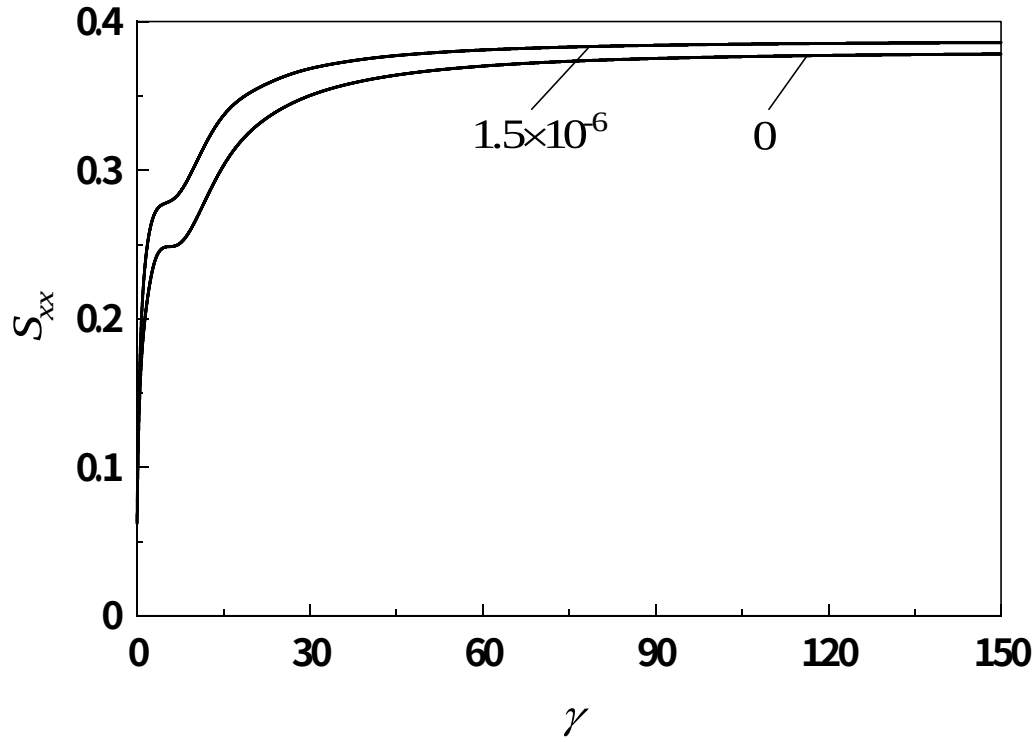

Figures 3.61 Transient behaviors of scalar order parameter S and S_{xx} versus strain at $\dot{\gamma}^*$=10 for β=0.9 when H_x^*=0 and 1.5×10^{-6}.

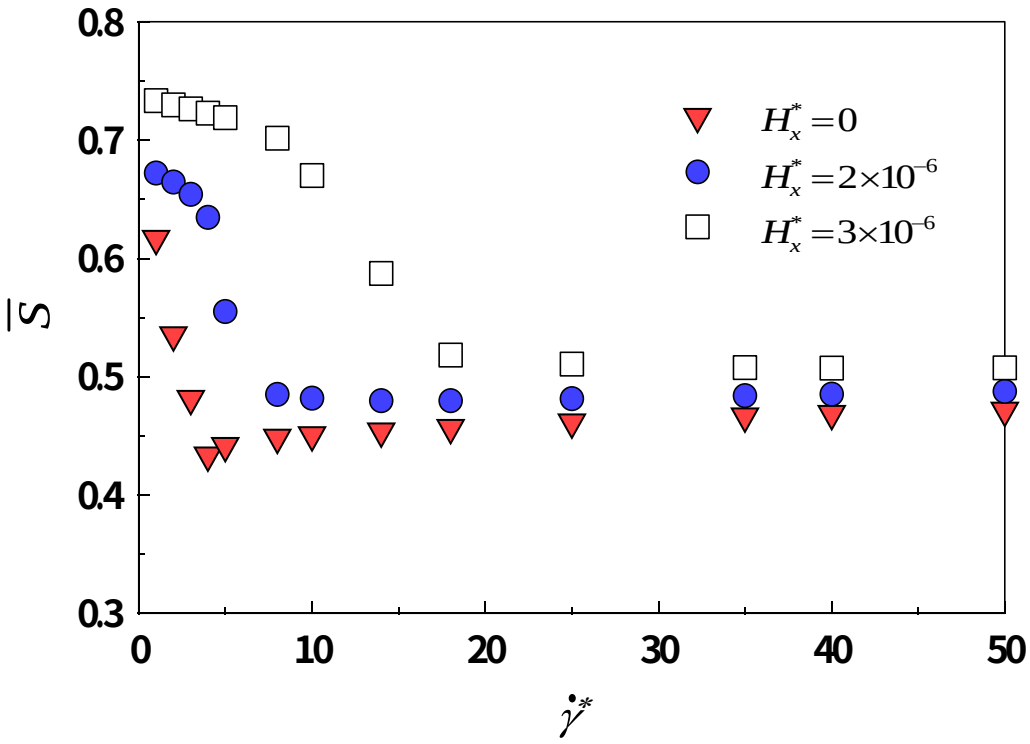

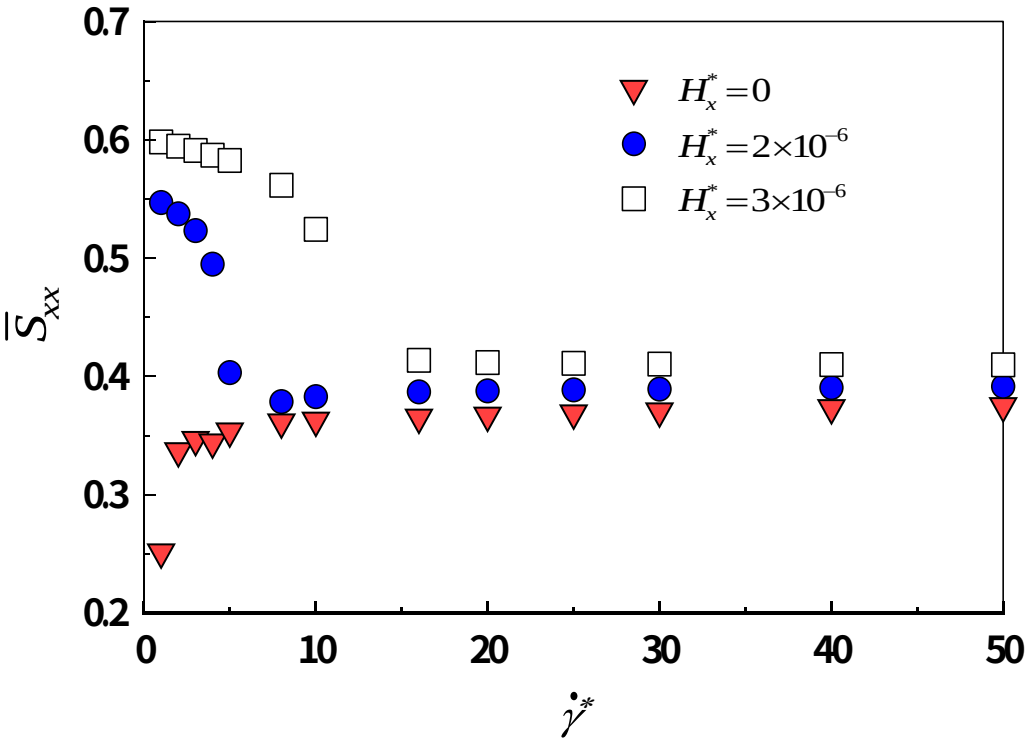

Figures 3.62 Average order parameter $\bar{S}$ and $\bar{S}_{xx}$ as a function of shear rate for β=0.9 at H_x^*=0, 1.5×10^{-6}, 2×10^{-6} and 3×10^{-6}.

3.4.3.2 The Magnetic Field along the *y*-axis

In this section, we will discuss the simulation results when the magnetic field is parallel to the velocity gradient direction. Figure 3.63 shows that the S_2 changes with time at $\dot{\gamma}^*$=1 for H_y*=0, 1.5×10^{-6} and 2×10^{-6}. The director almost aligns along the *y*-axis when H_y*=2×10^{-6}. *S* increases with the increasing strength of the magnetic field showed in Figure 3.64. When the shear rate is equal to 2 the final director will be decided by the torques caused by the flow and the magnetic field indirectly showed out in Figure 3.65. The scalar parameter *S* as the function of time at $\dot{\gamma}^*$=2 is plot in Figure 3.66 for H_y*=0, 1.5×10^{-6} and 2×10^{-6}. If further increasing the shear rate at $\dot{\gamma}^*$=6, the shear flow becomes stronger so that much more strength of the magnetic field is needed to align the director along the magnetic field as can be seen from Figure 3.67. *S* also is increased very quickly when the magnetic field is increased at 3×10^{-6} described in Figure 3.68. The time-averaged $\bar{S}$ as the function of the shear rate at H_y*=0, 1.5×10^{-6}, 2×10^{-6} and 3×10^{-6} is described in Figure 3.69. A high orientation state can be obtained at low shear rates.

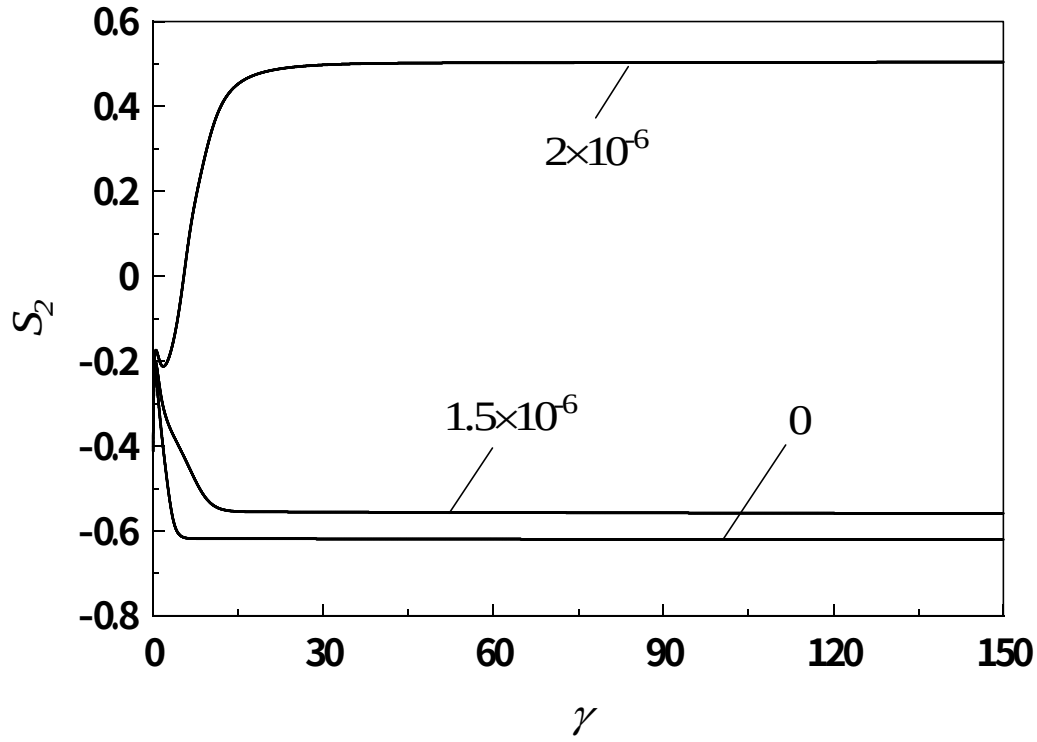

Figure 3.63 S_2 versus strain at $\dot{\gamma}^*$ =1 for β=0.9 when H_y^*=0, 1.5×10^{-6} and 2×10^{-6}.

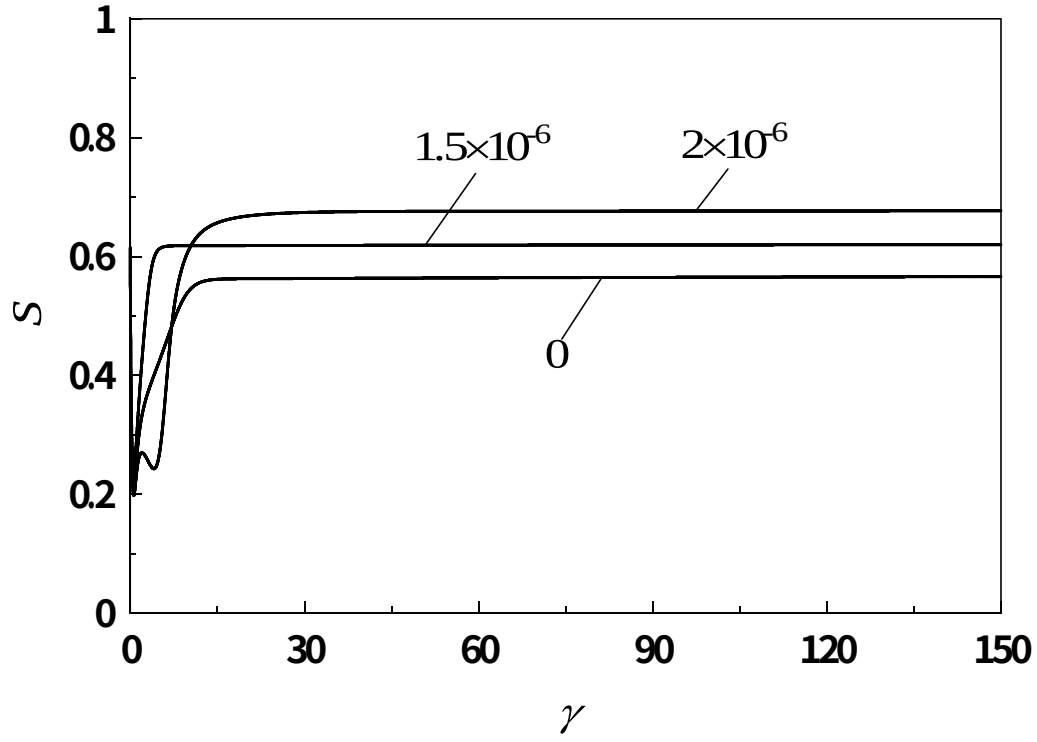

Figure 3.64 Transient behaviors of scalar order parameter S versus strain at $\dot{\gamma}^*$ =1 for β=0.9 when H_y^*=0, 1.5×10^{-6} and 2×10^{-6}.

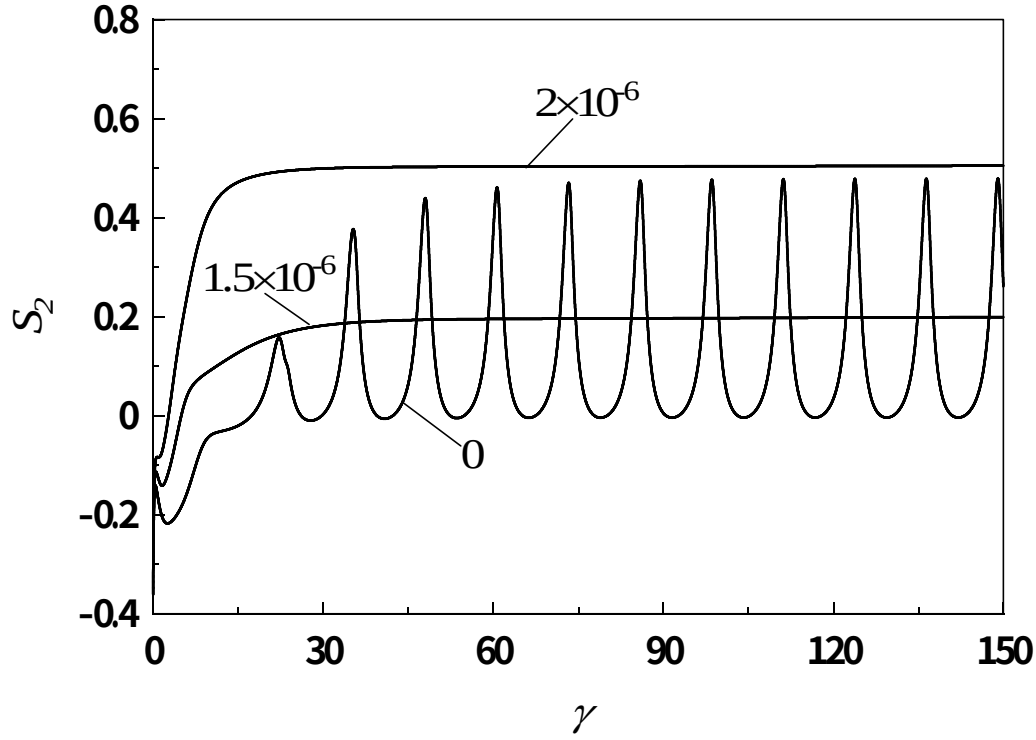

Figure 3.65 S_2 versus strain at $\dot{\gamma}^*$=2 for β=0.9 when H_y^*=0, 1.5×10^{-6} and 2×10^{-6}.

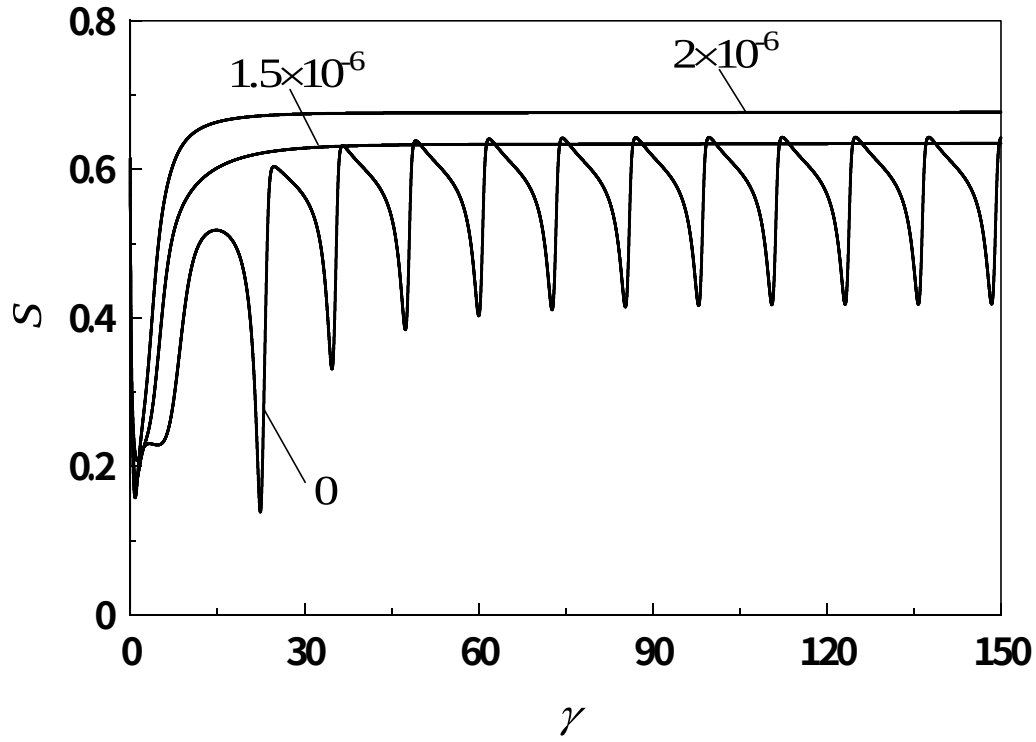

Figure 3.66 Transient behaviors of scalar order parameter S versus strain at $\dot{\gamma}^*$=2 for β=0.9 when H_y^*=0, 1.5×10^{-6} and 2×10^{-6}.

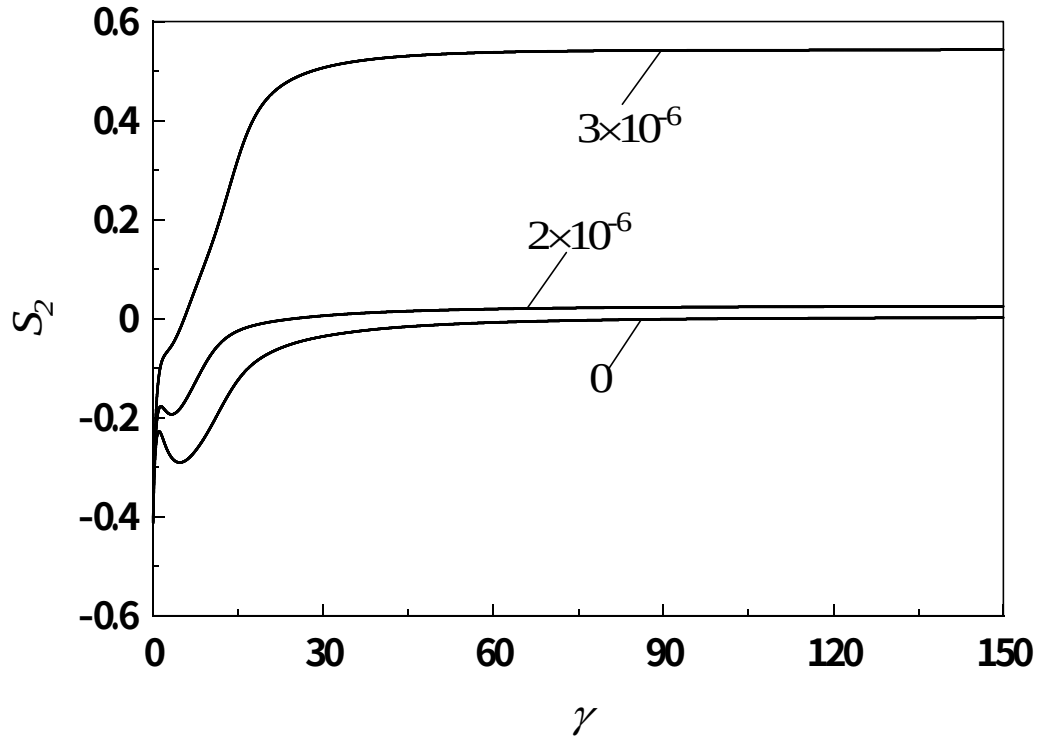

Figure 3.67 S_2 versus strain at $\dot{\gamma}^*$ =6 for β=0.9 when H_y^*=0, 2×10^{-6} and 3×10^{-6}.

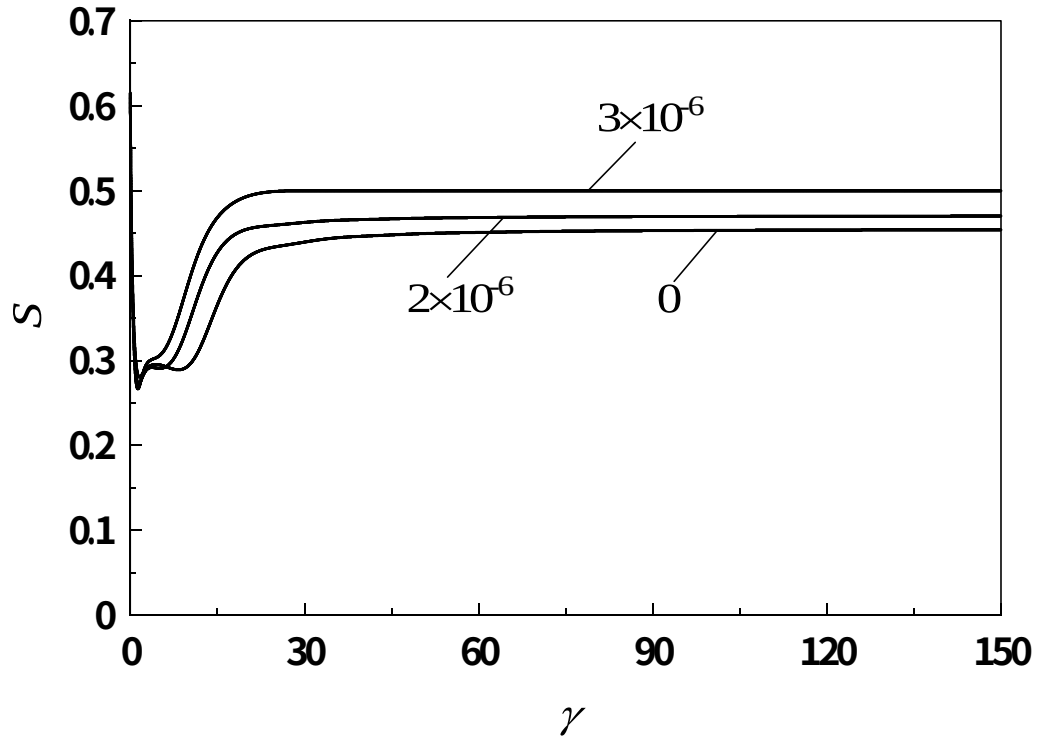

Figure 3.68 Transient behaviors of scalar order parameter S versus strain at $\dot{\gamma}^*$ =6 for β=0.9 when H_y^*=0, 2×10^{-6} and 3×10^{-6}.

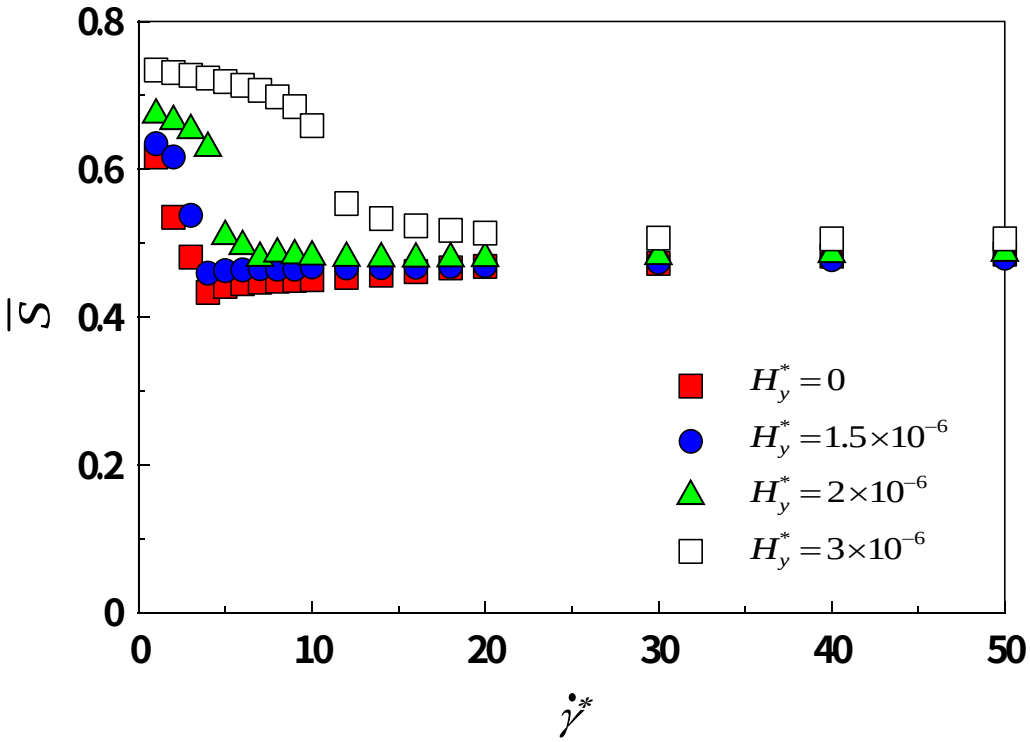

Figure 3.69 Average order parameter $\bar{S}$ as a function of shear rate for β=0.9 at H_y^*=0, 1.5×10^{-6}, 2×10^{-6} and 3×10^{-6}.

3.5 Conclusions

In this chapter the effect of the magnetic field along the *x*-axis and the *y*-axis on the out-of-plane case is investigated under the simple shear flow. Doi equation is solved without any approximation. The computation results are mainly analyzed and discussed according to the quantity S_2, the scalar parameter S and S_{xx}. When the initial director is along the *x*-axis, it doesn't rotate out from the shear plane again. And the three modes, tumbling, wagging and aligning, are observed as the increasing shear rate, respectively. However, if the initial director is along the vorticity direction, namely the *z*-axis, the log-rolling orientation state where the average orientation is always perpendicular to the shear plane is detected at low shear rates. It can be seen that the director is controlled to align along the magnetic field in the shear plane if the strength of the magnetic field is stronger enough. With the increasing shear rate the shear plane becomes an attractor for the director that is aligned along the flow direction. The torque caused by the applying magnetic field accelerates the rotational velocity of the director into the shear plane. Finally we also consider a general situation that the director lies in the *x*-*z* plane at

φ=-50^{o}. In this case the shear plane also is an attractor for the director at low shear rates.

In particular the molecular alignment along the flow direction under the magnetic field along the *x*-axis is investigated. The molecular alignment along the flow also can be increased by applying the proper magnetic field.

Finally the detail simulation results at β=0.9 are also presented. It can be seen that the time-averaged scalar order parameter $\overline{S}$ and $\overline{S}_{xx}$ is lower than the ones when β=1.0 at the same calculation conditions.

From the simulation results a conclusion can be made that the magnetic field can eliminate the log-rolling orientation state and control the director to align the direction of the magnetic field. The strength of the LCPs can be efficiently improved by applying the magnetic field.

References:

1. Doi, M., *J. Polym. Sci. Polym. Phys. Ed.* **19**, 229 (1981)
2. Zuniga, I. and Leslie, F. M., *Liq.Cryst.* **5**, 725 (1985)
3. Larson, R.G. and Öttinger, H.C., *Macromolecules* **24**, 6270 (1991)
4. Bhandar, A.S. and Wiest, J.M., *J. Colloid Interface Sci.* 257, 371 (2003)
5. Bhandar, A.S., Piao, M., Lane, A.M., and Wiest, J.M., *J. Colloid Interface Sci.* 268, 246 (2003)
6. Larson, R.G., *The structure and rheology of complex fluids*, 443 (1999) Oxford University press.

Chapter 4

Conclusions

This thesis gave a detailed presentation of computer simulation of the effect of the magnetic field on molecular orientation of nematic LCPs under the simple shear flow. In particular, the effect of the magnetic field on the major orientation direction, the scalar order parameter, and the flow-orientation mode transition are analyzed and discussed with the Doi theory directly solved without any approximation closures. Figures 4.1 describe how the moment caused by the flow and the magnetic field acts on the director. The arrows represent the moment direction. The intensity of the moment on the director is showed by the changes of the color on the arrows. The flow is along the *x*-axis. Two cases are considered in this dissertation: a) the magnetic field is applied parallel to the flow, namely, along the *x*-axis; b) the magnetic field is perpendicular to the flow, namely, along the *y*-axis. The moment caused by the flow along the *x*-axis always rotates the director. As shown as in Figures 4.1, when the director is parallel to the *y*-axis, the moment acting on the director is strongest. On the other hand, the moment is zero when it is parallel to the direction of flow. In Figure 4.1(a), the magnetic field is imposed along the *x*-axis. It can be seen that the torque caused by the magnetic field has the tendency to rotate the director along the *x*-axis. In this case the flow-orientation direction is along the magnetic field-orientation direction. However, when the magnetic field is parallel to the *y*-axis, the flow-orientation direction is perpendicular to the magnetic field-orientation direction. The final director will be

determined through the competition of the moments caused by the flow and the magnetic field. The conclusions are presented below.

1) Conclusions for in-plane case:

In this case the director always is confined into the shear plane so that the probability orientation function is symmetry to the shear plane. The simulation results are presented from two aspects: 1) the magnetic field along the flow direction (*x*-direction); 2) the magnetic field parallel to the velocity gradient direction (*y*-direction). When the magnetic field is imposed in the flow direction, the scalar parameter becomes higher for entire shear rate regime because of the magnetic field. Also, the existence of the new aligning state is found at low shear rate regime in which the effect of the shear flow prevails the effect of the magnetic force, and the rotation of individual molecules is suppressed. On the other hand, for the case of the magnetic field along the velocity gradient direction, the magnetic fields drastically affect on the steady angle of the major orientation direction, in addition to the effects mentioned above.

The effect of the molecular length by setting the molecular formation coefficient β=0.9 on the orientation behavior of the director also is discussed in the two cases that the magnetic field is along the *x*-direction and *y*-direction. Compared with the simulation results obtained at β=1.0 the major difference is the effect of the magnetic field along the *x*-axis on the flow-orientation mode, where the wagging state doesn't disappear with the increasing magnetic field. 31

2) Conclusions for the out-of-plane case:

Since the director has the chance to rotate out of the shear plane, the method has to be considered to control it in order to obtain the arbitrary desired molecular orientation configurations which enhance the functionality of LCP materials. The Doi theory also is used to solve this problem, in which the asymmetry of the probability orientation function is allowed. As discussed in the paper written by Larson and Öttinger in 1991 the initial director will decide the final orientation state of the director. Therefore, in this part three position of the director is chose: 1) along the flow direction, 2) along the vorticity direction, and 3) in the *x*-*z* plane and the degree with respect to the *z*-axis at $\varphi=-50^{o}$. And the effect of the magnetic field on the orientation state in the three cases also is investigated, respectively. When the initial director is along the *x*-axis, it doesn't rotate out from the shear plane again. And the three modes, tumbling,

wagging and aligning, are observed as the increasing shear rate, respectively. However, if the initial director is along the vorticity direction, namely the *z*-axis, the log-rolling orientation state where the average orientation is always perpendicular to the shear plane is detected at low shear rates. It can be seen that the director is controlled to align along the magnetic field in the shear plane if the strength of the magnetic field is stronger enough. Finally when the director lies in the *x*-*z* plane at φ=-50^{o}, the shear plane also is an attractor for the director at low shear rates.

In particular the molecular alignment along the flow direction under the magnetic field along the *x*-axis is investigated. Through the simulation results a conclusion can be made that except the log-rolling orientation state where the director always is perpendicular to the shear plane the molecular alignment along the flow direction will be increased by applying the magnetic field along the flow direction.

Finally the detail simulation results at β=0.9 are also presented. It can be seen that the time-averaged scalar order parameter $\overline{S}$ and $\overline{S}_{xx}$ is lower than the ones when β=1.0 at the same calculation conditions.

Through the simulation results presented in this thesis the performance of LCP material can be freely tailored by applying the appropriate strength of the magnetic field. It is an efficient way to make an improvement on the performance of LCP materials.

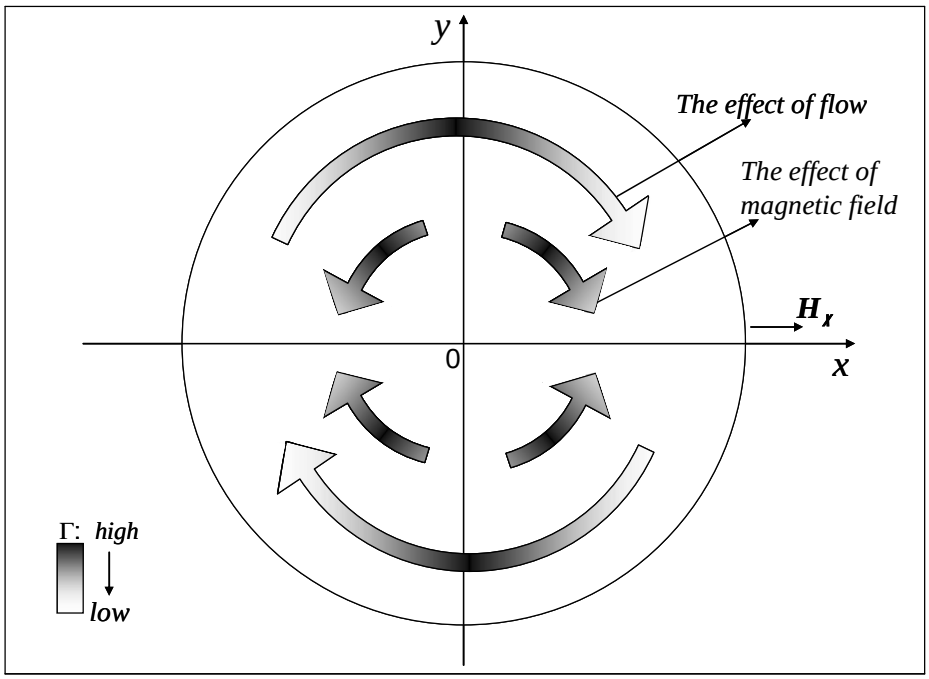

(a) Magnetic field is along the *x*-axis

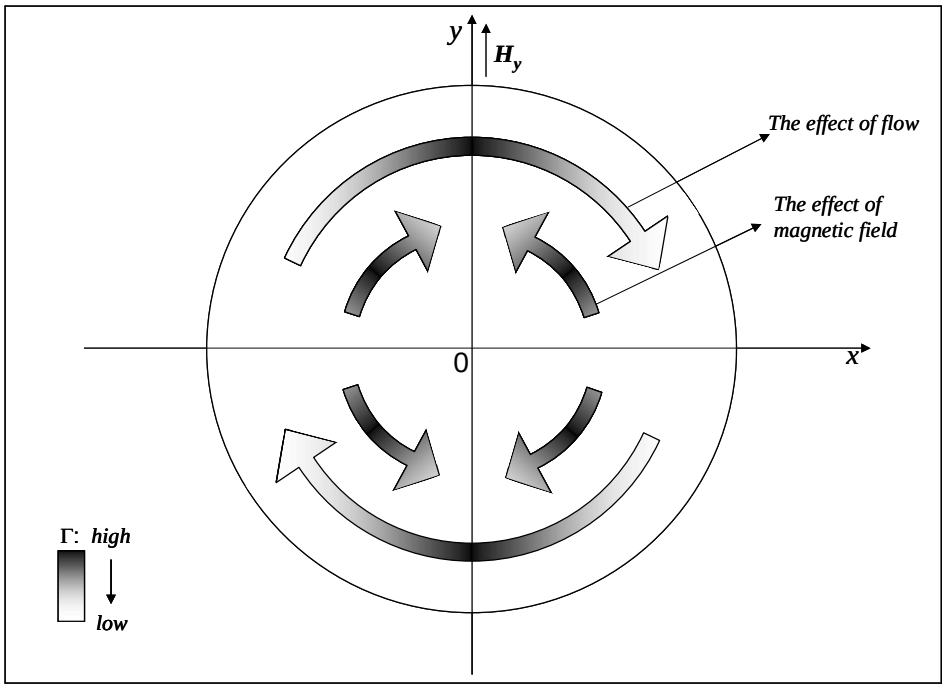

(b) Magnetic field is along the *y*-axis

Figures 4.1 Moment caused by the flow and the magnetic field

Acknowledgments

It is with great pleasure that I acknowledge my supervisor Professor Tomohiro Tsuji and co-supervisor Professor Shigeomi Chono. They give me many constructive comments and valuable suggestions. Because of their continuous guidance and encouragement in the course of this dissertation I finish this project.

Furthermore I would like to thanks all the members in our lab, especially, my tutor Erami Takafumi.

Last but not least, I especially want to give thanks to my family (my parents and my husband) for their support and encouragement in my study period.